THE BEHAVIOR OF LNG VAPOR CLOUDS:

Wind-Tunnel Simulation of 40 M^3 LNG Spill Tests at China Lake Naval Weapons Center, California

FINAL REPORT

(July 1979 - July 1981)

Prepared by

D. E. Neff and R. N. Meroney

Fluid Mechanics and Wind Engineering Program
Department of Civil Engineering
Colorado State University
Fort Collins, Colorado 80523

CER81-82DEN-RNM1

for

GAS RESEARCH INSTITUTE

Contract No. 5014-352-0203

GRI Project Manager

Steve J. Wiergma

Environment, Safety and Distribution Research Division

July 1981

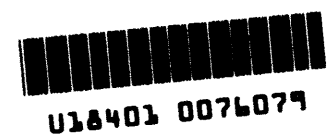

GRI DISCLAIMER

LEGAL NOTICE: This report was prepared by Colorado State University as an account of work sponsored by the Gas Research Institute (GRI). Neither GRI, members of GRI, not any person acting on behalf of either:

a. Makes any warranty or representation, expressed or implied with respect to the accuracy, completeness, or usefulness of the information contained in this report, or that the use of any information, apparatus, method or process disclosed in this report may not infringe privately owned rights; or

b. Assumes any liability with respect to the use of, or for damages resulting from the use of, any information, apparatus, method, or process disclosed in this report.

50272-101

REPORT DOCUMENTATION PAGE	1. REPORT NO. GRI 80/0094	2.	3. Recipient's Accession No.

4. Title and Subtitle

THE BEHAVIOR OF LNG VAPOR CLOUDS: Wind-Tunnel Simulation of 40 M^3 LNG Spill Tests at China Lake Naval Weapons Center, Calif

5. Report Date July 1981

6.

7. Author(s)

D. E. Neff and R. N. Meroney

8. Performing Organization Rept. No. CER81-82DEN-RNM1

9. Performing Organization Name and Address

Civil Engineering Department
Colorado State University
Fort Collins, Colorado 80523

10. Project/Task/Work Unit No.

11. Contract(C) or Grant(G) No.

(C)
(G) 5014-352-0203

12. Sponsoring Organization Name and Address

Gas Research Institute
8600 West Bryn Mawr Avenue
Chicago, Illinois 60631

13. Type of Report & Period Covered Final (July 1979 - July 1981)

14.

15. Supplementary Notes

16. Abstract (Limit: 200 words)

Wind-tunnel transient concentration data were obtained from modeling tests which reproduced gaseous dispersion from five different forty cubic meter or less liquefied natural gas (LNG) spills performed at China Lake Naval Weapons Center during the spring and summer of 1980. Comparisons in the transient concentration data between these modeled tests and the field tests indicated which parameters are dominant in the modeling process. Model tests which reproduced the wind shear and turbulence structure of the approach wind reproduced the concentration patterns measured at the field site. This result reinforced the predictive reliability of wind tunnel modeling of larger volume spills.

17. Document Analysis a. Descriptors

Liquefied Natural Gas, wind tunnel, dispersion of heavy plumes, vapor cloud dispersion

b. Identifiers/Open-Ended Terms

c. COSATI Field/Group

18. Availability Statement:	19. Security Class (This Report)	21. No. of Pages
	20. Security Class (This Page)	22. Price

(See ANSI-Z39.18) See Instructions on Reverse

OPTIONAL FORM 272 (4-77)
(Formerly NTIS-35)
Department of Commerce

RESEARCH SUMMARY

Title	The Behavior of LNG Vapor Clouds: Wind-Tunnel Simulation of 40 M^3 LNG Spill Tests at China Lake, California
	Accession Code: GRI-80/0094 GRI Contract Number: 5014-352-0203
Contractor	Civil Engineering Department Colorado State University
Principal Investigators	D. E. Neff and R. N. Meroney
Time Span	July 1979 - July 1981 Final Report
Major Achievements	Wind-tunnel transient concentration data were obtained from modeling tests which reproduced gaseous dispersion from five different field liquefied natural gas (LNG) spills performed at China Lake Naval Weapons Center during the spring and summer of 1980. Comparisons of the transient concentration data obtained in the modeled tests and those obtained in the field tests indicate which parameters are dominant in the modeling process. The model test that reproduced the wind shear and turbulence structure of the approach wind reproduced the concentration patterns measured at the field site. This result reinforced the predictive reliability of wind tunnel modeling of larger volume spills.
Recommendations	A larger number of field experiments should be performed over sites that exhibit a greater effective surface roughness and lower wind speeds.

From this data base and data collected from the wind-tunnel modeling of each spill, a more quantitative estimate of the accuracy of physical modeling can be determined. Since the results from the wind tunnel models of the present field test series are quite acceptable, the results from wind tunnel experiments covering a larger range of release conditions should be used to validate numerical models.

Description of Work Completed

A terraced 1:240 scale model of the China Lake Naval Weapons Center and a set of eight aspirated hot-wire katharometer probes to measure transient concentrations of modeled LNG spill situations were constructed. Numerical programs were written to sample and hold instantaneous data from hot-wire anemometer probes for real time analysis on a Hewlett-Packard System 1000. Measurements of mean velocities, turbulent intensities, spectra, and correlations over the naval weapons site model have been documented. Laboratory measurements of concentration for ten pre-field tests were completed and presented in the Interim 1979-1980 annual report. Laboratory measurements on the physical simulations of the forty cubic meter LNG spill series were completed. Five different field tests, Burros 4, 5, 7, 8, and 9, were simulated. Burro 8 was modeled by three different methodologies, two being at a model

length scale factor of 1:240 but different source gas specific gravities and one at a scale factor of 1:85. Burro 9 was also modeled by two different methods, one at a model scale factor of 1:240, the other at a scale factor of 1:85. Burros 4, 5, and 7 were each modeled by one test only at a scale factor of 1:240. The data from these runs were reduced into tables of pertinent values. From these tables, plots of ground-level peak concentration contours, time progression curves of the lower flammability limit (LFL), and the flammable zone as a function of centerline distance and time were prepared. Simulated concentration time histories of the different modeled tests were plotted for downwind spacial positions similar to those obtained during the actual field tests.

GRI Comment

Previous studies had indicated that the wind tunnel would be a useful tool for predicting the extent of downwind hazards associated with the release of heavy gases. Utilizing inert gaseous mixtures, Colorado State University had used wind tunnel experimental results to predict mean and transient vapor concentration contours and the overall plume geometry and behavior under various weather conditions and hence help the U.S. Department of Energy plan its large-scale field experiments to validate dispersion theories. The post-field-test wind

tunnel experiments reported here were conducted and analyzed to validate the predictive reliability of wind tunnel modeling of larger volume spills. CSU's results have verified that the wind-shear and turbulence-structure parameters are dominant in the modeling process and have reinforced the predictive reliability of wind tunnel modeling. GRI intends to use wind tunnel modeling to verify concepts (e.g., water curtains, vortex shedders and vapor fences) for increasing the dispersion of vapor clouds resulting from accidential LNG spills. Wind tunnel experiments will also be used to validate numerical models for vapor dispersion. Future field experiments at low wind speeds and with rough terrain are not planned at this time. If data from such experiments become available, GRI will be most interested in conducting associated wind-tunnel modeling of the spill tests to provide a more quantitative estimate of the accuracy of physical modeling.

TABLE OF CONTENTS

LIST OF TABLES

LIST OF FIGURES

LIST OF FIGURES (Continued)

LIST OF FIGURES (Continued)

LIST OF FIGURES (Continued)

LIST OF SYMBOLS

Dimensions are given in terms of mass (m), length (L), time (t), moles (n), and temperature (T).

Symbol	Definition	
A	Area	$[L^2]$
C_p	Specific heat capacity at constant pressure	$[L^2t^{-2}T^{-1}]$
C_p^*	Molar specific heat capacity at constant pressure	$[L^2mt^{-2}T^{-1}n^{-1}]$
D	Source diameter	$[L]$
g	Gravitational acceleration	$[Lt^{-2}]$
h	Local plume depth	$[L]$
k	Thermal conductivity	$[mLT^{-1}t^{-3}]$
L	Length	$[L]$
M	Molecular weight	$[mn^{-1}]$
n	Mole	$[n]$
p	Velocity power law exponent	
Q	Volumetric rate of gas flow	$[L^3t^{-1}]$
T	Temperature	$[T]$
ΔT	Temperature difference across some reference layer	$[T]$
t	Time	$[t]$
u_*	Friction velocity	$[Lt^{-1}]$
U	Velocity	$[Lt^{-1}]$
V	Volume	$[L^3]$
W	Plume vertical velocity	$[Lt^{-1}]$
x	General downwind coordinate	$[L]$
y	General lateral coordinate	$[L]$
z	General vertical coordinate	$[L]$
z_o	Surface roughness parameter	$[L]$

LIST OF SYMBOLS (continued)

Symbol	Definition	
δ	Boundary layer thickness	[L]
Λ	Integral length scale of turbulence	[L]
$\Delta\rho$	Density difference between source gas and air	$[mL^{-3}]$
ρ	Density	$[mL^{-3}]$
σ	Standard deviation	
χ	Mole fraction of gas component	
Ω	Angular velocity of earth = 0.726×10^{-4} (radians/sec)	$[t^{-1}]$
λ_p	Peak wavelength	[L]
ν	Kinematic viscosity	$[L^2t^{-1}]$

Subscripts

a	Air
Ar	Argon
b.o.	Boiloff
g	Gas
i	Cartesian index
LNG	Liquefied Natural Gas
m	Model
NG	Natural gas
o	Reference conditions
p	Prototype
s	Source gas

1.0 INTRODUCTION

Natural gas is a highly desirable form of energy for consumption in the United States. Its conversion to heat energy for home and industrial use is achieved with very little environmental impact, and a sophisticated distribution network already services a major part of the country. Recent efforts to expand this nation's natural gas supply include the transport of natural gas in a liquid state from distant gas fields. Although the likelihood is extremely small, an accident during storage and transport of liquid natural gas may result in a relatively large environmental risk [1,2]. To transport and store liquefied natural gas (LNG) it is cooled to a temperature of -162°C. At this temperature if a storage tank on a ship or land were to rupture and the contents spill out onto the earth's surface, rapid boiling of the LNG would ensue and the liberation of a potentially flammable vapor could would result. Past studies [3,4] have demonstrated that the cold LNG vapor plume will remain negatively buoyant for a long time and thus represents a ground-level hazard. This hazard will extend downwind until the atmosphere has diluted the LNG vapor below the lower flammability limit (a local concentration for methane below 5 percent by volume).

It is important that accurate predictive models for LNG vapor cloud physics be developed, so that the associated hazards of transportation and storage may be evaluated. Various industrial and governmental agencies have sponsored a combination of analytical, empirical, and physical modeling studies to analyze problems associated with the transportation and storage of LNG. Since these models require simplifying assumptions to permit the development of tractable solution procedures

one should perform atmospheric scale tests to validate the accuracy of the models.

A multitask research program has been designed by a complementary Gas Research Institute (GRI)/Department of Energy (DOE) effort to address the problem of preditive methods in LNG hazard analysis. One aspect of this program, the physical simulation of LNG vapor dispersion in a meteorological wind tunnel is the subject of this report. The complete sub-program research contract, GRI contract number 5014-352-0203 consists of four tasks.

Task 1: Laboratory Support Tests for the Forty Cubic Meter LNG Spill Series at China Lake, California.

Task 2: Physical Simulation in Laboratory Wind Tunnels of the 1980 LNG Spill Tests performed at China Lake, California.

Task 3: Laboratory Simulation of Idealized Spills on Land and Water.

Task 4: Laboratory Tests Defining LNG Plume Interaction with Surface Obstacles.

Task one was presented in the July 1980 annual report. Tasks three and four will be presented in separate reports. Task two, the physical simulation in laboratory wind tunnels of the 1980 LNG spill tests performed at China Lake, California, is the sole subject of this report.

Five different field tests, Burros 4, 5, 7, 8, and 9, were simulated in a laboratory wind tunnel[1]. Burro 8 was simulated by three different models. One at a length scale of 1:240 and a source gas specific gravity of 1.38, one at a length scale of 1:240 and a source gas specific gravity of 4.18, and one at a length scale of 1:85 and a

[1]The "burro" test series designate the 40-cubic meter LNG spill tests performed at the Naval Weapons Test Center in 1980.

source gas specific gravity of 1.38. Burro 9 was simulated by two different models both with source gas specific gravities of 1.38. One was at a model length scale of 1:85 the other was at a model length scale of 1:240. Burro 4, 5, and 7 were each simulated by one model each whose length scales were 1:240 and whose source gas specific gravities were 1.38.

The velocity and concentration data for each model test were summarized into contour plots and graphic presentations. Comparisons with the available field data were made.

The methods employed in the physical modeling of atmospheric and plume motion are discussed in Chapter 2. The details of model construction and experimental measurements are described in Chapter 3. Chapter 4 discusses the test program and results obtained. Chapter 5 summarizes the comparison between modeled data and field data. Chapter 6 summarizes the conclusions from this study.

2.0 MODELING OF PLUME DISPERSION

To obtain a predictive model for a specific plume dispersion problem one must quantify the pertinent physical variables and parameters into a logical expression that determines their interrelationships. This task is achieved implicitly for processes occurring in the atmospheric boundary layer by the formulation of the equations of conservation of mass, momentum, and energy. These equations with site and source conditions and associated constituitive relations are highly descriptive of the actual physical interrelationship of the various independent (space and time) and dependent (velocity, temperature, pressure, density, etc.) variables.

These generalized conservation statements subjected to the typical boundary conditions of atmospheric flow are too complex to be solved by present analytical or numerical techniques. It is also unlikely that one could create a physical model for which exact similarity exists for all the dependent variables over all the scales of motion present in the atmosphere at a reduced geometric scale. Thus, one must resort to various degrees of approximation to obtain a predictive model. At present purely analytical or numerical solutions of plume dispersion are unavailable because of the classical problem of turbulent closure [5]. Such techniques rely heavily upon empirical input from observed or physically modeled data. The combined empirical-analytical-numerical solutions have been combined into several different predictive approaches by Pasquill [6] and others. The estimates of dispersion by these approaches are often crude; hence, they should only be used when the approach and site terrain are uniform and without obstacles. Boundary layer wind tunnels are capable of physically modeling plume

processes in the atmosphere under certain restrictions. These restrictions are discussed in the next few sections.

2.1 PHYSICAL MODELING OF THE ATMOSPHERIC BOUNDARY LAYER

The atmospheric boundary layer is that portion of the atmosphere extending from ground level to a height of approximately 100 meters within which the major exchanges of mass, momentum, and heat occur. This region of the atmosphere is described mathematically by statements of conservation of mass, momentum, and energy [7]. The general requirements for laboratory-atmospheric-flow similarity may be obtained by fractional analysis of these governing equations [8]. This methodology is accomplished by scaling the pertinent dependent and independent variables and then casting the equations into dimensionless form by dividing through by one of the coefficients (the inertial terms in this case). Performing these operations on such dimensional equations yields dimensionless parameters commonly known as:

Reynolds number	$Re = U_o L_o / \nu_o$	$= \frac{\text{Inertial Force}}{\text{Viscous Force}}$
Bulk Richardson number	$Ri = [(\Delta T)_o / T_o] \, (L_o / U_o^2) \, g_o$	$= \frac{\text{Gravitational Force}}{\text{Inertial Force}}$
Rossby number	$Ro = U_o / L_o \Omega_o$	$= \frac{\text{Inertial Force}}{\text{Coriolis Force}}$
Prandtl number	$Pr = \nu_o / (k_o / \rho_o C_{p_o})$	$= \frac{\text{Viscous Diffusivity}}{\text{Thermal Diffusivity}}$
Eckert number	$Ec = U_o^2 / C_{p_o} \, (\Delta \bar{T})_o$	

For exact similarity between different flows which are described by the same set of equations, each of these dimensionless parameters must be equal for both flow systems. In addition to this requirement, there must be similarity between the surface-boundary conditions.

Surface-boundary condition similarity requires equivalence of the following features:

a. Surface-roughness distributions,

b. topographic relief, and

c. surface-temperature distribution.

If all the foregoing requirements are met simultaneously, all atmospheric scales of motion ranging from micro to mesoscale could be simulated within the same flow field for a given set of boundary conditions [9]. However, all of the requirements cannot be satisfied simultaneously by existing laboratory facilities; thus, a partial or approximate simulation must be used. This limitation requires that atmospheric simulation for a particular wind-engineering application must be designed to simulate most accurately those scales of motion which are of greatest significance for the given application.

2.1.1 Partial Simulation of the Atmospheric Boundary Layer

A partial simulation is practically realizable only because the kinematics and dynamics of flow systems above a certain minimum Reynolds number are independent of the magnitude of this number [10,11]. The magnitude of the minimum Reynolds number will depend upon the geometry of the flow system being studied. Halitsky [12] reported that for concentration measurements on a cube placed in a near uniform flow field the Reynolds number required for invariance of the concentration distribution over the cube surface and downwind must exceed 11,000. Because of this invariance exact similarity of Reynolds parameter is neglected when physically modeling the atmosphere.

When the flow scale being modeled is small enough such that the turning of the mean wind directions with height is unimportant,

similarity of the Rossby number may be relaxed. For the case of dispersion of LNG or neutral plume near the ground level the Coriolis effect on the plume motion would be extremely small.

The Eckert number for air is equivalent to $0.4\ Ma^2\ (\frac{T_o}{\Delta T_o})$ where Ma is the Mach number [5]. For the wind velocities and temperature differences which occur in either the atmosphere or the laboratory flow the Eckert number is very small; thus, the effects of energy dissipation with respect to the convection of energy is negligible for both model and prototype. Eckert number equality is relaxed.

Prandtl number equality is easily obtained since it is dependent on the molecular properties of the working fluid which is air for both model and prototype.

Bulk Richardson number equality may be obtained in special laboratory facilities such as the Meteorological Wind Tunnel at Colorado State University [13].

Quite often during the modeling of a specific flow phenomenon it is sufficient to model only a portion of a boundary layer or a portion of the spectral energy distribution. This relaxation allows more flexibility in the choice of the length scale that is to be used in a model study. When this technique is employed it is common to scale the flow by any combination of the following length scales, δ, the portion of the boundary layer to be simulated; z_o, the aerodynamic roughness; Λ_i, the integral length scale of the velocity fluctuations, or λ_p, the wavelength at which the peak spectral energy is observed.

Unfortunately many of the scaling parameters and characteristic profiles are difficult to obtain in the atmosphere. They are infrequently known for many of the sites at which a model study is to

be performed. To help alleviate this problem Counihan [14] has summarized measured values of some of these different parametric descriptions for the atmospheric flow at many different sites and flow conditions.

2.2 PHYSICAL MODELING OF LNG PLUME MOTION

In addition to modeling the turbulent structure of the atmosphere in the vicinity of a test site it is necessary to scale the LNG plume source conditions properly. One approach would be to follow the methodology used in Section 2.1, i.e., writing the conservation statements for the combined flow system followed by fractional analysis to find the governing parameters. An alternative approach, the one which will be used here, is that of similitude [8]. The method of similitude obtains scaling parameters by reasoning that the mass ratios, force ratios, energy ratios, and property ratios should be equal for both model and prototype. When one considers the dynamics of gaseous LNG plume behavior the following nondimensional parameters of importance are identified [12,15,16,17].[1,2]

$$\text{Mass Ratio} = \frac{\text{mass flow of LNG plume}}{\text{effective mass flow of air}}$$

$$= \frac{\rho_s W_s A_s}{\rho_a U_a A_a} = \frac{\rho_s Q}{\rho_a U_a L^2}$$

[1] It has been assumed that the dominant transfer mechanism is that of turbulent entrainment. Thus the transfer processes of heat conduction, convection, and radiation are negligible.

[2] The scaling of plume Reynolds number is also a significant parameter. Its effects are invariant over a large range thus making it possible to scale the distribution of mean and turbulent velocities and relax exact parameter equality.

Momentum Ratio $= \dfrac{\text{inertia of LNG plume}}{\text{effective inertia of air}}$

$$= \frac{\rho_s W_s^2 A_s}{\rho_a U_a^2 A_a} = \frac{\rho_s Q^2}{\rho_a U_a^2 L^4}$$

Densimetric Froude No. (Fr) $= \dfrac{\text{effective inertia of air}}{\text{buoyancy of LNG plume}}$

$$= \frac{\rho_a U_a^2 A_a}{g(\rho_g - \rho_a)\forall_s} = \frac{U_a^2}{g\left(\frac{\rho_s - \rho_a}{\rho_a}\right)L}$$

Volume Flux Ratio $= \dfrac{\text{Volume flow of LNG plume}}{\text{effective volume flow of air}}$

$$= \frac{Q}{UL^2}$$

To obtain simultaneous simulation of these four parameters at a reduced geometric scale it is necessary to maintain equality of the plume specific gravity ratio ρ_s/ρ_a.

2.2.1 Partial Simulation of LNG Plume Motion

The restriction to an exact variation of the density ratio for the entire life of a plume is difficult to meet for LNG plumes which simultaneously vary in molecular weight and temperature. To emphasize this point more clearly, consider the mixing of two volumes of gas, one being the source gas, $\forall_s$, the other being ambient air, $\forall_a$. Consideration of the conservation of mass and energy for this system yields [16][1]:

$$\frac{\rho_g}{\rho_a} = \frac{\frac{\rho_s}{\rho_a}\forall_s + \forall_s}{\left(\frac{T_a}{T_s}\forall_s + \forall_a\right)\left(\frac{C_{p_s}M_s}{C_{p_a}M_a}\forall_s + \forall_a\right)\Big/\left(\frac{C_{p_s}M_s}{C_{p_a}M_a}\frac{T_a}{T_s}\forall_s + \forall_a\right)}$$

[1]The pertinent assumption in this derivation is that the gases are ideal and properties are constant.

If the temperature of the air, T_a, equals the temperature of the source gases, T_s, or if the product, C_pM, is equal for both source gas and air then the equation reduces to:

$$\frac{\rho_g}{\rho_a} = \frac{\frac{\rho_s}{\rho_a} V_s + V_a}{V_s + V_a} \tag{2-8}$$

Thus for two prototype cases: 1) an isothermal plume and 2) a thermal plume which is mostly composed of air, it does not matter how one models the density ratio as long as the initial density ratio value is equal for both model and prototype.

For a plume where temperature, molecular weight, and specific heat are all different from that of the ambient air, e.g., a cold natural gas plume, equality in the variation of the density ratio upon mixing must be relaxed slightly if one is to model utilizing a gas different from that of the prototype.[1] In most situations this deviation from exact similarity is small (see discussion Section 2.3.2).

Scaling of the effects of heat transfer by conduction, convection, or radiation cannot be reproduced when the model source gas and environment are isothermal. Fortunately in a large majority of industrial plumes the effects of heat transfer by conduction, convection, and radiation from the environment are small enough that the plume buoyancy essentially remains unchanged. In the specific case of a cryogenic liquid spill the influence of heat transfer on cold dense gas dispersion can be divided into two phases. First, the temperature (and hence specific gravity) of the plume at exit from a containment tank and

[1] If one were to use a gas whose temperature is different from that of the ambient air then consideration of similarity in the scaling of the energy ratios must be considered.

surrounding dike area is dependent on the thermal diffusivity of the tank-dike-spill surface materials, the volume of the tank-dike structure, the actual boiloff rate, and details of the spill surface geometry. A second plume phase involves the heat transfer from the ground surface beyond the spill area which lowers plume density.

It is tempting to try to simulate the entire transient spill phenomenon in the laboratory including spill of cryogenic fluid into the dike, heat transfer from the tank and dike materials to the cryogenic fluid, phase change of the liquid and subsequent dispersal of cold gas downwind. Unfortunately, the different scaling laws for the conduction and convection suggest that markedly different time scales occur for these various processes as the length scale changes. Since the volume of dike material storing sensible heat scales with the cube of the length scale whereas the pertinent surface area scales as the square of the length scale one perceives that heat is transferred to a model cold plume much too rapidly within the model containment structures. This effect is apparently unavoidable since a material having a thermal diffusivity low enough to compensate for this effect does not appear to exist. Calculations for the full-scale situation suggest minimal heating of a cold gas plume by the tank-dike structure thus it may suffice to cool the model tank-dike walls to reduce the heat transfer to a cold model vapor and study the resultant cold plume.

Boyle and Kneebone [18] released under equivalent conditions room temperature propane and LNG onto a water surface. The density of propane at ambient temperatures and methane at -161°C relative to air are the same. Using the modified Froude number as a model law they

concluded that the dispersion characteristics were equivalent within experimental error.

A mixture of 50% helium and 50% nitrogen pre-cooled to 115°K was released from model tank-dike systems by Meroney et al. [19], to simulate equivalent LNG spill behavior. There was no guarantee that these experiments reproduced quantitatively similar situations in the field. Rather it was expected that the gross influences of different heat transfer conditions could be determined. Since the turbulence characteristics of the flow are dominated by roughness, upstream wind profile shape, and stratification one expects the Stanton number in the field will equal that in the model, and heat transfer rates in the two cases should be in proper relation to plume entrainment rates. On the other hand, if temperature differences are such that free convection heat transfer conditions dominate, scaling inequalities may exist; nonetheless, model dispersion rates would be conservative.

Visualization experiments performed with equivalent dense isothermal and dense cold plumes revealed no apparent change in plume geometry. Concentration data followed similar trends in both situations. No significant differentiation appeared between insulated versus heat conducting ground surfaces or neutral versus stratified approach flows.

The influence of latent heat release by moisture upon the buoyancy of a plume is a function of the quantity of water vapor present in the plume and the humidity of the ambient atmosphere. Such phase change effects on plume buoyancy can be very pronounced in some prototype situations. Figure 1 displays the variation of specific gravity from a spill of liquefied natural gas in atmospheres of different humidities.

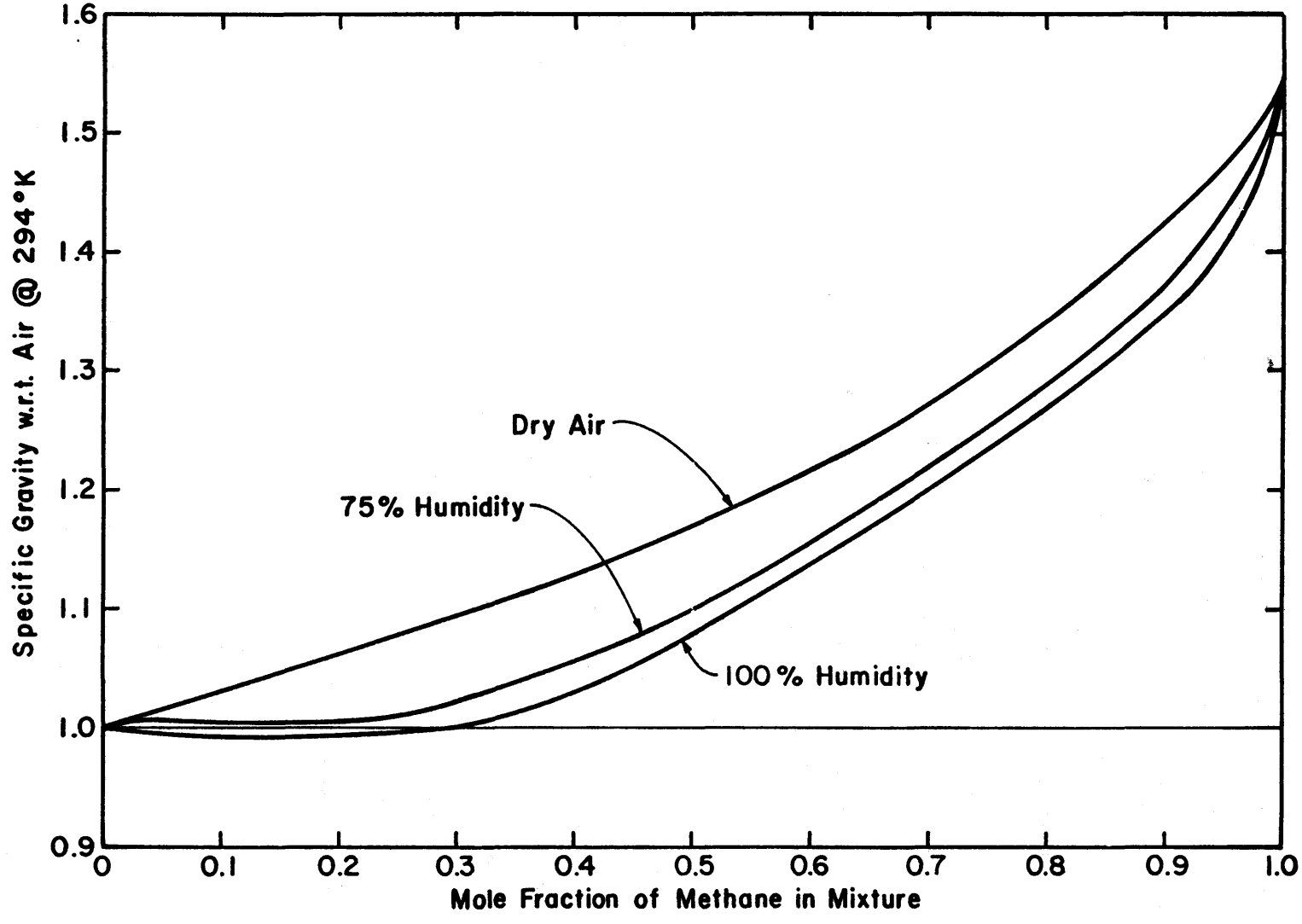

Figure 1. Specific Gravity of LNG Vapor - Humid Atmosphere Mixtures

For a LNG vapor plume humidity effects are thus shown to reduce the extent in space and time of plume buoyancy dominance on plume motion. Hence a dry adiabatic model condition should be conservative.

A reasonably complete simulation may be obtained in some situations even when a modified density ratio ρ_s/ρ_a is stipulated. The advantage of such a procedure is demonstrated most clearly by the statement of equality of Froude Numbers.

$$\left(\frac{U_a^2}{(\frac{\rho_s}{\rho_a} - 1)Lg}\right)_m = \left(\frac{U_a^2}{(\frac{\rho_s}{\rho_a} - 1)Lg}\right)_p$$

Solving this equation to find the relationship between model velocity and prototype velocity yields:

$$(U_a)_m = \left(\frac{S.G._m - 1}{S.G._p - 1}\right)^{\frac{1}{2}} \left(\frac{1}{L.S.}\right)^{\frac{1}{2}} (U_a)_p$$

where S.G. is the specific gravity, (ρ_s/ρ_a), and L.S. is the length scale, (L_p/L_m). By increasing the specific gravity of the model gas compared to that of the prototype gas, for a given length scale, one increases the reference velocity used in the model. It is difficult to generate a flow which is similar to that of the atmospheric boundary layer in a wind tunnel run at very low wind speeds. Thus the effect of modifying the model specific gravity extends the range of flow situations which can be modeled accurately. But unfortunately during such adjustment of the specific gravity of the model gases at least two of the four similarity parameters listed must be neglected. The options as to which two of these parameters to retain, if any, depends upon the physical situation being modeled. Two of the three possible options are listed below.

(1) Froude No. Equality
Momentum Ratio Equality
Mass Ratio Inequality
Velocity Ratio Inequality[1]

(2) Froude No. Equality
Momentum Ratio Inequality
Mass Ratio Inequality
Velocity Ratio Equality

Both of these schemes have been used to model plume dispersion downwind of an electric power plant complex by Isyumov [16] and Meroney [20] respectively.

The modeling of the plume Reynolds number is relaxed in all physical model studies. This parameter is thought to be of small importance since the plume character will be dominated by background atmospheric turbulence soon after its emission. But, if one was interested in plume behavior near the source, then steps should be taken to assure that the plume in the model is fully turbulent.

2.3 MODELING OF PLUME DISPERSION FOR PRESENT STUDY

In the sections above a review of the extent to which wind tunnels can model plume dispersion in the atmospheric boundary layer has been presented. In this section these arguments will be applied to the specific case of an LNG spill at the China Lake Naval Weapons Center.

2.3.1 Physical Modeling of the China Lake Atmospheric Surface Layer

In order to obtain a proper wind-tunnel scaling of the China Lake surface layer winds the approach flow characteristics must be similar. To achieve these upstream flow conditions, the wind tunnel must be modified through the introduction of surface roughness elements and

[1]When this technique is employed distortion in velocity scales or similarly volume flow rates requires that a correction be applied to the measured concentration field.

boundary layer trip devices in such a way that similarity is obtained in both the mean velocity variation with height and the characteristic length scales of turbulence. A convenient parameter which characterizes the mean velocity variation with height is z_o, the aerodynamic roughness height [10], as defined by log-linear description of velocity variation in a boundary layer. A convenient parameter which characterizes the scales of turbulent velocity fluctuations is Λ_i, the integral scale of turbulence [5].

The conditions in the wind tunnel were adjusted until both of these length scales were in the same proportion to their atmospheric equivalents (obtained from Counihan [14]) as the geometric length scale chosen for the model terrain construction. This optimal geometric length scale was chosen to be 1:240. Unfortunately the expected values of these scaling parameters as cited by Counihan [14] for sites similar to the China Lake topography were very much different than the values obtained from field instrumentation during the Burro Test Series. To compensate for these large errors due to improper length scaling, modeling tests were also performed at a length scale of 1:85. At this length scale the mean velocity variation with height scaled much more accurately.

2.3.2 Physical Modeling of the China Lake LNG Spill Plume

The buoyancy of a plume resulting from an LNG spill is a function of both the mole fraction of methane and temperature. If the plume entrains air adiabatically, then the plume would remain negatively buoyant for its entire lifetime. If the humidity of the atmosphere were high then the state of buoyancy of the plume will vary from negative to weakly positive. These conclusions are born out in Figure 1, which

illustrates the specific gravity of a mixture of methane at boiloff temperature with ambient air and water vapor.

Since the adiabatic plume assumption will yield the most conservative downwind dispersion estimates this situation was simulated. (Conservative is defined here to be highest peak concentrations furthest downwind.) Several investigators have confirmed that the Froude number is the parameter which governs plume spread rate, trajectory, plume size and entrainment during initial dense plume dilution [15,18,22,23]. The modeling of momentum is not of critical importance for a ground source released over a fairly large area. The equality of model and prototype specific gravity was relaxed so that either pure Argon gas (specific gravity at 1.38) or pure Freon-12®[1] (specific gravity of 4.18) could be used for the model source gas. The Froude number was maintained at equal values by adjusting reference wind speed.

Argon provides almost eight times the detection sensitivity for instantaneous concentration measurements as the carbon dioxide used in previous studies [19]. The variation of specific gravity with equivalent observed mole fraction of methane for these different gases is plotted in Figure 2. The use of an isothermal dense model gas such as Argon or Freon-12® in place of cold methane vapor also results in a slight distortion of the local dynamic forces acting on equivalent plume volumes as the gas mixes. Unfortunately this distortion is not conservative. The thermal capacitance properties of methane result in plumes which are more dense than the model equivalent. This results in less rapid prototype mixing. Analytical approximations based on the integral entrainment box model of Fay [23] suggest that buoyancy forces are more

[1]Registered trademark of DuPont Co.

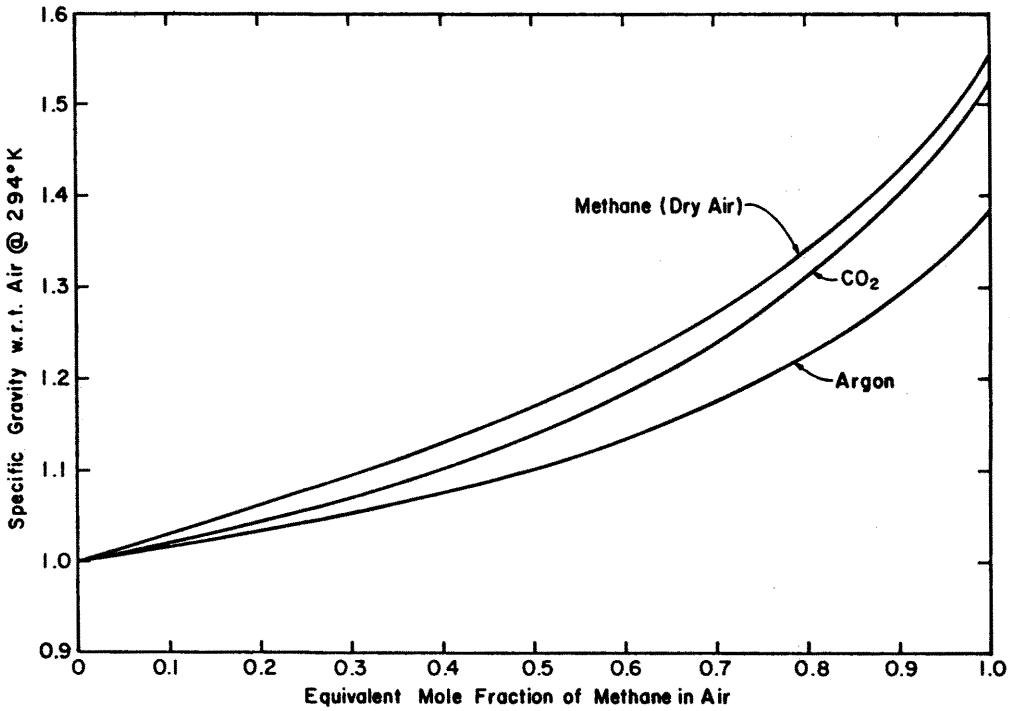

Figure 2. Specific Gravity of Gas-Air Mixtures

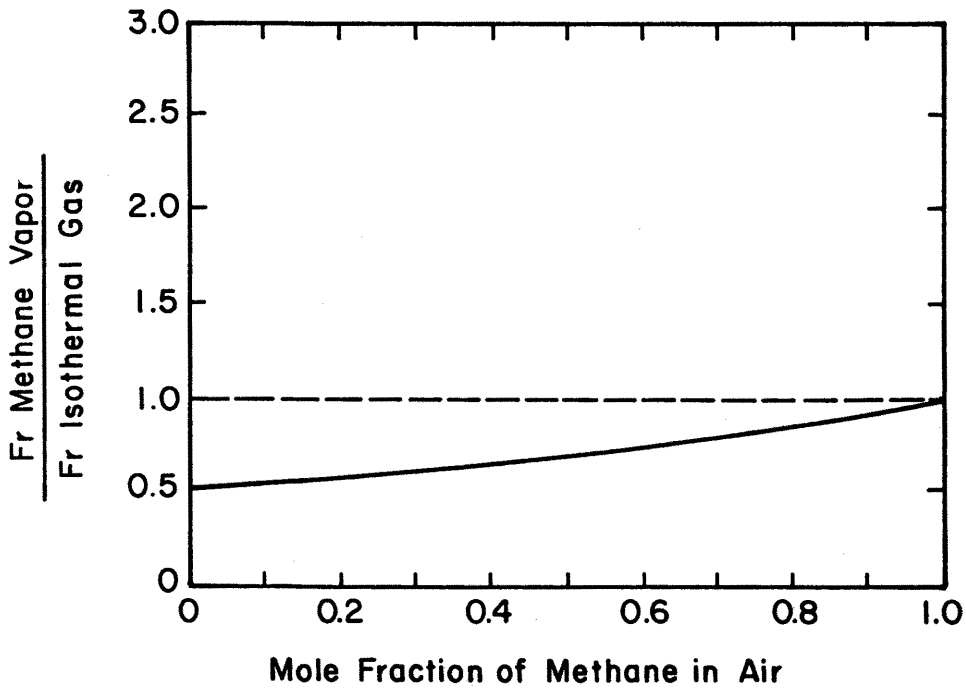

Figure 3. Variation of Isothermal Plume Behavior from Equivalent Cold Methane Plume Behavior

at equivalent time and space positions during adiabatic mixing of methane. Let $Fr = \frac{U(h)^2}{g \frac{\Delta\rho}{\rho_a} h}$ be a local Froude number, where h is local plume depth, $U(h)$ is wind speed at plume depth, h, and $\Delta\rho/\rho_a$ is a local density difference ratio. Then given a power law wind profile $U(h) \sim h^p$ one finds

$$\frac{Fr_{\text{isothermal gas}}}{Fr_{\text{LNG vapor}}} = \frac{(1+\chi S)(\beta+(1-\beta)\theta)}{(\beta(1+\chi S)+(1+S)(1-\beta)\theta)} \left[\frac{(1+\chi S+\chi(1+S)\theta}{(1-\chi\theta)(1+\chi S)} \right]^{2p} \left[\frac{R_{LNG}}{R_{iso}}\right]^{2-4p}$$

where χ = mole fraction methane vapor

R = local plume spread

$\beta = 1 - M_a/M_s \cong -0.81$

$\theta = 1 - T_s/T_a \cong 0.6$

$S = (Cp_s^*/Cp_a^* - 1) \cong 0.22$

p = velocity power law exponent $\cong 0.5$.

The variation of this Froude number ratio with equivalent mole fraction methane is plotted in Figure 3. Over most of the concentration range where buoyancy forces are dominant the variation of Froude number is reasonably simulated by the isothermal model gas. Indeed, integral-model calculations predict equal or slightly higher concentration values at equivalent times.

The actual source condition, boiloff rate per unit area over the time duration of the spill, for a spill of LNG on land is highly unpredictable. There were no data on the variable area and variable volume nature of the different LNG tests conducted at China Lake thus the source conditions were approximated by assuming a steady boiloff rate for the duration of the spill over a constant area.

Since the thermally variable prototype gas was simulated by an isothermal simulation gas, the concentration measurements observed in the model must be adjusted to equivalent concentrations that would be measured in the field. This relationship which is derived in Appendix A is:

$$\chi_p = \frac{\chi_m}{\chi_m + (1 - \chi_m)\frac{T_s}{T_a}}$$

where

χ_m = volume or mole fraction measured during the model tests,

T_s = source temperature of LNG during field conditions,

T_a = ambient air temperature during field conditions, and

χ_p = volume or mole fraction in the field.

3.0 DATA AQUISITION AND ANALYSIS

The methods used to make laboratory measurements and the techniques used to convert these measured quantities to meaningful field equivalent quantities are discussed in this section. Attention has been drawn to the limitations in the techniques in an attempt to prevent misinterpretation or misunderstanding of the results presented in the next section. Some of the methods used are conventional and need little elaboration.

3.1 WIND-TUNNEL FACILITIES

The Environmental Wind Tunnel (EWT) shown in Figure 4 was used for all tests performed. This wind tunnel, specially designed to study atmospheric flow phenomena, incorporates special features such as adjustable ceiling, rotating turntables, transparent boundary walls, and a long test section to permit reproduction of micrometeorological behavior at smaller length scales. Mean wind speeds of 0.10 to 12 m/s can be obtained in the EWT. A boundary layer depth of 1 m thickness at 6 m downstream of the test entrance can be obtained with the use of the vortex generators at the test section entrance and surface roughness on the floor. The flexible test section roof on the EWT is adjustable in height to permit the longitudinal pressure gradient to be set to zero. The vortex generators at the tunnel entrance were followed by 10 m of smooth floor, and a 3 m approach ramp to either the 1:240 or the 1:85 scaled topography of the China Lake site.

3.2 MODEL

Based on atmospheric data over sites similar to that of the China Lake site it was decided that the best reproduction of the surface wind characteristics would be at a model scale of 1:240. The topography of the China Lake terrain for this model scale was simulated by the

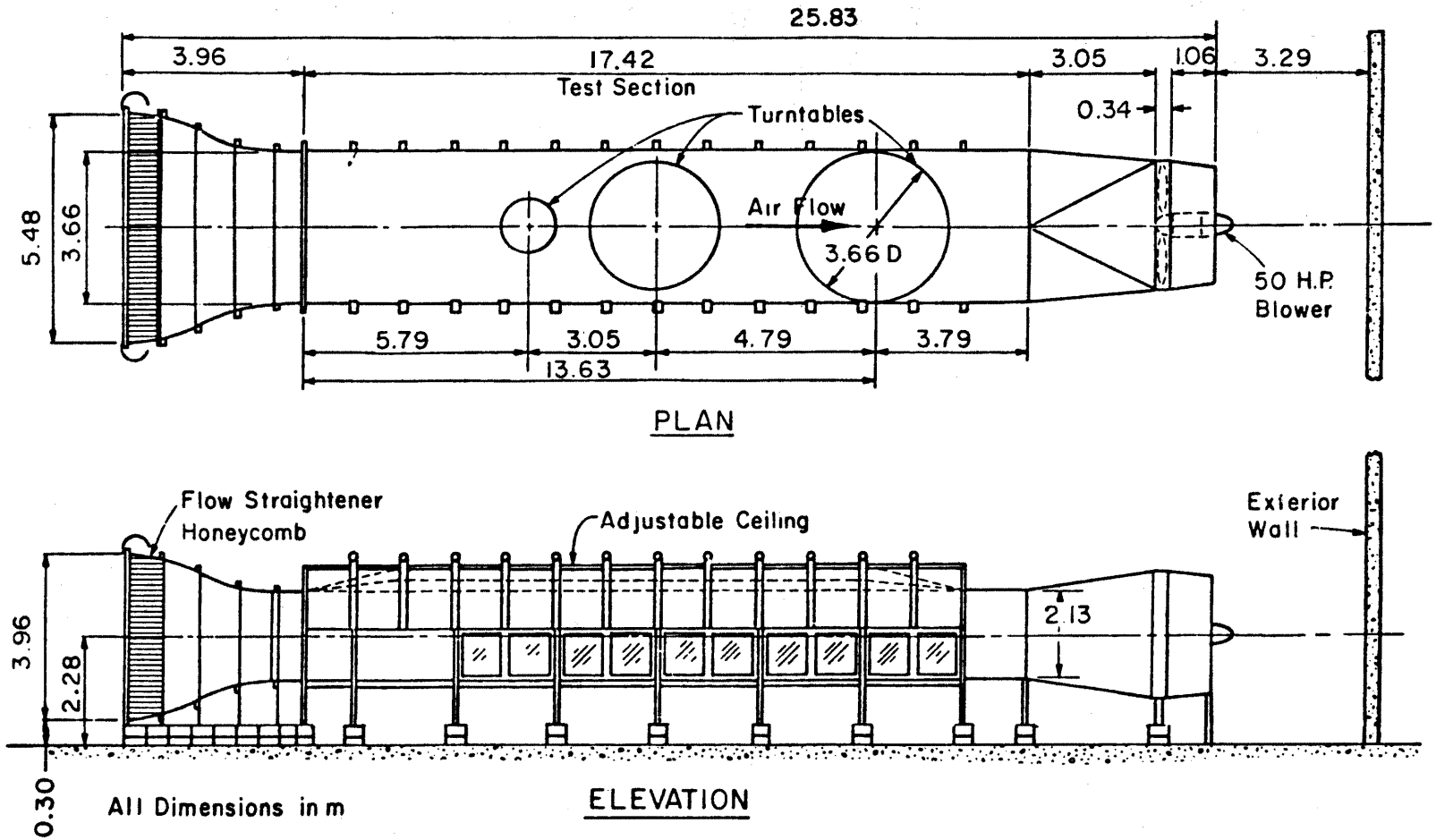

Figure 4. Environmental Wind Tunnel

construction of a layered model, each layer (1.3 mm tack board) was representative of a one-foot elevation change at the site. A hole was cut in the center of the spill pool to accommodate the appropriate size area source, and buildings and roads were placed on the model for reference points. Figure 5 is a photograph of this topographic model. Later after the acquisition of actual surface wind data at the China site during the Burro Test Series it was observed that a model scale of 1:85 provided a more accurate representation of the China Lake surface winds. Fortunately an old model of China Lake topography at a scale of 1:85 from a previous study [24] was still on hand. This model was constructed of 0.64 cm thick styrofoam sheets thus each layer was representative of 0.54 m elevation change. The model was modified to include most recent terrain and structure changes. For both model scales the source gas stored in a pressurized cylinder was directed through a solenoid valve, a flowmeter, and into the circular area source mounted in the model pond area.

3.3 FLOW VISUALIZATION TECHNIQUES

Smoke was used to define plume behavior over the China Lake site. The smoke was produced by passing the simulation gas through a container of titanium tetrachloride located outside the wind tunnel. The plume was illuminated with arc-lamp beams. A visible record was obtained by means of pictures taken with a Speed Graphic camera utilizing Polaroid film for immediate examination. Additional color slides were obtained with a 35 mm camera.

3.4 WIND PROFILE AND TURBULENCE MEASUREMENTS

Velocity profile measurements, reference wind speed conditions, and turbulence measurements were obtained with a Thermo-Systems Inc. (TSI)

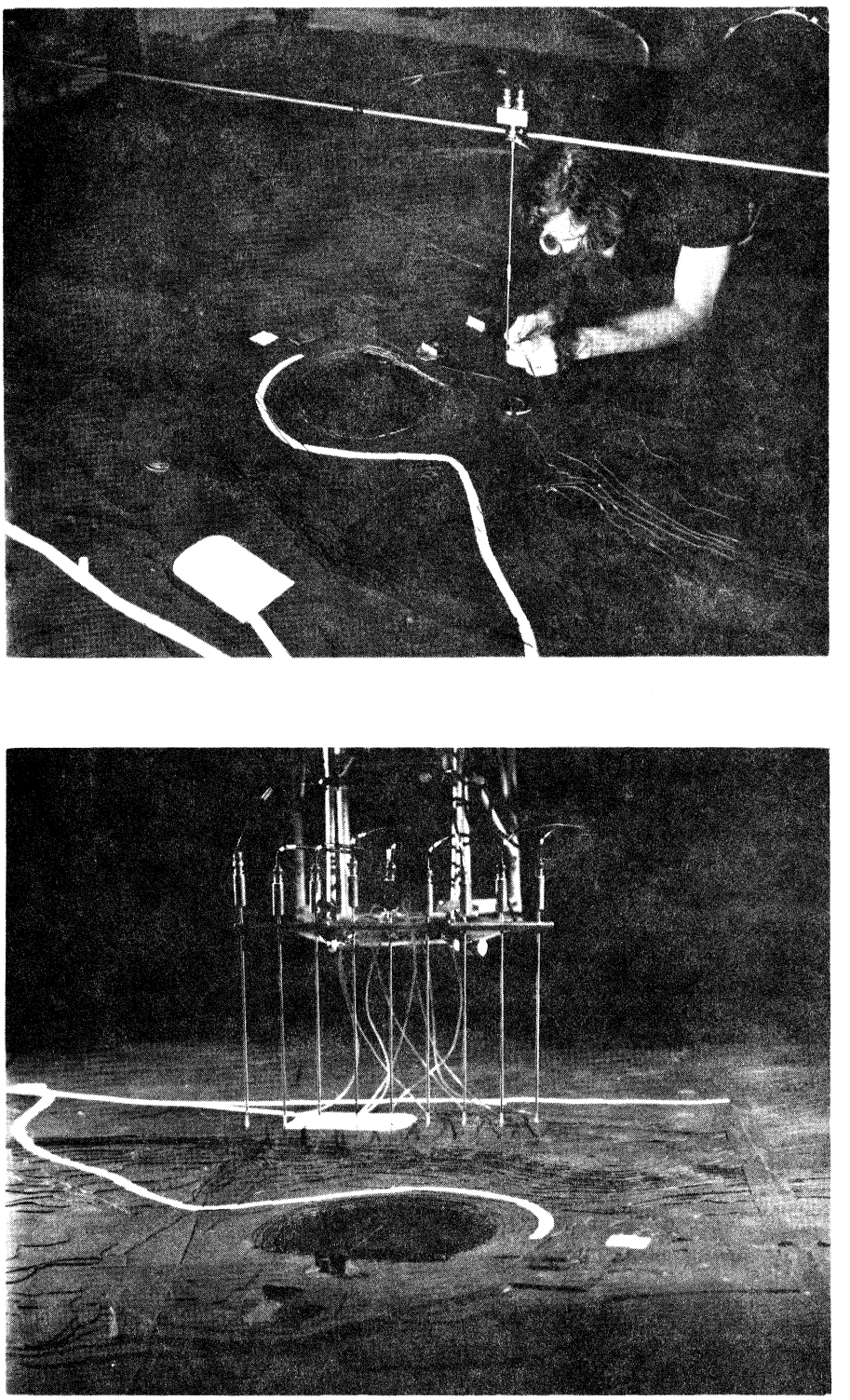

Figure 5. China Lake Naval Weapons Center Spill Site Model Scale 1:240

1050 anemometer and a TSI model 1210 hot-film probe. Since the voltage response of these anemometers is nonlinear with respect to velocity, a multi-point calibration of system response versus velocity was utilized for data reduction.

The velocity standard utilized in the present study was that depicted in Figure 6. This consisted of a Matheson model 8116-0154 mass flowmeter, a Yellowsprings thermistor, and a profile conditioning section constructed by the Colorado State University shop. The mass flowmeter measures mass flow rate independent of temperature and pressure, the thermistor measures the temperature at the exit conditions, and the profile conditioning section forms a flat velocity profile of very low turbulence at the position where the probe is to be located. Incorporating a measurement of the ambient atmospheric pressure and a profile correction factor permits the calibration of velocity at the measurement station from 0.1-2.0 m/s ±5.0 cm/s or ±10 percent whichever is smaller.

During calibration of the single film anemometer, the anemometer voltage response values over the velocity range of interest were fit to an expression similar to that of King's law [25] but with a variable exponent. The accuracy of this technique is approximately ±2 percent of the actual longitudinal velocity.

The velocity sensors were mounted on a vertical traverse and positioned over the measurement location on the model. The anemometer responses were fed to a Preston analog-to-digital converter and then directly to a HP-1000 minicomputer for immediate interpretation. The HP-1000 computer also controls probe position. A flow chart depicting the control sequence for this process is presented in Figure 7.

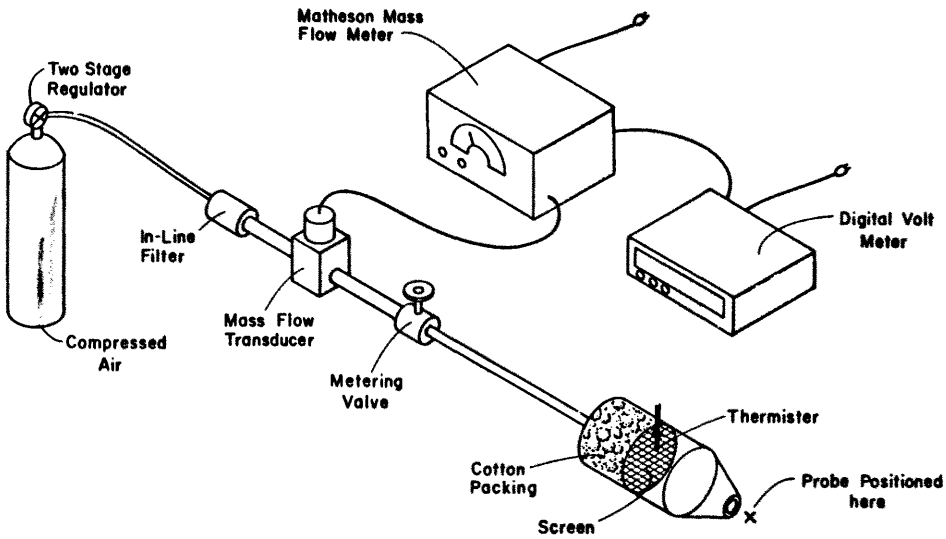

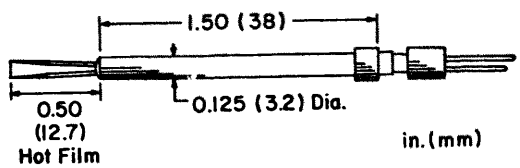

TSI Single Film Sensor

Figure 6. Velocity Probes and Velocity Standard

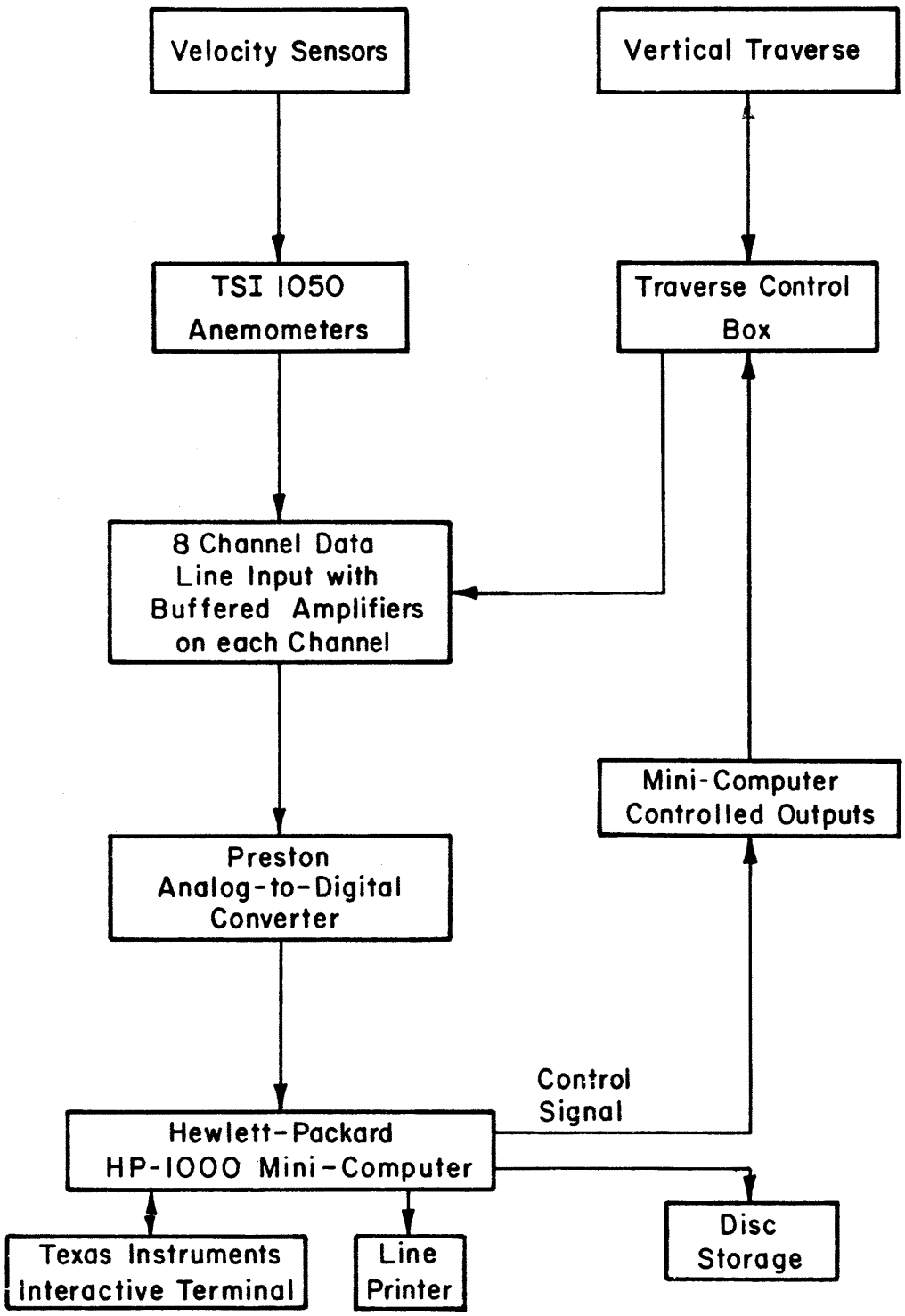

Figure 7. Velocity Data Reduction Flow Chart

3.5 CONCENTRATION MEASUREMENTS

To obtain the concentration time histories at points downwind of the spill site a rack of eight hot-wire aspirating probes was designed and constructed. A layout of this design is presented in Figure 8. The films on these probes were replaced with 0.005 in. platinum wire to improve signal-to-noise characteristics. These eight instantaneous concentration sensors were connected to an eight-channel TSI hot-wire anemometer system. The output voltages from the TSI unit are conditioned for input to the analog-to-digital converter by a DC-supression circuit, a passive low-pass filter circuit tuned to 100 Hz, and an operational amplifier of times five gain. A schedule of this process is shown in Figure 9.

3.5.1 Hot-Wire Aspirating Probe

The basic principles governing the behavior of aspirating hot-wire probes have been discussed by Blackshear and Fingerson [26], Brown and Rebollo [27], and Kuretsky [28]. A vacuum source sufficient to choke the flow through the small orifice just downwind of the sensing element was applied. This wire was operated in a constant temperature mode at a temperature above that of the ambient air temperature. A feedback amplifier maintained a constant overheat resistance through adjustment of the heating current. A change in output voltage from this sensor circuit corresponds to a change in heat transfer between the hot wire and the sampling environment.

The heat transfer rate from a hot wire to a gas flowing over it depends primarily upon the wire diameter, the temperature difference between the wire and the gas, the thermal conductivity and viscosity of the gas, and the gas velocity. For a wire in an aspirated probe with a

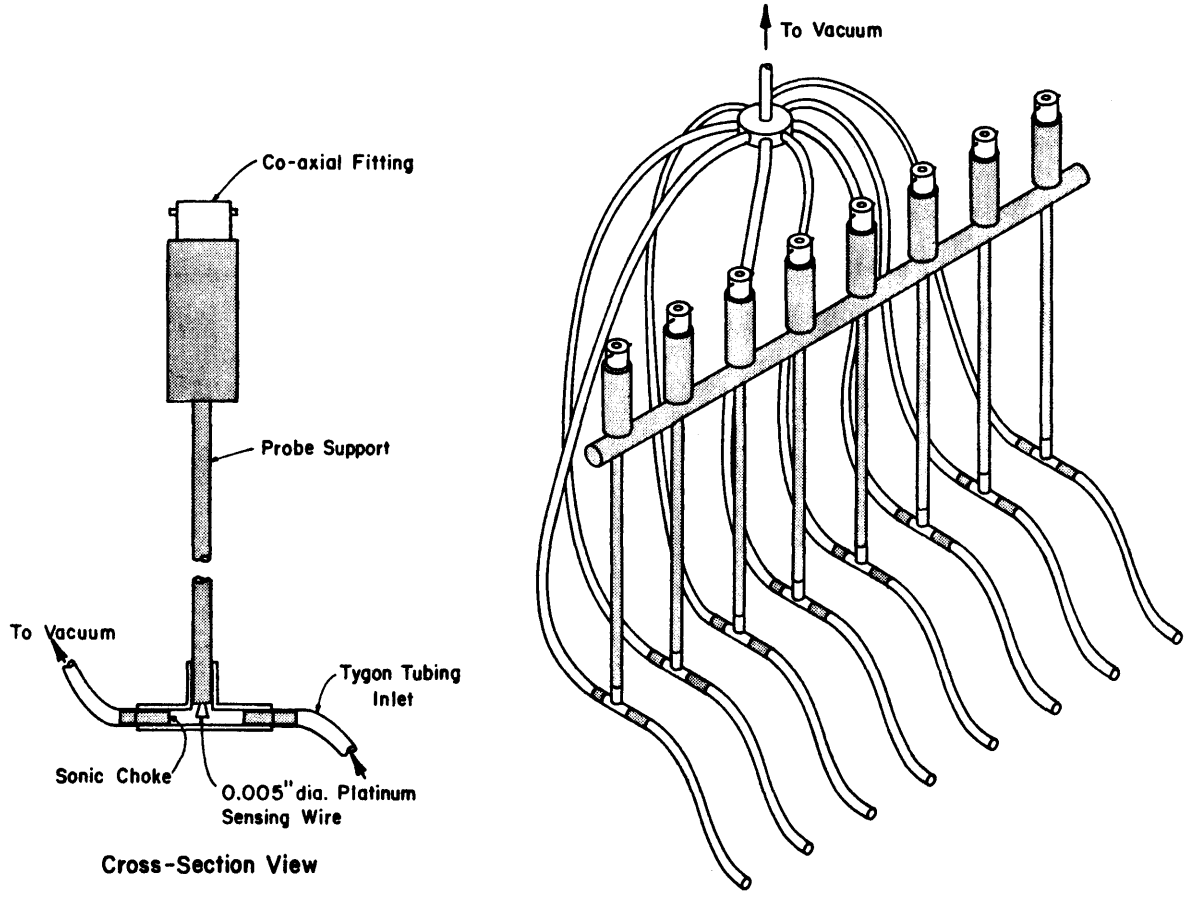

Figure 8. Hot-wire Katharometer Probes

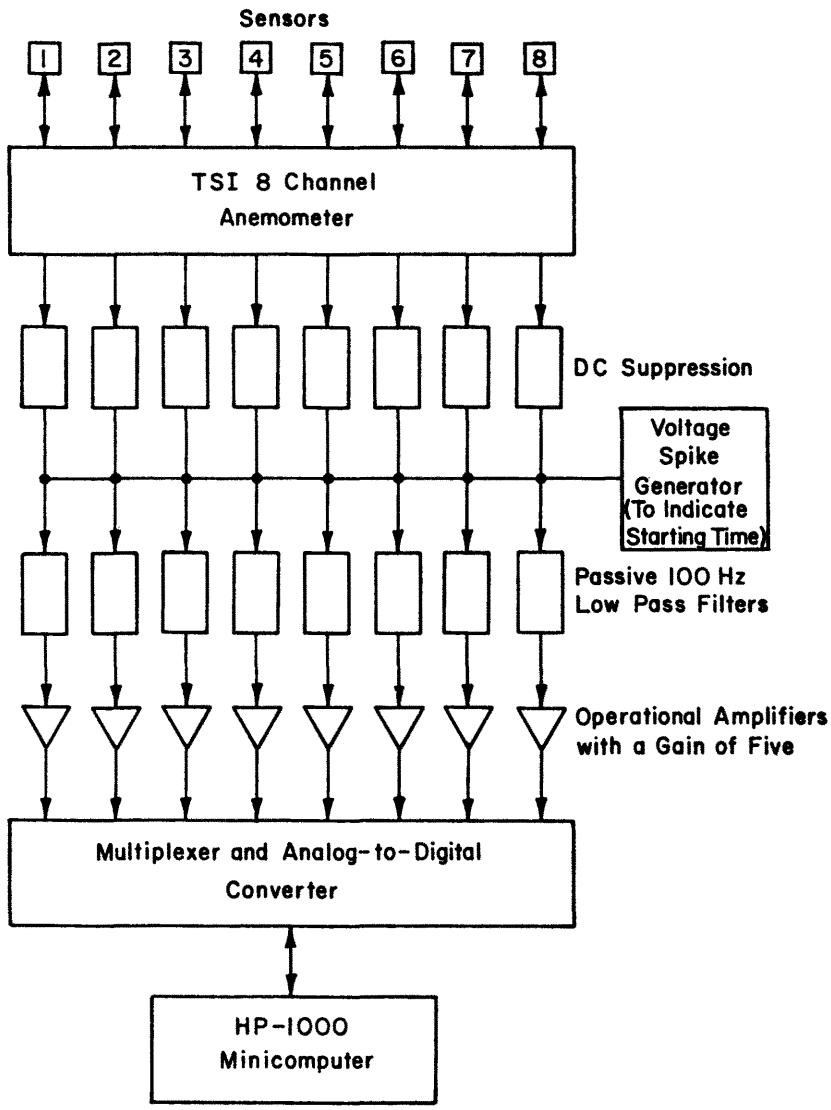

Figure 9. Block Diagram Katharometer Array

sonic throat, the gas velocity can be expressed as a function of the ratio of the probe cross-sectional area at the wire position to the area at the throat, the specific heat ratio, and the speed of sound in the gas. The latter two parameters, as well as the thermal conductivity and viscosity of the gas mentioned earlier, are determined by the gas composition and temperature. Hence, for a fixed probe geometry and wire temperature, the heat transfer rate, or the related voltage drop across the wire is a function of only the gas composition and temperature. Since all tests performed in this study were in an isothermal flow situation the wire response was only a function of gas composition.

During probe calibration known compositions of either Argon-air or Freon 12-air mixtures were passed through a pre-heat exchanger to condition the gas to the tunnel temperature environment. These known compositions for the Argon-air calibration systems were drawn from bottles of prepared gas composition provided by Matheson Laboratories. For the Freon 12-air calibration system known compositions were produced from pure Freon 12 and pure air being passed through a Matheson gas proportioner. An overheat ratio (temperature of wire/ambient temperature) of 1.65 was used to maximize signal response while maintaining acceptable noise and signal drifting levels.

3.5.2 Errors in Concentration Measurement

The effective sampling area of the probe inlet is a function of the probe aspiration rate and the distribution of approach velocities of the gases to be sampled. A calculation of the effective sampling area during all tests suggests that the effective sampling area was approximately 0.5 cm^2. Thus the resolution of the concentration measurements as applied to the China Lake site is 2.9 m^2 or 0.36 m^2 for the 1:240 and 1:85 scaled models respectively.

The travel time from the sensor to the sonic choke limits the upper frequency response of the probe. At high frequencies the correlation between concentration fluctuation and velocity fluctuations (velocity fluctuations are a result of the changes of sonic velocity with concentration) at the sensor begin to decline. The CSU aspirated probe is expected to have a 1000 Hz upper frequency response, but, to improve signal-to-noise characteristics, the signal was filtered at 100 Hz. This is well above the frequencies of concentration fluctuations that were expected to occur.

The accumulative error, due to the combined effect of calibration uncertainties and nonlinear voltage drifting during the testing time, is estimated to be approximately ±20 percent of component value in the range of 5-15 percent equivalent methane concentrations.

4.0 TEST PROGRAM RESULTS

Five different field tests, Burros 4, 5, 7, 8, and 9, were simulated. Burro 8 was modeled by three different methodologies, two being at a model length scale factor of 1:240 but different source gas specific gravities and one at a scale factor of 1:85. Burro 9 was modeled by two different methods, one at a model scale factor of 1:240, the other at a scale factor of 1:85. Burros 4, 5, and 7 were each modeled by one test only at a scale factor of 1:240.

Table 1 summarizes the pertinent field test conditions for the five tests simulated. The following equations were used to convert field values to model values,

$$L_m = \frac{1}{L.S.} L_p \ ,$$

$$U_m = \left(\frac{S.G._m - 1}{S.G._p - 1}\right)^{1/2} \left(\frac{L_m}{L_p}\right)^{1/2} U_p \ ,$$

$$Q_m = \left(\frac{S.G._m - 1}{S.G._p - 1}\right)^{1/2} \left(\frac{L_m}{L_p}\right)^{5/2} Q_p \ ,$$

$$t_m = \left(\frac{S.G._p - 1}{S.G._m - 1}\right)^{1/2} \left(\frac{L_m}{L_p}\right)^{1/2} t_p \ ,$$

where L is length, U is wind speed, Q is plume flow rate at the source, t is time, L.S. is length scale factor, and S.G. is the plume specific gravity at the source. The subscripts m and p indicate model and prototype (field) conditions respectively.

Table 2 summarizes the pertinent model test conditions for all eight runs performed. Table 3 and Figures 10-1 to 10-8 show a comparison between the different field tests wind data and the simulated model tests wind data. It is seen from these that the wind shear

Table 1. Field Test Conditions

	Burro-4	Burro-5	Burro-7	Burro-8	Burro-9
Spill Quantity (m^3 liquid)	35.3	35.8	39.4	28.4	24.2
Spill Rate (m^3/min liquid)	12.1	11.6	14.7	16.0	18.4
Time Duration of Spill (s)	175	185	161	107	79
Time to Equilibrium Boiloff (s)	33	32	35	36	38
Time to Pool Breakup (s)	190	200	177	123	97
Time to Complete Evaporation (s)	205	215	192	138	112
Equilibrium Boiloff Rate (m^3/s gas at 111°K)	46.0	44.1	55.8	60.8	69.9
Equilibrium Pool Radius (m)	12.3	12.0	13.5	14.1	15.1
Mean Wind Speed (Upwind)					
(m/s at 1 m height)	9.3	7.3	8.6	1.9	5.3
(m/s at 2 m height)	9.6	7.8	8.8	2.0	6.1
(m/s at 3 m height)	10.2	8.3	9.5	2.1	6.3
(m/s at 8 m height)	10.8	9.2	10.	2.6	6.8
Mean Local Longitudinal Turbulent Intensity (% at 2 m height)	11	17	14	9	13
Mean Wind Direction (Degrees from North at 2 m height)	218	218	208	235	232
Standard Deviation of Wind Direction (Degrees at 2 m height)	7.3	11.1	5.2	5.6	4.4
Temperature (°C at 2 m height)	35	40	34	33	35
Average Lapse Rate (°C/100 m)	6	8	3	-1.6	2
Richardson Number at 2 m height	-0.085	-0.13	-0.027	0.141	-0.023
*Roughness Length, z_o (m)	$4x10^{-5}$	$4x10^{-5}$	$4x10^{-5}$	$4x10^{-5}$	$4x10^{-5}$
*Friction Velocity, u_* (m/s)	0.34	0.29	0.32	0.06	0.21
Flux Froude Number at 3 m height and Equilibrium Conditions+	105.2	57.7	76.9	0.8	20.1

+$Fr = \frac{U^3 D}{(\frac{\rho_s - \rho_a}{\rho_a})gQ}$

*Values supplied by Lawrence Livermore Laboratory

Table 2. Model Test Conditions

	RUN NO. 1	RUN NO. 2	RUN NO. 3	RUN NO. 4	RUN NO. 5	RUN NO. 7	RUN NO. 8	RUN NO. 9
Field Run Number	Burro-8	Burro-9	Burro-8	Burro-4	Burro-5	Burro-7	Burro-8	Burro-9
Model Scale	1:240	1:85	1:85	1:240	1:240	1:240	1:240	1:240
Plume Specific Gravity, $\frac{\rho_s}{\rho_a}$	4.18	1:38	1:38	1:38	1:38	1:38	1:38	1:38
Plume Release Rate, Q (ccs)	164	874	760	44	42	53	58	66
Time Duration of Release, Δt (s)	2.9	10.3	13.9	13.5	14.2	12.4	8.2	6.1
Source Diameter, D (cm)	11.7	35.6	33.0	10.2	10.0	11.2	11.7	12.6
Mean Wind Speed, U	32 @ 1.25 cm	57 @ 3.6 cm	18 @ 3.6 cm	55 @ 1.25 cm	45 @ 1.25 cm	51 @ 1.25 cm	11 @ 1.25 cm	34 @ 1.25 cm
Mean Wind Direction (Degrees from North)	215	232	215	218	218	208	215	232
Stability	neutral	neutral	neutral	neutral	neutral	neutral	neutral	neutral
Roughness Length, Z_o (cm)	0.01	0.01	0.01	0.01	0.01	0.01	0.01	0.01
Friction Velocity, U_*	2.65	3.87	1.22	4.56	3.73	4.23	0.91	2.82
Flux Froude Number, Fr+	0.7 @ 1.25 cm	20.0 @ 3.6 cm	0.7 @ 3.6 cm	103.5 @ 1.25 cm	58.2 @ 1.25 cm	75.2 @ 1.25 cm	0.7 @ 1.25 cm	20.2 @ 1.25 cm

$$^{+}Fr = \frac{U^3 D}{(\frac{\rho_s - \rho_a}{\rho_a})gQ}$$

Table 3. Wind Field Comparisons

	Mean Wind Speed				Local Turbulent Intensity (% @ 2m)	Roughness[+] Length, z_o (m)	Friction Velocity, u_* (m/s)		Eulerian Integral Length Scale (m)
	(m/s @ 1m)	(m/s @ 2m)	(m/s @3m)	(m/s @8m)					
Run No. 1	0.9	1.7	2.1	2.5	30	9.1×10^{-2}	0.21		50
Burro 8	1.9	2.0	2.1	2.6	9	5.0×10^{-3}	0.14	.06	
Run No. 2	5.6	5.8	6.3	6.7	13	3.9×10^{-4}	0.28		14.5
Burro 9	5.3	6.1	6.3	6.8	13	4.0×10^{-4}	0.28	.21	
Run No. 3	1.9	1.9	2.1	2.1	20	3.0×10^{-4}	0.09		19.8
Burro 8	1.9	2.0	2.1	2.6	9	5.0×10^{-3}	0.14	.06	
Run No. 4	6.6	8.0	10.2	12.1	26	4.7×10^{-2}	0.92		27.5
Burro 4	9.3	9.6	10.2	10.8	11	4.5×10^{-6}	0.30	.34	
Run No. 5	4.8	6.5	8.4	10.0	27	6.7×10^{-2}	0.80		21.9
Burro 5	7.3	7.8	8.3	9.2	17	4.1×10^{-4}	0.37	.29	
Run No. 7	5.4	7.3	9.5	11.3	11	6.7×10^{-2}	0.91		21.9
Burro 7	8.6	8.8	9.5	10	14	6.5×10^{-6}	0.29	.32	
Run No. 8	0.7	1.5	2.1	2.8	36	1.2×10^{-1}	0.24		33.6
Burro 8	1.9	2.0	2.1	2.6	9	5.0×10^{-3}	0.14	.06	
Run No. 9	2.7	4.7	6.0	7.2	30	9.1×10^{-2}	0.61		50
Burro 9	5.3	6.1	6.3	6.8	13	4.0×10^{-4}	0.28	.21	

[+]These values of z_o and u_* were obtained by CSU during a reanalysis of field data by a least squares fit to the velocity data at the heights of 1, 2, 3, and 8 meters only.

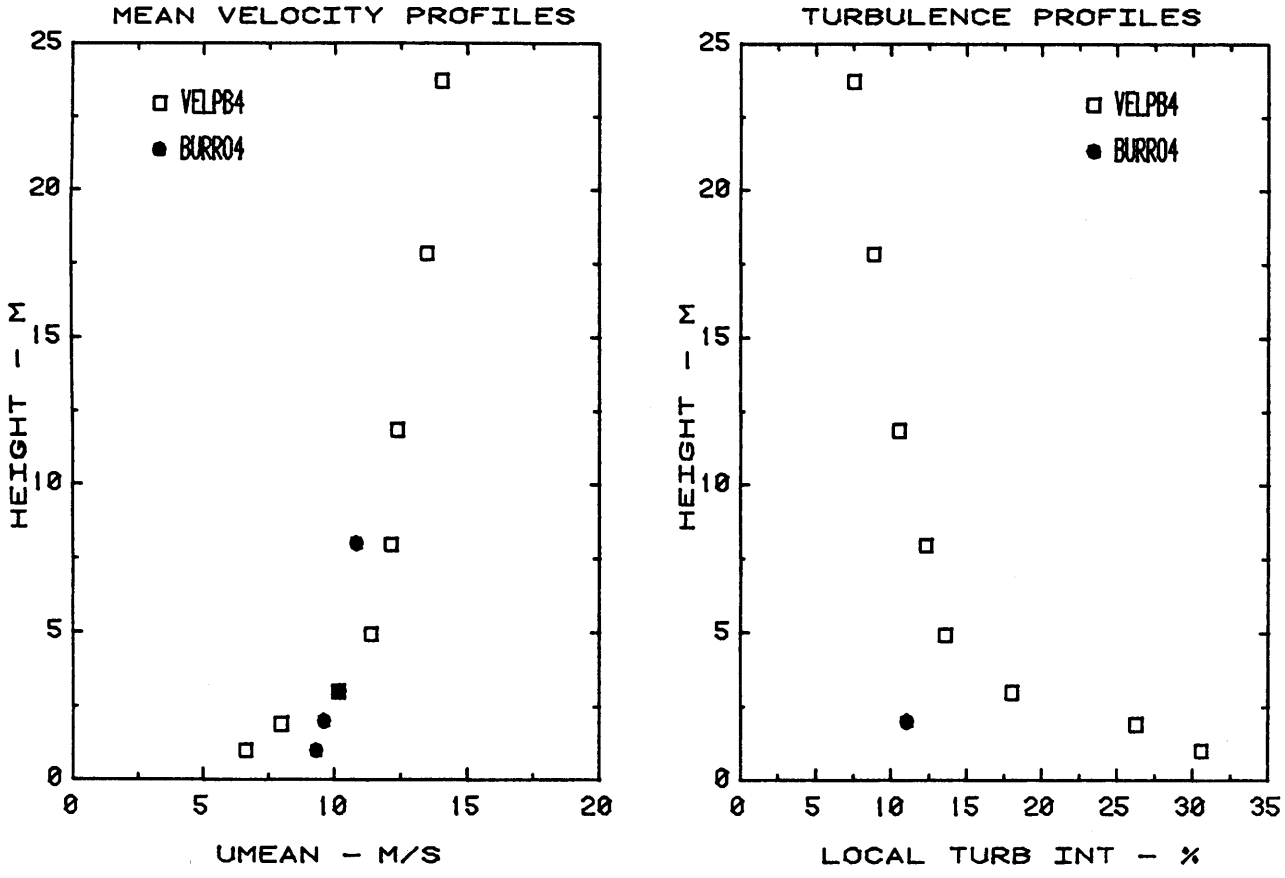

Figure 10-1. Velocity Field Comparison for Run 4 Simulation of Burro 4

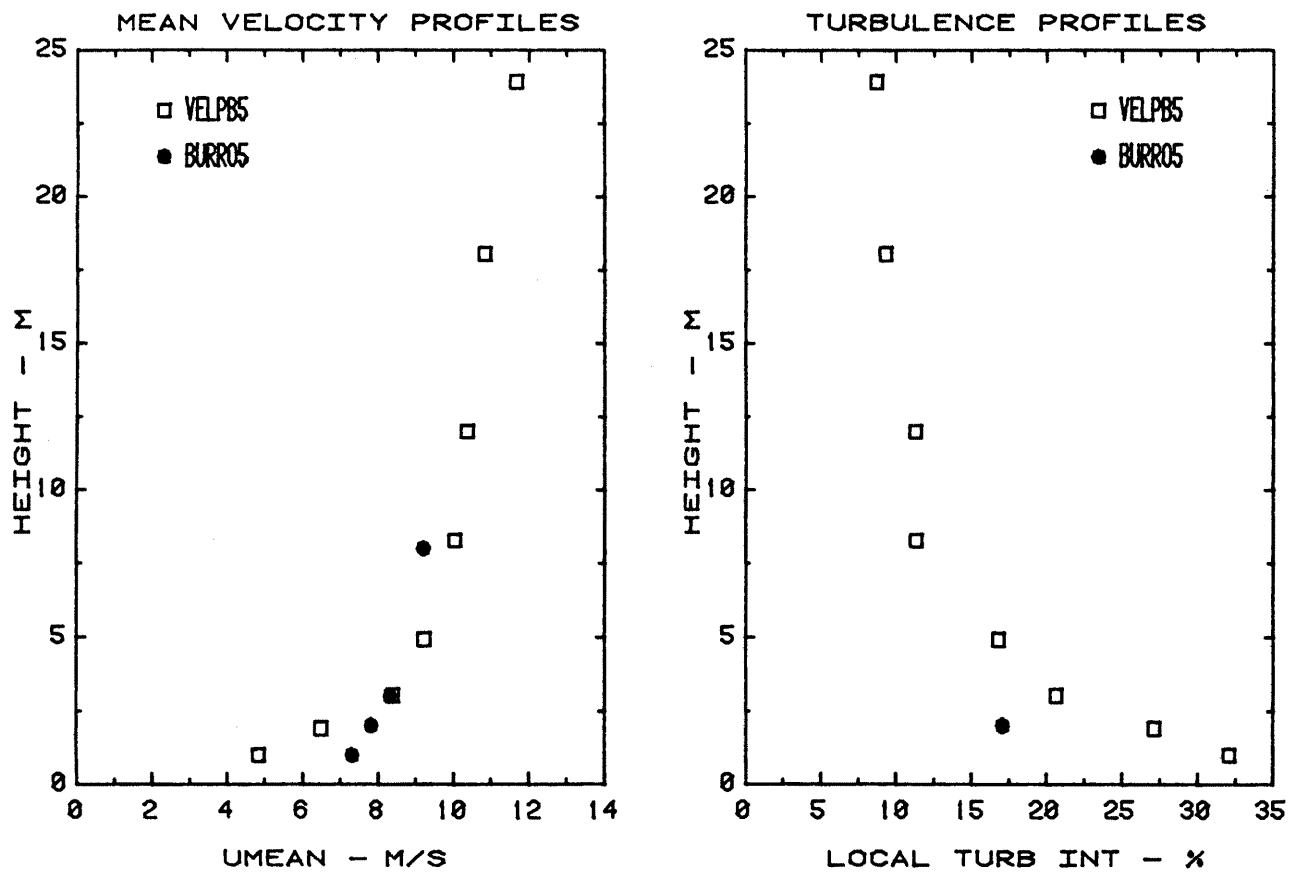

Figure 10-2. Velocity Field Comparison for Run 5 Simulation of Burro 5

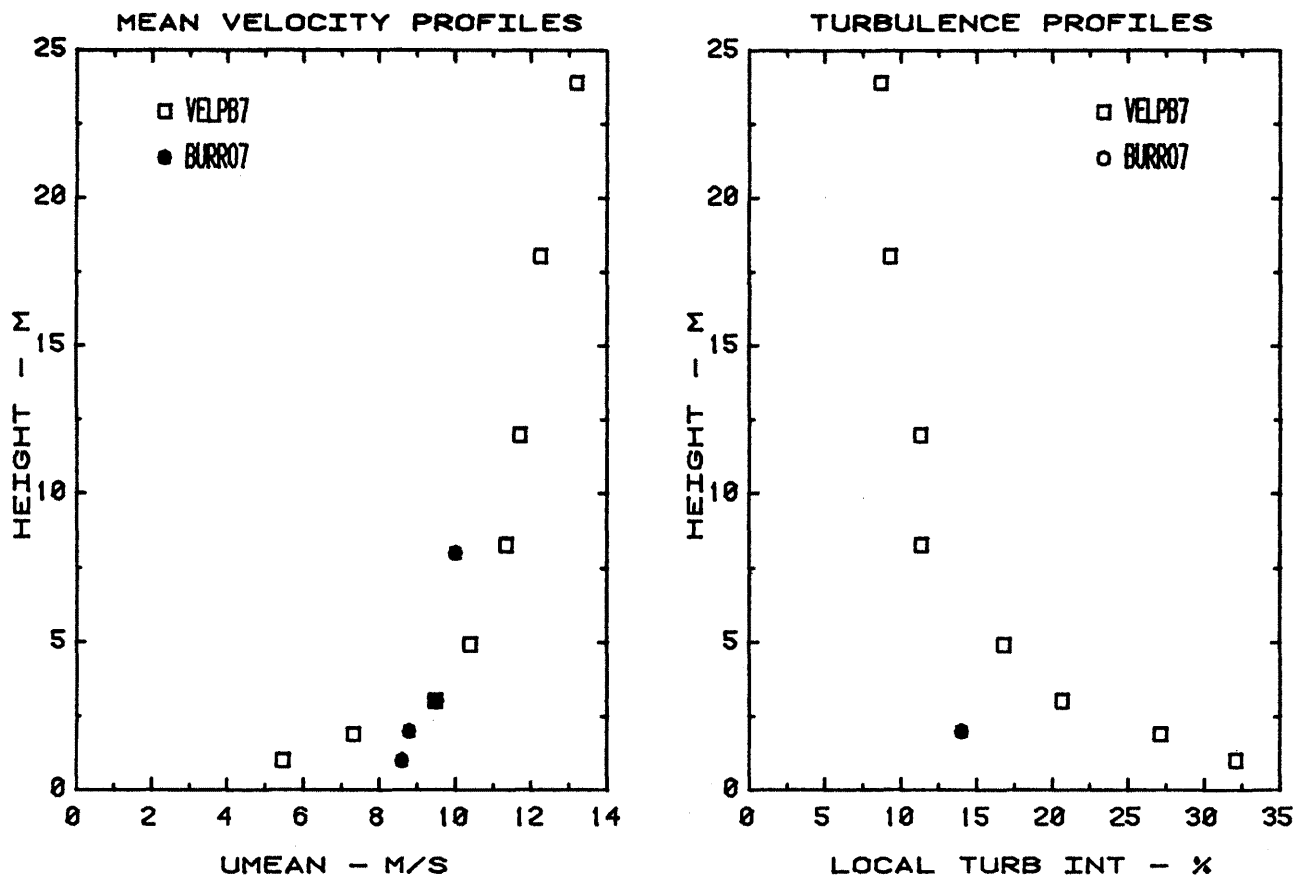

Figure 10-3. Velocity Field Comparison for Run 7 Simulation of Burro 7

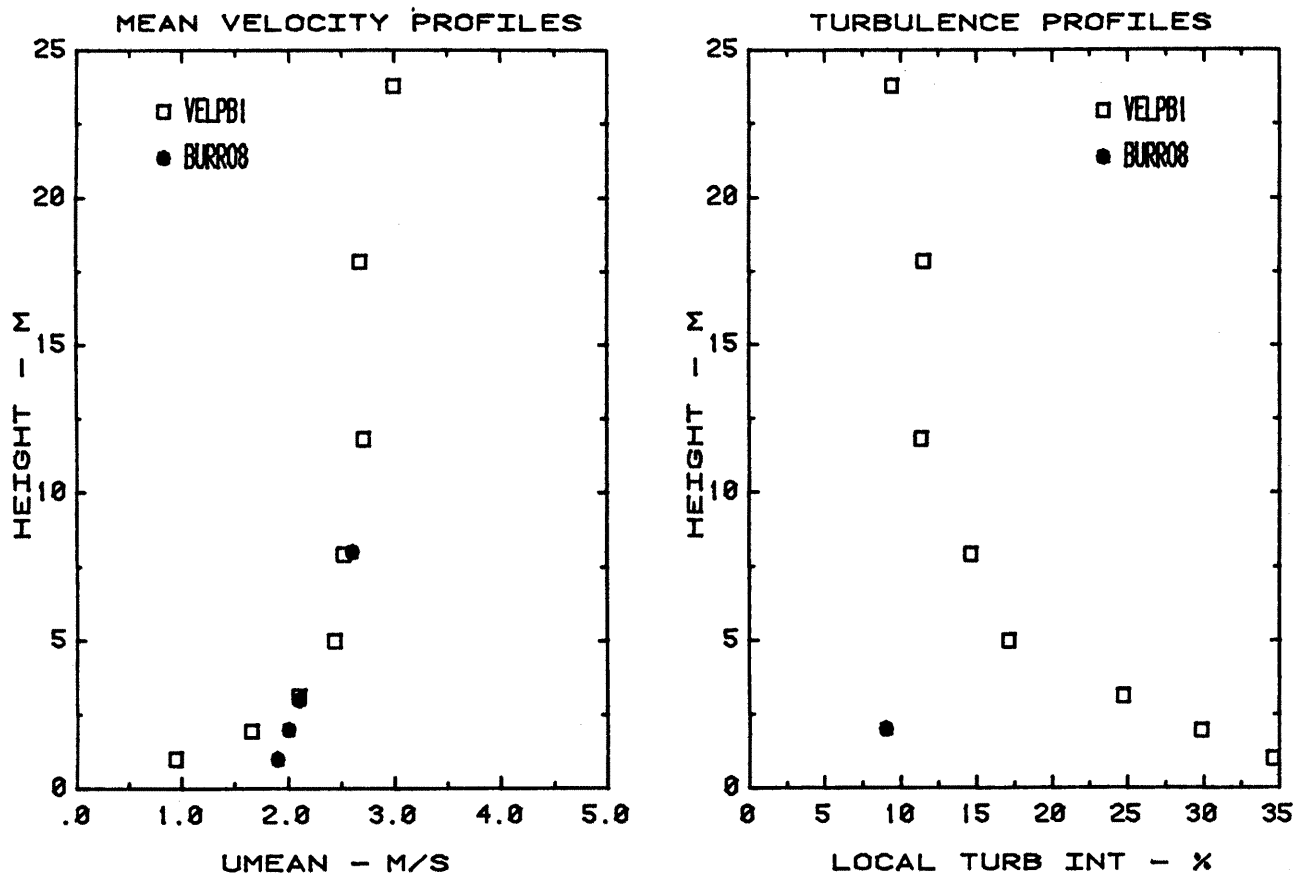

Figure 10-4. Velocity Field Comparison for Run 1 Simulation of Burro 8

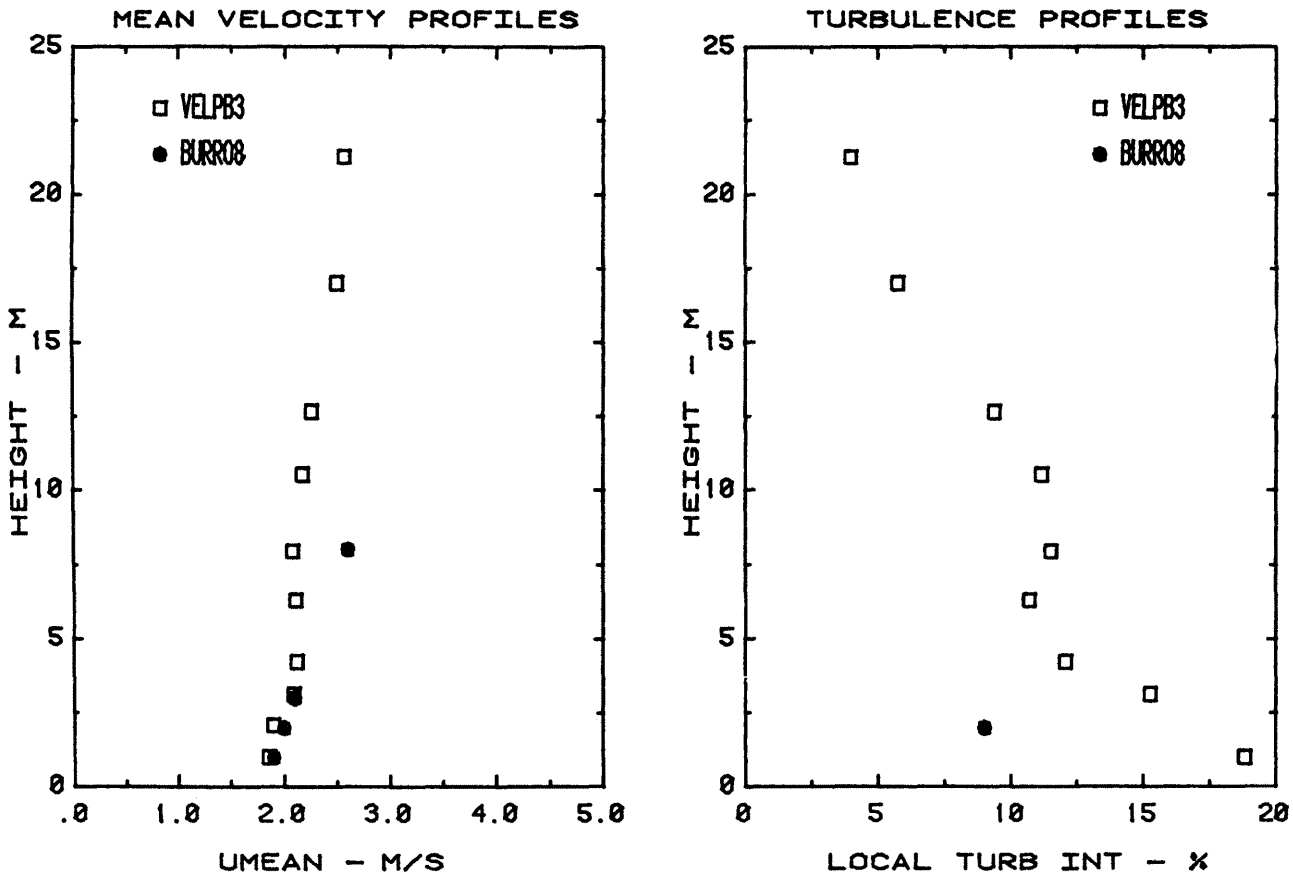

Figure 10-5. Velocity Field Comparison for Run 3 Simulation of Burro 8

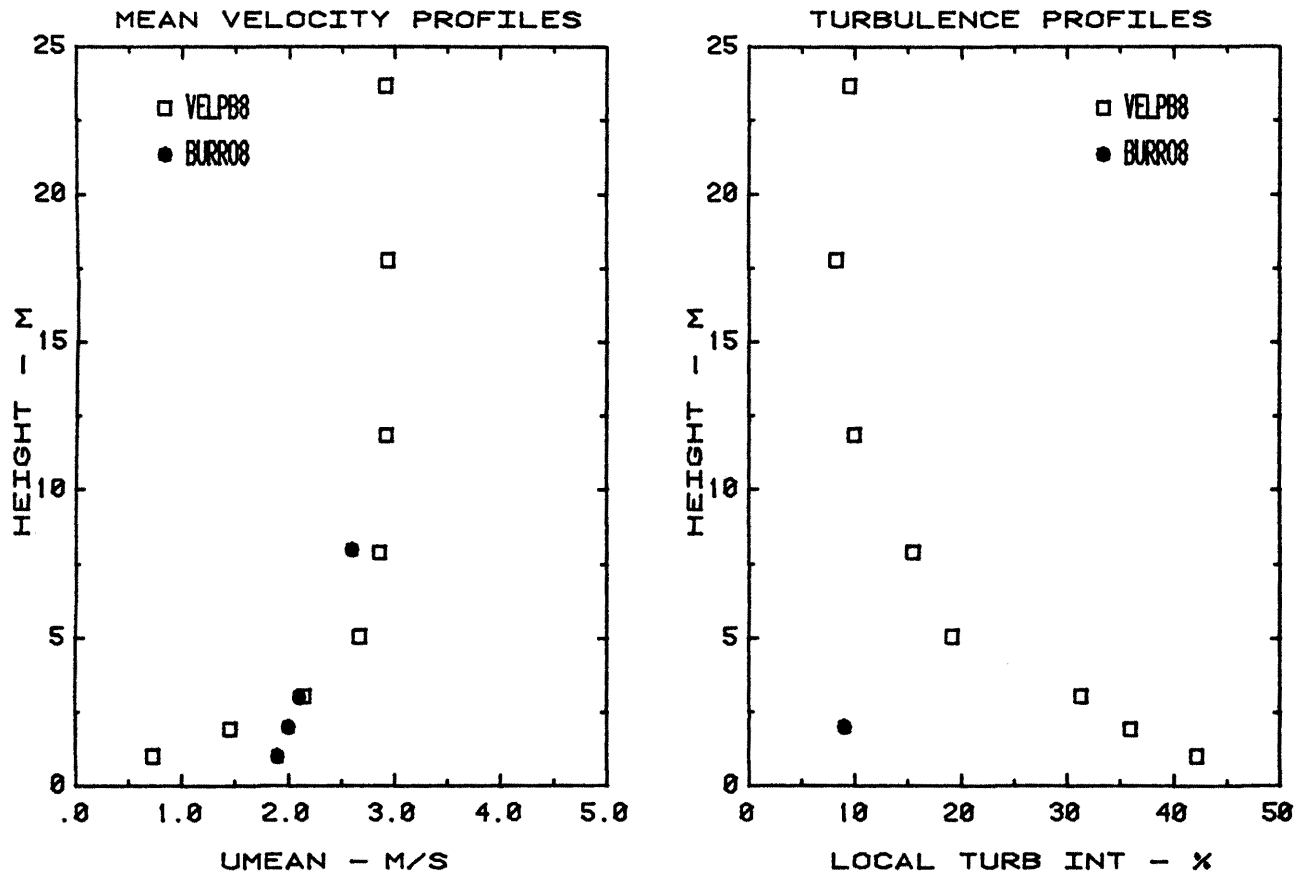

Figure 10-6. Velocity Field Comparison for Run 8 Simulation of Burro 8

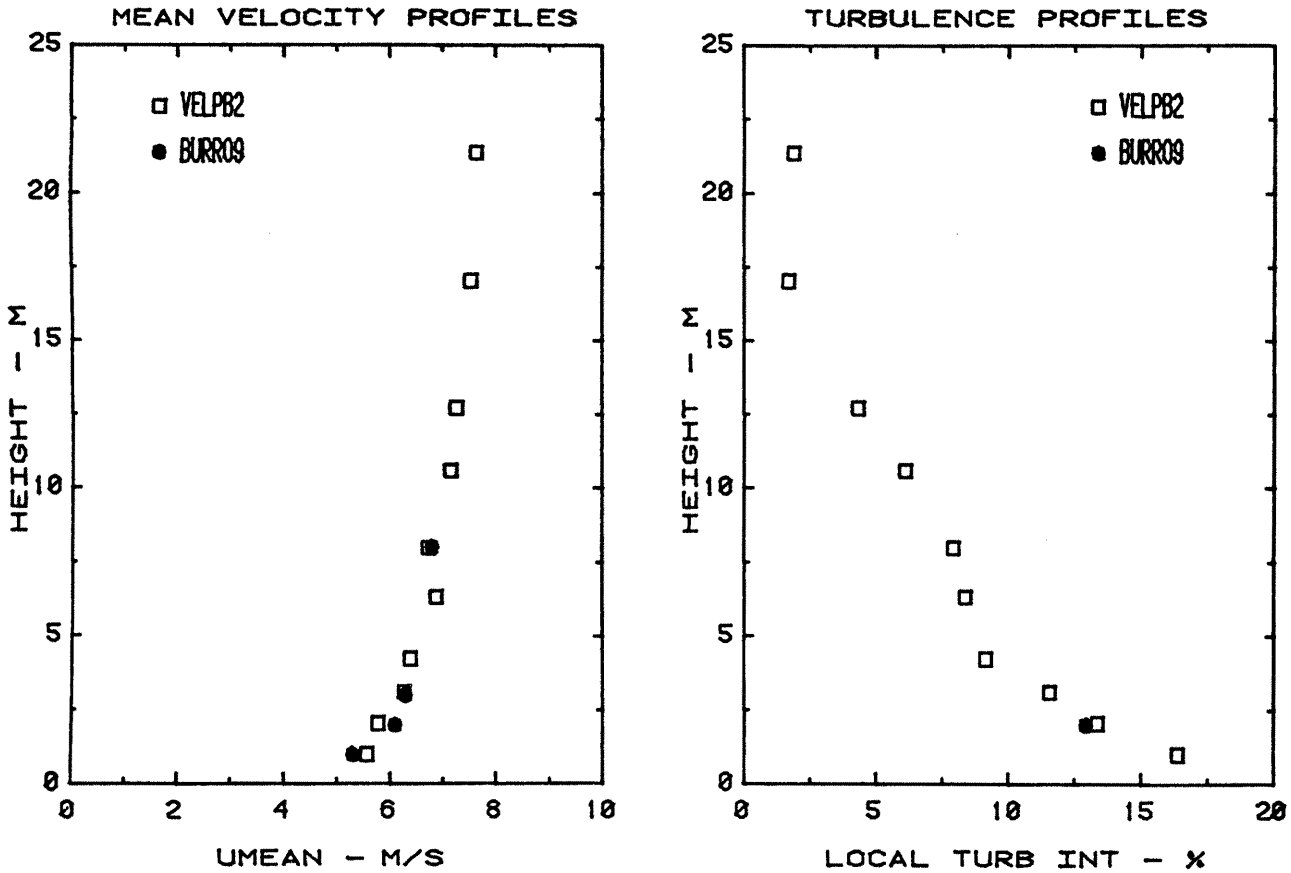

Figure 10-7. Velocity Field Comparison for Run 2 Simulation of Burro 9

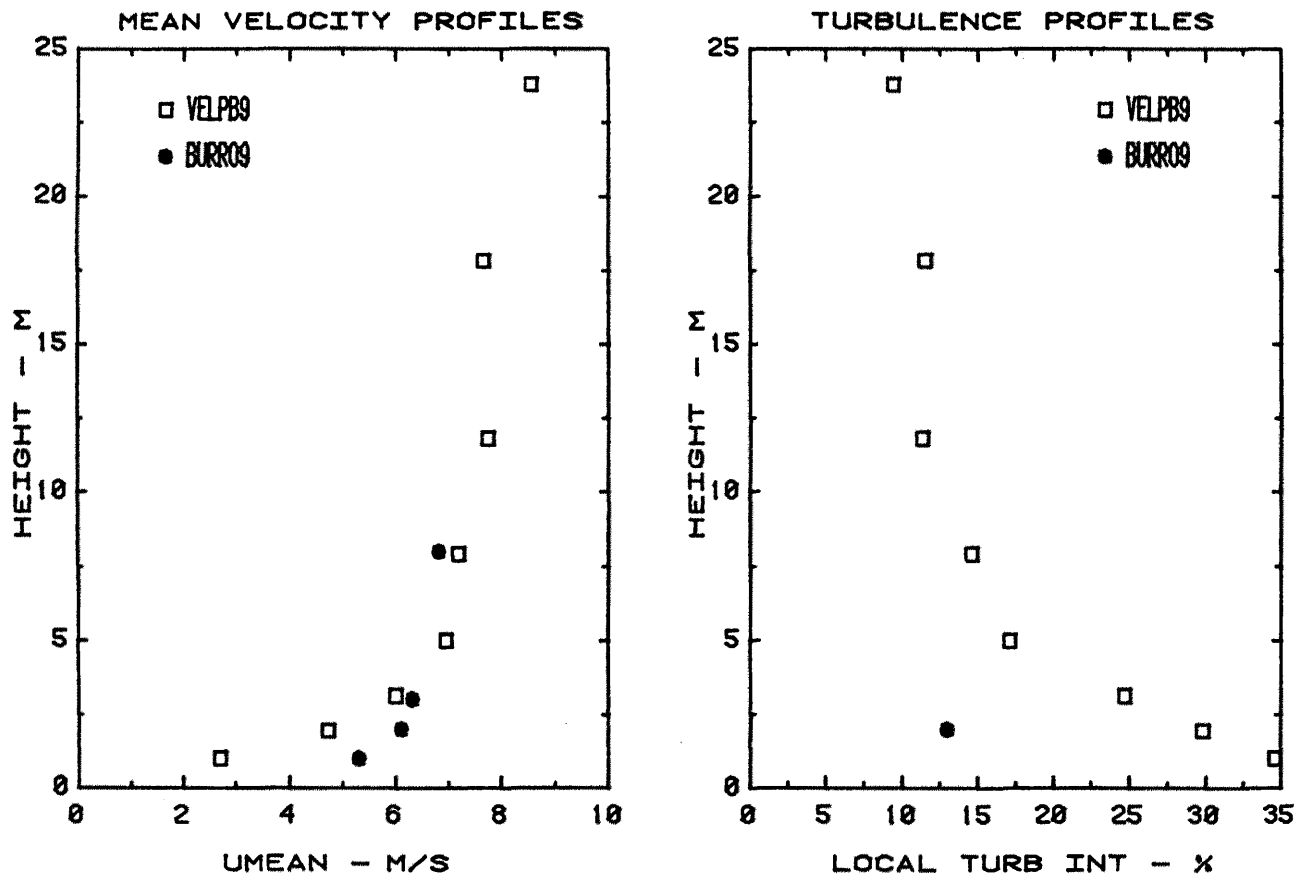

Figure 10-8. Velocity Field Comparison for Run 9 Simulation of Burro 9

profile with height for the 1:240 model scale (Runs 4, 5, 7, 8, 9) are not in very good agreement with field results. In order to improve the shear profile it was decided to perform additional simulations of Burros 8 and 9 at a model scale of 1:85. From Table 3 it is seen that these runs (numbers 2 and 3) have a better wind shear with height comparison. Because of the difficulty of obtaining wind field similarity[1] at extremely low wind-tunnel speeds (i.e., 11 cm/s for Burro 8 at a model scale of 1:240), it was decided to run an additional simulation of this test in which the specific gravity of the source plume was substantially increased. This change in model plume's specific gravity in Run 1 enabled the wind-tunnel reference velocity to be increased from 11 cm/s up to 32 cm/s for the simulation of Burro 8. Kothari and Meroney [29] have utilized a similar criterion for modeling negatively buoyant effluent discharge from a stack.

The data from these eight different runs were reduced into tables of pertinent values; see Appendix B for a complete listing. From these tables plots of the ground level peak concentration contours (Figures 11-1 to 11-8), time progression curves of the lower flammability limit (Figures 12-1 to 12-8), and the flammable zone as a function of time and centerline distance (Figures 13-1 to 13-4) were made. The concentration time histories of selected data points were stored on digital magnetic tape and later plotted in the form shown in Figures 14-1 and 14-2.

[1]At low wind speeds (<20 cm/s) in a smooth floor wind tunnel the turbulence dampening effect of the laminar sublayer penetrates up to heights which are of the same order as the plume height. In addition there is very little known about atmospheric turbulence at winds characteristic to Burro 8 (2.6 m/s at 8 m height). Thus proper scaling of this type of test is more or less a shot in the dark unless the spectral characteristics of the atmospheric winds are measured at the site. This data was not provided in the present study.

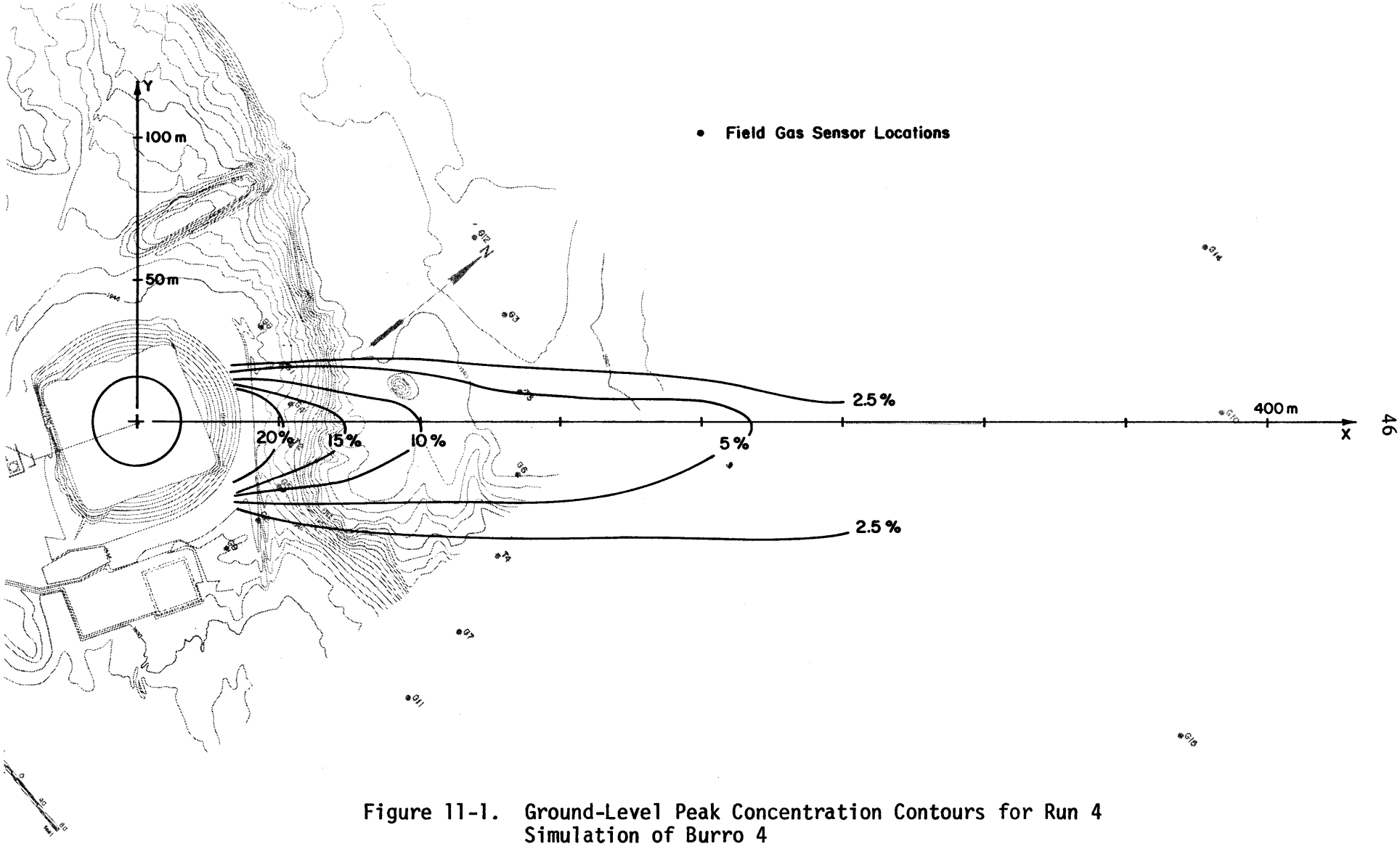

Figure 11-1. Ground-Level Peak Concentration Contours for Run 4 Simulation of Burro 4

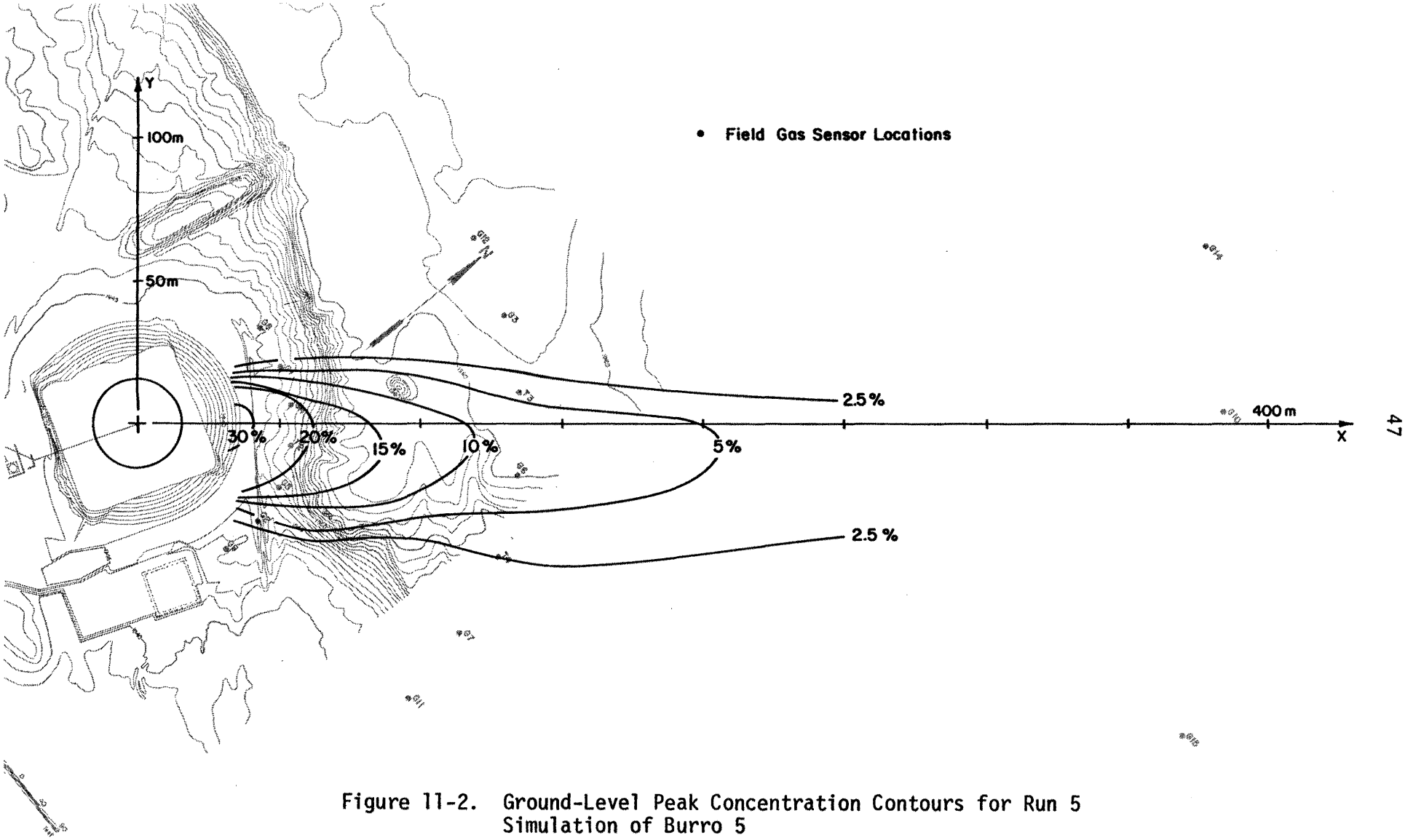

Figure 11-2. Ground-Level Peak Concentration Contours for Run 5 Simulation of Burro 5

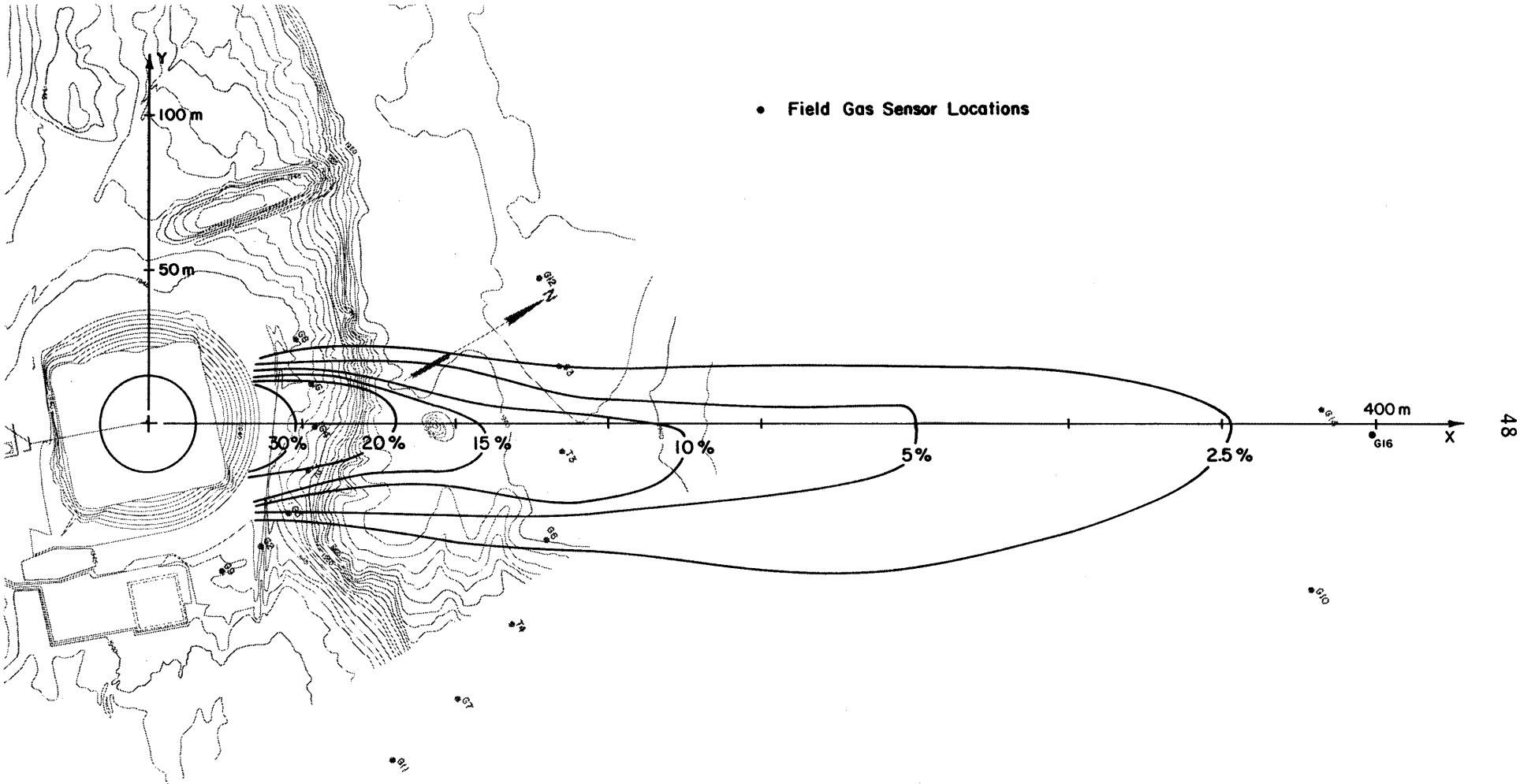

Figure 11-3. Ground-Level Peak Concentration Contours for Run 7 Simulation of Burro 7

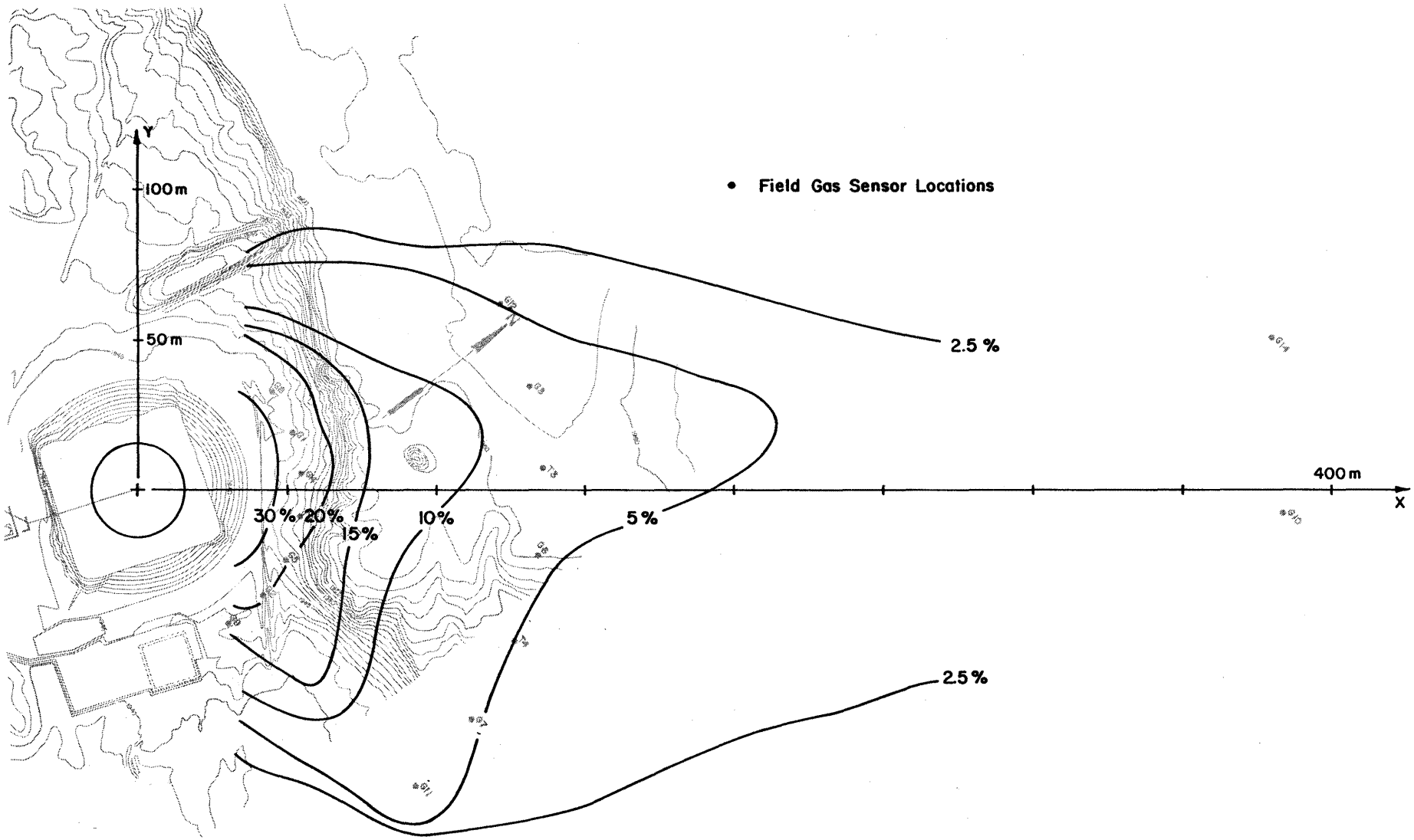

Figure 11-4. Ground-Level Peak Concentration Contours for Run 1 Simulation of Burro 8

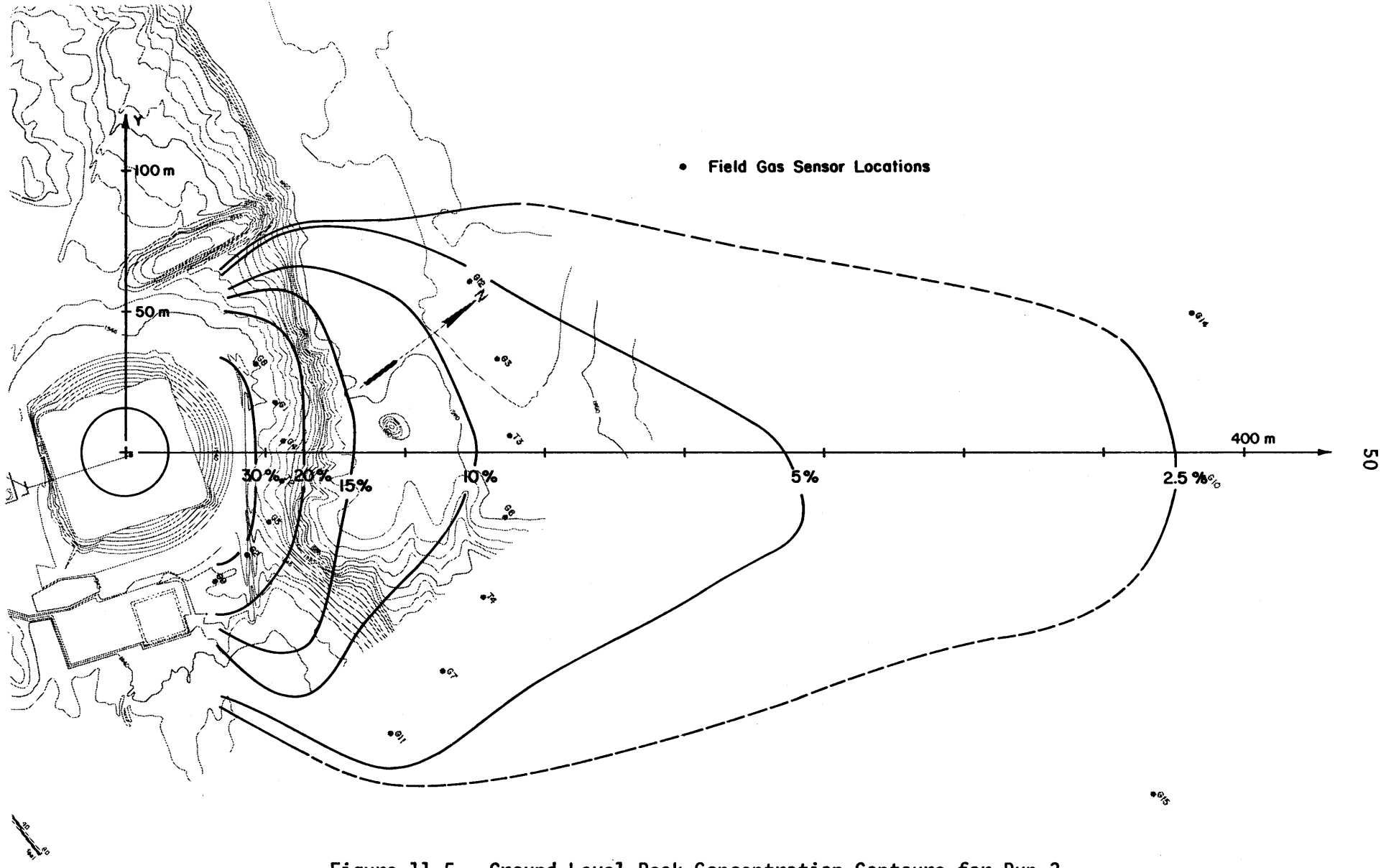

Figure 11-5. Ground-Level Peak Concentration Contours for Run 3 Simulation of Burro 8

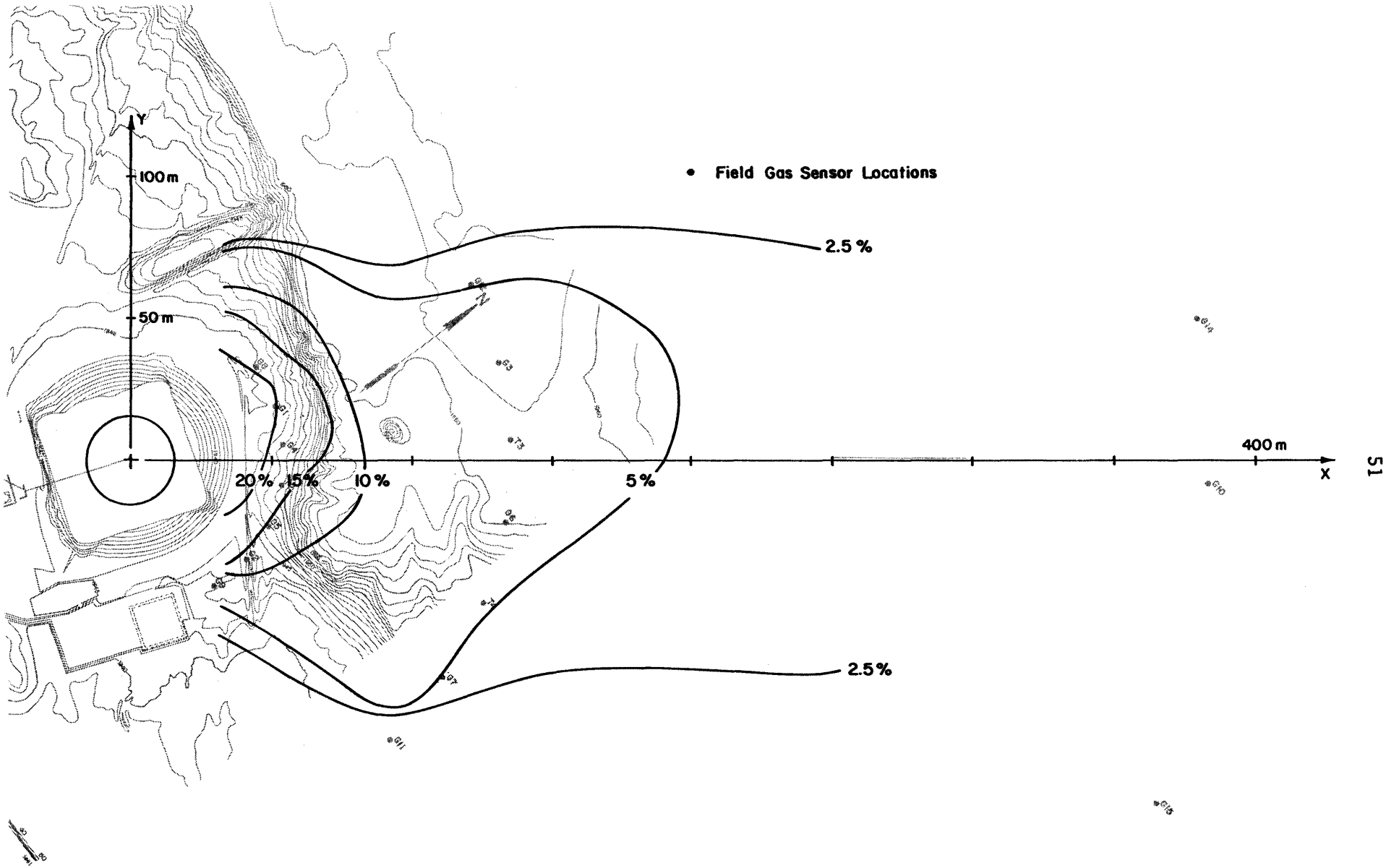

Figure 11-6. Ground-Level Peak Concentration Contours for Run 8 Simulation of Burro 8

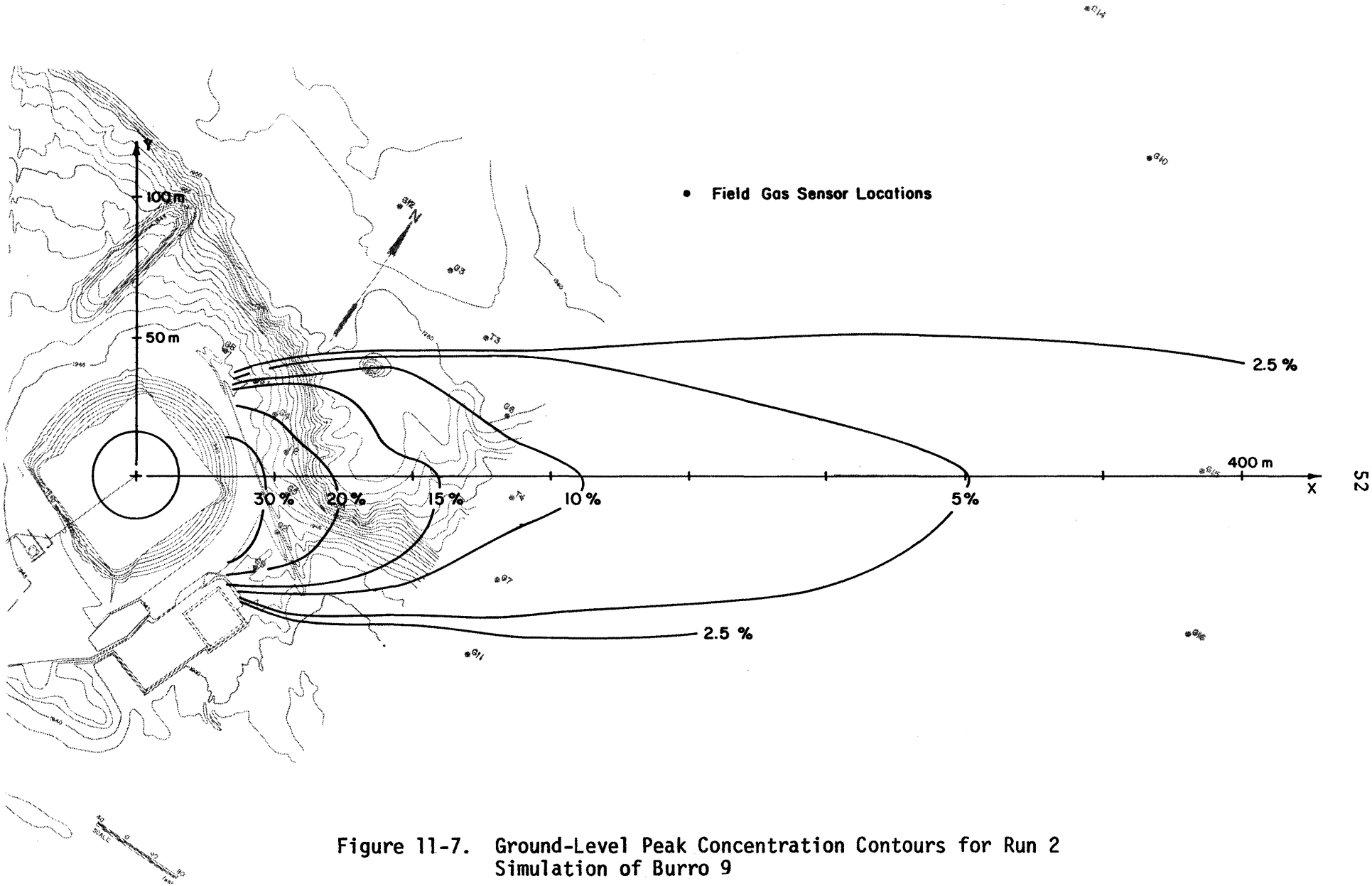

Figure 11-7. Ground-Level Peak Concentration Contours for Run 2 Simulation of Burro 9

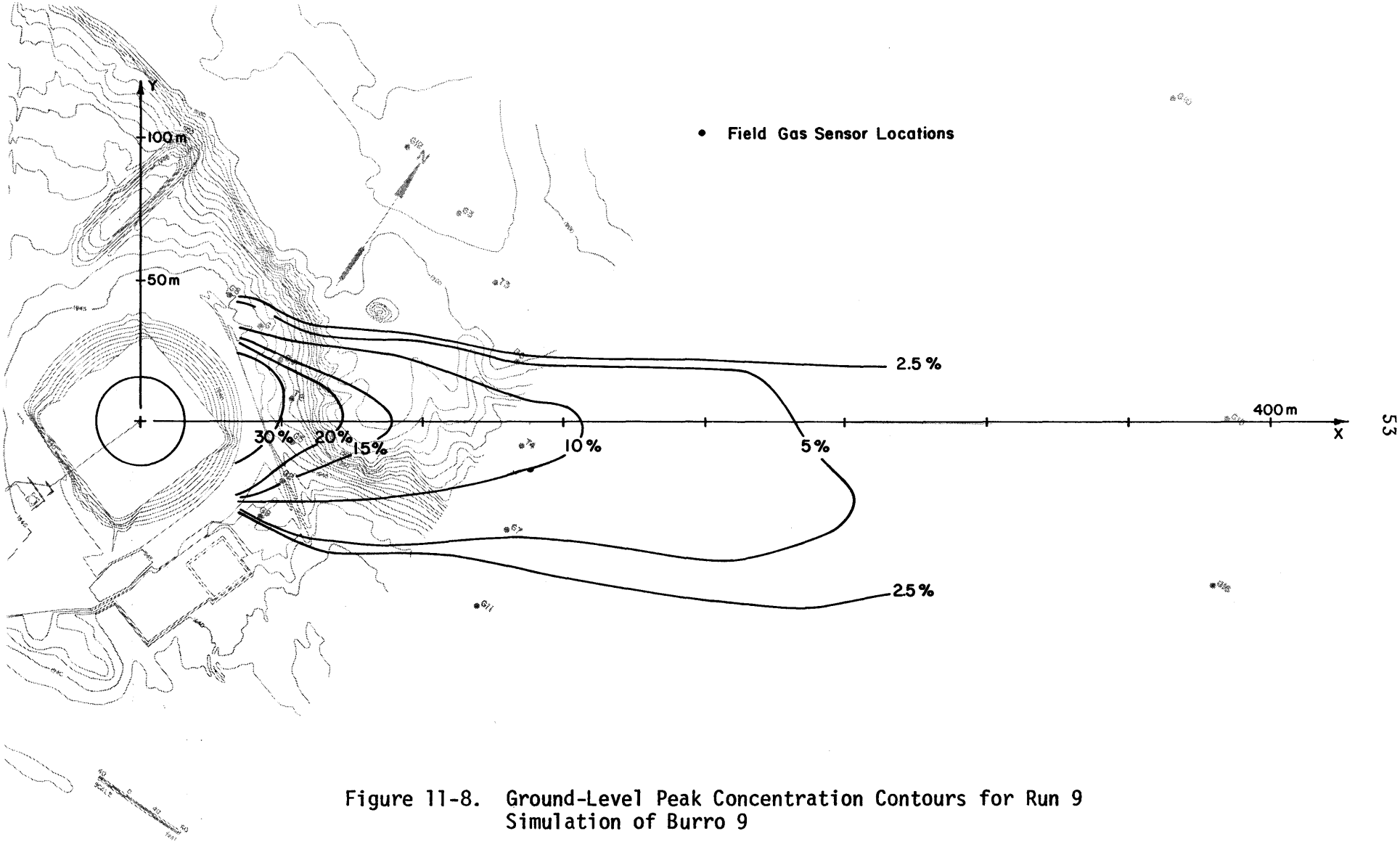

Figure 11-8. Ground-Level Peak Concentration Contours for Run 9 Simulation of Burro 9

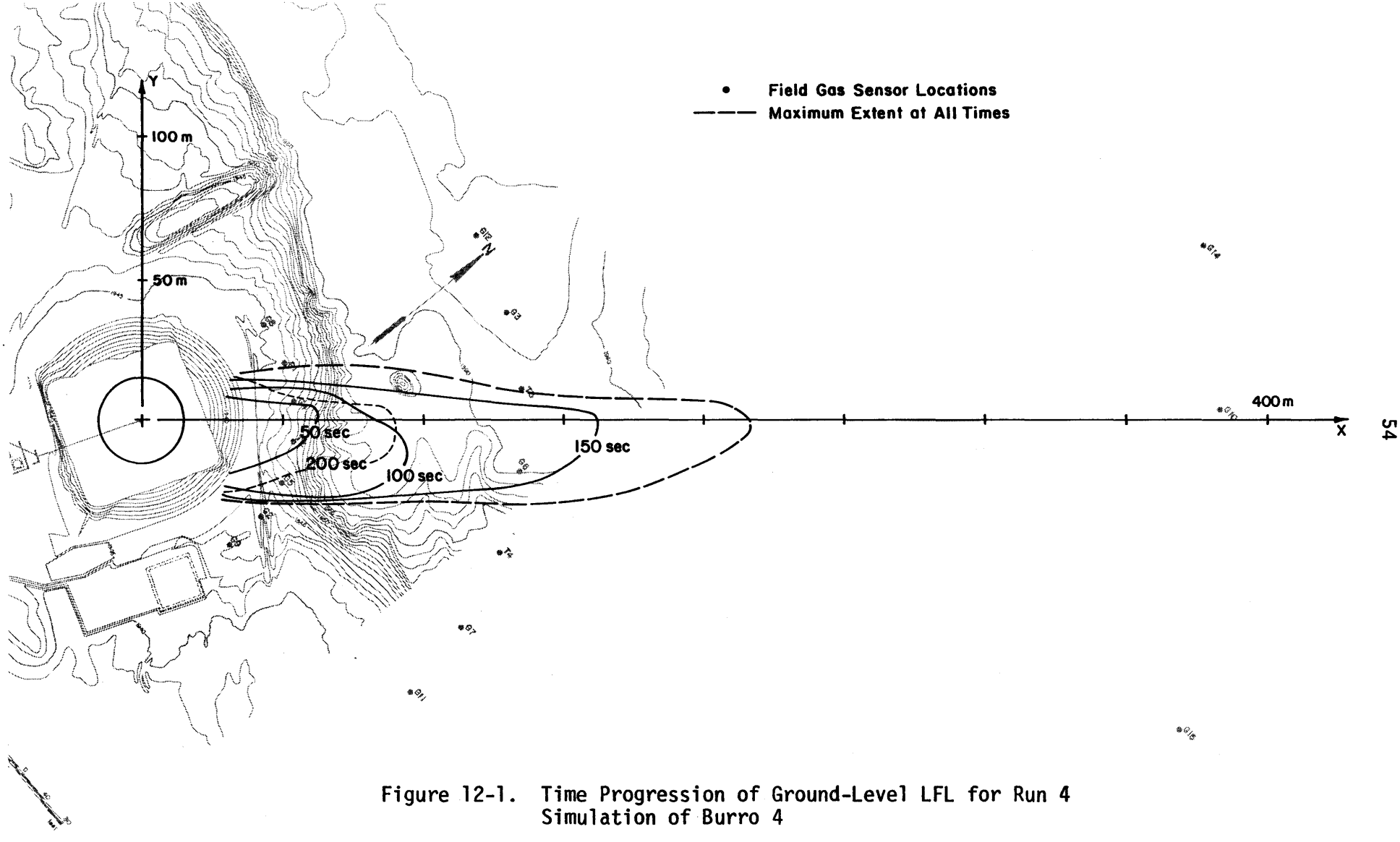

Figure 12-1. Time Progression of Ground-Level LFL for Run 4 Simulation of Burro 4

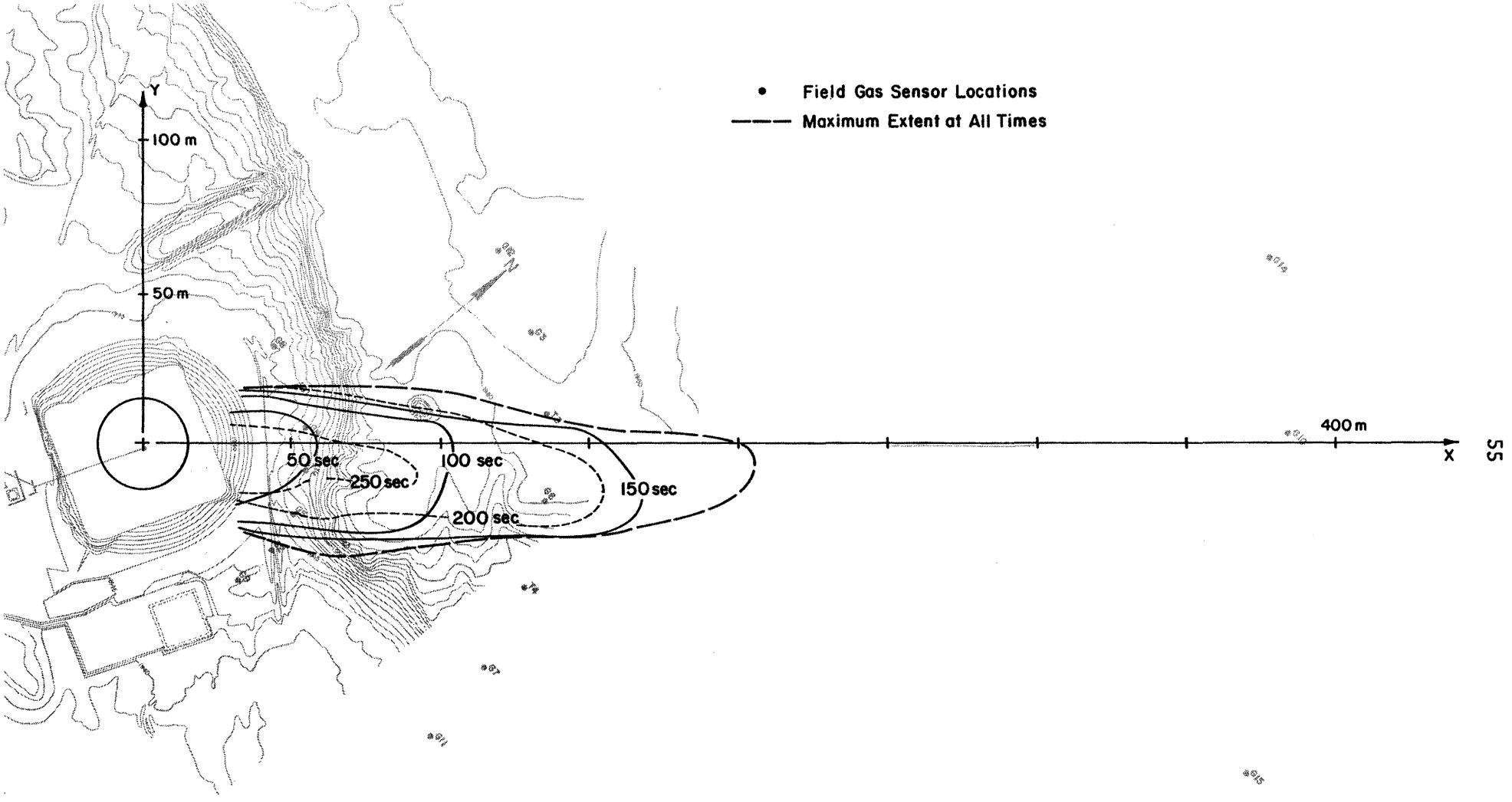

Figure 12-2. Time Progression of Ground-Level LFL for Run 5 Simulation of Burro 5

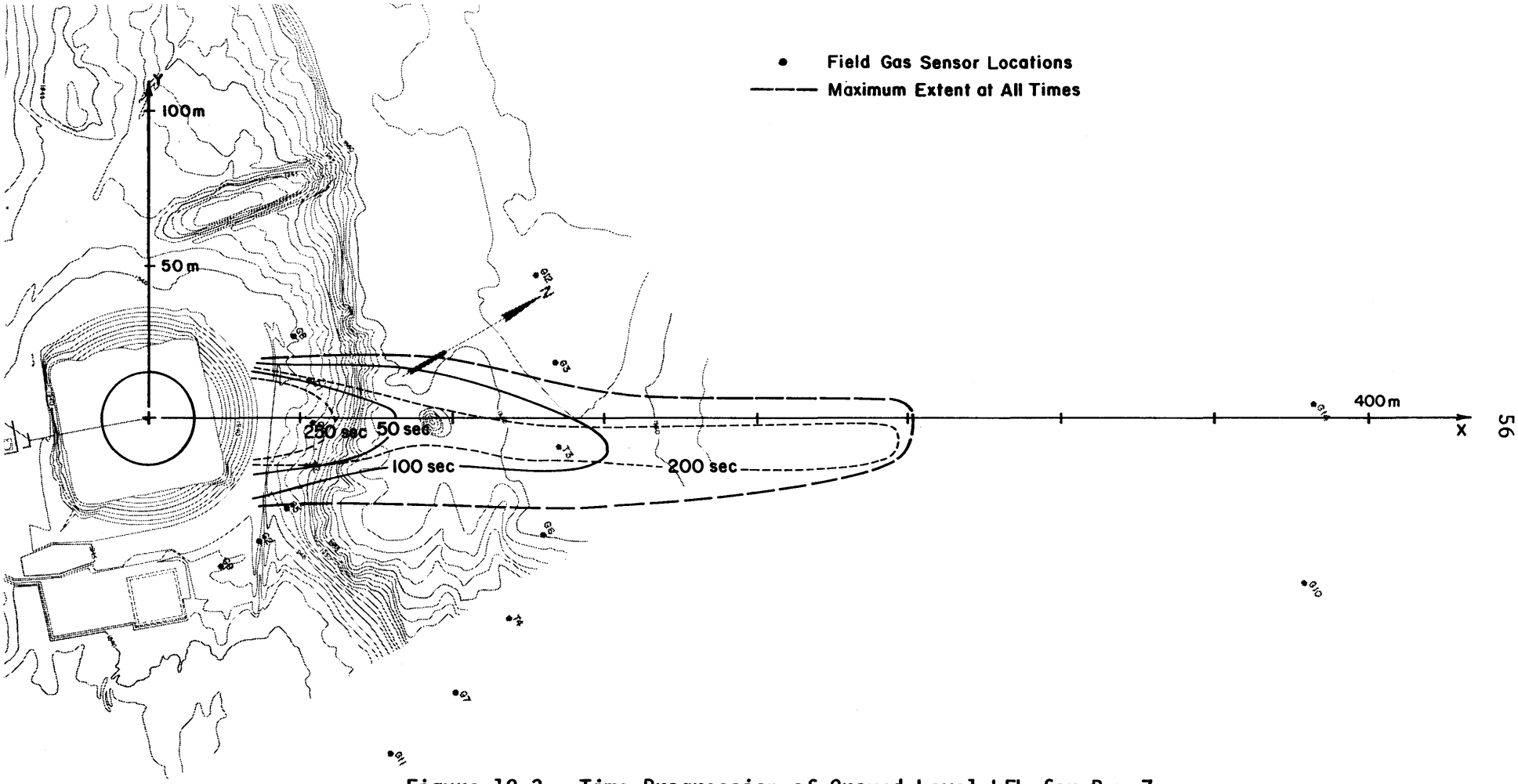

Figure 12-3. Time Progression of Ground-Level LFL for Run 7 Simulation of Burro 7

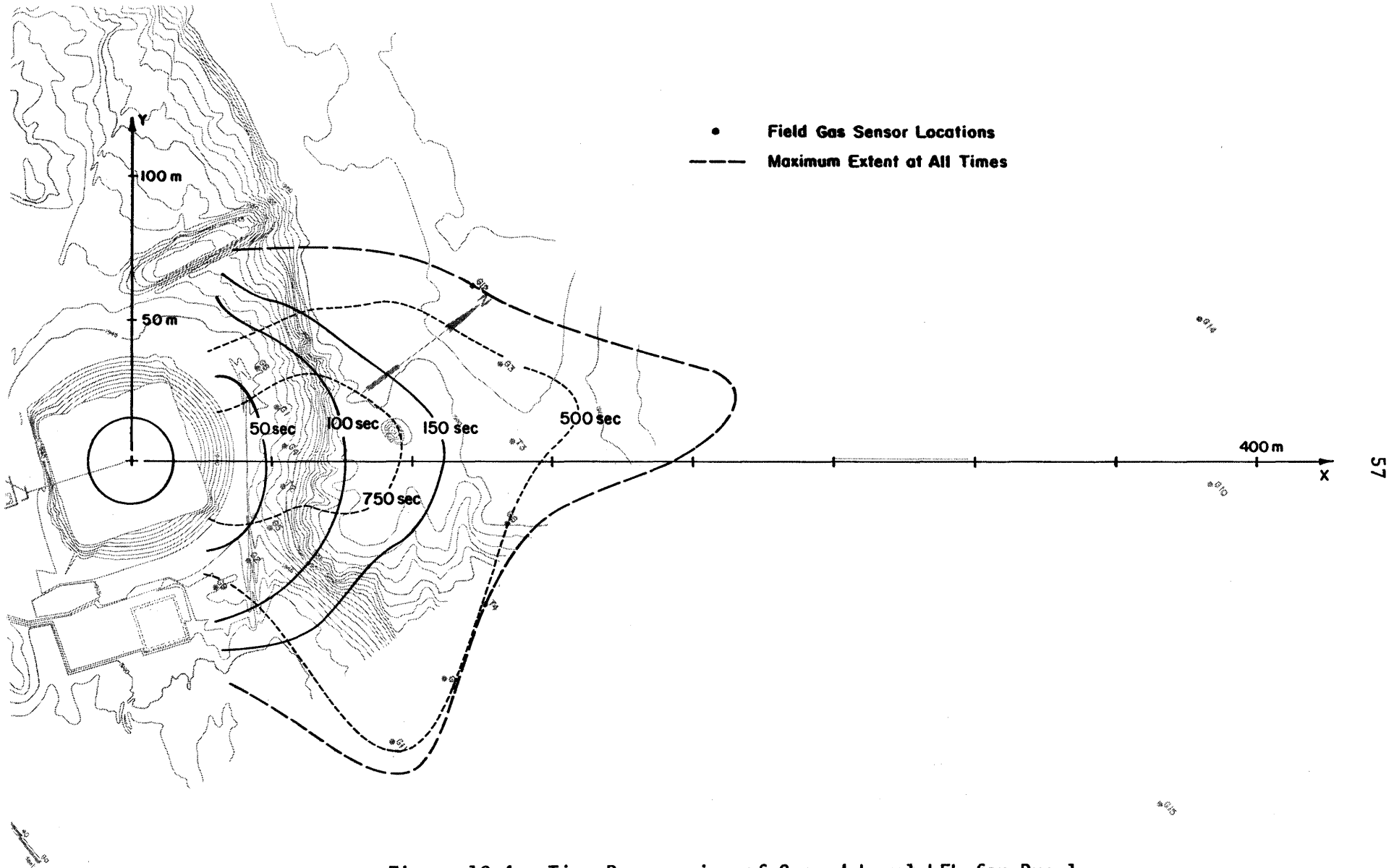

Figure 12-4. Time Progression of Ground-Level LFL for Run 1 Simulation of Burro 8

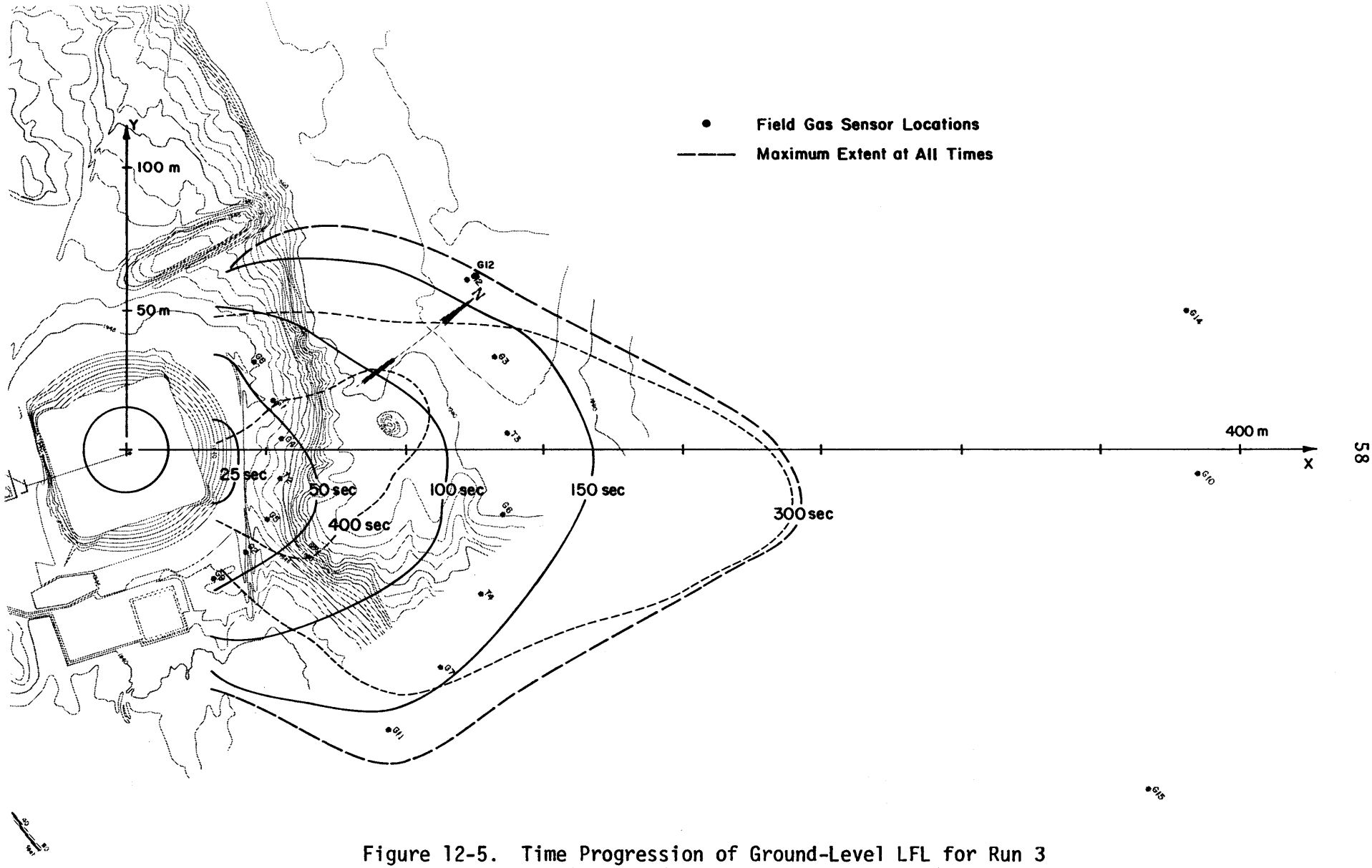

Figure 12-5. Time Progression of Ground-Level LFL for Run 3 Simulation of Burro 8

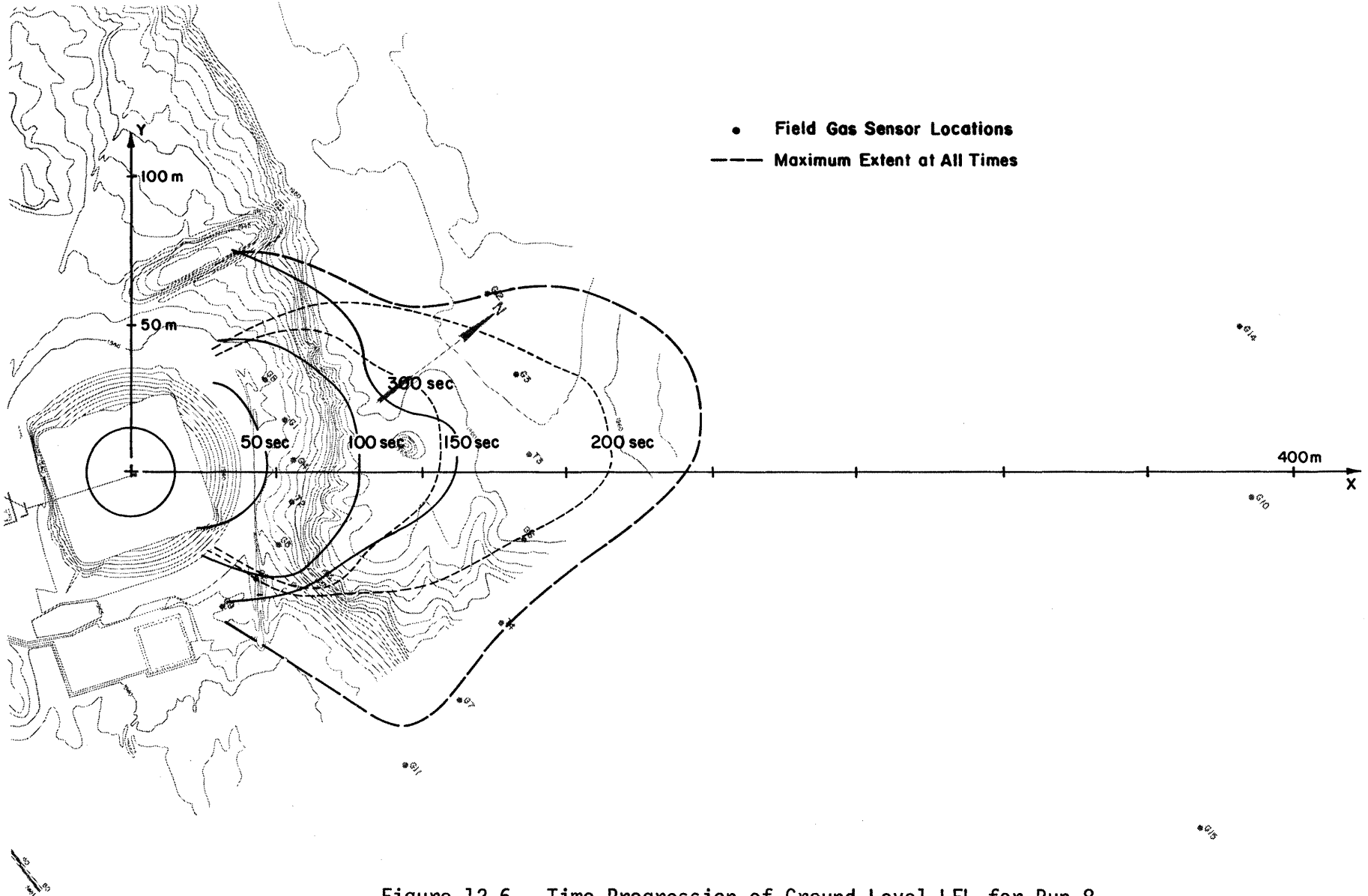

Figure 12-6. Time Progression of Ground-Level LFL for Run 8 Simulation of Burro 8

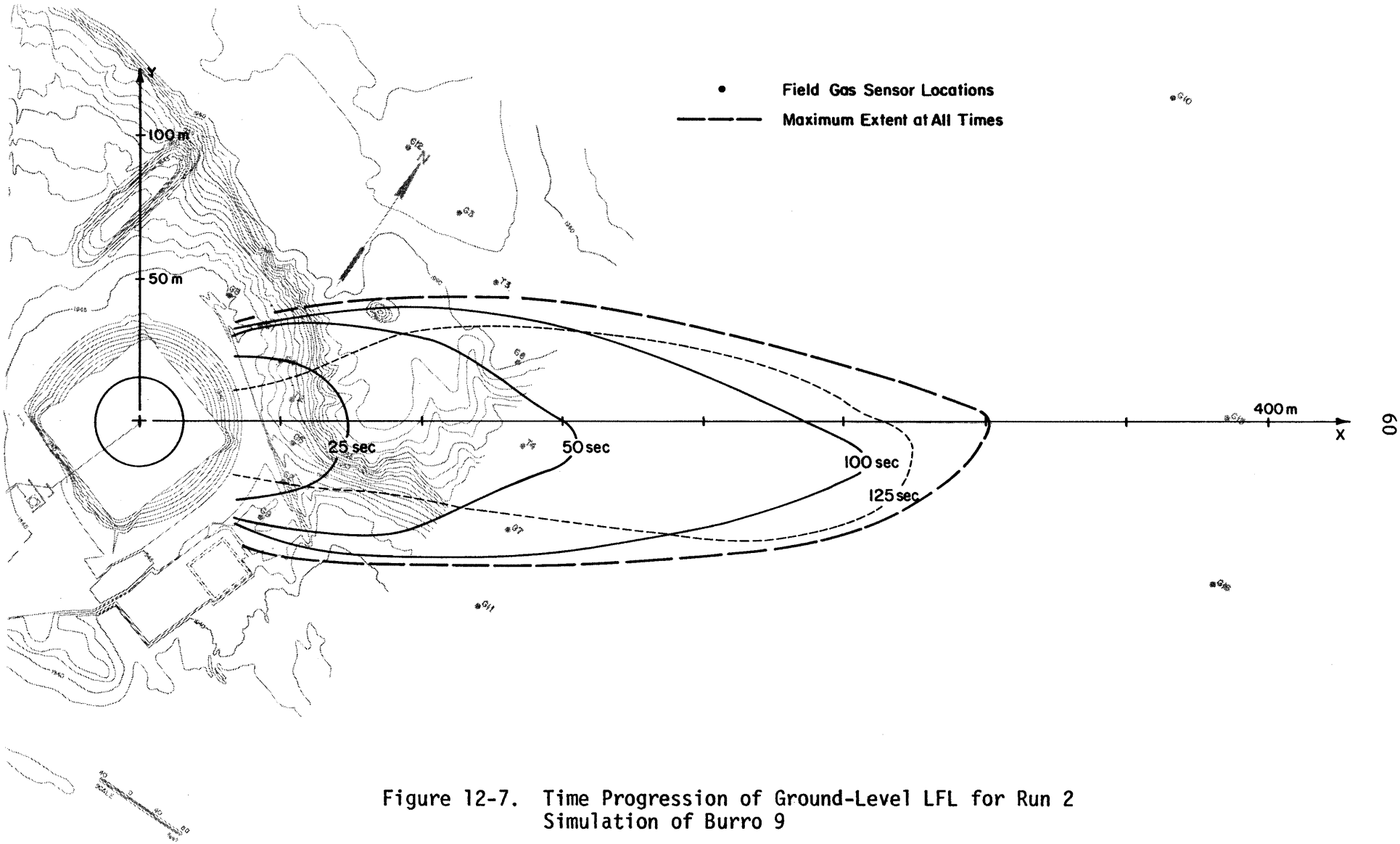

Figure 12-7. Time Progression of Ground-Level LFL for Run 2 Simulation of Burro 9

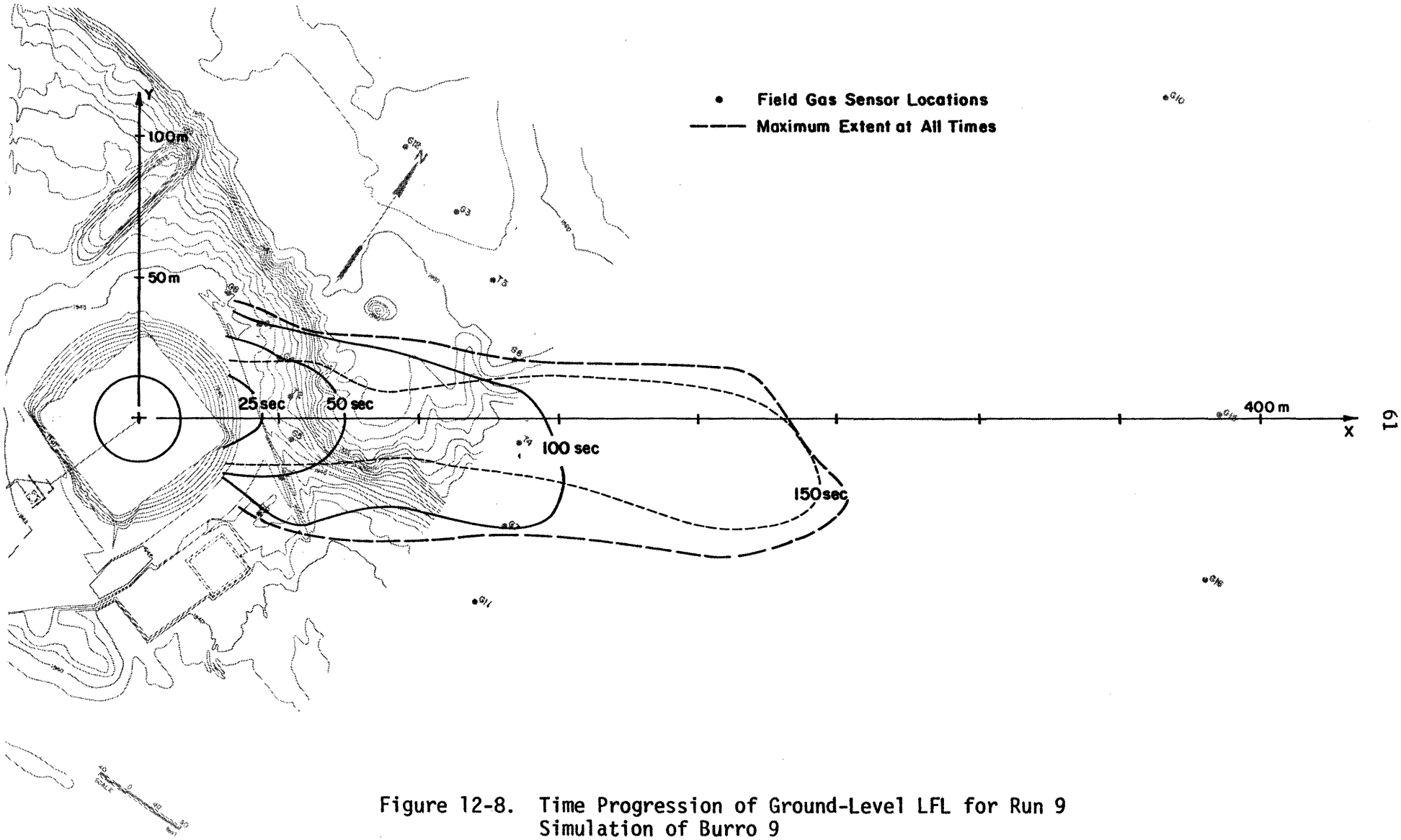

Figure 12-8. Time Progression of Ground-Level LFL for Run 9 Simulation of Burro 9

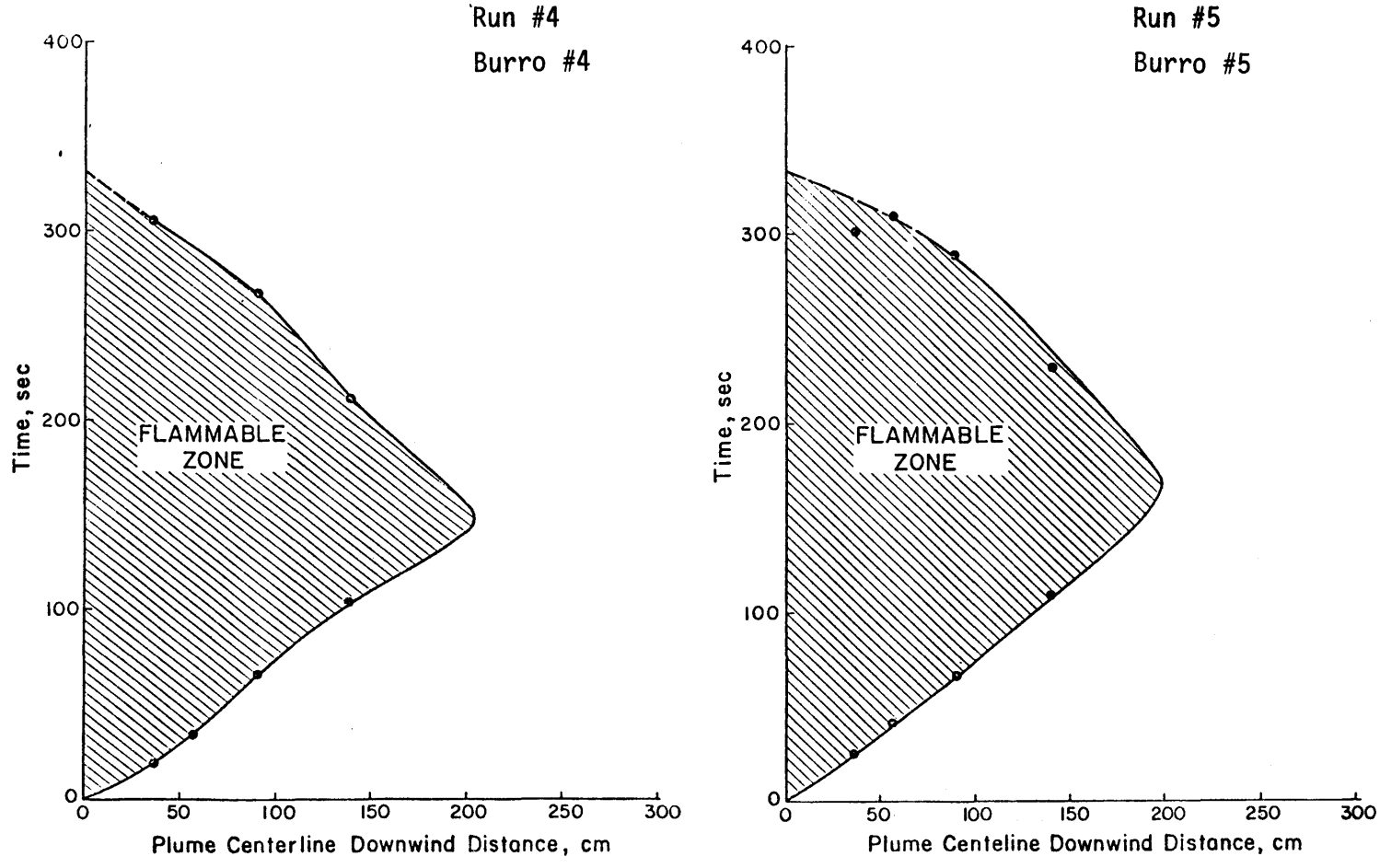

Figure 13-1. Extent of Flammable Zone as a Function of Distance and Time for Runs 4 and 5

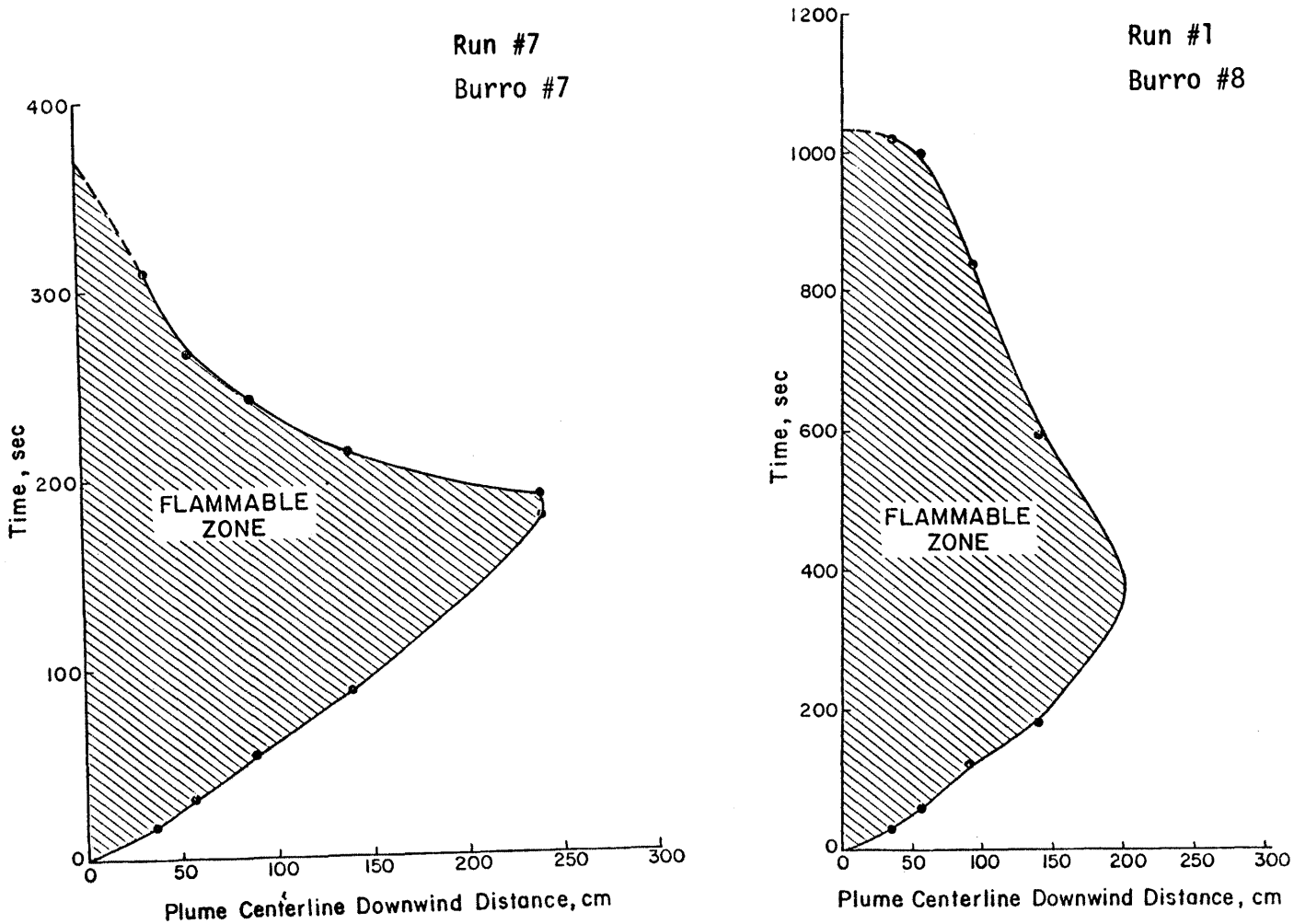

Figure 13-2. Extent of Flammable Zone as a Function of Distance and Time for Runs 7 and 1

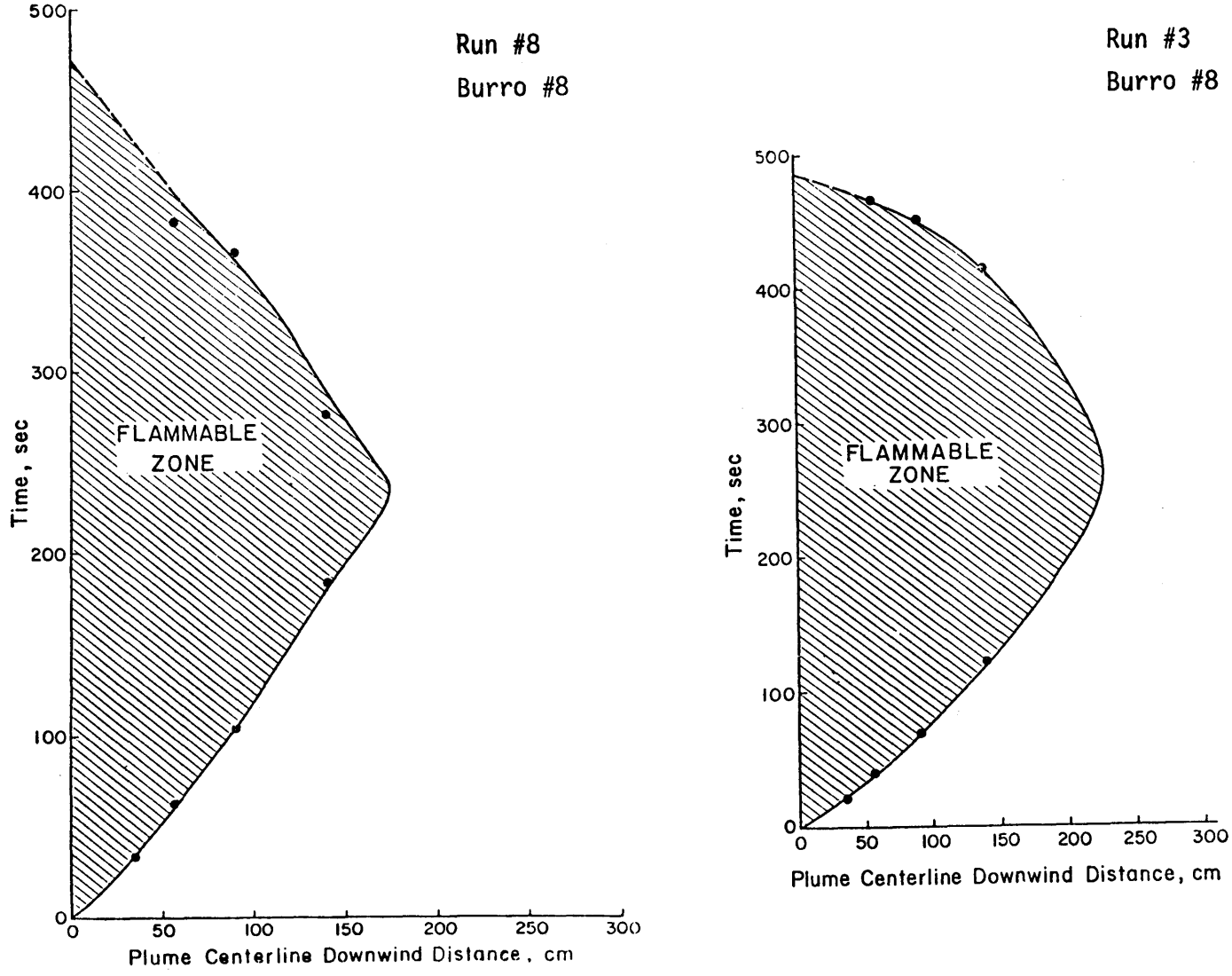

Figure 13-3. Extent of Flammable Zone as a Function of Distance and Time for Runs 8 and 3

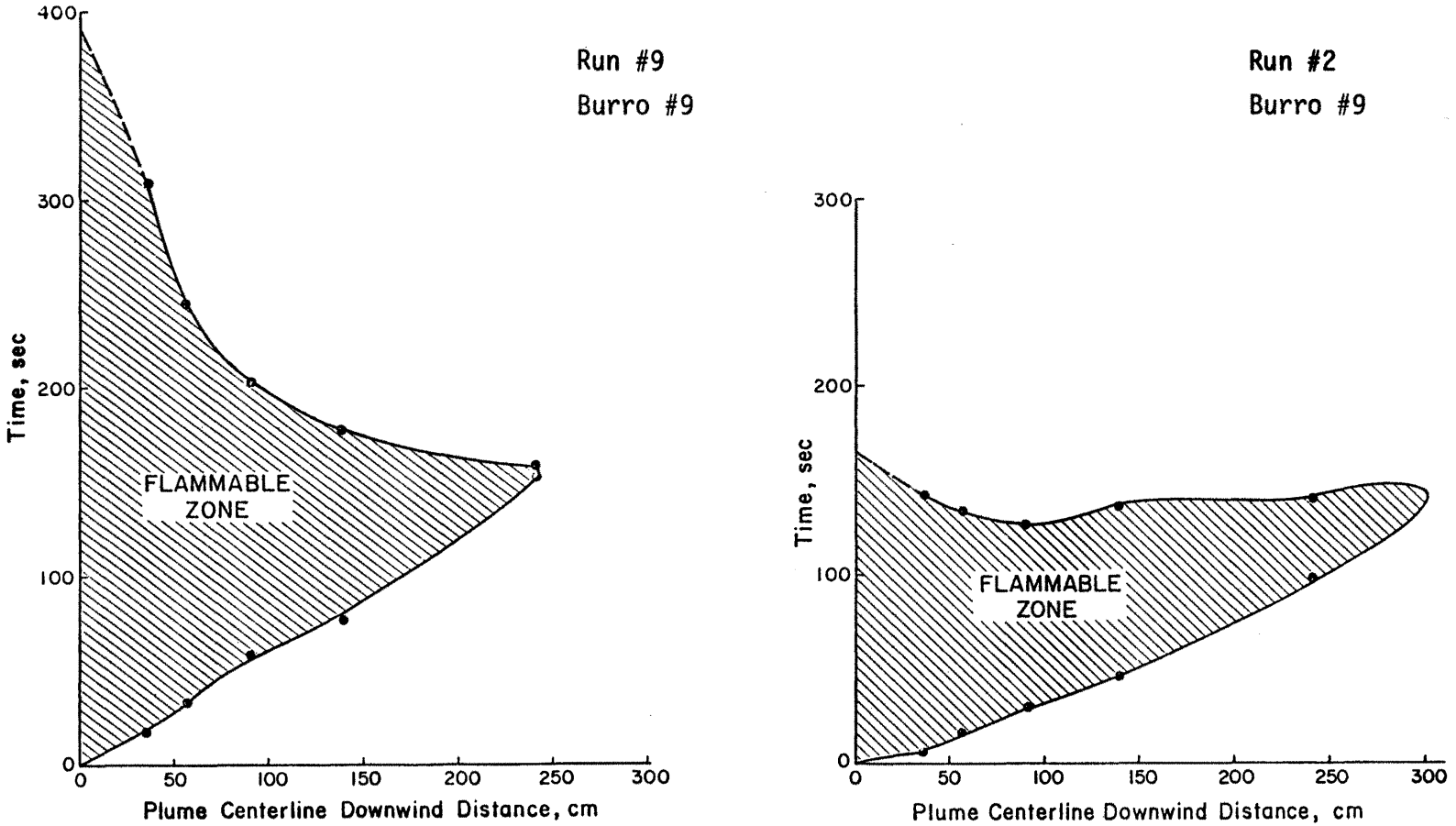

Figure 13-4. Extent of Flammable Zone as a Function of Distance and Time for Runs 9 and 2

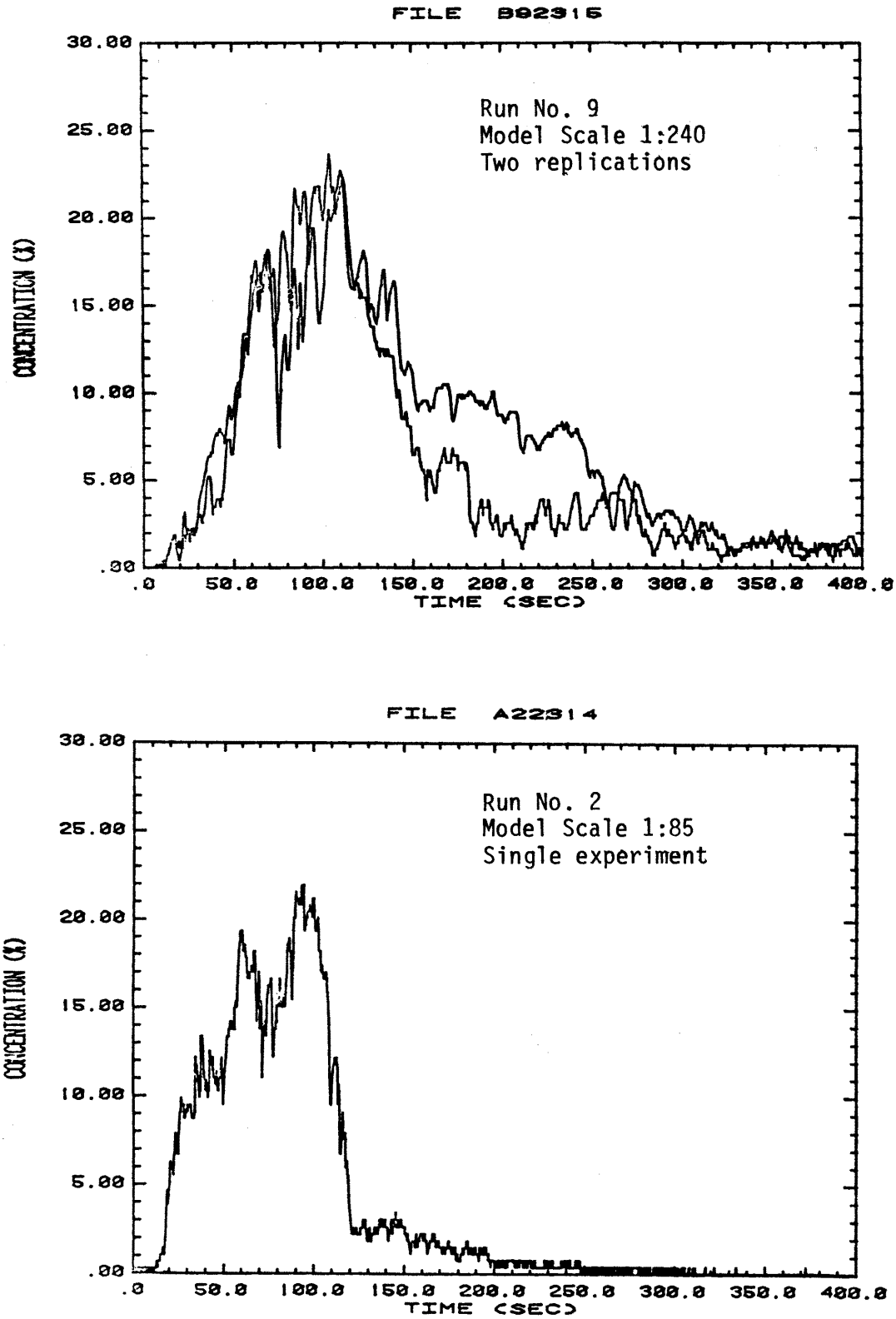

Figure 14-1. Concentration Time History Comparisons for Dfferent Modeling Scales - Burro 9

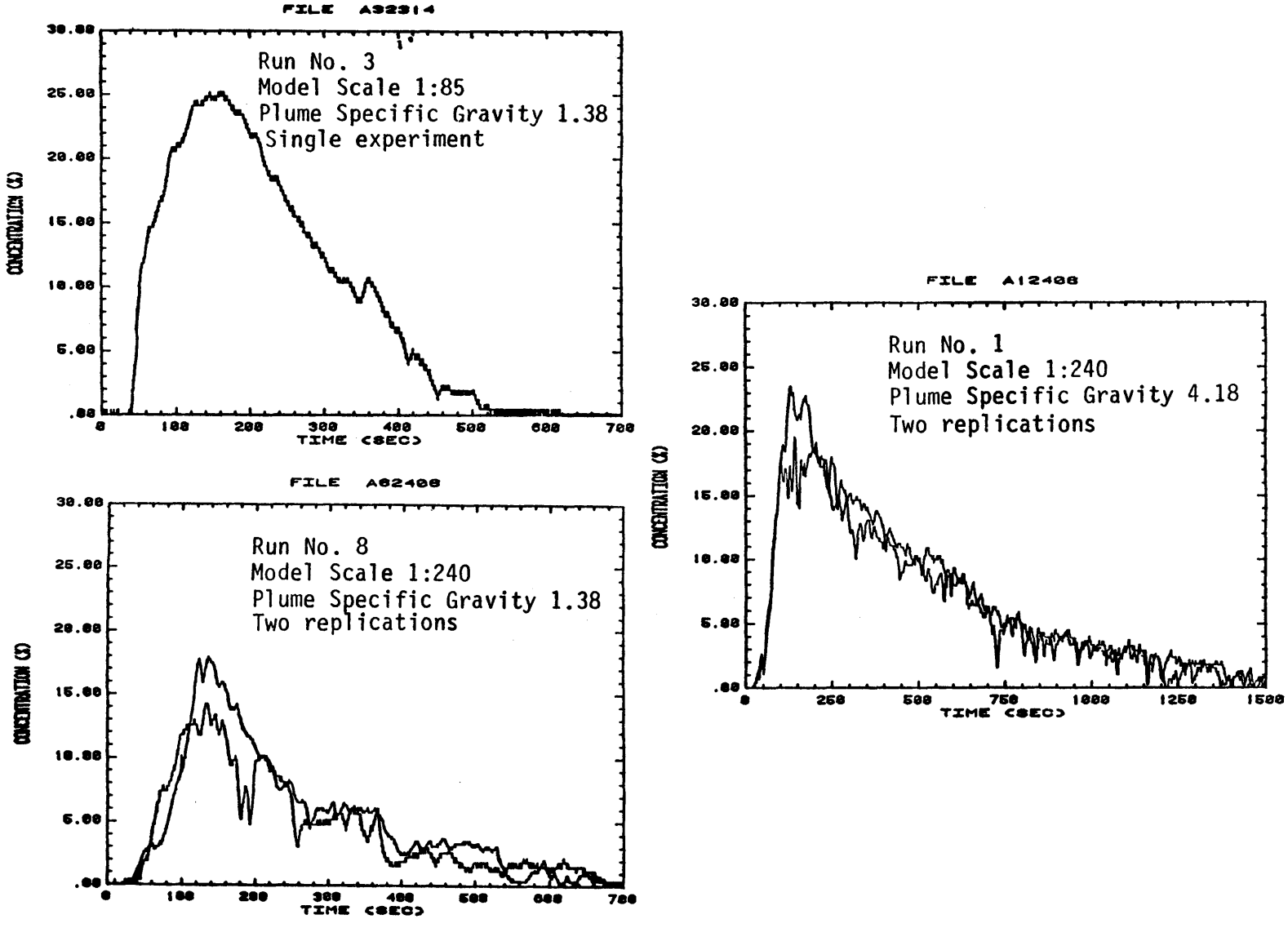

Figure 14-2. Concentration Time History Comparisons for Different Modeling Methodologies - Burro 8

From Figures 11-1 through 11-8 it is seen that the maximum distance to the lower flammability limit (LFL) varies from 200 to 300 meters downwind of the source for all simulations of the five Burro tests that were investigated. The comparison of this distance between the different modeling methodologies performed on Burros 8 and 9 is generally acceptable, ±20 percent, and visual comparison of the peak concentration contours in Figures 11-4, 11-5, 11-6 and in Figures 11-7, 11-8 show general agreement among the results. But the prediction consistency in the timing of the plume motion is less reliable. This is borne out in the plots of LFL time progressions in Figures 12-4, 12-5, 12-6 for Burro 8 and 12-7, 12-8 for Burro 9. Figures 14-1 and 14-2 of the concentration time histories at a similar spacial point also demonstrate differences in the time dependent character of the plume.

Several significant observations are readily seen by the comparison of the effect of model scale on the measured time-dependent characteristics of the plume. Figures 12-7 and 12-8 show the LFL time progression for measured plumes at a scale of 1:85 and 1:240 respectively for the simulation of Burro 9. Comparison of these two figures shows that at the 1:85 scale the plume growth rate in the downwind direction is almost twice as fast as that observed at the 1:240 scale. A similar conclusion is obtained from inspection of the concentration time histories presented in Figure 14-1. Also it is readily observed in Figure 14-1 that for the 1:85 scale model the rise and fall of initial and final plume concentrations is much more rapid than in the 1:240 scale-model case. An explanation of these differences in plume timing characteristics is portrayed in Figure 15; a comparison of the mean velocity and turbulent intensity profiles for Runs 2 (1:85 scale) and

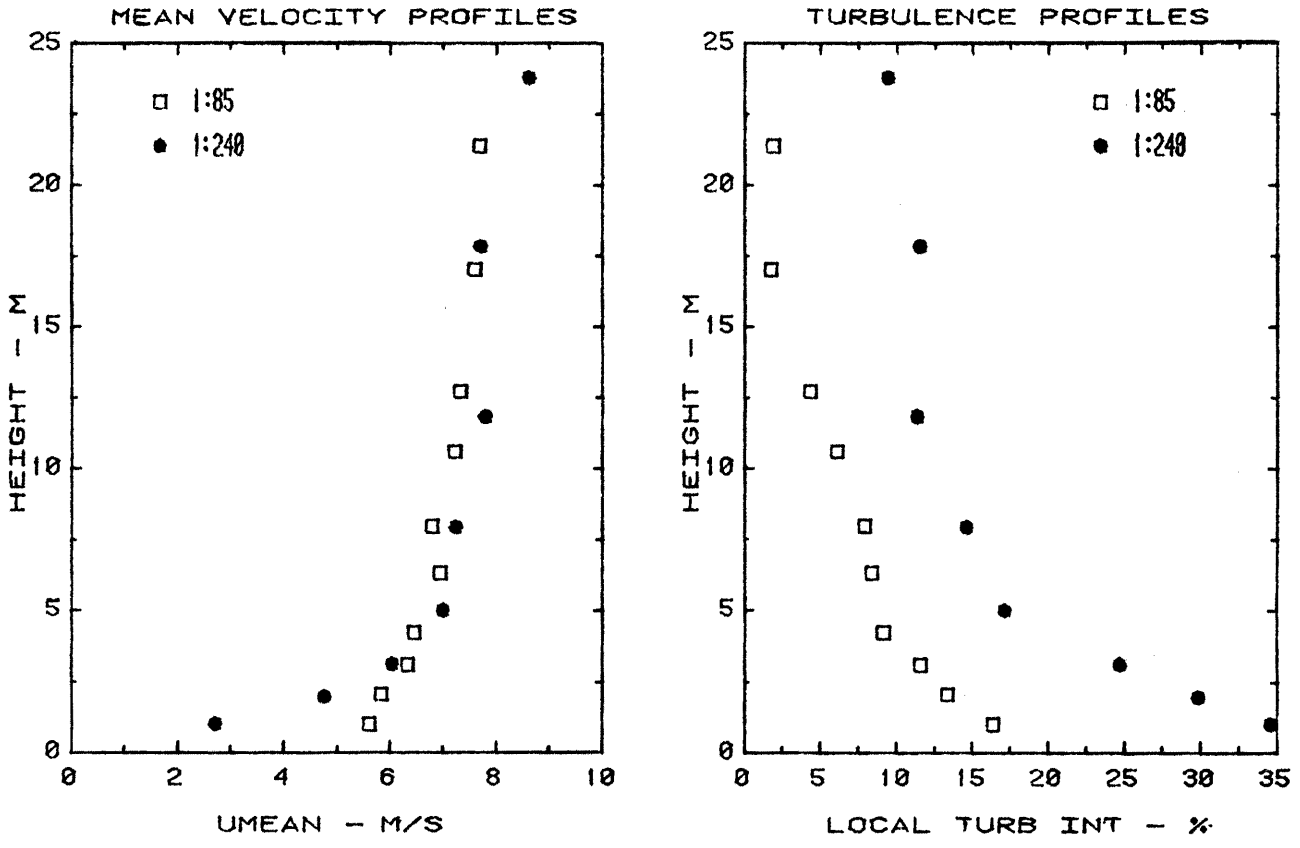

Figure 15. Model-Scale Effects on Wind Field Statistics for Burro 9

9 (1:240 scale). From this figure it is observed that the mean wind shear and the resultant intensity of turbulence is much greater for the 1:240 scale model. Since the velocity reference height for the calculation of plume similarity is three meters, the 1:240 scale model has much lower velocities below this height than the 1:85 scale model. This coupled with the result that the 1:85 scaled plume traveled at a much faster speed than the 1:240 scaled plume leads one to believe that for a 24 cubic meter LNG spill (Burro 9) the plume frontal velocities are primarily determined by the speed of the wind at heights below 3 meters. The increased wind shear and turbulence as modeled by the 1:240 scaled plume would in effect cause increased longitudinal dispersion of the plume. This would explain the comparatively slow rise and fall times of plume arrival and departure as seen in the 1:240 scaled plume data (Figure 14-1).

Similar modeling-scale characteristics that were discussed above for Burro 9 are also present for the scale comparisons observable in Burro 8. Figures 12-5 and 12-6 display the time progression of the LFL for model scales 1:85 and 1:240 respectively and Figure 14-2 displays the concentration time history comparisons for both model scales. The wind-profile comparison is retrievable through observation of the model data presented in Figures 10-5 and 10-6.

The modeling comparison between Run 1 and Run 8 which both simulate Burro 8 is generally favorable in the prediction of peak concentrations (Figures 11-4 and 11-6) and plume arrival and buildup characteristics (Figures 12-4, 12-6, and 14-2) but discrepancies appear in the prediction of plume decay rate (Figures 12-4, 12-6, and 14-2). Run 1 incorporates an enhanced modeling criteria in which the initial specific

gravity of the modeled plume is much greater than that of the field plume. This enables the usage of higher wind-tunnel velocities and hence more assurance of operating in a Reynolds number invariant regime (see section 2.2.1 for a more complete discussion). Both Runs 1 and 8 are at a model scale of 1:240 thus the only difference between them is the relaxation of the initial plume specific gravity requirement. These limited results would indicate that when only the peak downwind concentrations are of interest enhanced modeling may be a viable technique. When the duration of plume exposure is important this technique should be used with caution until more conclusive results or explanations of this behavior are obtained from experimental data. A pausible explanation of these differences is that increasing the plume source density relaxes the inertial interactions between the plumes mass, initially at rest, and the approach flow. The heavier the plume mass the longer it will take the approach flow to accelerate that mass up to its convective velocities; thus, the enhanced plume does not pass by the concentration sensor as fast as the plume simulated by a smaller source density.

5.0 FIELD DATA COMPARISONS

When comparing physical model predictions with field data of a complex diffusion process one must realize that many physical assumptions and approximations have been employed in the modeling process. A single field event has a large number of uncontrolled or poorly specified variables which have an affect on the resultant concentration field that are not completely accounted for in the modeling process. Specific limitations are discussed in the following paragraphs.

The source conditions of an LNG spill situation must be approximated since it is difficult to predict or measure the time dependent size and boiloff characteristics in the field let alone reproduce these characteristics in a model situation. During the model tests a simple on-off gas release at constant boiloff over a constant area was used.

The wind field into which an LNG plume is released is typically nonstationary. The plume may experience a wind field that is undergoing a change of mean wind speed, mean wind direction, and turbulent characteristics with time. Indeed some of these nonstationary effects were observed during the Burro Series. Burro 4 had significant wind direction changes and Burro 8 experienced a steadily declining wind speed throughout the test. These nonstationary factors were not modeled in the physical simulations. The wind characteristics were assumed to be constant, i.e., statistically stationary. These assumptions may lead to major differences between the resultant concentration fields depending on the severity of the nonstationarities during the field tests.

Even if the atmospheric wind field were stationary for the duration of a test, a single measurement of a time transient phenomenon, such as an LNG spill plume, would yield only a single datum point in the construction of a time dependent concentration probability distribution. Many replications of the same source conditions emitted into the same mean approach flow would be necessary to construct the entire probability distribution. But multiple releases with the same source conditions and wind fields are not possible in the atmosphere. In a model situation the source conditions and stationarity of the wind field are reproducible. Figures 14-1 and 14-2 show that two measurements of the concentration time history at the same spacial point in the same plume can yield fairly large variations. Thus even when a field test is performed in an approximately stationary wind field the measurements can only fall within some probabilistic concentration band. The width of this band can be estimated when the tests are repeated several times. During the model test series simulated spills were repeated up to four times.

Model data and field concentration data [30] are compared in three presentation formats; the peak plume centerline concentration decay with downwind distance, Figures 16-1 through 16-5, the concentration time histories for plume centerline stations, Figures 17-1 through 17-15 and ground level maximum concentration extent contours, Figures 18-1 through 18-8. The field gas concentration measurement stations are shown in Figure 19.

5.1 DATA QUALITY CONSTRAINTS ON MODEL/FIELD EVALUATIONS

The model was oriented in the wind tunnel based on the average and direction which occurred during the field tests. Since drift in

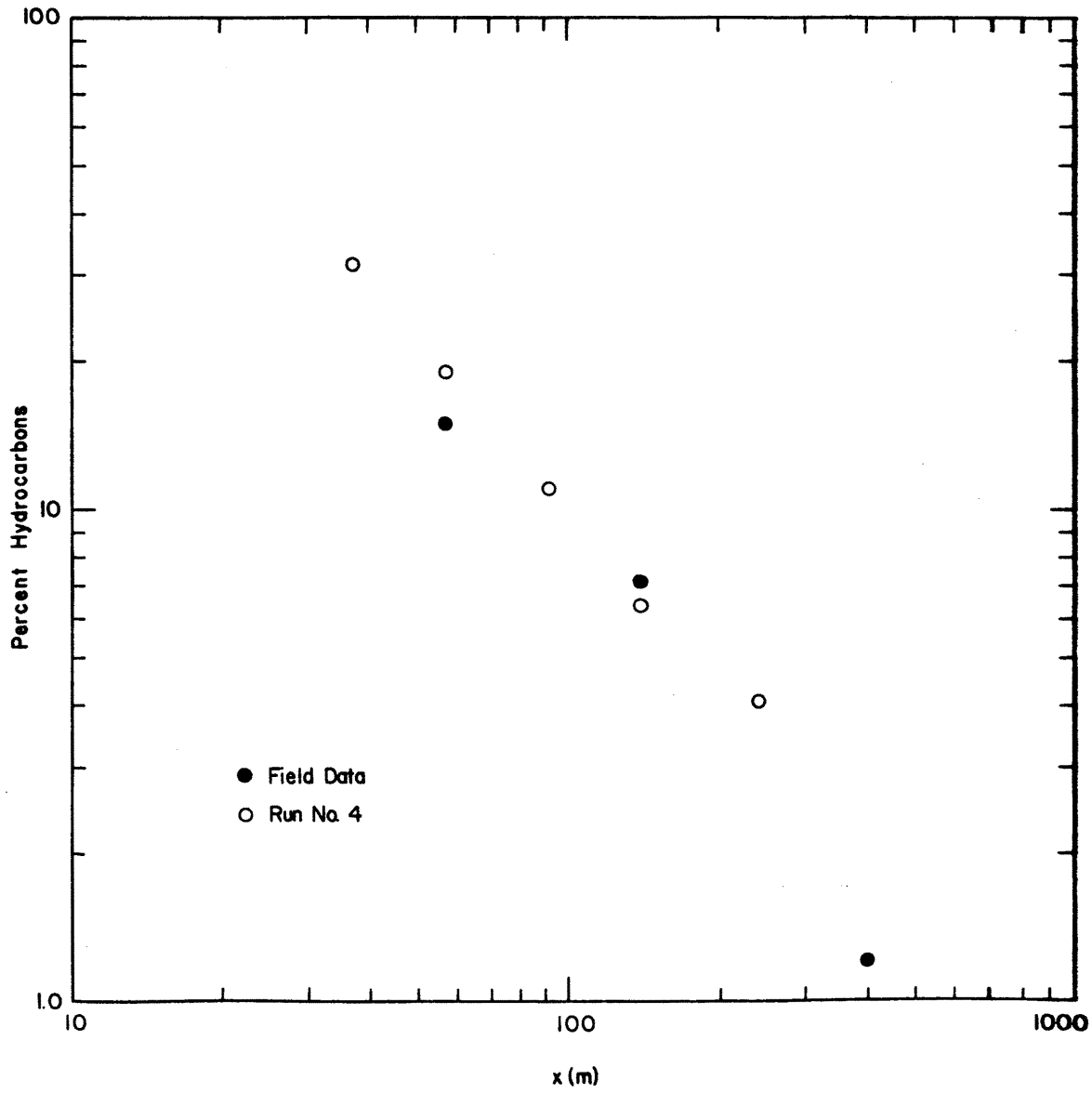

Figure 16-1. Peak Plume Centerline Concentration Decay with Downwind Distance at 1 meter height for Burro 4

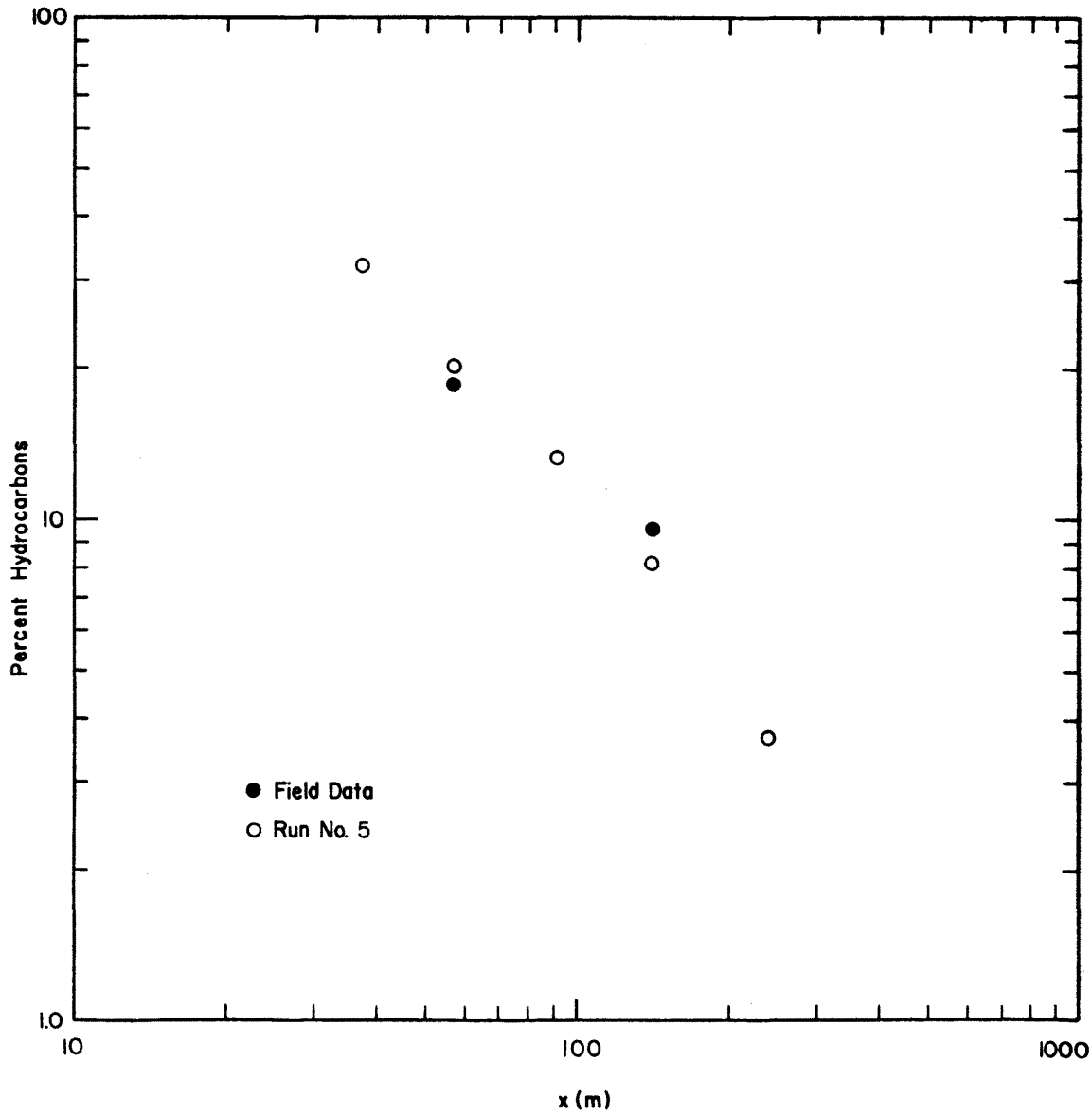

Figure 16-2. Peak Plume Centerline Concentration Decay with Downwind Distance at 1 meter height for Burro 5

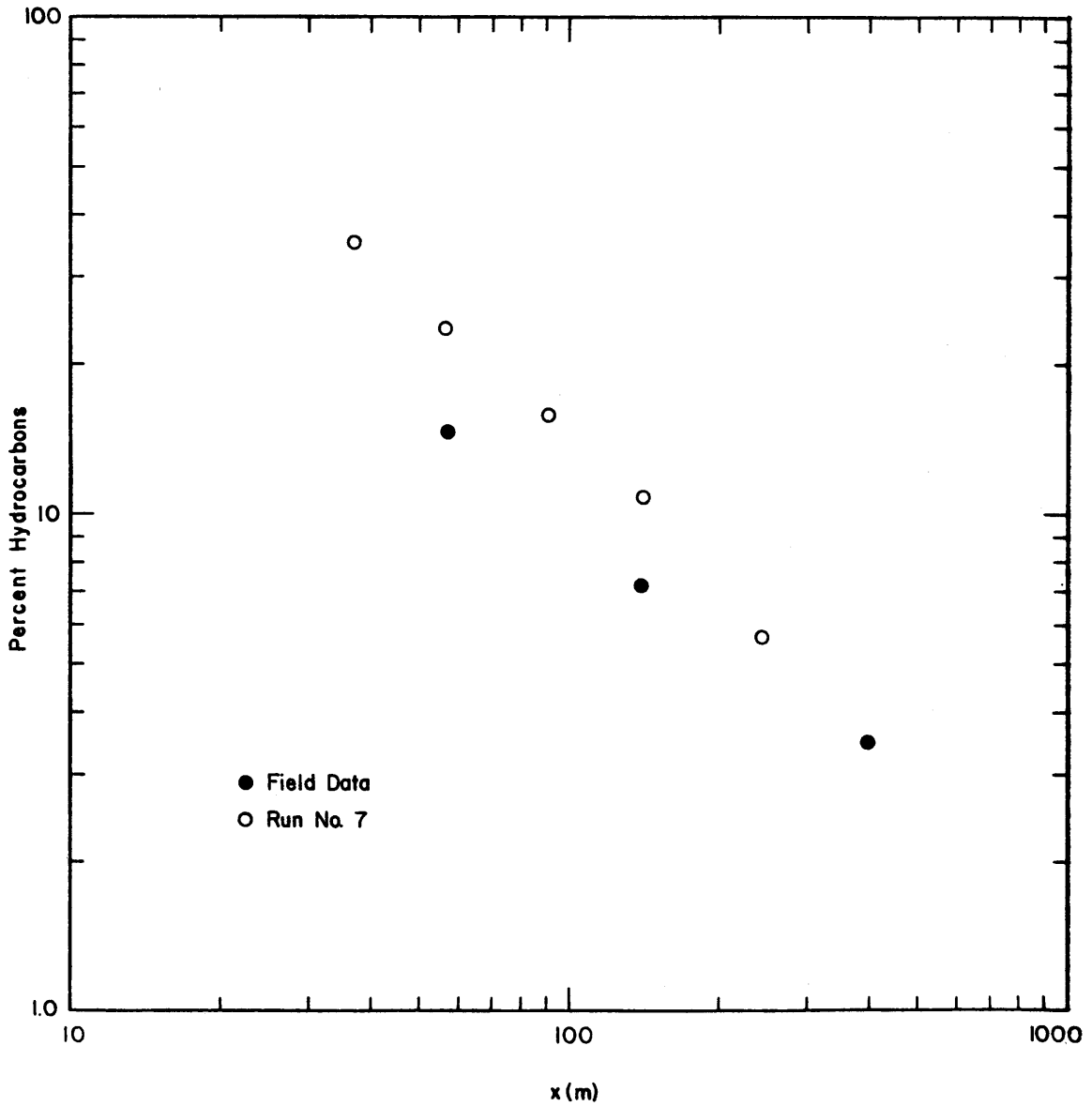

Figure 16-3. Peak Plume Centerline Concentration Decay with Downwind Distance at 1 meter height for Burro 7

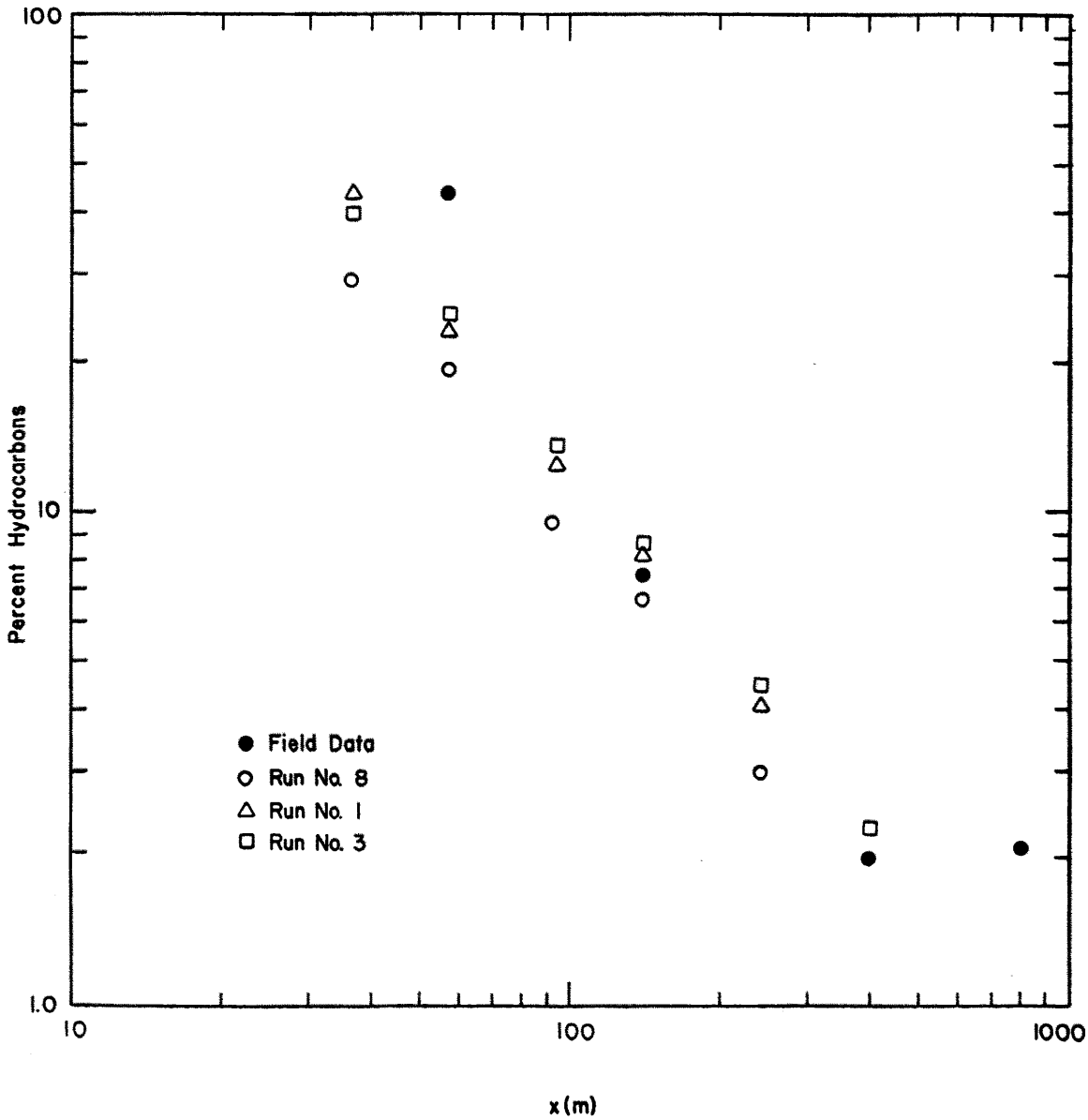

Figure 16-4. Peak Plume Centerline Concentration Decay with Downwind Distance at 1 meter height for Burro 8

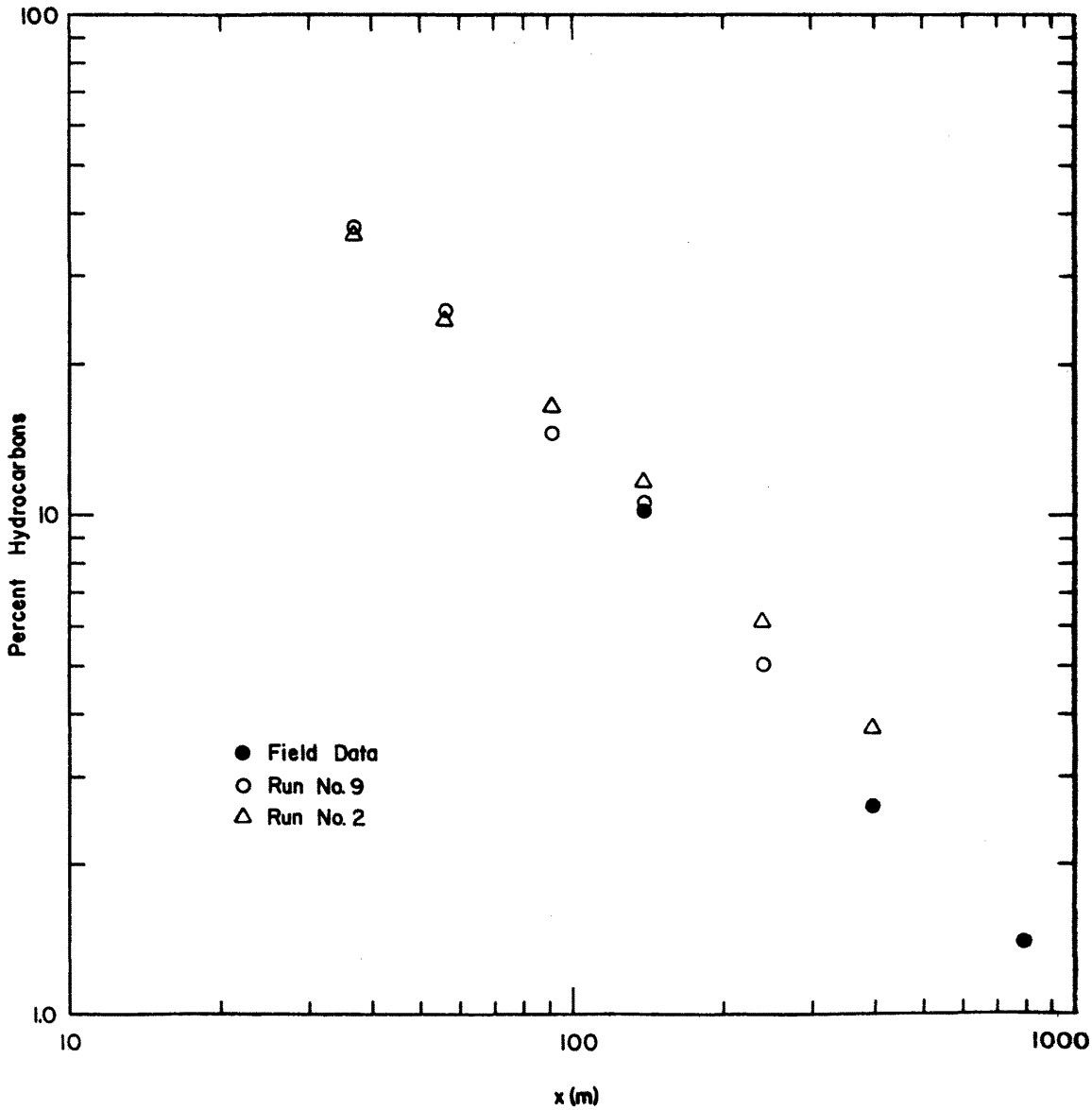

Figure 16-5. Peak Plume Centerline Concentration Decay with Downwind Distance at 1 meter height for Burro 9

Table 4. Figures 17 Reference Code

Figure Number	Run Number	Field Test[30]	Field Position[30] Station	Distance[+] (m)
17-1	4	Burro 4	G4	57
17-2	4	Burro 4	G3	140
17-3	5	Burro 5	T2	57
17-4	5	Burro 5	T3	140
17-5	7	Burro 7	G4	57
17-6	7	Burro 7	G3	140
17-7	1	Burro 8	T2	57
17-8	1	Burro 8	G6	140
17-9	3	Burro 8	T2	57
17-10	3	Burro 8	G6	140
17-11	8	Burro 8	T2	57
17-12	8	Burro 8	G6	140
17-13	2	Burro 9	T4	140
17-14	2	Burro 9	G15	400
17-15	9	Burro 9	T4	140

[+]These are radial distances to concentration sensors at 1 meter height.

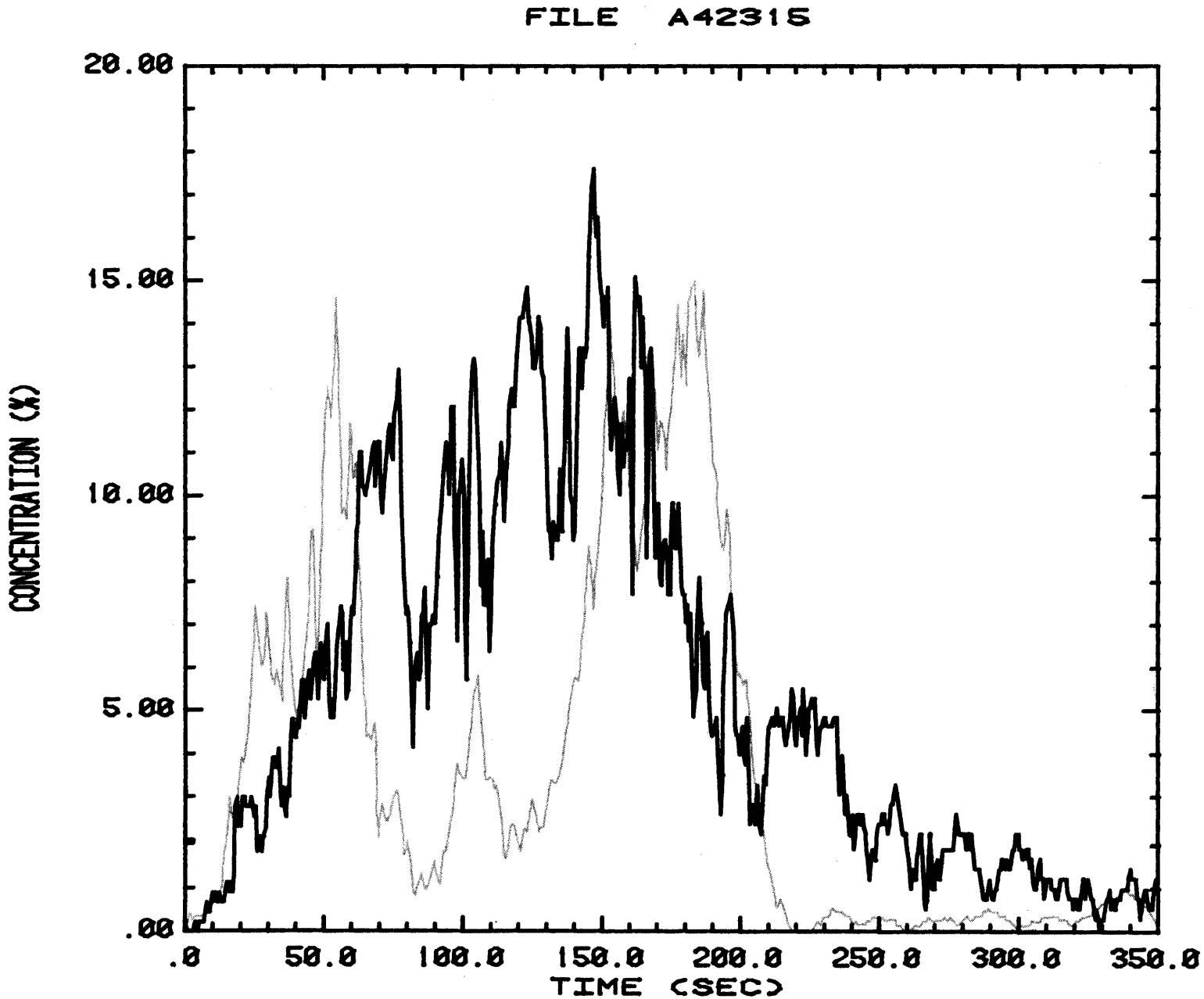

Figure 17-1. Concentration Time History Comparison between Burro 4 and Run 4, Position G4

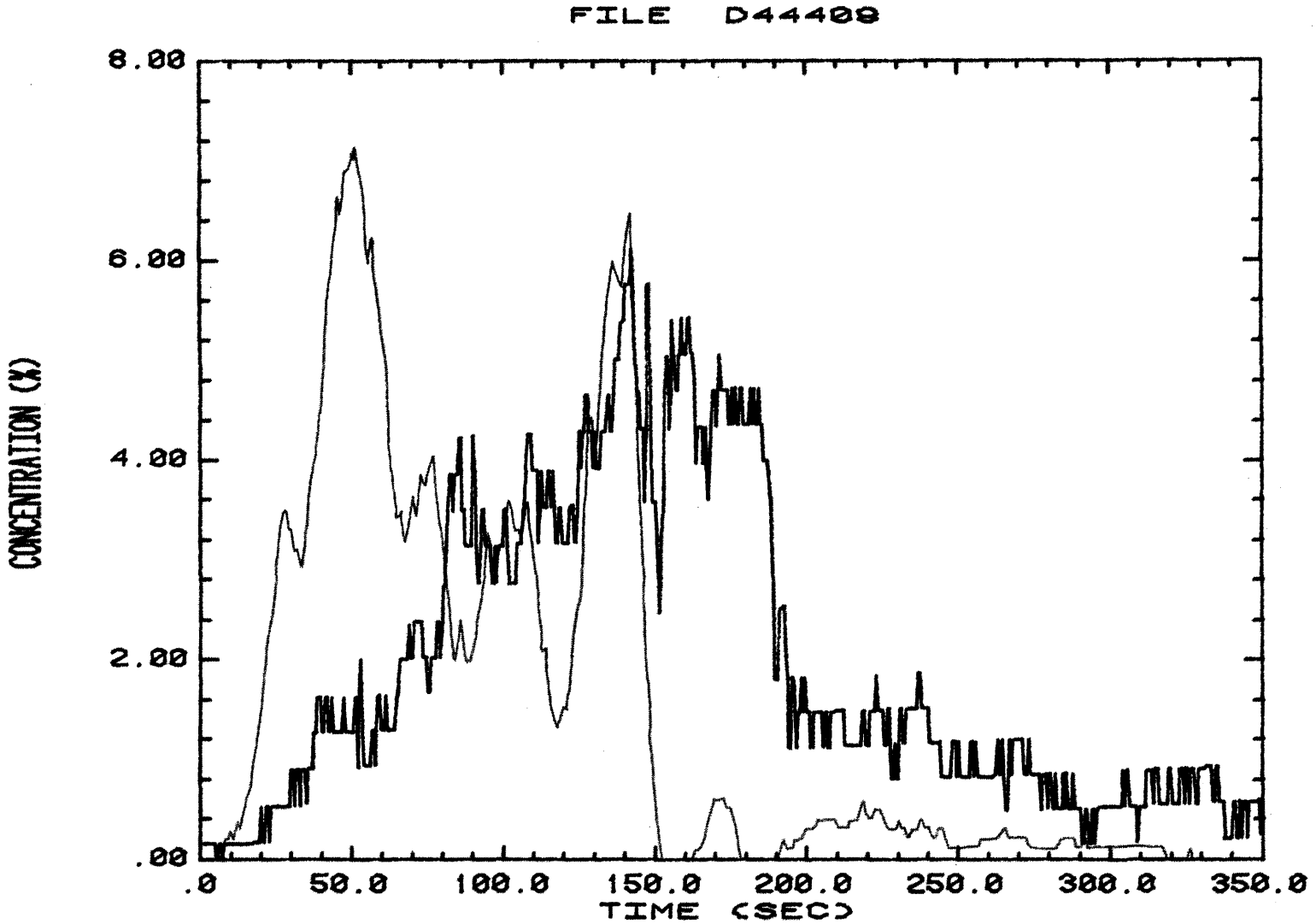

Figure 17-2. Concentration Time History Comparison between Burro 4 and Run 4, Position G3

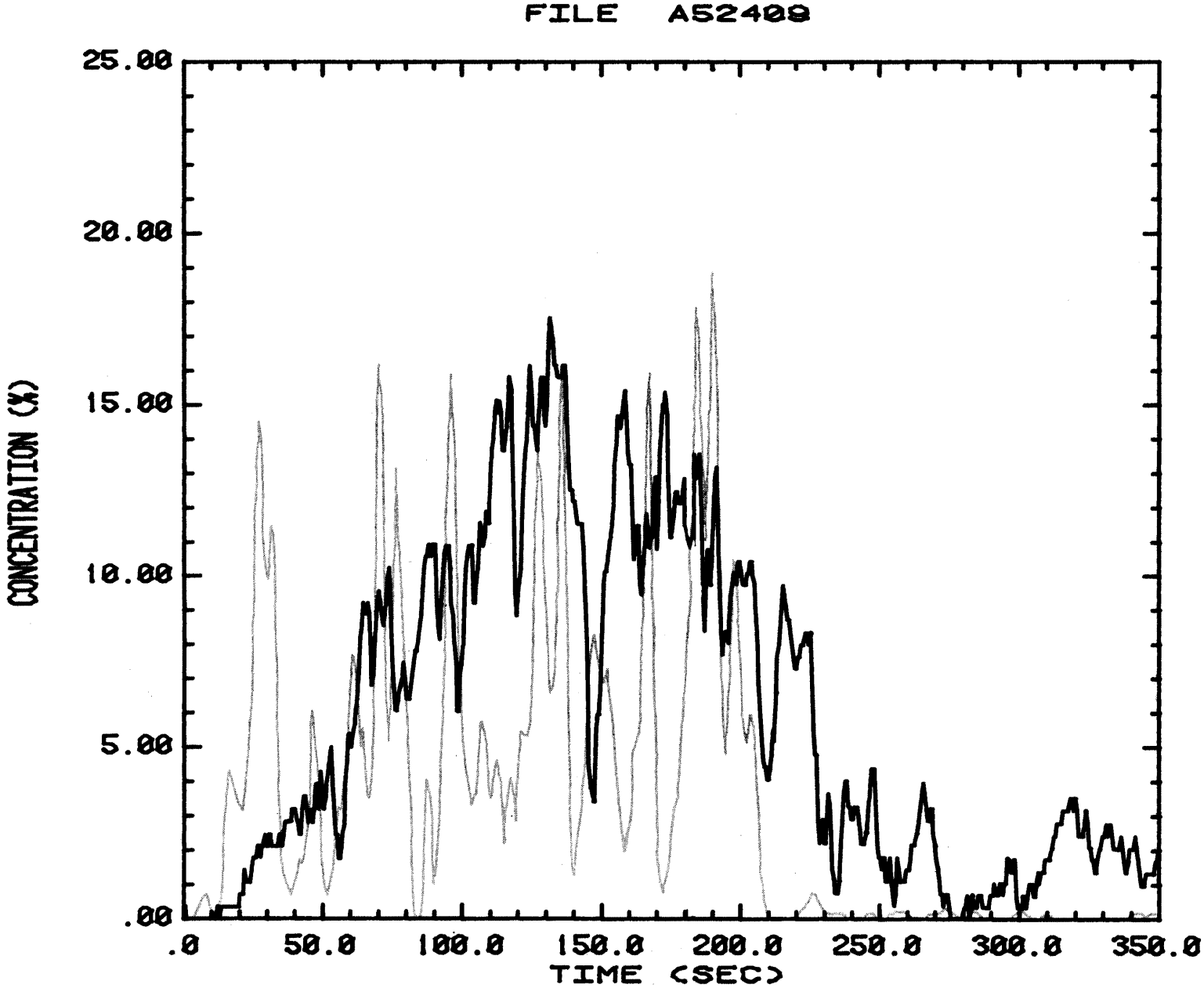

Figure 17-3. Concentration Time History Comparison between Burro 5 and Run 5, Position T2

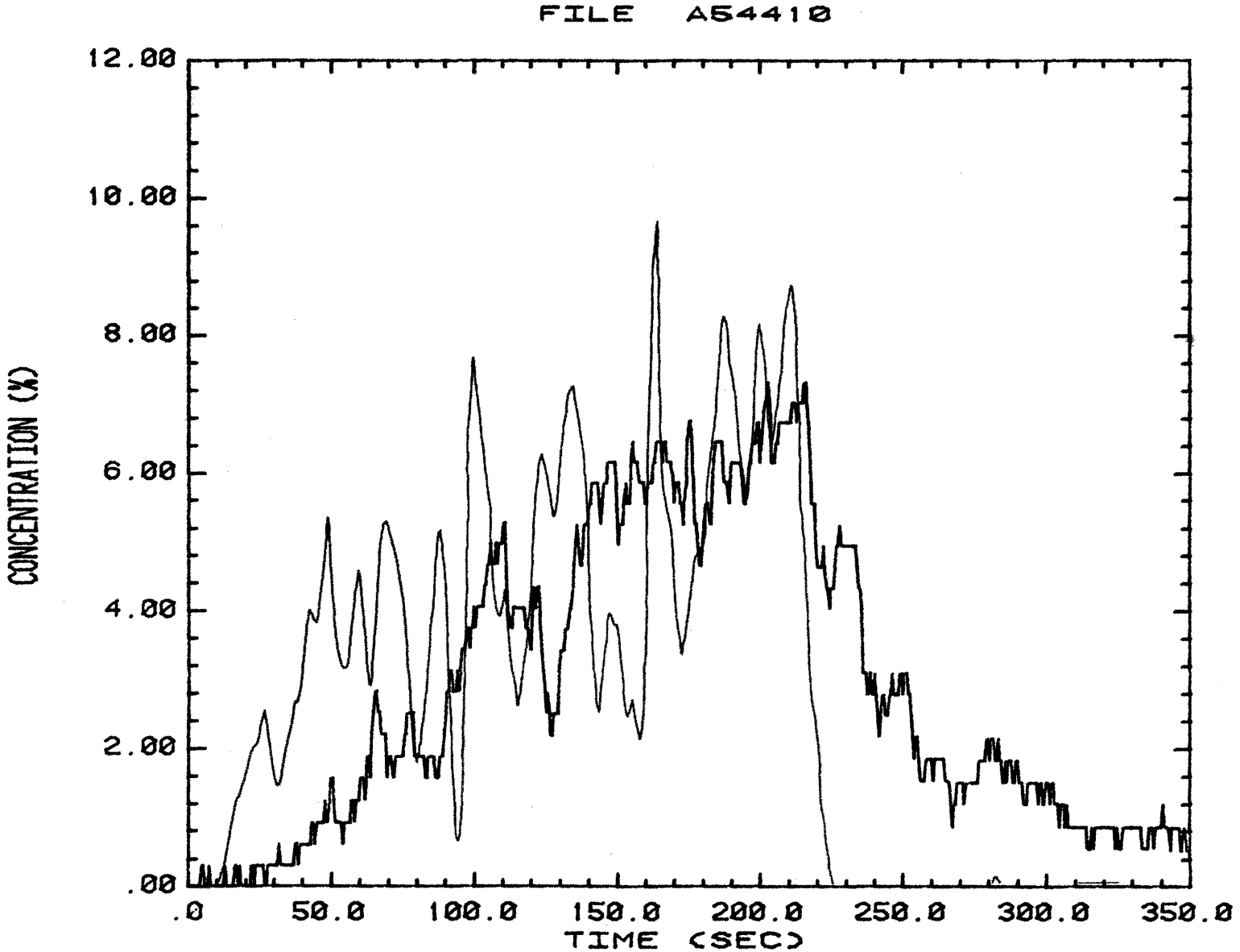

Figure 17-4. Concentration Time History Comparison between Burro 5 and Run 5, Position T3

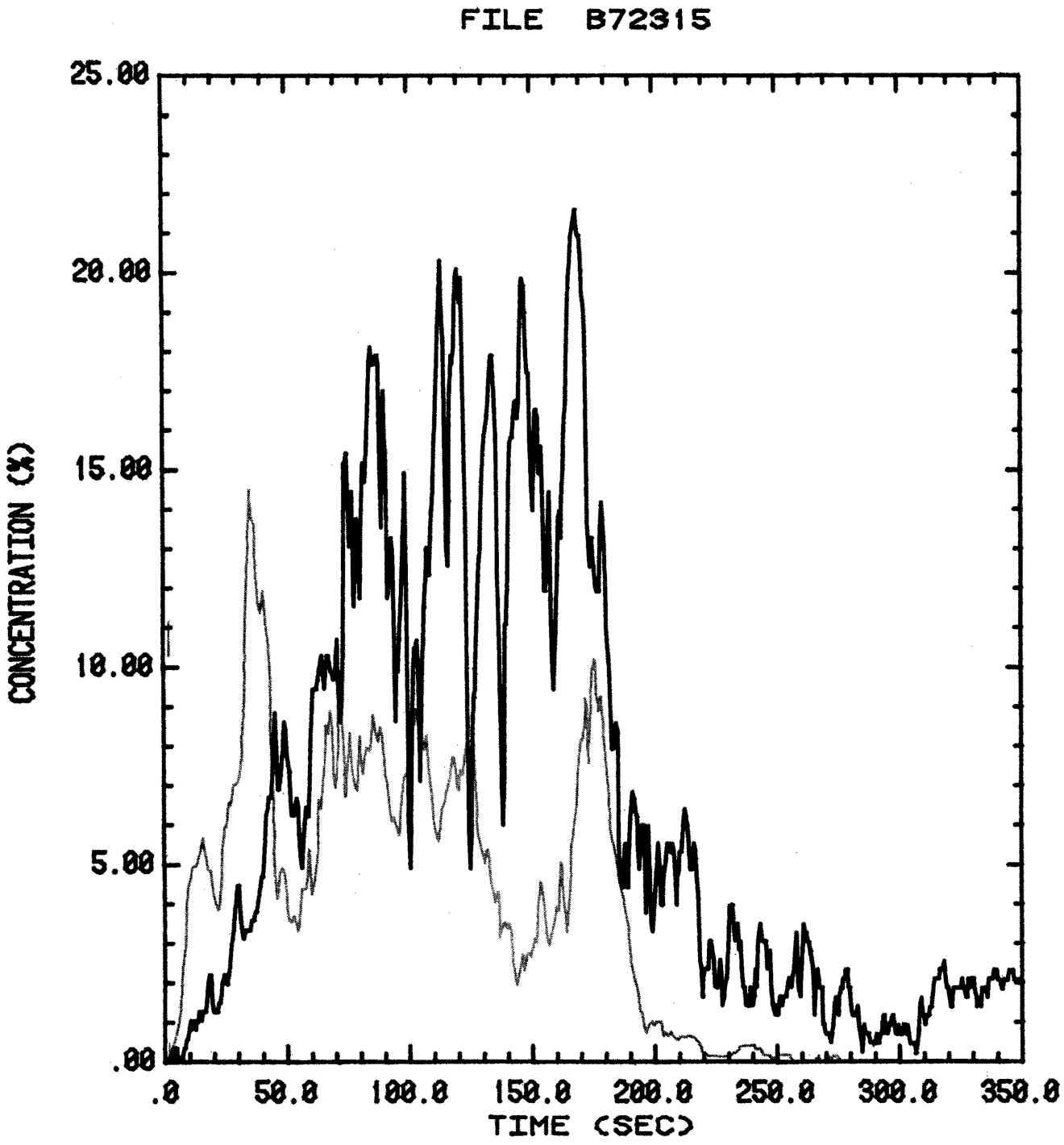

Figure 17-5. Concentration Time History Comparison between Burro 7 and Run 7, Position G4

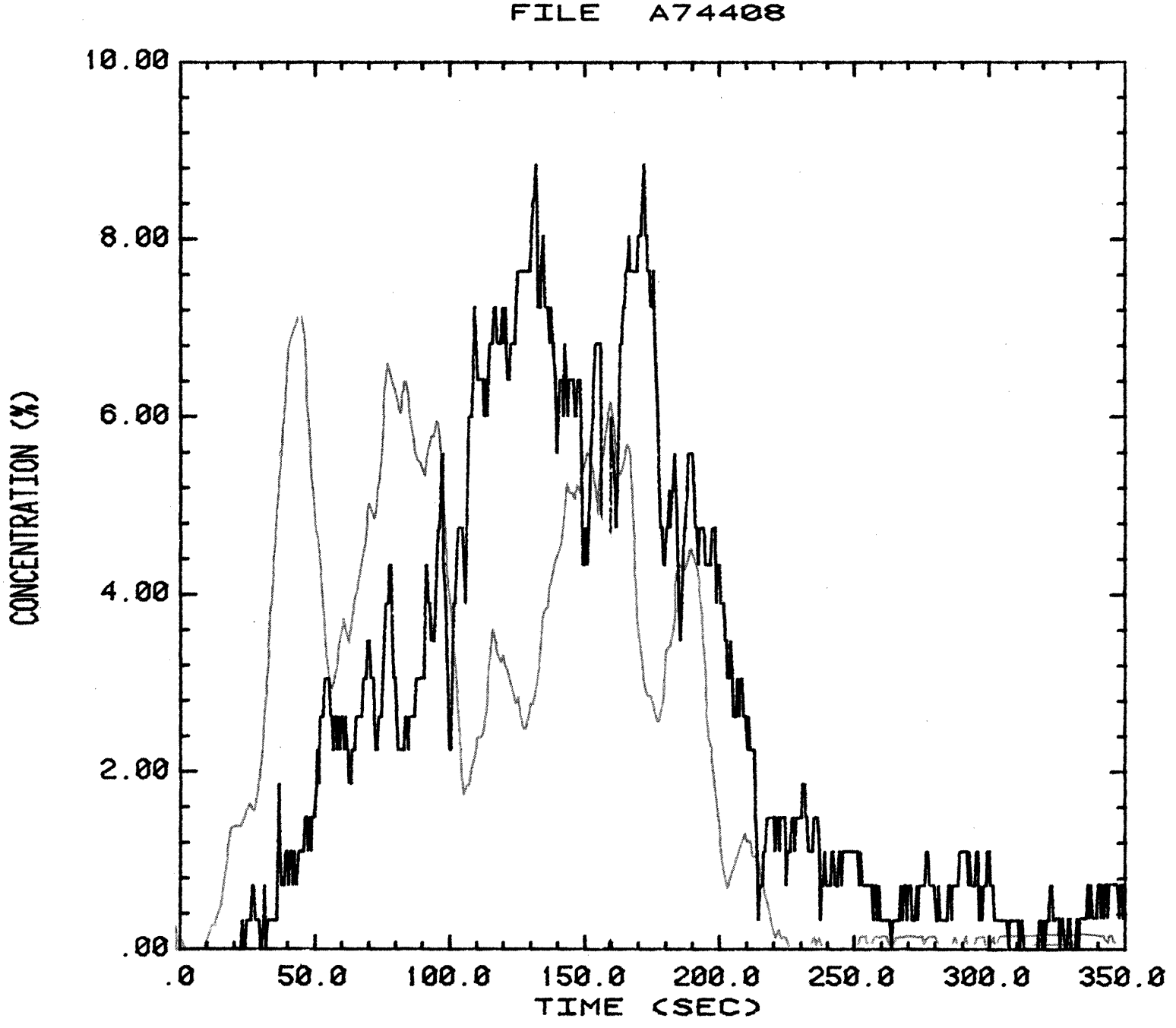

Figure 17-6. Concentration Time History Comparison between Burro 7 and Run 7, Position G3

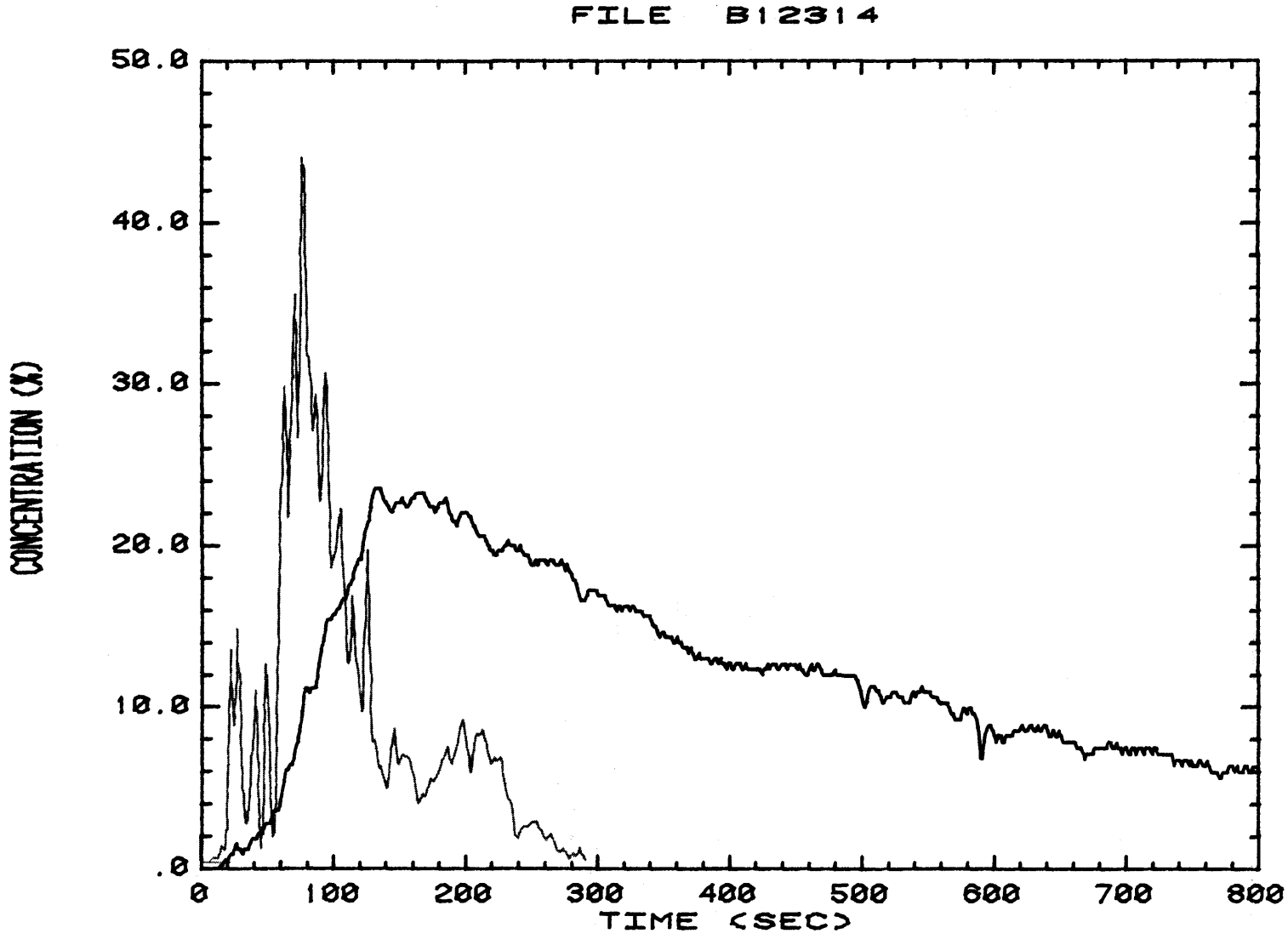

Figure 17-7. Concentration Time History Comparison between Burro 8 and Run 1, Position T2

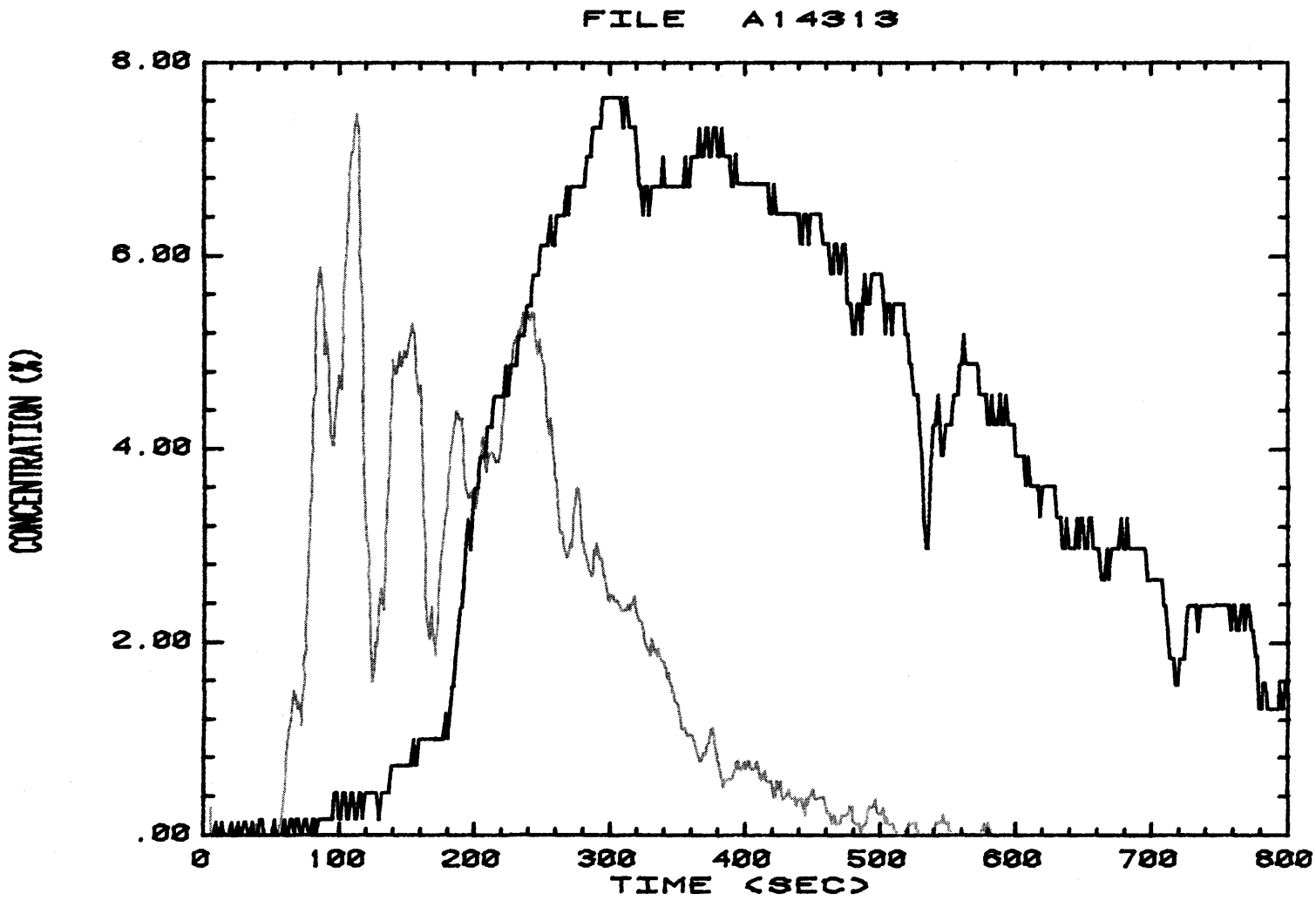

Figure 17-8. Concentration Time History Comparison between Burro 8 and Run 1, Position G6

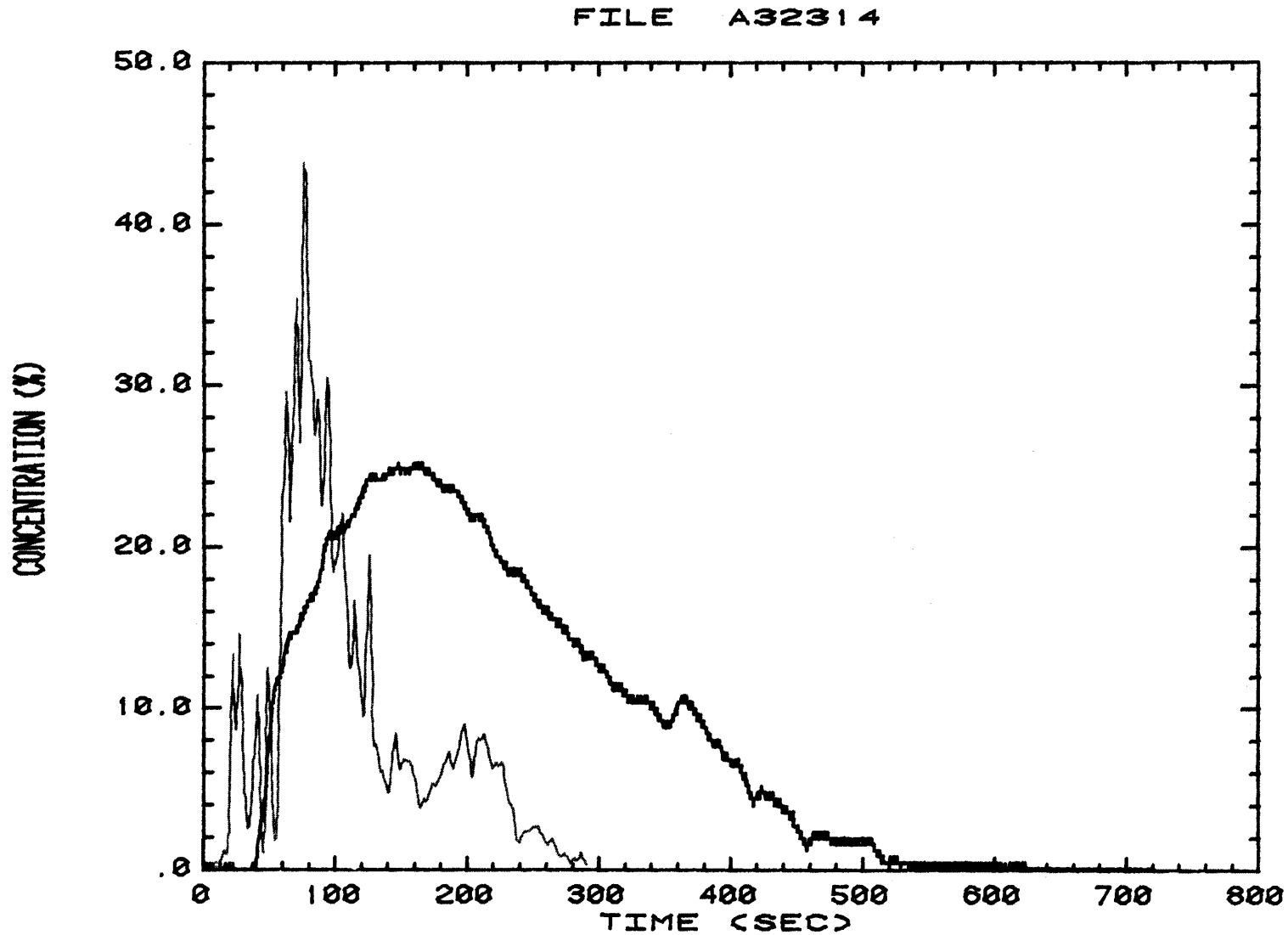

Figure 17-9. Concentration Time History Comparison between Burro 8 and Run 3, Position T2

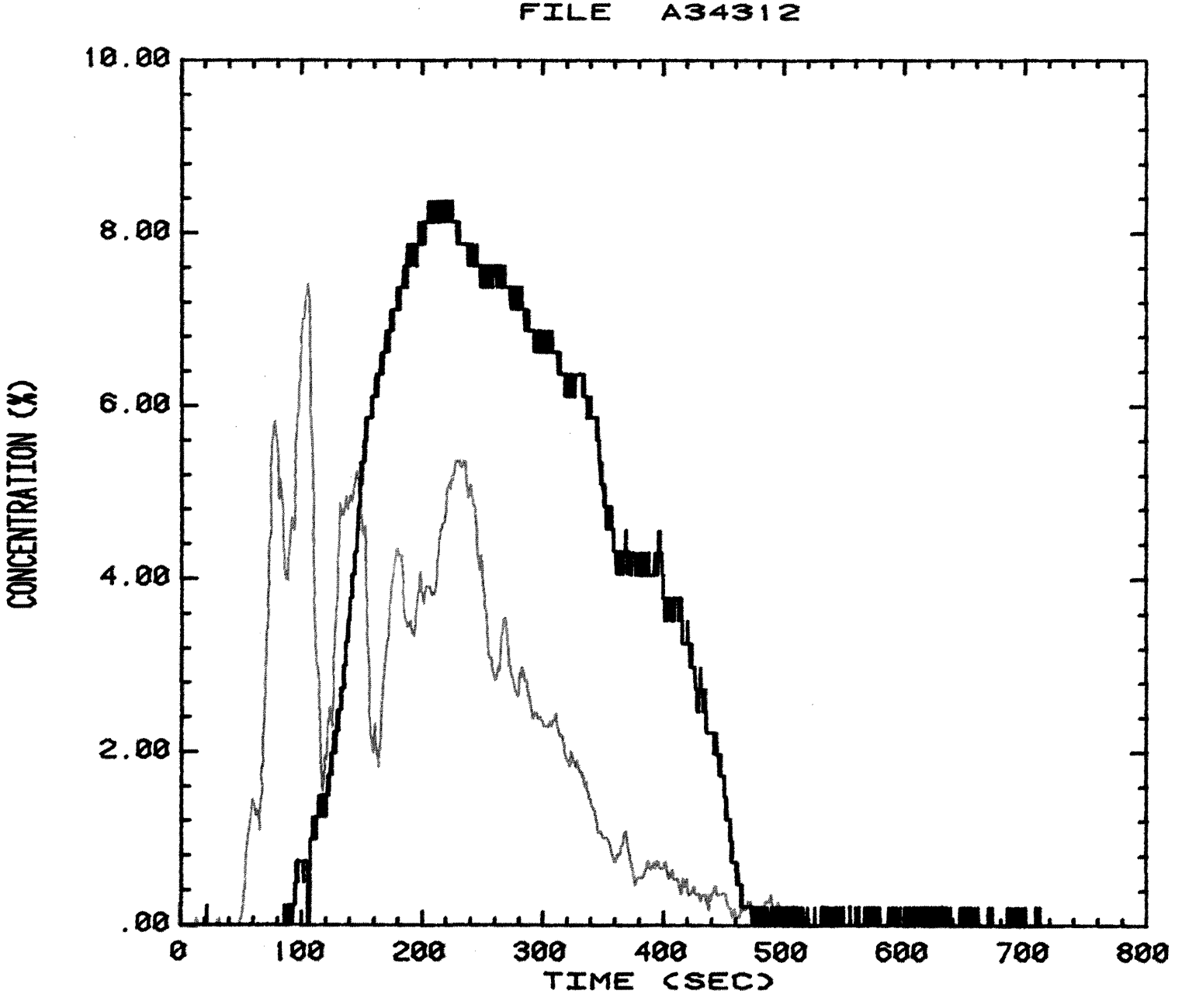

Figure 17-10. Concentration Time History Comparison between Burro 8 and Run 3, Position G6

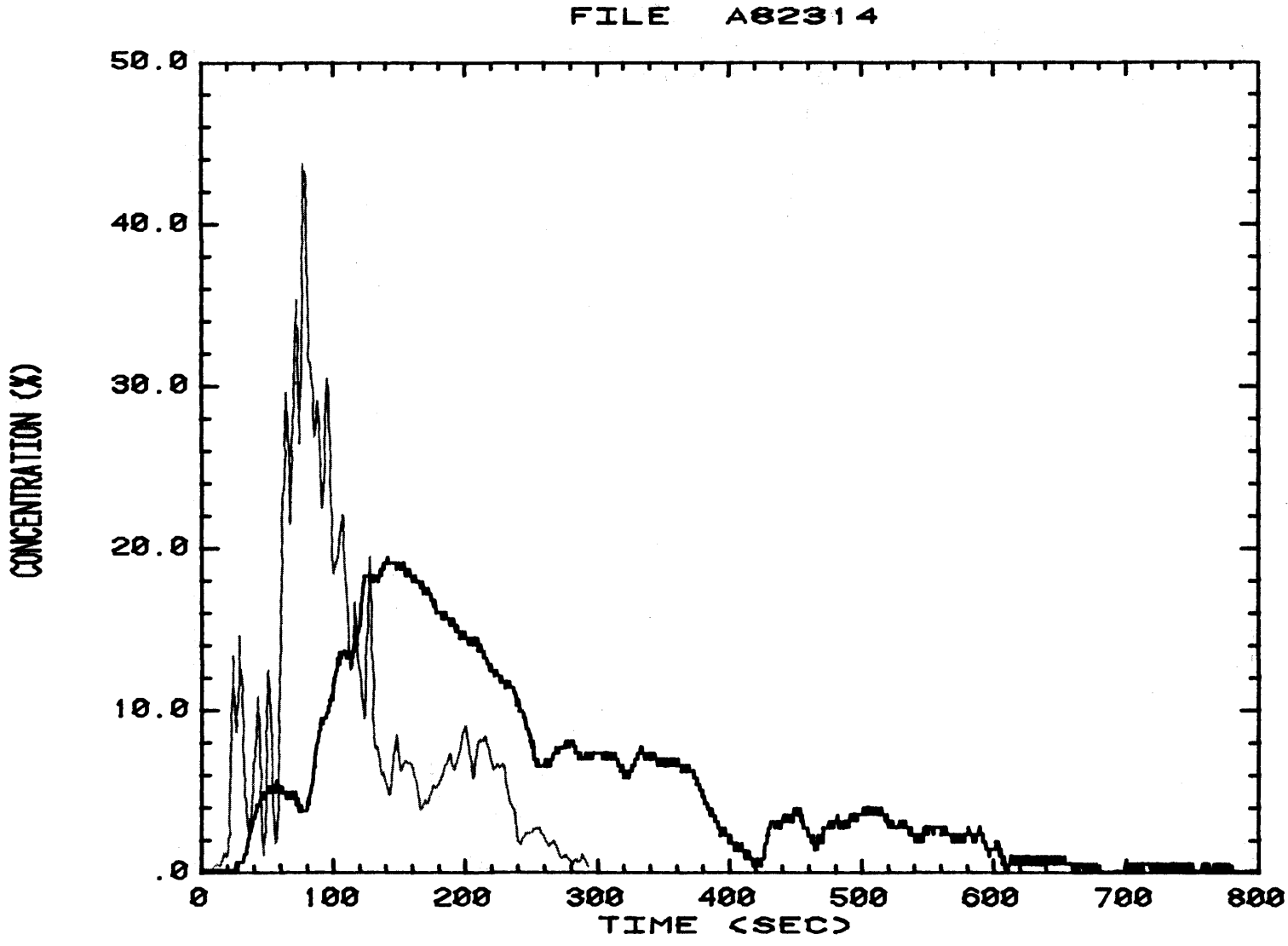

Figure 17-11. Concentration Time History Comparison between Burro 8 and Run 8, Position T2

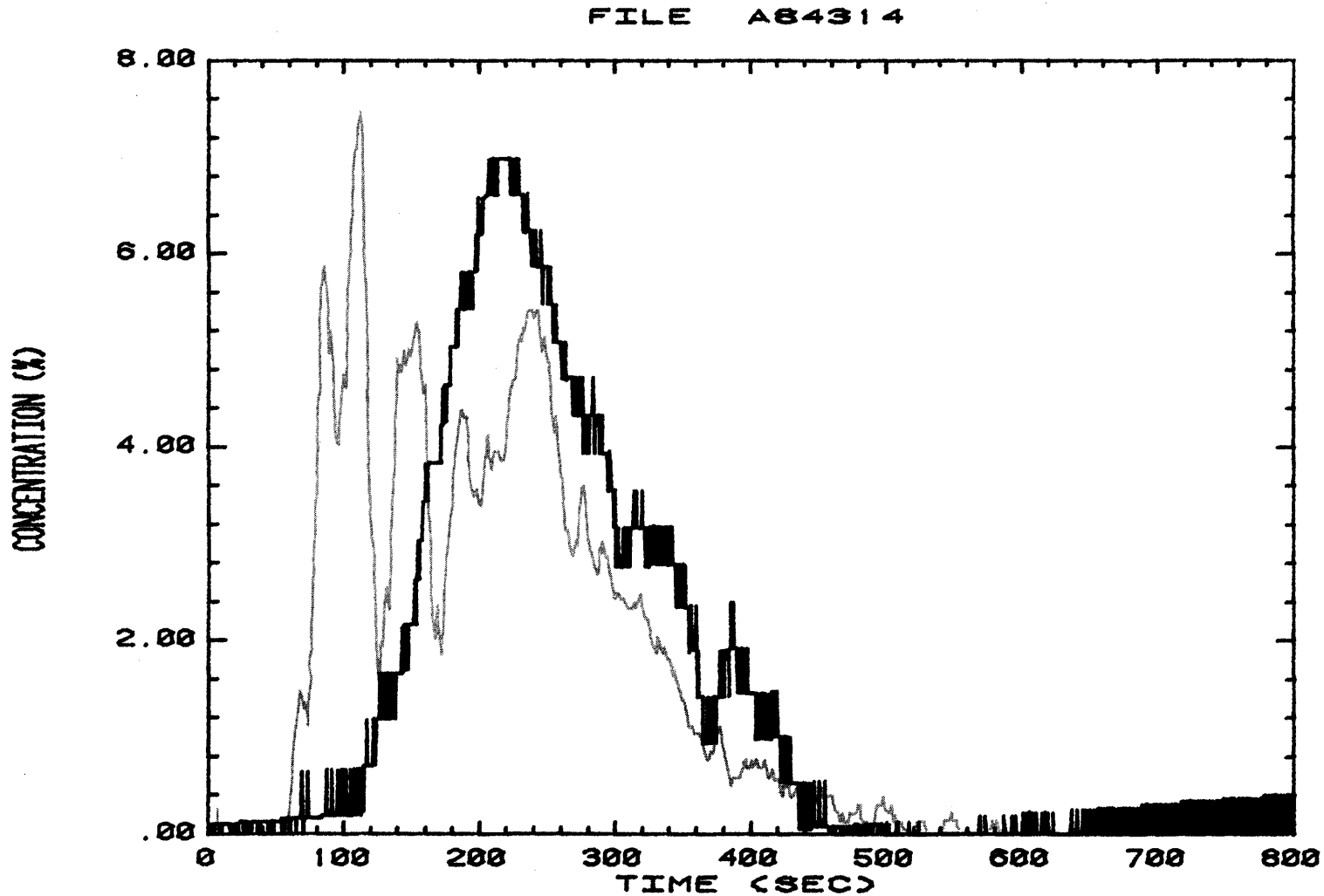

Figure 17-12. Concentration Time History Comparison between Burro 8 and Run 8, Position G6

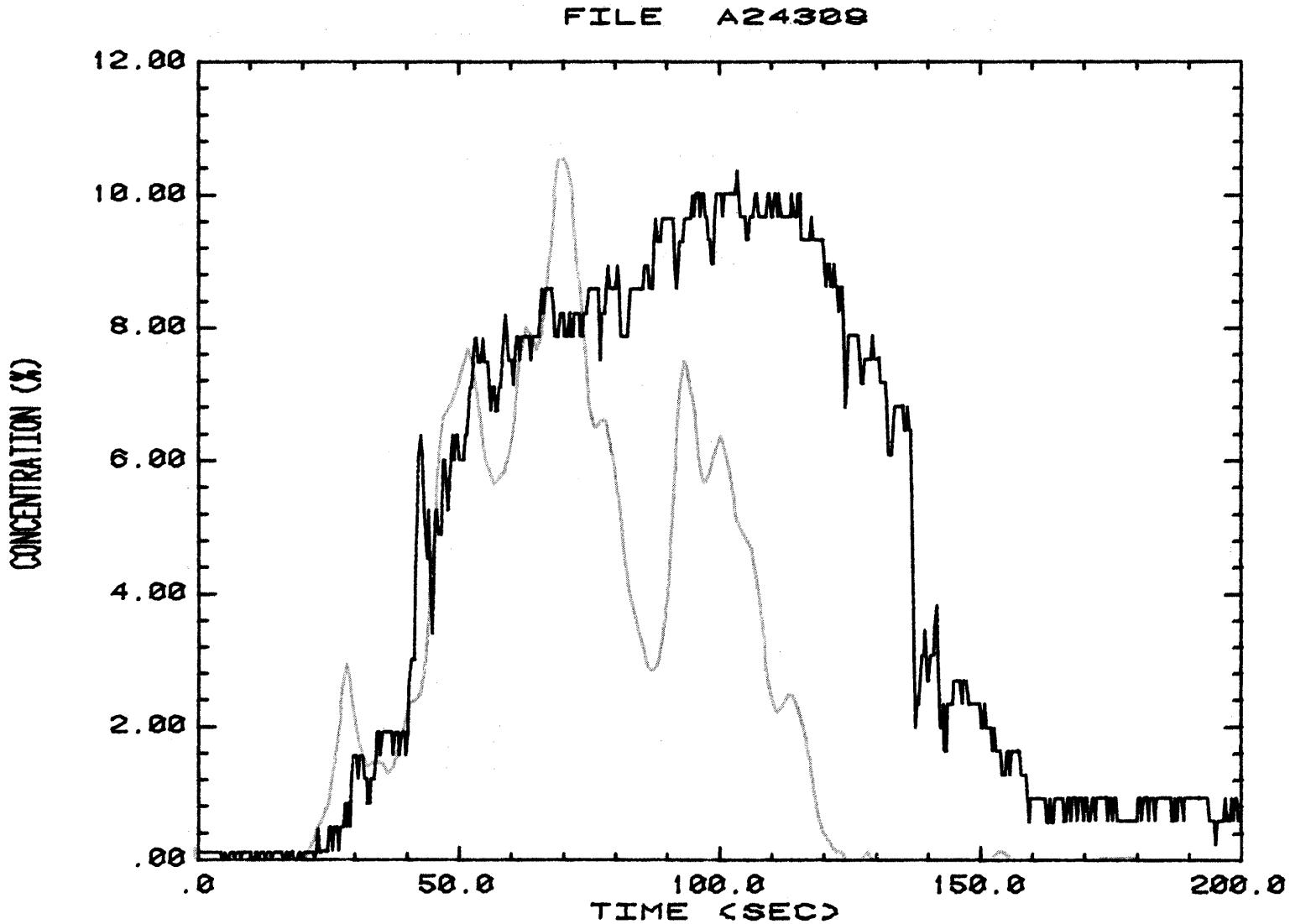

Figure 17-13. Concentration Time History Comparison between Burro 9 and Run 2, Position T4

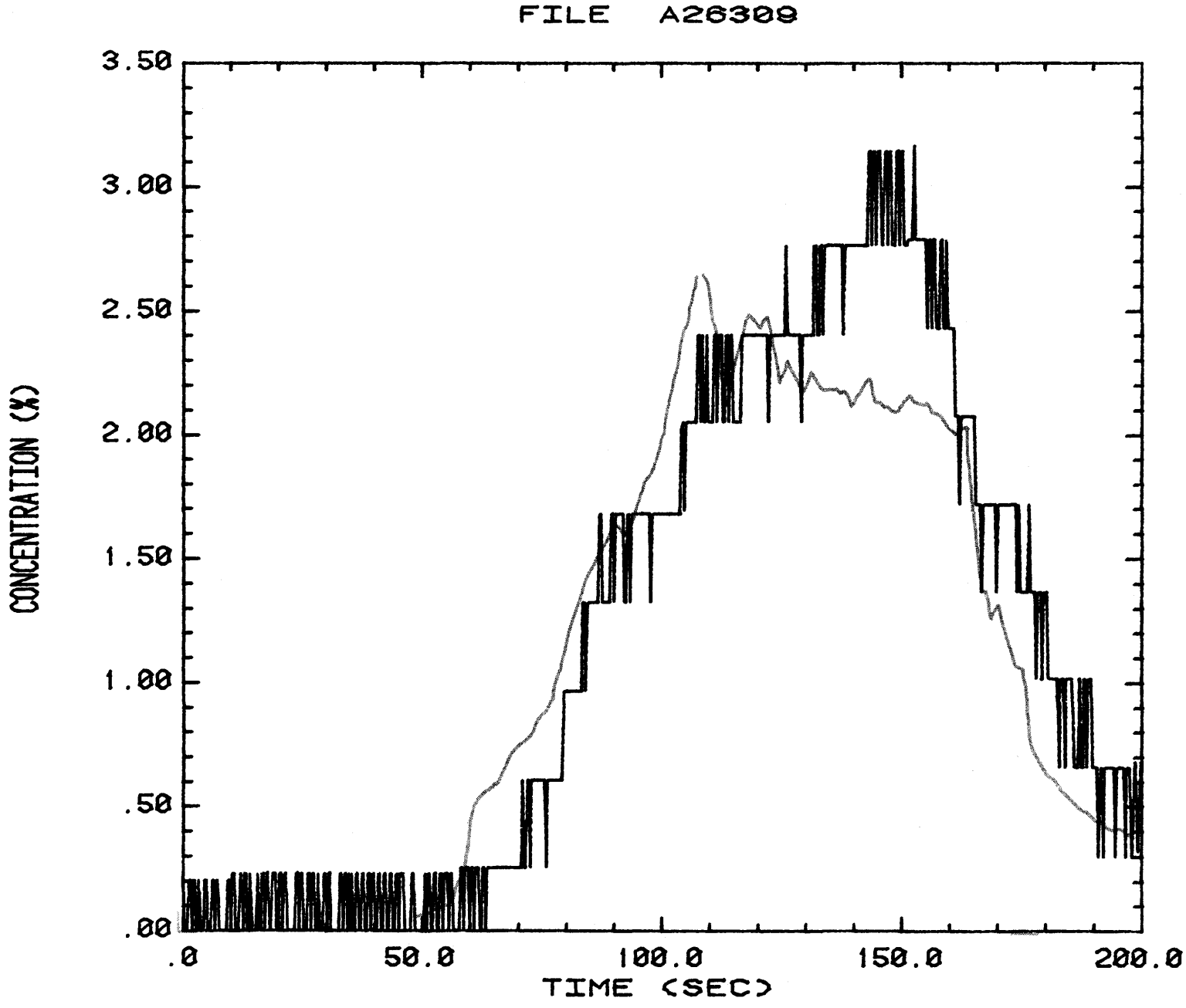

Figure 17-14. Concentration Time History Comparison between Burro 9 and Run 2, Position G15

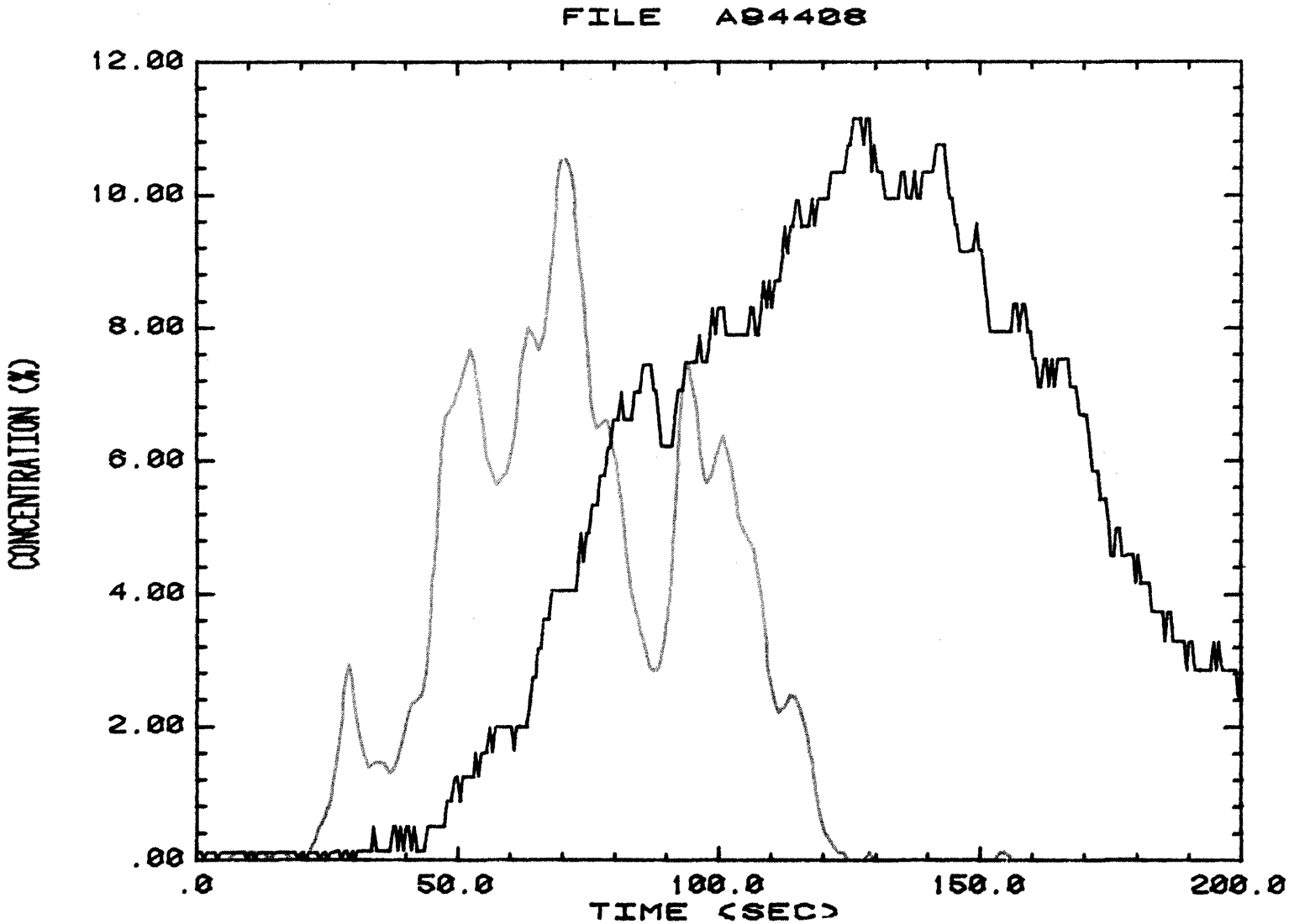

Figure 17-15. Concentration Time History Comparison between Burro 9 and Run 9, Position T4

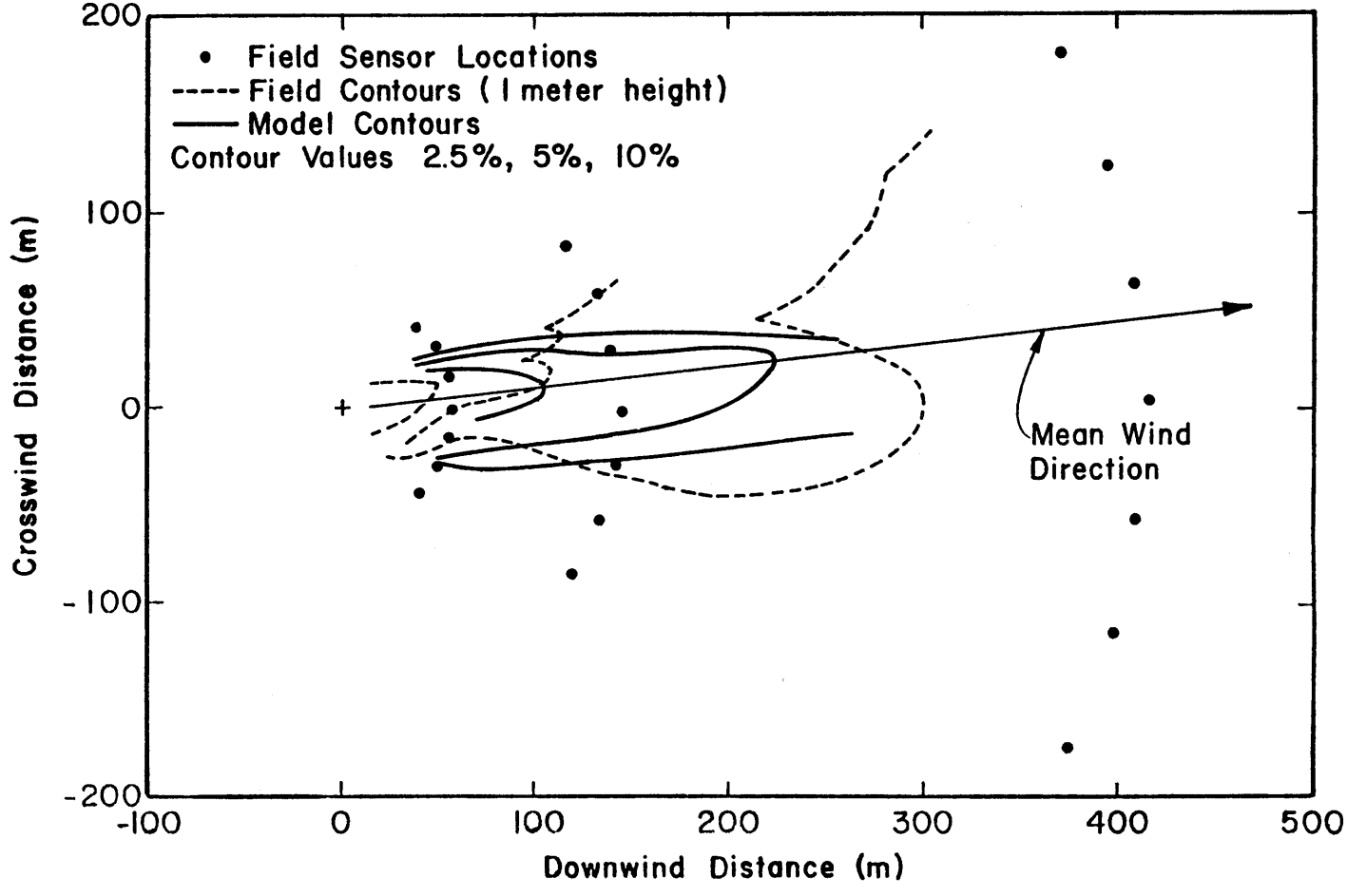

Figure 18-1. Ground Level Concentration Extent Comparison between Burro 4 and Run 4

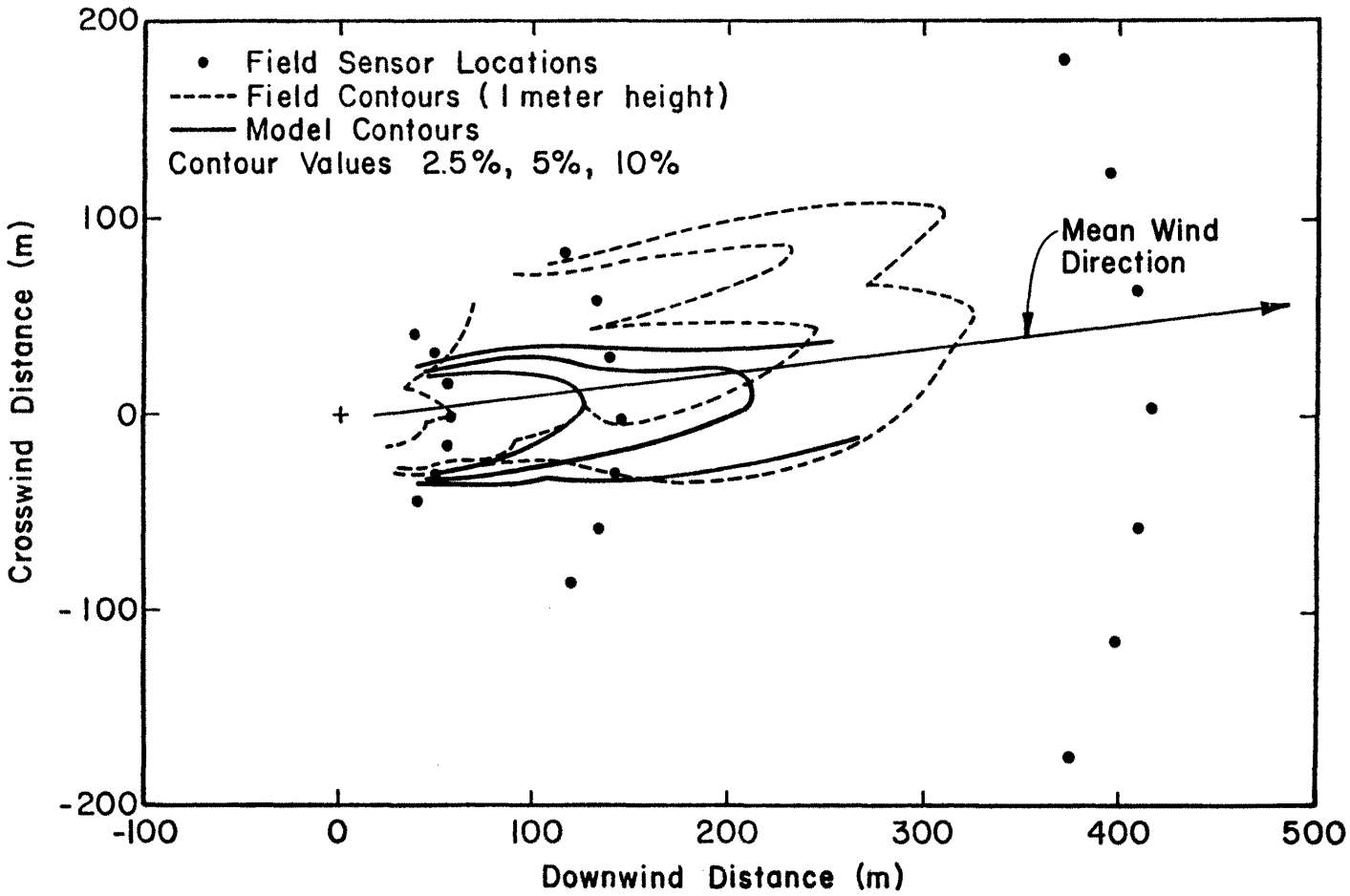

Figure 18-2. Ground Level Concentration Extent Comparison between Burro 5 and Run 5

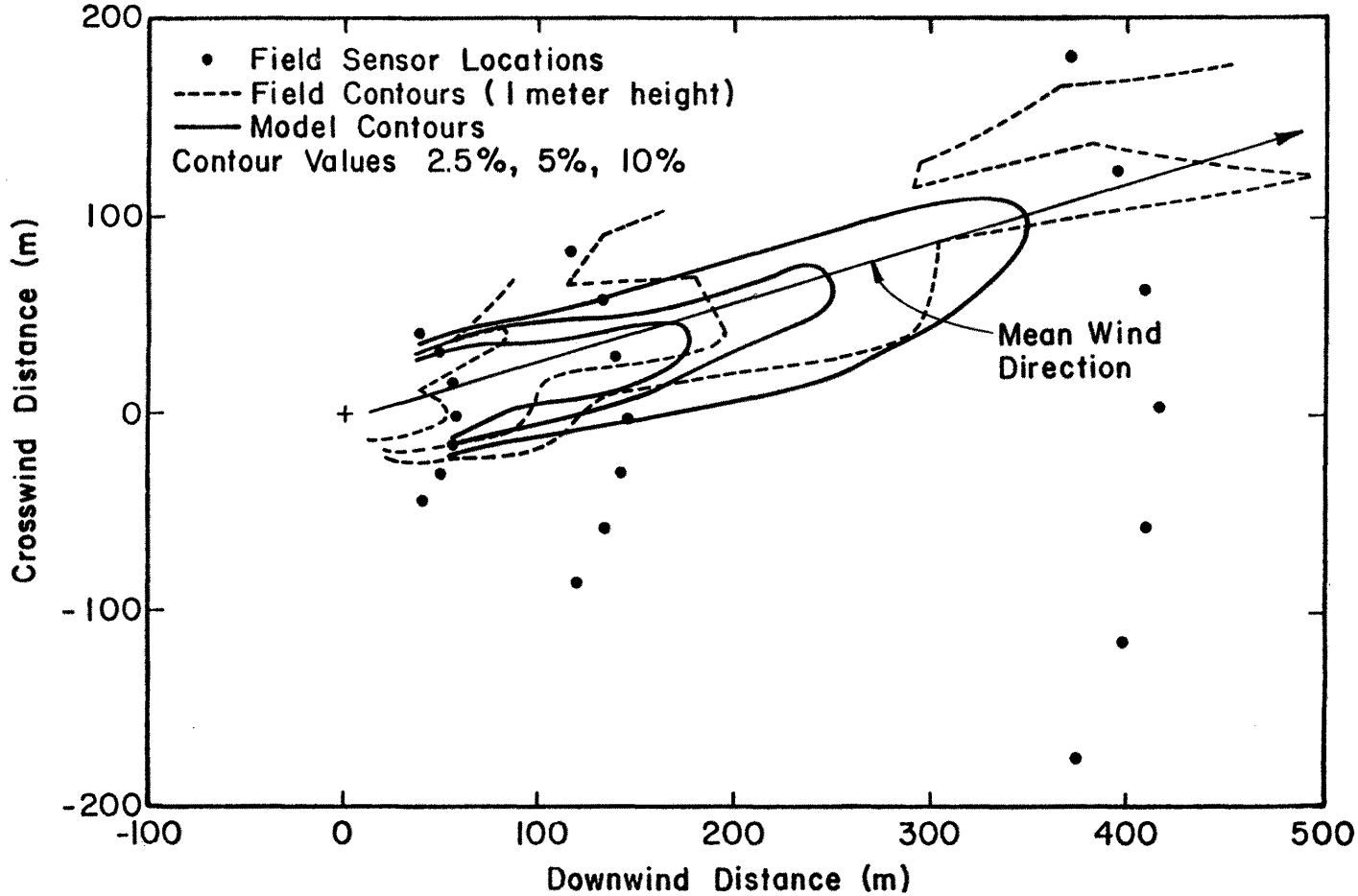

Figure 18-3. Ground Level Concentration Extent Comparison between Burro 7 and Run 7

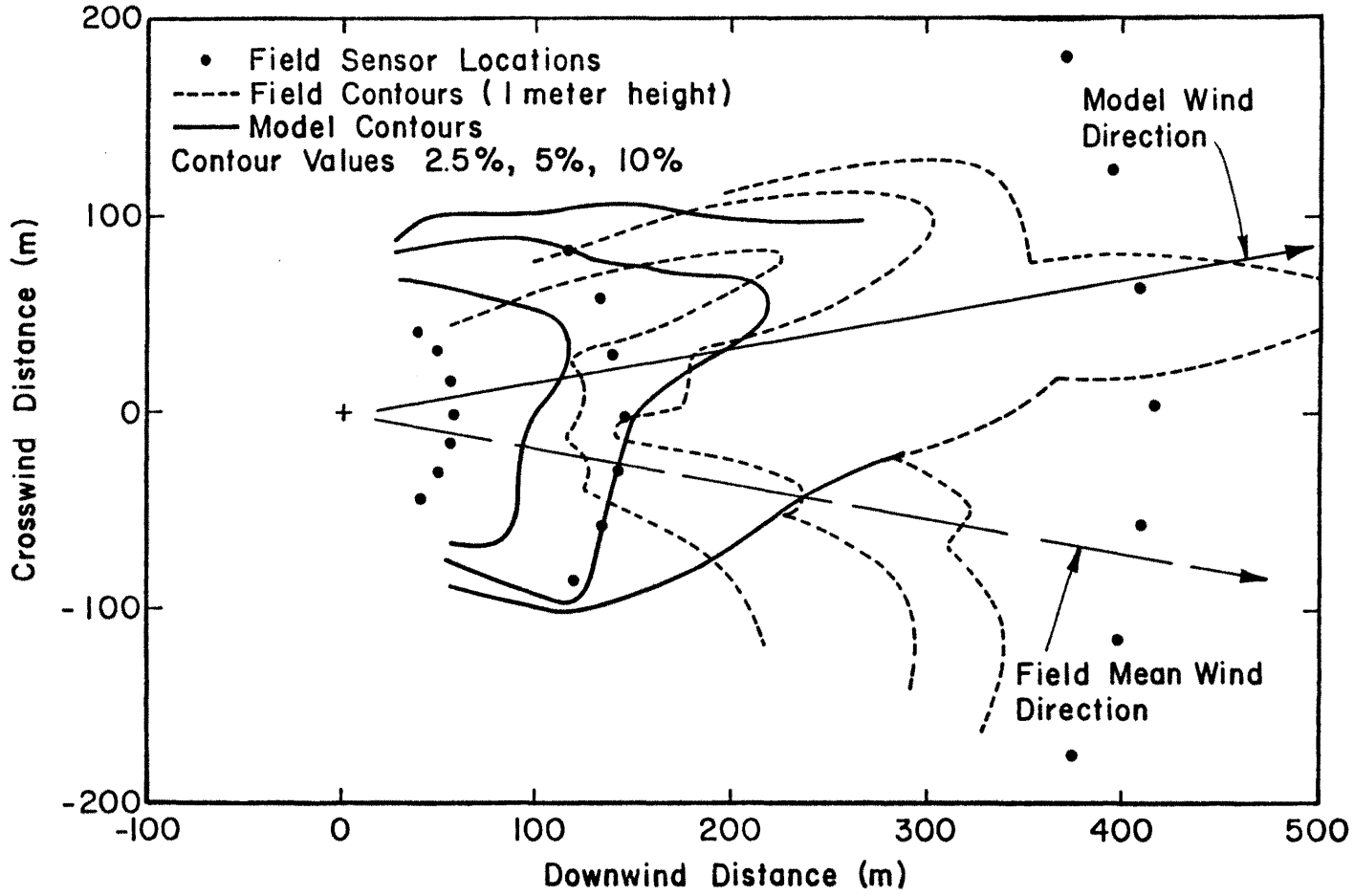

Figure 18-4. Ground Level Concentration Extent Comparison between Burro 8 and Run 1

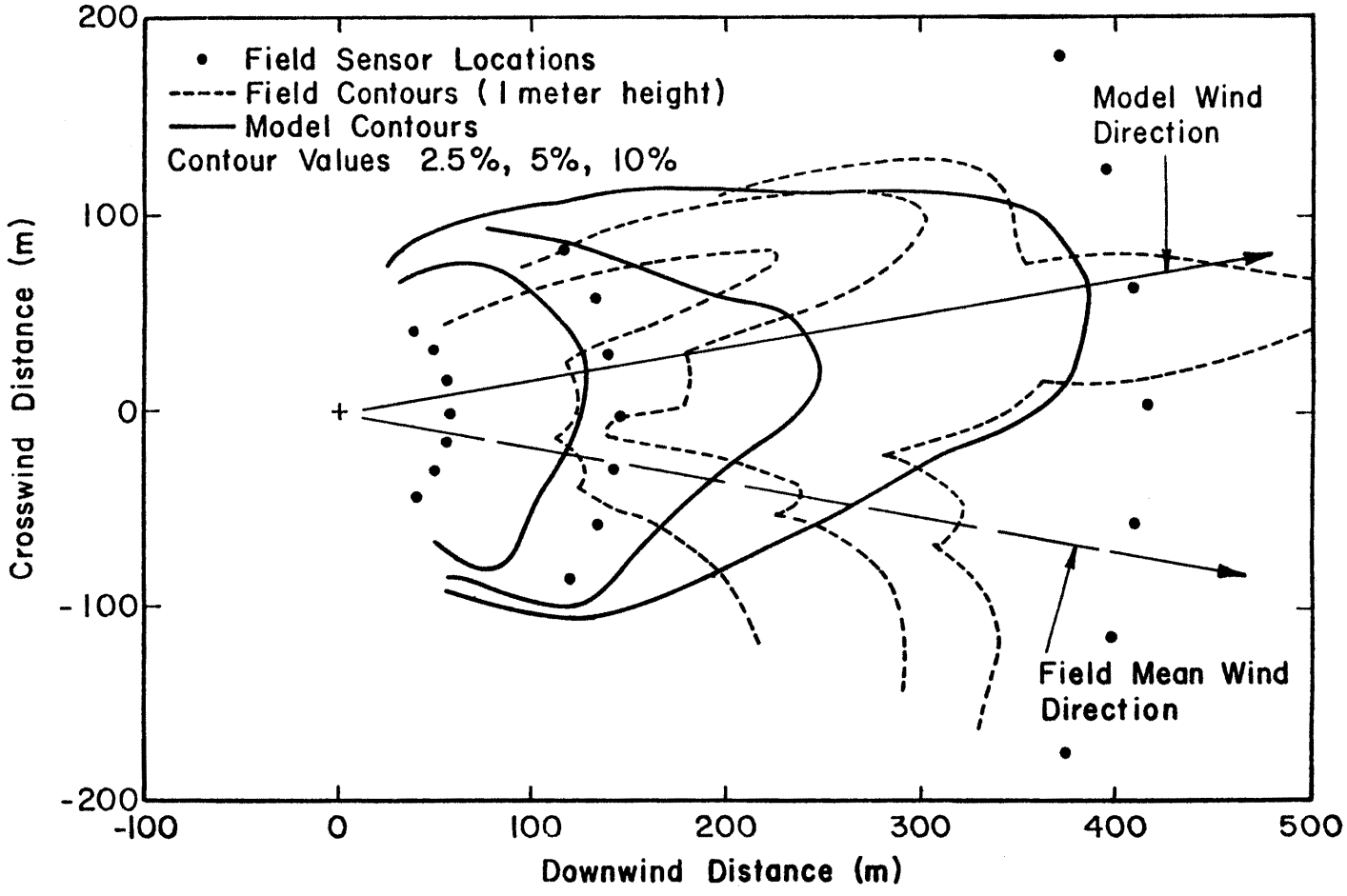

Figure 18-5. Ground Level Concentration Extent Comparison between Burro 8 and Run 3

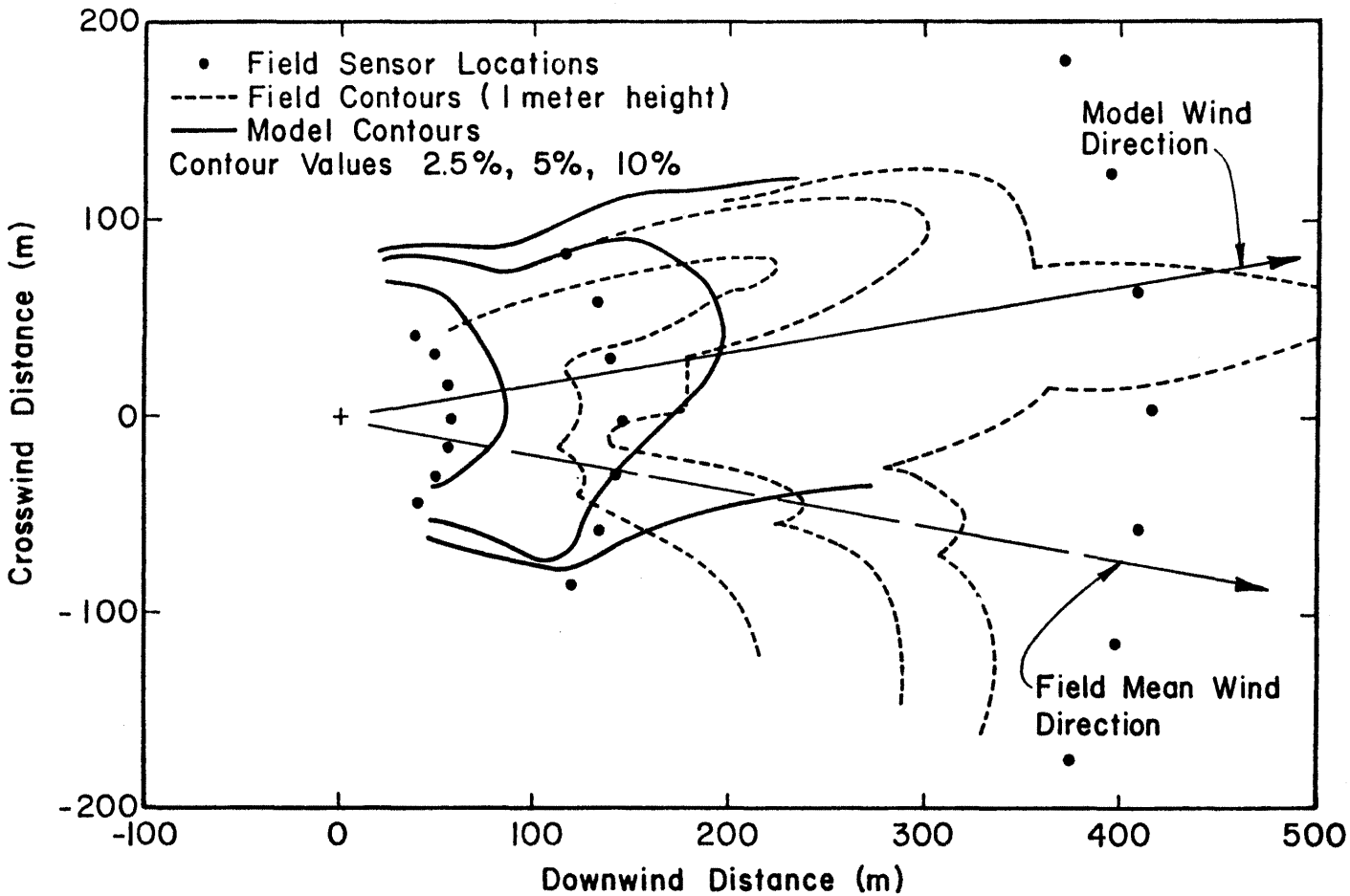

Figure 18-6. Ground Level Concentration Extent Comparison between Burro 8 and Run 8

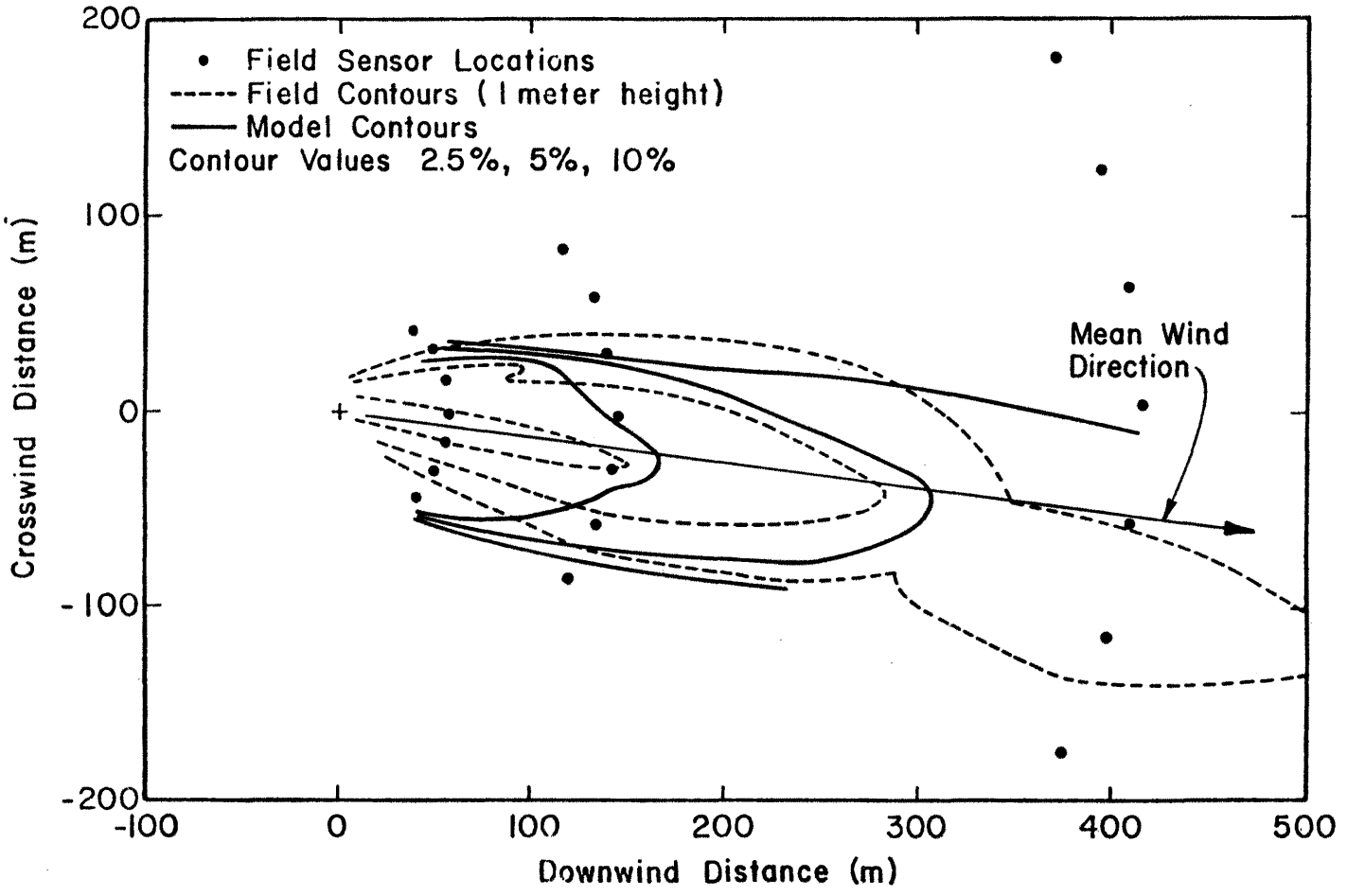

Figure 18-7. Ground Level Concentration Extent Comparison between Burro 9 and Run 2

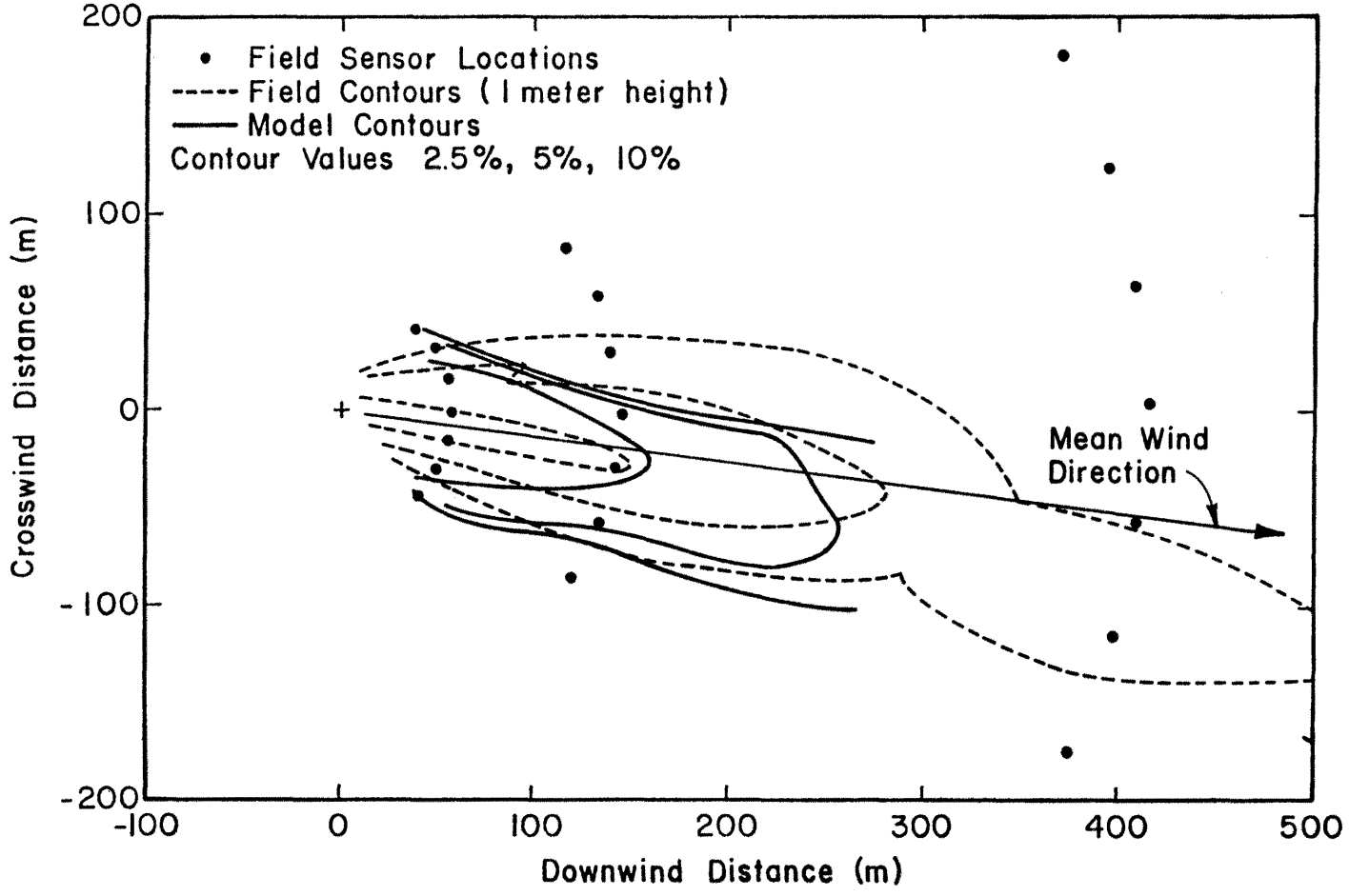

Figure 18-8. Ground Level Concentration Extent Comparison between Burro 9 and Run 9

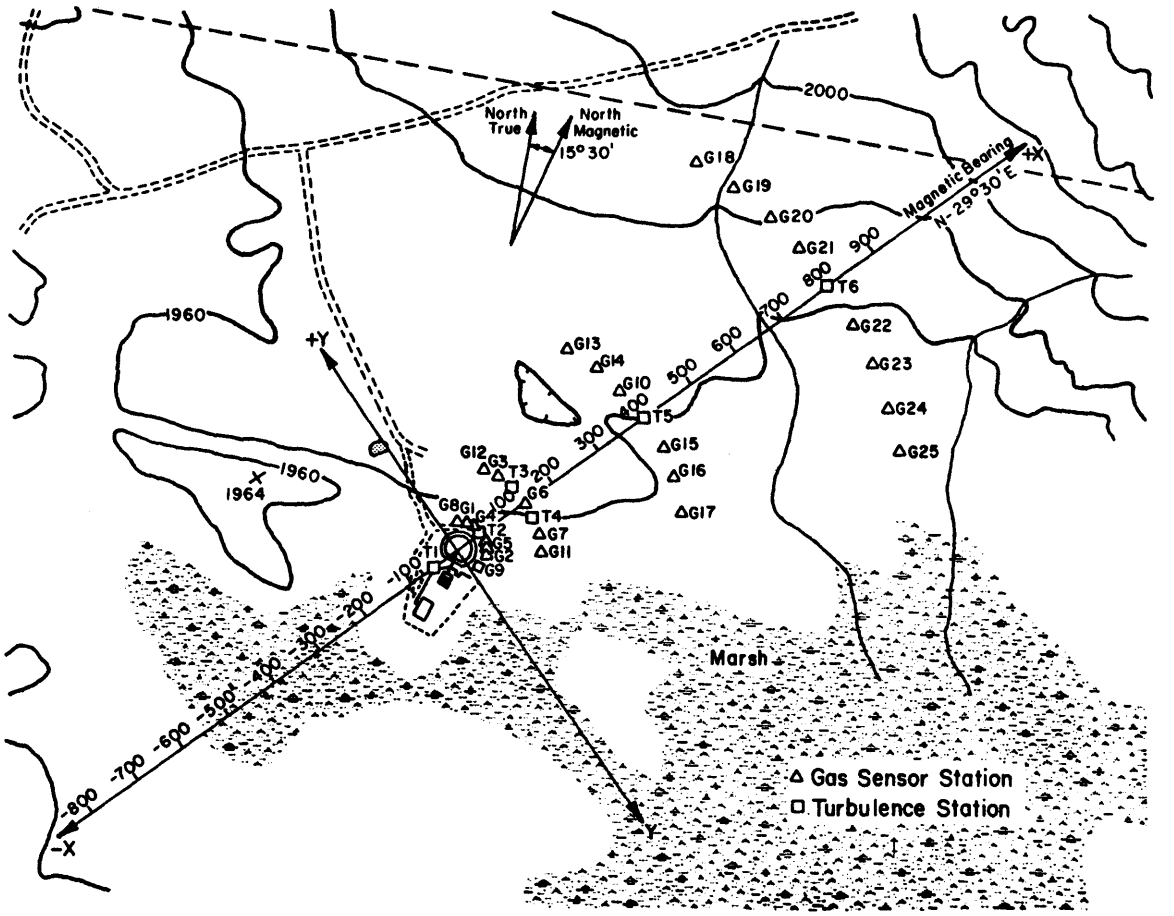

Figure 19. Field Gas Sensor Location Map

wind approach vector was sometimes substantial during the field tests some liberty was taken during the model/field comparisons to compare plume centerline values even when they were not measured at spatially equivalent locations. Unfortunately for the case of the model Runs 1, 3, and 8 which were intended to model Burro 8 the topographic model was incorrectly turned to 215° from the North rather than the 235° as specified by the field measured mean wind direction. Nonetheless comparisons are made with the field data by rotating the measured model data 20° to coincide with the field wind direction. It is unfortunate that this mistake occurred since Burro 8 was the run most susceptable to the influences of topography. The comparisons shown in Figures 16-4, 17-7 through 17-12, and 18-4 through 18-6 should be viewed somewhat skeptically when drawing conclusions about model-field comparisons. Indeed it may be better to interpret Runs 1, 3, and 8 as releases performed under equivalent source and wind field conditions to Burro 8 but for a different approach wind direction.

On Figures 17-1 through 17-15 the black line trace is that of the modeled data and the gray line trace is that of the field data. The step-like irregularities observed in some of the modeled data concentration time history plots (Figure 17-2 for example) are due to the five millivolt bin size of the analog-to-digital converter that was employed. The field data in these plots have been averaged in time to 10 seconds. No such average was employed on the modeled data.

The field data presented on Figures 16 and 17 are actual concentration readings obtained from field sensors. The presentation of actual concentration sensor time histories in the Lawrence Livermore Laboratory (LLL) report on field data [30] was limited to the plume

centerline sensor positions. To obtain the concentration structure of the different Burro Series plumes at off-centerline values it was necessary to use LLL's interpolated plots of ground level (1 meter height) concentration contours at specific times in the plume history. Unfortunately LLL used a simple linear interpolation of concentrations between sensor arrays. This procedure leads to nonsystematic errors of relatively large magnitude because of the large distances between sensor arrays (see Figure 19). Figure 20 conveys the source of these errors. The actual plume concentration contours of some hypothetical plume are shown for two different times t_1 and t_2. Below these actual plume contours are shown what the predicted contours from a linear interpolation such as that used by LLL would yield. The linear interpolation causes the predicted plume to leap forward as it passes each sensor array. It will also underpredict concentrations as the plumes leading edge approaches the next sensor array. Such leaping behavior (by as much as 200 meters) is seen very clearly in the plots presented by LLL [30].[1]

Nonetheless it is desirable to have some form of comparison of the lateral plume structure between the model and the field; hence, plots presented by LLL were used to find the concentration contours of maximum

[1]To estimate concentration contours more accurately one should use an interpolation scheme that is based on the plumes advective time scale (leading edge velocity) and knowledge that as a section of the plume moves downwind its concentrations will decay in a power law fashion with downwind distance. The arrival time of the plume for Burro 8 at each sensor array suggests that the advective time scale for the plume is nearly the same as the mean wind speed at 2 meters height. No concentration should be present at downwind distances greater than $u \cdot t$, where t is the time from release. The approximate form of the power law decay could be obtained from the decay of the peak concentrations for all time (like those presented in Figures 16-1 through 16-5). The use of an advective time scale should prevent errors such as are noted in Figure 20. Otherwise frontal location errors are approximately the same as the spacing of the sensor arrays.

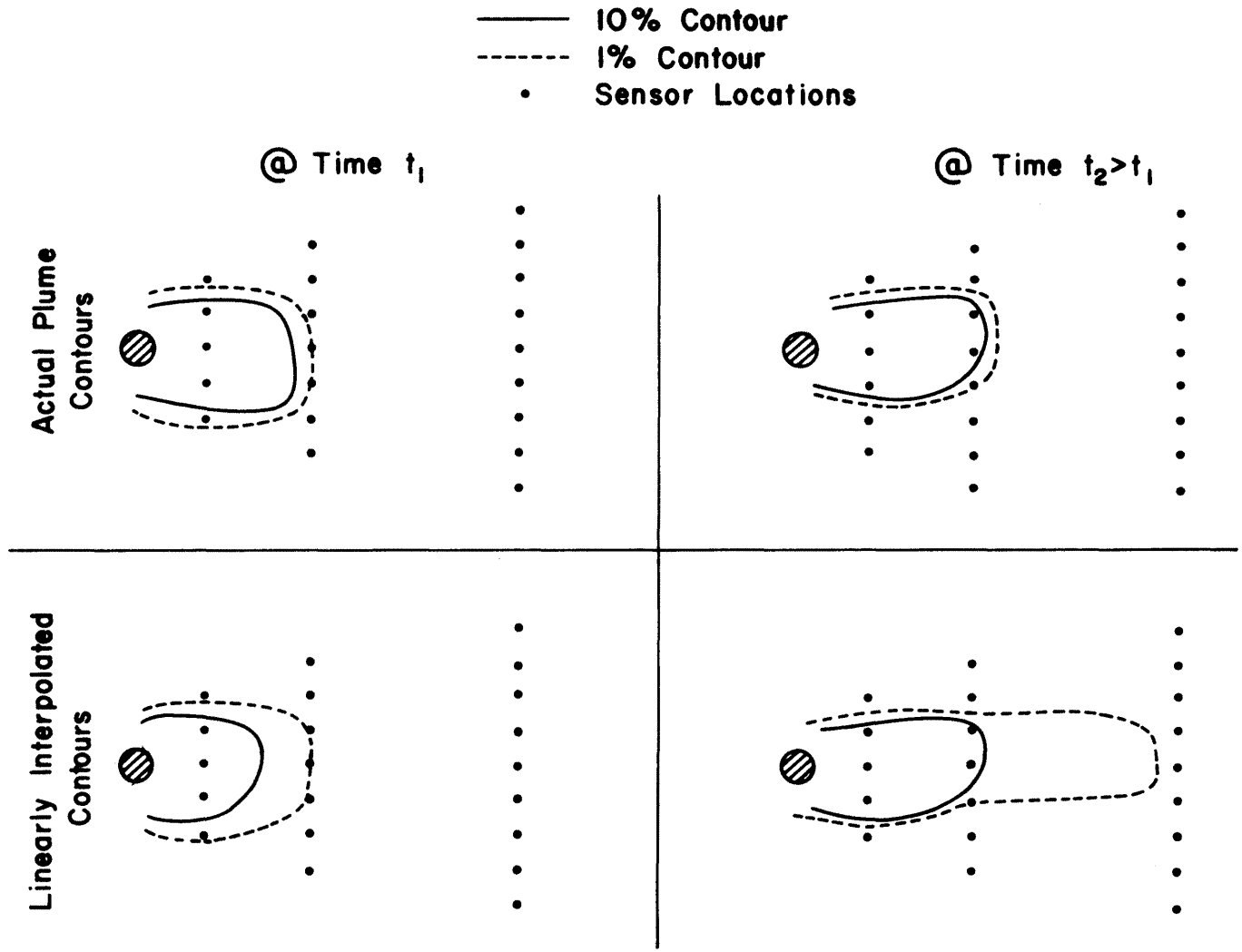

Figure 20. Explanatory Diagram of Linear Interpolation Errors

plume extent and are presented in Figures 18-1 through 18-8. The field sensor locations are presented on these figures to permit the reader to locate those areas where such comparisons are most valid. The comparison of field concentration measurements with model values in between sensor locations should be considered cautiously in light of interpolation errors in the field data discussed previously.

5.2 PEAK CENTERLINE CONCENTRATION DECAY

From an inspection of Figure 16-1 through 16-5 of the peak plume centerline concentration decay with downwind distance it is seen that the physical model data correlated fairly well with the field data for all runs except that of Burro 7 (Figure 16-3) and the 57 and 400 meter field concentration values for Burro 8 (Figure 16-4).

During the test, Burro 7, the wind speed was fairly high causing the plume to be narrow. With a narrow plume the possibility is large that the plume centerline, where the concentrations are the highest, is located between two measurement stations in the field. The peak concentration ground level contours for model Run 7 (Figure 11-3) show large variations in concentration values between the field measurement stations. Since the measurement grid spacing in the model was finer than that used in the field, the actual plume centerline values were more likely to be measured. The net effect would be the same as that depicted in Figure 16-3, that is, the model concentration values are consistently greater than or equal to those measured in the field.

The large difference between the modeled and measured field values found at the 57 and 400 meter station in Burro 8 (see Figure 16-4) is probably due to a combination of several factors that are not seen on a

simple presentation of plume centerline decay. The field data showed that there was a large influence of topography on the Burro 8 plume. This caused the plume to lobe outward on both sides of the centerline. Unfortunately the model topography was incorrectly oriented by 20° during the model runs 1, 3, and 8. A combination of model orientation errors and marginal plume simulation at low wind speeds lead to the discrepancies observed in Figure 16-4.

5.3 CONCENTRATION TIME HISTORIES

Comparison of the actual concentration time histories at similar downwind positions for each run reveals many of the pertinent physical similarities and differences between modeled and field data. Figures 17-1 through 17-15 as described in Table 4 present this comparison. The actual locations at the spill site of these field stations are presented in Figure 19.

Figures 17-1 and 17-2 display some of the effects of field test mean wind direction nonstationarities. In Figure 17-1 a distinctive double peak is observed in the field concentration data at times 55 seconds and 150 seconds. These peaks can be directly correlated with major shifts in the mean wind direction during the field test Burro 4. Thus the plume was advected into and away from the fixed measurement location during its progression downwind. This phenomenon is observable in Figure 17-2 where it is seen that measurement station G3 recorded the plume to have passed completely by at 150 seconds whereas the spillage of LNG onto the pool lasted 175 seconds. As discussed earlier, nonstationarities such as these were not modeled in the wind-tunnel.

The field data in Figures 17-3 and 17-4 reflect the influence of an unstable atmospheric stability during the Burro 5 test. The magnitude of the mean standard deviation of wind direction, the mean local longitudinal turbulent intensity, and the Richardson number suggests that Burro 5 took place in a fairly turbulent atmosphere. The large excursions in concentration magnitude measured within the plume for Burro 5 is a direct result of this highly turbulent atmosphere. This highly fluctuating character was unique to Burro 5. Since Burro 5 was modeled using a neutral atmospheric condition, these large excursions of plume concentration are not present in the modeled data. The magnitude of the peaks in the unstable field data are similar to those in the modeled data; however, mean concentration values are much lower in the unstable case. This emphasizes the importance of fast response instrumentation to measure concentrations in an LNG vapor cloud, particularly in an unstable atmosphere.

In Figures 17-5 and 17-6 for Burro 7 the discrepancy in concentration magnitudes is probably due to the same narrow plume effect mentioned earlier in the discussion of Figure 16-3. Since the plume was very narrow the field sensors may have missed the actual centerline of the plume where the concentrations would be highest.

The field data generally shows smaller plume arrival times and greater plume concentrations at early times than the 1:240 scale model data. The field data also display a more sudden falloff in plume concentration with plume passage. Figures 10-1, 10-2, 10-3, 10-4, 10-6, and 10-8 suggest a possible explanation for these differences in plume timing characteristics during the 1:240 scaled runs. These figures

provide a comparison between the mean velocity and turbulent intensity profiles for the 1:240 scaled-model data and the field data. The mean wind shear and the resultant intensity of turbulence is much greater during the 1:240 scale model runs. The velocity reference height for the calculation of plume similarity is three meters. These modeled runs have much lower velocities below this height than the field tests, which suggests that frontal velocities for these plumes are primarily determined by the speed of the wind at heights below three meters. The greater wind shear and turbulence during these modeled runs would cause increased longitudinal dispersion of the plume, hence, the slow rise and fall times of model plume concentrations.

During the 1:85 scale model experiments the wind field similarity was far superior to those scaled at 1:240, Figures 10-5 and 10-7. In particular, Run 2 (see Figure 10-7) shows almost exact similarity to the Burro 9 field test in both its wind shear and turbulent intensity. Thus arrival time and rise time characteristics should agree better than that of the 1:240 scale model. Figures 17-13 and 17-14 display such agreement between concentration time history comparisons for the Burro 9 test and a 1:85 scale model.

The wind shear similarity between the 1:85 scaled model Run 3 and Burro 8 was also quite good (see Figure 10-7), but a discrepancy remains in the arrival time characteristics (see Figures 17-9 and 17-10). Part of this difference is most certaintly due to variability in the wind speed experienced through the duration of the Burro 8 field test. The mean wind speed declined from 2.7 meters/second at the start of the spill to 1.7 meters/second at later times. As the field test was modeled at an average wind speed of 2 meters/second wind variability

would account for most of the discrepancies in arrival time characteristics. Also the model topographic orientation error confuses the issue.

5.4 GROUND LEVEL CONCENTRATION CONTOURS

A comparison of model and field lateral concentration distributions may have limited value because of interpolation procedures used by LLL [30]. As mentioned earlier in section 5.1 the field contours between sensor arrays could be in error by the distance between each array. In addition by plotting arbitrary time slices one examines only single concentration cross sections from a highly fluctuating time history. The actual peak concentration information, upon which all model maximum ground level extent contours were based, was not retrievable from the data in reference [30]. Field data plotted on Figures 18-1 through 18-8 for the maximum ground level extent of the 2.5, 5, and 10 percent concentrations may be incorrect.

A qualitative evaluation of modeled and actual plume widths can be made from Figures 18. Figures 18-1 to 18-3 suggest that the wind tunnel simulations generally underpredict the plume width for Burros 4, 5, and 7. Variations in the mean wind direction during the field experiment explain this phenomenon. These nonstationary aspects of the atmospheric wind variations were not modeled during the physical simulations.

As noted on Figures 18-4 to 18-6 the model experiments to simulate Burro 8 were incorrectly oriented. A clockwise rotation of the model data contours by 20° overlays the data sets and reveals that the southern plume edge is well beyond the field sensor array. A similar pattern is noted in the field data.

The Burro 8 field plume appears to bifurcate into two lobes whereas the model data does not show as extreme a bifurcation. The field lobing may be exaggerated by artificial large forward leaping of the plumes frontal concentrations resulting from the linear interpolation scheme used by LLL. Recall also that the model's wind orientation was directly into a hill (see Figure 11-5) which inhibits plume travel. The field plume was such that half the plume was directed into the hill and half the plume traveled out onto relatively flat terrain. This orientation would tend to split the plume. One must also recognize, however, that the behavior of atmospheric turbulence at low wind speeds (<2 m/s) is not well understood and the extremely low wind tunnel velocities required to model these wind speeds ($\lesssim$20 cm/s) may result in a substantial loss in wind field similarity.

Figures 18-7 and 18-8 display results from the 1:85 and 1:240 simulations of Burro 9, respectively. The overall plume width during the 1:85 simulation is quite good; however, at high concentrations the model predicts a much wider plume structure. No explanation for this behavior is apparent.

The longest distance measured to the LFL (5 percent) level for all the field tests was ~420 meters at a 3 meter height during Burro 8. Unfortunately due to the 20° topographic orientation mistake a comparison to model results for this worst case situation cannot be made. An isothermal physical model would not predict an elevated plume maximum.

6.0 SUMMARY AND RECOMMENDATIONS

The purpose of this study was to provide assistance during the U.S. Department of Energy sponsored field test preparation for the 1979-1980 forty cubic meter spill series at China Lake, California, and post-field test reproduction of those field tests. Small-scale models of the LNG release pond and surrounding topography at China Lake, Naval Weapons Testing Center, were placed in a meteorological wind tunnel capable of simulating the appropriate meteorological conditions. Transient concentrations of LNG vapor were determined by sampling concentrations of tracer gas released from the LNG spill area.

6.1 DISPERSION CHARACTERISTICS PERCEIVED FROM PRE-FIELD TEST SERIES

Ten pre-field model configurations were examined over a 1:240 scale model of the China Lake test site. Three wind speeds (3, 5, and 7 m/sec), two spill rates (15 and 30 m^3/min) and five wind orientations were considered. Based on visual examination of the site a wind field was produced characterized by an equivalent 4.3 cm roughness and a power law exponent of 0.18. Concentration measurements revealed that:

- Topographical effects are significant. Modest hill slopes of 1:10 can detain dense plumes and reduce longitudinal distances to LFL. Shallow valleys and gorges may channel the plume and sustain high concentrations.
- Accelerated boiloff rates of a finite amount of LNG may result in slightly modified LFL distances; however, the influence of a two-fold variation in boiloff rate is barely discernable in the results.
- An increased travel distance to a given concentration with increased wind speed was clearly apparent for wind speeds between 3 and 5 m/sec. This is in marked contrast to the passive dispersion of clouds where there is an inverse dependence on wind speed.
- Maximum LFL distances appear to lie between 250 and 350 meters.

6.2 COMPARISON OF LABORATORY AND POST-FIELD EXPERIMENTS

An importance objective of this study was to compare the physical model and field data through the principles of similarity and to determine how well the physical model can simulate actual atmospheric dense gas dispersion.

Field-model comparisons for each of the five different Burro tests simulated are summarized below:

- The 1:240 scale model of Burro 4 reproduced the peak centerline concentration decay with downwind distance. The arrival and departure concentration structure of the model plume was significantly different from the field because of poor modeling of the approaching wind profile at a 1:240 scale. Lateral plume extent comparisons indicate that deviations in the mean wind direction observed in the field caused the field plume to be wider than the model plume.

- The 1:240 scale model of Burro 5 displayed all the same comparison characteristics as that of Burro 4 above. In addition to these comments it was observed the concentrations in the interior of the field plume fluctuated much more than in the model plume. This difference is attributed to the highly turbulent atmosphere as a result of an unstable potential temperature gradient into which the plume was released. The model simulation was in a neutral wind field condition.

- The 1:240 scale model of Burro 7 did not reproduce the centerline concentration decay with downwind distance. This disagreement is attributed to the Burro 7 plume being very narrow. It is likely the plume center was missing the field concentration sensors. The arrival and departure structure of the model plume was significantly different from the field because of poor modeling of the approaching wind profile at a 1:240 scale. Lateral plume extent comparisons indicate that deviations in the mean wind direction observed in the field caused the field plume to be wider than the model plume. This wind direction variation often caused the plume to leave the bounds of the sensor array.

- Three different types of model simulations were intended to simulate Burro 8. Unfortunately the models topographic orientation was in error by 20° toward the north and the wind speeds were low enough in these tests for the topography to have a large influence on plume behavior. This error in wind direction prevents a complete evaluation of a model-field comparison, but several comments can still be made. There is a comparison discrepancy in the plume arrival times at the first sensors positions where topography differences are not yet present. This is attributed to the declining mean wind speed that occurred over the history of the Burro 8 plume. The wind tunnel models cannot reproduce nonstationarities such as a declining mean

wind speed, and a wind speed in between the actual extremes was used for modeling purposes. This choice caused the model plumes to be initially advected at a lower speed than that of the field plume. The field plume showed a stronger tendency to lobe than the model plume, but this difference could be a result of topographic orientation errors. The comparison between the two model runs 1 and 8 indicate that the distortion of plume initial density to obtain higher wind tunnel operating speeds results in a significant loss in plume similarity. The Burro 8 plume had the longest distance of any of the Burro tests to LFL (5 percent) concentrations. This concentration extreme was measured at a height of 3 meters and not at the height of 1 meter at the same tower. This significant affect of plume lofting was not modeled in the wind tunnel.

- Two different types of model simulations were made on the Burro 9 plume. One was at the standard scale of 1:240, and the other was at a scale of 1:85 to better approximate the mean shear and total turbulent intensity reported in the Burro 9 wind field summary. Both simulations show good agreement with the field data for the peak centerline concentration decay with downwind distance. The replication of the arrival and departure structure of the model-field plume comparison was greatly improved by the more accurate representation of the approaching wind characteristics at the 1:85 scale. The total lateral extent was better represented at the 1:85 scale. Overall the 1:85 model scale simulation of Burro 9 had excellent agreement. The only serious descrepancy observed is the model shows a much larger lateral plume width at the 10 percent concentration level. No explanation of this behavior could be found.

From these different test comparisons it is concluded that:

- Nonstationary effects such as variations of mean wind speed and mean wind direction exist in the field tests. These effects were accounted for in the physical model.

- Field plume thermal effects definitely caused plume lofting in the plume most susceptible to thermal heating, Burro 8. This effect was not simulated by an isothermal physical model.

- Distortion in the similarity of the approach wind field between model and field do not have a large effect on the comparison of actual and modeled peak concentration extents for all time. But these distortions cause large differences in the arrival and departure structure of the plumes tested.

- For the one test comparison in which good wind field similarity in mean shear and total turbulent intensity was obtained, Burro 9-Run 2, the concentration field comparison was generally excellent.

- There are most definitely limits to the range of possible field test conditions for which an accurate physical model can be developed. These limits are associated with large releases at low winds over terrain of low roughness. Burro 8's thermal lofting suggest that it falls into this category. No conclusions about the total loss of similarity can be made due to the modeling error in topographic orientation.

6.3 RECOMMENDATIONS

From the knowledge gained from the present study the following recommendations are made.

- The field data from the Burro test series should be presented in a format, as suggested within this report, which does not cause the very large errors that were found to exist in the linear interpolation scheme that was used. Since a time slice progression of plume concentration contours can very easily miss the peak concentration information it would be helpful to future users of this field data base if presentations similar to the format used to report model data within this report were used, i.e., the maximum ground level extent of different concentration values and ground level time progressions of the LFL.

- In the present study only the 1:85 scaled model (Run 2) of Burro 9 achieved a good similarity in the approach flow and the concentration field comparisons were very acceptable. Burros 4 and 8 both exhibited characteristics that cannot be modeled. But Burro tests 5 and 7 could be resimulated by a wind tunnel model in which improved wind comparisons are obtained by proper adjustment of model scale and thermal stability.

- Beyond the present field test series a larger data base of field experiments should be performed over sites which exhibit a greater effective roughness and lower wind speeds. From this data base and data collected from the associated wind tunnel modeling of each spill a more quantitative estimate of the accuracy of physical modeling can be determined.

- For future wind tunnel modeling studies of time dependent phenomena such as those of LNG spills, multiple replications of each concentration time history should be obtained. The ensemble mean and variance of the time dependent concentration signal at each spacial point can can be constructed from such data. Such ensemble averaging would greatly improve the ability to estimate the quality of field-model correlations.

REFERENCES

1. Fay, J. A. (1973) "Unusual Fire Hazard of LNG Tanker Spills," Combustion Science and Technology, Vol. 7, pp. 47-49.

2. Burgess, D. S., Biardi, J., and Murphy, J. N. (1972) "Hazards of Spillage of LNG into Water," Bureau of Mines, MIPR No. Z-70099-9-12395.

3. American Gas Association (1974) "LNG Safety Program, Interim Report on Phase II Work," Report on American Gas Association Project IS-3-1, Battelle Columbus Laboratories.

4. Neff, D. E., Meroney, R. N., and Cermak, J. E. (1976) "Wind Tunnel Study of Negatively Buoyant Plume Due to an LNG Spill," Report prepared for R & D Associates, California, Fluid Dynamics and Diffusion Laboratory Report CER76-77DEN-RNM-JEC22, Colorado State University, Fort Collins, Colorado, 241 p.

5. Hinze, J. O. (1975) Turbulence, McGraw-Hill, 790 p.

6. Pasquill, F. (1974) Atmospheric Diffusion, D. von Nostrand Co., 429 p.

7. Cermak, J. E. (1971) "Laboratory Simulation of the Atmospheric Boundary Layer," AIAA Jl., Vol. 9, No. 9, pp. 1746-1754, September.

8. Kline, S. J. (1965) Similitude and Approximation Theory, McGraw-Hill, 229 p.

9. Cermak, J. E. (1975) "Applications of Fluid Mechanics to Wind Engineering, A Freeman Scholar Lecture," J. of Fluid Engineering, Vol. 97, Ser. 1, No. 1, pp. 9-38.

10. Schlichting, H. (1968) Boundary Layer Theory, McGraw-Hill, New York.

11. Zoric, D. and Sandborn, V. A. (1972) "Similarity of Large Reynolds Number Boundary Layers," Boundary-Layer Meteorology, Vol. 2, No. 3, March, pp. 326-333.

12. Halitsky, J. (1969) "Validation of Scaling Procedures for Wind Tunnel Model Testing of Diffusion Near Buildings," Geophysical Sciences Laboratory, Report No. TR-69-8, New York University, New York.

13. Plate, E. J. and Cermak, J. E. (1963) "Micro-Meteorological Wind-Tunnel Facility: Description and Characteristics," Fluid Dynamics and Diffusion Laboratory Report CER63-ELP-JEC9, Colorado State University, Fort Collins, Colorado.

14. Counihan, J. (1975) "Adiabatic Atmospheric Boundary Layers: A Review and Analysis of Data from the Period 1880-1972," Atmospheric Environment, Vol. 9, pp. 871-905.

15. Hoot, T. G., et al. (1974) "Wind Tunnel Tests of Negatively Buoyant Plumes," Fluid Dynamics and Diffusion Laboratory Report CER73-74TGH-RNM-JAP-13, Colorado State University, Fort Collins, Colorado, October.

16. Isyumov, N., Jandali, T., and Davenport, A. G., "Model Studies and the Prediction of Full Scale Levels of Stack Gas Concentrations," APCA Journal, Vol. 26, No. 10, October 1976.

17. Snyder, W. H. (1972) "Similarity Criteria for the Application of Fluid Models to the Study of Air Pollution Meteorology," Boundary Layer Meteorology, Vol. 3, No. 1, September.

18. Boyle, G. J. and Kneebone, A. (1973) "Laboratory Investigation into the Characteristics of LNG Spills on Water, Evaporation, Spreading and Vapor Dispersion," Shell Research, Ltd., Report to API, March.

19. Meroney, R. N., Neff, D. E., Cermak, J. E., and Megahed, M. (1977) "Dispersion of Vapor from LNG Spills - Simulation in a Meteorological Wind Tunnel," Report prepared for R & D Associates, California, Fluid Dynamics and Diffusion Laboratory Report CER76-77RNM-JEC-DEN-MM57, Colorado State University, Fort Collins, Colorado, 151 p.

20. Meroney, R. N., et al. (1974) "Wind Tunnel Study of Stack Gas Dispersal at the Avon Lake Power Plant," Fluid Dynamics and Diffusion Laboratory Report CER73-74RNM-JEC-BTY-SKN35, Colorado State University, Fort Collins, Colorado, April.

21. Kothari, K. M. and Meroney, R. N. (1979) "Building Effects on National Transonic Facility Exhaust Plume," A Technical Report Prepared for NASA, Hampton, Virginia, also, Colorado State University Report CER79-80KMK-RNM35.

22. Bodurtha, F. T., Jr. (1961) "The Behavior of Dense Stack Gases," J. of APCA, Vol. 11, No. 9, pp. 431-437.

23. van Ulden, A. P. (1974) "On the Spreading of a Heavy Gas Released Near the Ground," Loss Prevention and Safety Promotion Seminar, Delft, Netherlands, 6 p.

24. Fay, J. A. (1980) "Gravitational Spread and Dilution of Heavy Vapor Clouds," Second International Symposium on Stratified Flows, the Norwegian Institute of Technology, Trondheim, Norway, 24-27 June.

25. Sandborn, V. A. (1972) Resistance Temperature Transducers, Metrology Press, 545 p.

26. Blackshear, P. L., Jr., and Fingerson, L. (1962) "Rapid Response Heat Flux Probe for High Temperature Gases," ARS Journal, November 1962, pp. 1709-1715.

27. Brown, G. L. and Rebollo, M. R. (1972) "A Small, Fast Response Probe to Measure Composition of a Binery Gas Mixture," AIAA Journal, Vol. 10, No. 5, pp. 649-752.

28. Kuretsky, W. H. (1967) "On the Use of an Aspirating Hot-Film Anemometer for the Instantaneous Measurement of Temperature," Thesis, Master of Mechanical Engineering, University of Minnesota, Minneapolis, Minnesota.

29. Kothari, K. M. and Meroney, R. N. (1979) "Building Effects on National Transonic Facility Exhaust Plume," A Technical Report Prepared for NASA, Hampton, Virginia, also, Colorado State University Report CER79-80KMK-RNM35, 43 p.

30. Koopman, R. P., Kamppinen, L. M., Hogan, W. J., and Lind, C. D. (1981) "Burro Series Data Report LLNL/NWC 1980 LNG Spill Tests," Lawrence Livermore Laboratory, Livermore, California, Report No. UCID-19075, June 1981.

APPENDIX A - THE CALCULATION OF MODEL SCALE FACTORS

As discussed previously in Section 2.3 the dominant scaling criteria for the simulation of LNG vapor cloud physics are the Froude number and the volume flux ratio. By setting these parameters equal for model and prototype one obtains the following relationships.

$$(U_a)_m = \left(\frac{S.G._m - 1}{S.G._p - 1}\right)^{1/2} \left(\frac{1}{L.S.}\right)^{1/2} (U_a)_p$$

$$Q_m = \left(\frac{S.G._m - 1}{S.G._p - 1}\right)^{1/2} \left(\frac{1}{L.S.}\right)^{5/2} Q_p$$

$$L_m = \left(\frac{1}{L.S.}\right) L_p$$

In addition to these scaling parameters which govern the flow physics one must also scale the mole fractions (concentrations) measured in the model to those that would occur in the prototype. This scaling is required since the number of moles being released in a thermal plume are different from the number of moles being released in a isothermal plume. To be more precise the relationship between the molar flow rate of source gas in the model and the prototype is

$$n_p = (T_m/T_p)\, n_{@m_{b.o.}} = (2.70)\, n_m$$

By definition the concentration of LNG vapor is expressed as:

$$\chi_p = n_{NG}/(n_{NG} + n_a)$$

Substituting model equivalents into the above expression yields

$$\chi_p = \frac{(T_m/T_p)_{@b.o.}\, n_{Ar}}{(T_m/T_p)_{@b.o.}\, n_{Ar} + n_a} = \frac{n_{Ar}}{n_{Ar} + n_a (T_p/T_m)_{@b.o.}}$$

or

$$\chi_p = \frac{\chi_m}{\chi_m + (1 - \chi_m)(0.37)}$$

This equation was used to correct the modeled measurements to those that would be observed in the field.

APPENDIX B - DATA TABLES

RUN NUMBER 1

FILE NAME	MODEL CONDITIONS: PEAK CONC. (%)	MODEL CONDITIONS: 1% ARR. TIME (SEC)	MODEL CONDITIONS: PEAK TIME (SEC)	MODEL CONDITIONS: 1% END TIME (SEC)	MODEL CONDITIONS: SUM (X-S)	POSITION: X (M)	POSITION: Y (M)	POSITION: Z (M)	PROTOTYPE CONDITIONS: PEAK CONC. (%)	PROTOTYPE CONDITIONS: 5% ARR. TIME (SEC)	PROTOTYPE CONDITIONS: 15% ARR. TIME (SEC)	PROTOTYPE CONDITIONS: PEAK TIME (SEC)	PROTOTYPE CONDITIONS: 15% END TIME (SEC)	PROTOTYPE CONDITIONS: 5% END TIME (SEC)	PROTOTYPE CONDITIONS: SUM (X-S)
A113308	.4	0.0	6.2	0.0	.01	36.5	84.0	0.0	1.0	0.	0.	230.	0.	0.	.88
A113309	1.6	4.2	5.3	6.6	.03	36.5	72.0	0.0	4.3	0.	0.	197.	0.	0.	2.54
A113310	1.0	3.6	4.0	9.0	.13	36.5	60.0	0.0	10.2	135.	0.	147.	0.	239.	12.37
A113311	10.4	2.5	3.9	15.9	.57	36.5	48.0	0.0	23.9	95.	116.	145.	256.	467.	51.64
A113312	11.9	1.8	3.4	16.2	.80	36.5	36.0	0.0	26.7	74.	96.	127.	304.	584.	71.88
A113313	12.2	1.1	2.8	25.0	1.12	36.5	24.0	0.0	27.4	46.	65.	105.	391.	805.	100.3
A113314	12.7	.8	2.4	36.3	1.98	36.5	12.0	0.0	44.3	40.	61.	124.	485.	1014.	169.3
A113315	19.4	.7	2.1	36.2	1.76	36.5	0.0	0.0	39.4	31.	64.	116.	415.	965.	154.1
B113308	.6	0.0	5.8	0.0	.01	36.5	84.0	0.0	1.5	0.	0.	215.	0.	0.	1.05
B113309	1.3	4.5	4.6	5.5	.02	36.5	72.0	0.0	5.1	170.	0.	170.	0.	172.	2.14
B113310	3.3	3.2	5.3	9.8	.13	36.5	60.0	0.0	8.3	135.	0.	197.	0.	316.	12.60
B113311	10.1	2.4	3.7	12.2	.56	36.5	48.0	0.0	23.2	87.	102.	136.	288.	443.	51.07
B113312	11.4	1.8	4.0	19.1	.82	36.5	36.0	0.0	27.1	68.	86.	147.	317.	535.	73.19
B113313	16.4	1.2	3.1	26.4	1.25	36.5	24.0	0.0	34.6	47.	65.	114.	393.	735.	110.2
B113314	20.3	.9	3.4	37.7	2.09	36.5	12.0	0.0	44.8	40.	53.	126.	495.	1069.	177.4
B113315	22.0	.6	3.0	34.3	1.77	36.5	0.0	0.0	40.8	41.	56.	113.	439.	914.	153.2
A114408	21.5	.8	3.2	34.0	1.88	36.5	0.0	0.0	41.1	39.	55.	127.	418.	988.	163.2
A114409	21.5	1.0	3.2	35.6	1.83	36.5	-12.0	0.0	42.5	41.	65.	117.	399.	916.	157.5
A114410	14.1	1.1	3.5	35.0	1.13	36.5	-24.0	0.0	30.8	50.	73.	129.	336.	860.	101.3
A114411	9.6	1.7	3.8	23.3	.76	36.5	-36.0	0.0	22.6	64.	98.	141.	267.	539.	69.14
A114412	7.6	2.1	4.4	12.8	.44	36.5	-48.0	0.0	16.9	89.	159.	163.	246.	436.	41.01
A114413	4.6	2.6	5.4	10.4	.24	36.5	-60.0	0.0	11.4	124.	0.	222.	0.	365.	22.80
A114414	3.2	4.0	7.1	10.3	.15	36.5	-72.0	0.0	8.8	162.	0.	262.	0.	336.	14.92
A114415	1.2	6.9	6.9	7.1	.02	36.5	-84.0	0.0	3.0	0.	0.	256.	0.	0.	1.94
B114408	23.4	1.0	3.0	35.1	1.87	36.5	0.0	0.0	44.7	40.	52.	113.	449.	1023.	161.4
B114409	22.4	1.0	3.1	34.9	1.77	36.5	-12.0	0.0	40.9	41.	62.	116.	403.	929.	153.8
B114410	17.5	1.0	3.7	38.7	1.09	36.5	-24.0	0.0	29.8	46.	80.	138.	330.	654.	98.52
B114411	9.5	1.7	4.0	17.8	.74	36.5	-36.0	0.0	22.2	62.	104.	147.	280.	594.	67.72
B114412	6.4	1.9	6.1	16.3	.57	36.5	-48.0	0.0	16.3	89.	127.	227.	259.	492.	53.32
B114413	4.2	3.2	5.6	12.0	.26	36.5	-60.0	0.0	10.7	124.	0.	209.	0.	379.	24.94
B114414	3.1	3.9	4.7	10.7	.13	36.5	-72.0	0.0	8.0	163.	0.	173.	0.	292.	12.40
B114415	1.0	5.2	5.2	5.2	.02	36.5	-84.0	0.0	2.7	0.	0.	193.	0.	0.	1.68
A124408	8.2	1.6	3.9	33.4	1.07	56.9	0.0	0.0	19.5	67.	96.	144.	252.	800.	100.2
A124409	7.9	1.8	3.9	35.0	.94	56.9	-12.0	0.0	18.9	82.	126.	144.	237.	744.	88.49
A124410	6.3	2.1	4.5	35.0	.71	56.9	-24.0	0.0	15.4	86.	165.	166.	176.	676.	67.80
A124411	4.4	2.4	4.9	22.5	.67	56.9	-36.0	0.0	17.7	101.	170.	181.	210.	658.	63.16
A124412	6.6	2.7	6.1	18.5	.57	56.9	-48.0	0.0	16.0	108.	182.	227.	246.	630.	53.55
A124413	6.8	3.3	7.2	16.9	.55	56.9	-60.0	0.0	16.6	133.	206.	265.	290.	609.	50.90
A124414	5.1	4.1	7.6	14.8	.32	56.9	-72.0	0.0	12.8	169.	0.	282.	0.	462.	30.78
A124415	3.8	5.1	7.3	12.8	.16	56.9	-84.0	0.0	9.0	249.	0.	282.	0.	443.	15.28
B124408	9.8	1.9	3.8	27.4	1.06	56.9	0.0	0.0	22.7	83.	111.	139.	295.	808.	97.61
B124409	9.0	2.2	4.6	26.3	.99	56.9	-12.0	0.0	21.0	93.	127.	157.	301.	742.	91.80
B124410	8.0	2.1	4.6	26.8	.72	56.9	-24.0	0.0	16.5	92.	165.	169.	218.	683.	68.68
B124411	5.7	2.3	5.7	27.6	.69	56.9	-36.0	0.0	14.0	96.	0.	212.	0.	682.	65.32
B124412	6.3	2.8	6.8	29.2	.61	56.9	-48.0	0.0	15.4	113.	190.	191.	194.	697.	57.00
B124413	6.4	3.3	6.8	19.0	.57	56.9	-60.0	0.0	16.0	129.	219.	250.	258.	594.	53.44
B124414	5.4	4.1	7.1	15.3	.37	56.9	-72.0	0.0	13.3	160.	0.	264.	0.	548.	35.51
B124415	4.4	4.7	7.4	17.0	.50	56.9	-60.0	0.0	14.6	133.	0.	216.	0.	599.	47.08
A125509	5.4	4.7	7.4	15.2	.34	56.9	-72.0	0.0	13.4	182.	0.	273.	0.	494.	32.15
A125510	2.8	6.4	8.2	11.3	.12	56.9	-84.0	0.0	7.2	277.	0.	305.	0.	378.	11.34

RUN NUMBER 1

FILE NAME	MODEL CONDITIONS: PEAK CONC. (%)	MODEL CONDITIONS: 1% ARR. TIME (SEC)	MODEL CONDITIONS: PEAK TIME (SEC)	MODEL CONDITIONS: 1% END TIME (SEC)	MODEL CONDITIONS: SUM (X-S)	POSITION: X (M)	POSITION: Y (M)	POSITION: Z (M)	PROTOTYPE CONDITIONS: PEAK CONC. (%)	PROTOTYPE CONDITIONS: 5% ARR. TIME (SEC)	PROTOTYPE CONDITIONS: 15% ARR. TIME (SEC)	PROTOTYPE CONDITIONS: PEAK TIME (SEC)	PROTOTYPE CONDITIONS: 15% END TIME (SEC)	PROTOTYPE CONDITIONS: 5% END TIME (SEC)	PROTOTYPE CONDITIONS: SUM (X-S)
A12511	.8	0.0	10.8	0.0	.01	56.9	-96.0	0.0	2.2	0.	0.	399.	0.	0.	1.25
A12512	1	0.0	1.0	0.0	0.00	56.9	-108.0	0.0	.3	0.	0.	37.	0.	0.	.11
A12513	.1	0.0	48.2	0.0	.01	56.9	-120.0	0.0	.3	0.	0.	1787.	0.	0.	.60
A12514	.1	0.0	33.3	0.0	0.00	56.9	-132.0	0.0	.4	0.	0.	1235.	0.	0.	.43
A12515	.1	0.0	37.7	0.0	0.00	56.9	-144.0	0.0	.2	0.	0.	1396.	0.	0.	.20
B12508	5.5	3.7	6.0	15.4	.47	56.9	-60.0	0.0	13.6	148.	0.	222.	0.	548.	44.12
B12509	4.8	4.8	7.5	13.8	.32	56.9	-72.0	0.0	11.9	193.	0.	277.	0.	494.	39.52
B12510	2.2	5.7	9.7	13.1	.14	56.9	-84.0	0.0	5.8	259.	0.	360.	0.	442.	13.22
B12511	.9	0.0	7.9	0.0	.03	56.9	-96.0	0.0	2.5	0.	0.	293.	0.	0.	2.74
B12512	.1	0.0	17.6	0.0	.01	56.9	-108.0	0.0	.3	0.	0.	654.	0.	0.	.51
B12513	.0	0.0	.1	0.0	.01	56.9	-120.0	0.0	.1	0.	0.	3.	0.	0.	1.42
B12514	.1	0.0	.1	0.0	.01	56.9	-132.0	0.0	.3	0.	0.	3.	0.	0.	1.51
B12515	.1	0.0	26.0	0.0	.01	56.9	-144.0	0.0	.4	0.	0.	962.	0.	0.	.80
A12308	.5	0.0	7.1	0.0	.01	56.9	84.0	0.0	1.2	0.	0.	264.	0.	0.	1.28
A12309	1.9	5.2	11.2	11.5	.08	56.9	72.0	0.0	3.0	415.	0.	415.	0.	422.	7.44
A12310	3.5	3.8	7.9	14.9	.25	56.9	60.0	0.0	8.9	157.	0.	292.	0.	464.	24.45
A12311	6.7	3.1	5.0	20.4	.59	56.9	48.0	0.0	16.3	122.	156.	187.	265.	566.	55.43
A12312	8.6	2.6	5.1	21.4	.80	56.9	36.0	0.0	20.3	104.	144.	190.	305.	745.	74.04
A12313	10.4	1.6	4.5	32.4	1.19	56.9	24.0	0.0	23.8	79.	123.	167.	376.	877.	108.5
A12314	9.9	1.5	4.4	37.4	1.30	56.9	12.0	0.0	21.0	67.	111.	163.	371.	996.	120.5
A12315	9.6	1.3	4.7	37.1	1.22	56.9	0.0	0.0	18.1	61.	95.	173.	338.	1005.	114.2
B12308	1.3	7.2	9.8	10.4	.05	56.9	84.0	0.0	3.3	0.	0.	363.	0.	0.	5.30
B12309	2.8	5.4	8.6	11.1	.13	56.9	72.0	0.0	7.1	225.	0.	317.	0.	397.	12.68
B12310	4.3	4.4	5.8	12.9	.22	56.9	60.0	0.0	9.5	170.	0.	215.	0.	393.	21.00
B12311	6.7	3.2	5.4	18.7	.58	56.9	48.0	0.0	16.2	132.	196.	199.	243.	621.	54.46
B12312	7.1	2.1	5.2	20.3	.79	56.9	36.0	0.0	18.5	89.	141.	193.	302.	697.	73.13
B12313	9.1	1.5	5.0	26.4	1.12	56.9	24.0	0.0	21.3	62.	98.	185.	381.	751.	102.3
B12314	10.2	1.4	5.6	32.9	1.30	56.9	12.0	0.0	23.6	64.	96.	132.	344.	965.	119.2
B12315	10.2	1.6	5.5	31.4	1.13	56.9	0.0	0.0	23.5	64.	96.	130.	308.	803.	104.1
C12308	.4	0.0	7.1	0.0	.01	56.9	84.0	0.0	1.2	0.	0.	264.	0.	0.	1.48
C12309	1.9	6.0	6.8	10.4	.07	56.9	72.0	0.0	4.9	0.	0.	253.	0.	0.	6.41
C12310	3.3	4.1	7.7	15.1	.23	56.9	60.0	0.0	8.4	187.	0.	286.	0.	436.	22.20
C12311	6.2	3.2	5.9	19.7	.59	56.9	48.0	0.0	15.2	135.	219.	219.	227.	587.	54.92
C12312	7.7	2.6	5.0	22.0	.82	56.9	36.0	0.0	18.4	102.	147.	187.	298.	702.	75.52
C12313	9.1	1.8	4.7	30.2	1.18	56.9	24.0	0.0	21.4	76.	122.	175.	387.	823.	108.0
C12314	9.7	1.8	5.1	35.8	1.27	56.9	12.0	0.0	22.5	73.	113.	190.	310.	940.	117.2
C12315	9.3	1.6	5.6	37.7	1.23	56.9	0.0	0.0	22.8	67.	101.	132.	290.	910.	113.7
A13308	.3	0.0	12.0	0.0	.01	91.2	84.0	0.0	.9	0.	0.	443.	0.	0.	1.25
A13309	2.0	10.0	11.6	13.4	.08	91.2	72.0	0.0	5.1	431.	0.	431.	0.	462.	7.78
A13310	3.8	5.3	9.4	16.4	.17	91.2	60.0	0.0	5.2	348.	0.	348.	0.	387.	16.67
A13311	3.2	4.9	6.7	18.8	.29	91.2	48.0	0.0	8.1	202.	0.	247.	0.	584.	28.44
A13312	4.6	4.0	6.6	18.0	.33	91.2	36.0	0.0	10.2	175.	0.	245.	0.	535.	31.69
A13313	5.5	3.4	6.0	26.3	.57	91.2	24.0	0.0	13.5	145.	0.	222.	0.	628.	54.58
A13314	5.1	3.0	6.4	26.2	.65	91.2	12.0	0.0	12.7	129.	0.	237.	0.	686.	61.85
A13315	4.5	3.0	6.4	30.0	.69	91.2	0.0	0.0	11.4	122.	0.	237.	0.	688.	65.95
B13308	.1	0.0	.2	0.0	.01	91.2	84.0	0.0	.2	0.	0.	7.	0.	0.	.88
B13309	1.4	6.8	8.6	9.2	.06	91.2	72.0	0.0	3.7	0.	0.	319.	0.	0.	5.70
B13310	1.5	4.2	6.4	12.9	.13	91.2	60.0	0.0	3.9	0.	0.	237.	0.	0.	13.00
B13311	2.1	3.7	6.3	18.0	.32	91.2	48.0	0.0	7.9	162.	0.	234.	0.	612.	31.24
B13312	2.7	3.4	6.8	20.1	.40	91.2	36.0	0.0	9.4	142.	0.	253.	0.	579.	39.53

RUN NUMBER 1

FILE NAME	MODEL CONDITIONS PEAK CONC. (%)	1% ARR. TIME (SEC)	PEAK TIME (SEC)	1% END TIME (SEC)	SUM (X-S)	PROTOTYPE CONDITIONS POSITION X (M)	Y (M)	Z (M)	PEAK CONC (%)	5% ARR. TIME (SEC)	15% ARR. TIME (SEC)	PEAK TIME (SEC)	15% END TIME (SEC)	5% END TIME (SEC)	SUM (X-S)
B13313	4.9	2.6	6.4	28.6	.60	91.2	24.0	0.0	12.2	111.	0.	239.	0.	668.	57.93
B13314	4.6	2.8	4.6	27.3	.65	91.2	12.0	0.0	11.5	119.	0.	169.	0.	852.	61.79
B13315	4.2	2.8	4.8	25.0	.58	91.2	0.0	0.0	10.5	122.	0.	176.	0.	659.	55.55
A13408	4.2	3.0	6.3	23.8	.57	91.2	0.0	0.0	10.6	127.	0.	233.	0.	621.	55.27
A13409	4.0	2.9	6.2	24.2	.56	91.2	-12.0	0.0	10.0	132.	0.	228.	0.	662.	53.87
A13410	2.6	3.1	4.8	18.3	.36	91.2	-24.0	0.0	6.8	139.	0.	179.	0.	507.	35.43
A13411	2.4	3.1	8.6	20.0	.28	91.2	-36.0	0.0	6.1	209.	0.	317.	0.	341.	27.67
A13412	2.2	5.1	6.9	16.6	.20	91.2	-48.0	0.0	5.8	239.	0.	256.	0.	268.	19.84
A13413	3.0	4.1	7.0	19.0	.27	91.2	-60.0	0.0	7.7	199.	0.	261.	0.	403.	26.65
A13414	3.1	5.4	6.7	19.7	.29	91.2	-72.0	0.0	7.9	210.	0.	249.	0.	528.	28.36
A13415	3.1	5.4	7.3	18.5	.30	91.2	-84.0	0.0	7.8	222.	0.	271.	0.	582.	28.89
B13408	4.3	3.0	7.1	26.5	.61	91.2	0.0	0.0	10.8	119.	0.	264.	0.	738.	56.89
B13409	4.3	3.0	5.1	25.6	.65	91.2	-12.0	0.0	10.9	132.	0.	190.	0.	777.	59.19
B13410	2.9	3.3	5.2	26.9	.41	91.2	-24.0	0.0	7.4	145.	0.	191.	0.	440.	39.66
B13411	2.6	3.6	6.8	20.6	.32	91.2	-36.0	0.0	6.7	166.	0.	252.	0.	353.	30.98
B13412	1.9	4.8	7.6	16.0	.23	91.2	-48.0	0.0	5.0	0.	0.	283.	0.	0.	23.08
B13413	2.6	4.2	7.3	16.5	.27	91.2	-60.0	0.0	6.6	210.	0.	271.	0.	507.	26.33
B13414	3.3	5.1	7.6	17.9	.28	91.2	-72.0	0.0	8.4	218.	0.	283.	0.	544.	27.62
B13415	3.0	5.4	7.1	16.2	.25	91.2	-84.0	0.0	7.7	225.	0.	262.	0.	541.	24.03
A13508	2.5	4.9	6.7	17.6	.24	91.2	-60.0	0.0	6.4	207.	0.	247.	0.	368.	23.28
A13509	2.2	5.2	8.3	18.4	.30	91.2	-72.0	0.0	8.2	219.	0.	308.	0.	600.	27.99
A13510	2.6	5.8	10.0	18.4	.24	91.2	-84.0	0.0	6.8	247.	0.	372.	0.	496.	22.66
A13511	2.0	7.0	11.0	18.1	.23	91.2	-96.0	0.0	7.7	283.	0.	409.	0.	579.	25.68
A13512	2.0	9.1	10.0	13.5	.06	91.2	-108.0	0.0	5.3	372.	0.	372.	0.	373.	6.10
A13513	.1	0.0	23.6	0.0	.01	91.2	-120.0	0.0	.3	0.	0.	873.	0.	0.	1.03
A13514	.2	0.0	12.4	0.0	.01	91.2	-132.0	0.0	.4	0.	0.	459.	0.	0.	1.23
A13515	.3	0.0	2.6	0.0	.02	91.2	-144.0	0.0	.8	0.	0.	95.	0.	0.	1.91
B13508	2.4	5.0	6.9	15.2	.21	91.2	-60.0	0.0	6.3	207.	0.	256.	0.	434.	20.89
B13509	2.2	5.1	7.2	15.6	.26	91.2	-72.0	0.0	8.3	210.	0.	265.	0.	535.	25.45
B13510	2.5	5.8	7.6	16.2	.21	91.2	-84.0	0.0	6.6	246.	0.	282.	0.	483.	20.12
B13511	2.8	7.1	9.1	16.0	.20	91.2	-96.0	0.0	7.3	288.	0.	338.	0.	507.	19.12
B13512	2.3	8.0	10.0	13.0	.08	91.2	-108.0	0.0	5.9	329.	0.	369.	0.	379.	8.29
B13513	.1	0.0	10.9	0.0	.01	91.2	-120.0	0.0	.4	0.	0.	405.	0.	0.	.94
B13514	.1	0.0	1.6	0.0	.01	91.2	-132.0	0.0	.4	0.	0.	59.	0.	0.	.51
C13508	[illegible]	4.7	6.9	15.6	.21	91.2	-60.0	0.0	6.1	216.	0.	255.	0.	292.	20.09
C13509	[illegible]	5.0	7.2	18.4	.26	91.2	-72.0	0.0	7.6	216.	0.	268.	0.	548.	24.80
C13510	[illegible]	5.5	9.2	14.2	.19	91.2	-84.0	0.0	6.5	245.	0.	341.	0.	462.	18.92
C13511	[illegible]	6.6	8.3	14.3	.19	91.2	-96.0	0.0	7.8	261.	0.	307.	0.	492.	18.55
C13512	[illegible]	8.3	8.4	11.8	.06	91.2	-108.0	0.0	5.8	311.	0.	313.	0.	41.	5.96
C13513	.0	0.0	.1	0.0	.01	91.2	-120.0	0.0	.1	0.	0.	3.	0.	0.	1.42
C13514	.1	0.0	.1	0.0	.02	91.2	-132.0	0.0	.3	0.	0.	3.	0.	0.	1.57
C13515	.2	0.0	36.8	0.0	.02	91.2	-144.0	0.0	.4	0.	0.	1365.	0.	0.	1.88
A14408	2.4	4.4	8.2	22.2	.36	139.9	0.0	0.0	6.3	213.	0.	305.	0.	471.	35.48
A14409	2.6	4.4	7.6	21.9	.42	139.9	-12.0	0.0	6.6	237.	0.	283.	0.	522.	40.70
A14410	1.9	5.0	12.2	21.0	.31	139.9	-24.0	0.0	4.9	0.	0.	451.	0.	0.	30.72
A14411	1.7	5.5	10.1	15.7	.24	139.9	-36.0	0.0	4.4	0.	0.	373.	0.	0.	24.03
A14412	1.5	6.8	8.0	16.1	.17	139.9	-48.0	0.0	3.8	0.	0.	298.	0.	0.	16.33
A14413	1.6	6.4	14.0	16.6	.18	139.9	-60.0	0.0	4.2	0.	0.	519.	0.	0.	18.01
A14414	1.7	6.7	9.0	16.7	.17	139.9	-72.0	0.0	4.4	0.	0.	332.	0.	0.	16.39
A14415	1.3	7.8	9.6	19.8	.11	139.9	-84.0	0.0	3.5	0.	0.	354.	0.	0.	10.92

RUN NUMBER 1

FILE NAME	MODEL CONDITIONS: PEAK CONC. (%)	1% ARR. TIME (SEC)	PEAK TIME (SEC)	1% END TIME (SEC)	SUM (X-S)	POSITION X (M)	POSITION Y (M)	POSITION Z (M)	PROTOTYPE CONDITIONS: PEAK CONC. (%)	5% ARR. TIME (SEC)	15% ARR. TIME (SEC)	PEAK TIME (SEC)	15% END TIME (SEC)	5% END TIME (SEC)	SUM (X-S)
@14408	2.4	4.7	6.6	22.6	.41	139.9	0.0	0.0	6.3	228.	0.	245.	0.	536.	40.36
@14409	2.4	4.6	7.3	23.8	.38	139.9	-12.0	0.0	6.2	216.	0.	270.	0.	399.	37.02
@14410	1.9	5.4	6.8	19.2	.28	139.9	-24.0	0.0	5.0	0.	0.	253.	0.	0.	27.47
@14411	1.6	6.0	7.7	16.2	.21	139.9	-36.0	0.0	4.3	0.	0.	285.	0.	0.	20.66
@14412	1.6	6.9	8.8	11.3	.13	139.9	-48.0	0.0	4.1	0.	0.	328.	0.	0.	13.14
@14413	1.5	6.4	8.3	11.6	.14	139.9	-60.0	0.0	3.8	0.	0.	307.	0.	0.	13.79
@14414	1.4	7.1	8.7	15.1	.15	139.9	-72.0	0.0	3.8	0.	0.	322.	0.	0.	14.73
@14415	1.2	8.2	8.4	12.3	.06	139.9	-84.0	0.0	3.0	0.	0.	311.	0.	0.	6.04
@14308	.9	0.0	11.4	0.0	.04	139.9	84.0	0.0	2.3	0.	0.	422.	0.	0.	4.02
@14309	1.0	8.3	10.3	11.6	.09	139.9	72.0	0.0	2.7	0.	0.	381.	0.	0.	8.69
@14310	1.3	8.9	10.7	12.2	.10	139.9	60.0	0.0	3.3	0.	0.	396.	0.	0.	9.55
@14311	1.8	6.4	8.4	16.9	.19	139.9	48.0	0.0	4.7	0.	0.	313.	0.	0.	18.21
@14312	1.7	6.1	12.8	16.1	.19	139.9	36.0	0.0	4.4	0.	0.	474.	0.	0.	19.09
@14313	3.0	5.2	8.0	18.9	.37	139.9	24.0	0.0	7.6	233.	0.	295.	0.	565.	36.39
@14314	2.8	4.6	7.8	18.6	.38	139.9	12.0	0.0	7.3	216.	0.	289.	0.	569.	36.96
@14308	.8	0.0	12.7	0.0	.04	139.9	84.0	0.0	2.2	0.	0.	470.	0.	0.	3.65
@14309	1.4	9.1	10.3	13.5	.12	139.9	72.0	0.0	3.7	0.	0.	382.	0.	0.	11.51
@14310	1.4	8.7	9.6	14.6	.13	139.9	60.0	0.0	3.7	0.	0.	357.	0.	0.	12.80
@14311	1.9	6.0	9.6	17.0	.22	139.9	48.0	0.0	5.0	0.	0.	357.	0.	0.	21.80
@14312	1.9	5.7	9.2	20.3	.23	139.9	36.0	0.0	5.1	339.	0.	339.	0.	341.	22.60
@14313	3.0	4.1	8.0	23.8	.48	139.9	24.0	0.0	7.8	200.	0.	296.	0.	753.	46.28
@14314	3.0	4.5	8.3	24.0	.50	139.9	12.0	0.0	7.7	227.	0.	307.	0.	659.	48.17
@14315	2.6	4.2	8.3	23.4	.44	139.9	0.0	0.0	6.6	210.	0.	307.	0.	594.	43.06
C14308	.8	0.0	12.7	0.0	.05	139.9	84.0	0.0	2.1	0.	0.	470.	0.	0.	4.62
C14309	1.2	8.8	9.6	12.9	.10	139.9	72.0	0.0	3.2	0.	0.	354.	0.	0.	9.95
C14310	1.5	7.0	9.6	13.7	.12	139.9	60.0	0.0	4.1	0.	0.	356.	0.	0.	12.14
C14311	2.1	6.1	8.5	17.4	.23	139.9	48.0	0.0	5.4	302.	0.	316.	0.	390.	22.51
C14312	2.2	6.1	8.9	17.3	.23	139.9	36.0	0.0	5.8	298.	0.	330.	0.	366.	22.83
C14313	3.4	4.3	8.1	22.1	.43	139.9	24.0	0.0	8.6	205.	0.	299.	0.	608.	41.55
C14314	3.3	4.6	8.6	22.0	.44	139.9	12.0	0.0	8.3	215.	0.	320.	0.	630.	42.29
C14315	2.9	4.0	7.6	23.8	.50	139.9	0.0	0.0	7.5	182.	0.	280.	0.	582.	48.05
A15308	.4	0.0	15.1	0.0	.03	242.4	84.0	0.0	1.0	0.	0.	560.	0.	0.	2.57
A15309	.7	0.0	13.4	0.0	.05	242.4	72.0	0.0	1.8	0.	0.	498.	0.	0.	5.10
A15310	.7	0.0	13.4	0.0	.08	242.4	60.0	0.0	1.9	0.	0.	496.	0.	0.	7.47
A15311	1.2	11.0	13.4	15.1	.15	242.4	48.0	0.0	3.1	0.	0.	496.	0.	0.	15.10
A15312	1.2	10.0	16.5	17.7	.19	242.4	36.0	0.0	3.2	0.	0.	611.	0.	0.	18.52
A15313	1.7	8.0	12.2	20.0	.26	242.4	24.0	0.0	4.6	0.	0.	453.	0.	0.	25.62
A15314	1.4	9.5	10.7	19.2	.21	242.4	12.0	0.0	3.7	0.	0.	397.	0.	0.	21.15
A15315	1.3	9.0	11.8	16.4	.18	242.4	0.0	0.0	3.3	0.	0.	436.	0.	0.	18.24
A15308	.3	0.0	18.8	0.0	.01	242.4	84.0	0.0	.7	0.	0.	695.	0.	0.	1.25
A15309	.6	0.0	17.5	0.0	.06	242.4	72.0	0.0	1.7	0.	0.	649.	0.	0.	6.41
A15310	.7	0.0	17.4	0.0	.09	242.4	60.0	0.0	2.0	0.	0.	645.	0.	0.	9.23
A15311	1.0	10.9	13.1	17.3	.16	242.4	48.0	0.0	2.8	0.	0.	486.	0.	0.	15.36
A15312	1.3	9.4	11.0	20.2	.20	242.4	36.0	0.0	3.3	0.	0.	408.	0.	0.	19.84
A15313	1.6	7.4	9.9	21.5	.28	242.4	24.0	0.0	4.1	0.	0.	368.	0.	0.	27.47
A15314	1.4	8.4	10.6	19.8	.27	242.4	12.0	0.0	3.7	0.	0.	391.	0.	0.	26.19
A15315	1.4	8.7	10.6	20.8	.26	242.4	0.0	0.0	3.8	0.	0.	394.	0.	0.	26.05
A15408	1.2	10.6	11.6	18.0	.19	242.4	0.0	0.0	3.1	0.	0.	431.	0.	0.	19.12
A15409	1.5	9.4	12.0	19.0	.24	242.4	-12.0	0.0	3.9	0.	0.	443.	0.	0.	24.11
A15410	1.2	9.5	11.0	16.2	.20	242.4	-24.0	0.0	3.1	0.	0.	406.	0.	0.	19.52

RUN NUMBER 1

FILE NAME	MODEL CONDITIONS: PEAK CONC. (%)	1% ARR. TIME (SEC)	PEAK TIME (SEC)	1% END TIME (SEC)	SUM (X-S)	POSITION X (M)	POSITION Y (M)	POSITION Z (M)	PROTOTYPE CONDITIONS: PEAK CONC. (%)	5% ARR. TIME (SEC)	15% ARR. TIME (SEC)	PEAK TIME (SEC)	15% END TIME (SEC)	5% END TIME (SEC)	SUM (X-S)
A15411	1.3	10.6	13.7	17.0	.20	242.4	-36.0	0.0	3.4	0.	0.	500.	0.	0.	19.41
A15412	1.1	14.2	14.2	14.4	.16	242.4	-48.0	0.0	2.9	0.	0.	528.	0.	0.	15.42
A15413	1.0	0.0	12.9	0.0	.14	242.4	-60.0	0.0	2.6	0.	0.	479.	0.	0.	13.77
A15414	.9	0.0	15.0	0.0	.11	242.4	-72.0	0.0	2.4	0.	0.	556.	0.	0.	11.11
A15415	.8	0.0	14.2	0.0	.09	242.4	-84.0	0.0	2.2	0.	0.	525.	0.	0.	8.69
B15408	1.3	10.2	12.7	16.6	.21	242.4	0.0	0.0	3.4	0.	0.	471.	0.	0.	20.49
B15409	1.4	9.2	11.3	18.4	.25	242.4	-12.0	0.0	3.7	0.	0.	418.	0.	0.	24.82
B15410	1.2	9.5	11.8	16.7	.21	242.4	-24.0	0.0	3.1	0.	0.	439.	0.	0.	20.66
B15411	1.1	11.5	11.5	15.8	.18	242.4	-36.0	0.0	2.9	0.	0.	425.	0.	0.	17.78
B15412	.9	0.0	12.8	0.0	.12	242.4	-48.0	0.0	2.5	0.	0.	474.	0.	0.	12.20
B15413	.9	0.0	10.9	0.0	.12	242.4	-60.0	0.0	2.3	0.	0.	405.	0.	0.	11.88
B15414	.8	0.0	10.4	0.0	.10	242.4	-72.0	0.0	2.1	0.	0.	384.	0.	0.	10.17
B15415	.8	0.0	11.6	0.0	.09	242.4	-84.0	0.0	2.1	0.	0.	430.	0.	0.	9.12

RUN NUMBER 2

FILE NAME	MODEL CONDITIONS PEAK CONC. (%)	1% ARR. TIME (SEC)	PEAK TIME (SEC)	1% END TIME (SEC)	SUM (X-S)	POSITION X (M)	Y (M)	Z (M)	PROTOTYPE CONDITIONS PEAK CONC. (%)	5% ARR. TIME (SEC)	15% ARR. TIME (SEC)	PEAK TIME (SEC)	15% END TIME (SEC)	5% END TIME (SEC)	SUM (X-S)
A21309	.1	0.0	11.8	0.0	0.00	36.5	45.9	0.0	.3	0.	0.	90.	0.	0.	.04
A21310	.2	0.0	11.1	0.0	.01	36.5	38.3	0.0	.5	0.	0.	85.	0.	0.	.24
A21311	6.6	6.8	11.1	14.5	.20	36.5	30.6	0.0	16.0	57.	85.	85.	87.	107.	4.02
A21312	12.2	3.0	10.8	15.8	.78	36.5	23.0	0.0	27.2	24.	50.	83.	109.	118.	14.57
A21313	12.1	2.3	12.0	22.4	1.02	36.5	15.3	0.0	27.1	18.	34.	92.	110.	117.	18.83
A21314	16.0	1.2	13.0	23.5	1.43	36.5	7.6	0.0	34.0	12.	26.	100.	120.	146.	25.87
A21315	16.0	.9	10.6	25.5	1.47	36.5	0.0	0.0	34.0	10.	18.	81.	115.	132.	26.38
B21308	.1	0.0	42.7	0.0	.01	36.5	53.6	0.0	.4	0.	0.	327.	0.	0.	.21
B21309	.1	0.0	1.2	0.0	0.00	36.5	45.9	0.0	.4	0.	0.	10.	0.	0.	.03
B21310	.5	0.0	13.6	0.0	.01	36.5	38.3	0.0	1.3	0.	0.	104.	0.	0.	.28
B21311	6.9	5.3	13.2	15.4	.38	36.5	30.6	0.0	16.6	44.	96.	101.	102.	110.	7.47
B21312	11.4	2.2	8.0	14.4	.73	36.5	23.0	0.0	25.7	24.	38.	62.	101.	107.	13.64
B21313	12.5	1.7	9.7	20.0	.95	36.5	15.3	0.0	27.8	16.	34.	74.	102.	127.	17.58
B21314	12.6	1.2	10.0	22.1	1.15	36.5	7.6	0.0	28.1	11.	27.	77.	109.	120.	21.06
B21315	13.7	.7	12.2	23.0	1.21	36.5	0.0	0.0	30.1	6.	21.	93.	106.	128.	22.03
A21408	19.0	.8	12.6	22.2	1.56	36.5	0.0	0.0	38.8	9.	20.	96.	110.	142.	27.51
A21409	18.0	1.1	11.9	26.6	1.31	36.5	-7.6	0.0	37.2	10.	17.	91.	110.	168.	23.91
A21410	15.5	.9	5.6	23.8	1.30	36.5	-15.3	0.0	33.1	12.	23.	43.	116.	127.	23.49
A21411	16.1	2.3	9.5	16.1	1.20	36.5	-23.0	0.0	34.1	21.	29.	73.	108.	115.	21.22
A21412	14.2	3.2	11.3	14.4	.66	36.5	-30.6	0.0	30.9	25.	53.	87.	103.	110.	12.12
A21413	6.7	7.4	11.8	12.7	.10	36.5	-38.3	0.0	16.2	58.	90.	91.	91.	97.	1.93
A21414	.1	0.0	.2	0.0	.02	36.5	-45.9	0.0	.3	0.	0.	2.	0.	0.	.32
A21415	.1	0.0	46.1	0.0	.02	36.5	-53.6	0.0	.3	0.	0.	353.	0.	0.	.32
B21408	17.0	1.1	11.8	24.3	1.38	36.5	0.0	0.0	35.6	11.	18.	90.	110.	127.	24.72
B21409	17.6	1.2	8.2	23.3	1.18	36.5	-7.6	0.0	36.7	12.	22.	63.	106.	134.	21.28
B21410	14.8	1.3	9.5	23.2	1.24	36.5	-15.3	0.0	31.9	12.	25.	73.	109.	135.	22.54
B21411	14.7	2.2	11.2	15.5	1.14	36.5	-23.0	0.0	31.8	19.	27.	86.	105.	117.	20.32
B21412	12.6	2.6	10.4	14.2	.63	36.5	-30.6	0.0	28.0	30.	36.	80.	102.	109.	11.80
B21413	3.1	9.0	9.2	9.6	.05	36.5	-38.3	0.0	8.0	70.	0.	70.	0.	71.	.94
B21414	.2	0.0	19.8	0.0	.02	36.5	-45.9	0.0	.5	0.	0.	152.	0.	0.	.47
B21415	.1	0.0	5.7	0.0	.02	36.5	-53.6	0.0	.3	0.	0.	44.	0.	0.	.46
A22408	11.1	2.0	12.6	17.8	.93	56.9	0.0	0.0	25.3	17.	40.	97.	108.	124.	17.81
A22409	8.3	2.1	8.6	17.9	.82	56.9	-7.6	0.0	19.7	18.	36.	66.	109.	123.	15.56
A22410	10.2	2.0	10.5	19.9	.95	56.9	-15.3	0.0	23.5	16.	36.	81.	108.	135.	17.92
A22411	9.3	2.5	11.0	15.8	.79	56.9	-23.0	0.0	21.7	21.	39.	84.	103.	117.	14.67
A22412	8.5	3.0	10.6	14.6	.52	56.9	-30.6	0.0	20.2	31.	48.	82.	97.	108.	9.86
A22413	6.9	4.6	11.2	14.1	.28	56.9	-38.3	0.0	16.6	47.	71.	86.	86.	102.	5.42
A22414	3.0	9.3	11.8	13.3	.05	56.9	-45.9	0.0	7.8	88.	0.	90.	0.	92.	1.01
A22415	.2	0.0	10.5	0.0	.01	56.9	-53.6	0.0	.5	0.	0.	81.	0.	0.	.11
B22408	11.7	2.3	13.0	20.6	1.02	56.9	0.0	0.0	26.4	21.	42.	99.	113.	134.	18.88
B22409	10.9	2.5	13.3	18.5	.94	56.9	-7.6	0.0	24.9	20.	38.	102.	115.	127.	17.64
B22410	8.6	2.3	12.4	20.1	.88	56.9	-15.3	0.0	20.3	19.	51.	95.	108.	132.	16.81
B22411	9.4	2.9	12.0	16.6	.75	56.9	-23.0	0.0	21.9	27.	51.	92.	112.	123.	14.17
B22412	8.0	3.3	12.1	15.8	.52	56.9	-30.6	0.0	19.0	26.	47.	93.	95.	115.	9.95
B22413	5.3	6.1	12.8	14.3	.20	56.9	-38.3	0.0	13.2	53.	0.	98.	0.	107.	3.90
B22414	.3	0.0	13.0	0.0	.01	56.9	-45.9	0.0	.8	0.	0.	99.	0.	0.	.20
B22415	.0	0.0	8.2	0.0	0.00	56.9	-53.6	0.0	.1	0.	0.	63.	0.	0.	.04
A22308	.2	0.0	18.1	0.0	.01	56.9	53.6	0.0	.4	0.	0.	139.	0.	0.	.23
A22309	.2	0.0	11.8	0.0	.01	56.9	45.9	0.0	.4	0.	0.	91.	0.	0.	.22
A22310	1.5	11.6	11.7	12.6	.02	56.9	38.3	0.0	4.0	0.	0.	89.	0.	0.	.50

RUN NUMBER 2

FILE NAME	MODEL CONDITIONS: PEAK CONC. (%)	1% ARR. TIME (SEC)	PEAK TIME (SEC)	1% END TIME (SEC)	SUM (X-S)	POSITION X (M)	Y (M)	Z (M)	PROTOTYPE CONDITIONS: PEAK CONC. (%)	5% ARR. TIME (SEC)	15% ARR. TIME (SEC)	PEAK TIME (SEC)	15% END TIME (SEC)	5% END TIME (SEC)	SUM (X-S)
A22311	6.8	5.4	10.3	15.0	.34	56.9	30.6	0.0	16.3	43.	78.	79.	85.	106.	6.65
A22312	7.9	3.7	11.2	15.7	.62	56.9	23.0	0.0	18.9	30.	40.	86.	102.	117.	11.82
A22313	8.6	2.8	11.5	19.7	.81	56.9	15.3	0.0	20.3	23.	59.	88.	102.	131.	15.47
A22314	9.4	2.4	12.4	19.7	.86	56.9	7.6	0.0	22.0	20.	57.	95.	110.	121.	16.32
A22315	10.2	2.0	12.8	21.1	.82	56.9	0.0	0.0	23.6	20.	55.	98.	101.	121.	15.67
B22308	.1	0.0	5.3	0.0	.02	56.9	53.6	0.0	.4	0.	0.	41.	0.	0.	.35
B22309	.2	0.0	19.8	0.0	.01	56.9	45.9	0.0	.4	0.	0.	151.	0.	0.	.27
B22310	2.1	11.0	11.4	11.8	.03	56.9	38.3	0.0	5.6	87.	0.	87.	0.	88.	1.04
B22311	6.2	5.3	12.3	15.8	.42	56.9	30.6	0.0	15.1	50.	94.	94.	97.	110.	8.13
B22312	7.1	3.4	11.0	17.5	.57	56.9	23.0	0.0	17.2	34.	65.	85.	100.	124.	10.95
B22313	8.4	2.8	12.2	18.9	.73	56.9	15.3	0.0	19.9	24.	56.	93.	110.	126.	13.91
B22314	10.5	2.1	12.6	17.7	.90	56.9	7.6	0.0	24.1	21.	49.	97.	109.	121.	16.81
B22315	9.1	2.0	8.9	20.4	.78	56.9	0.0	0.0	21.3	19.	45.	68.	99.	120.	14.85
A23408	.1	0.0	.0	0.0	.01	90.9	53.6	0.0	.2	0.	0.	0.	0.	0.	.19
A23409	.1	0.0	40.4	0.0	.02	90.9	45.9	0.0	.3	0.	0.	309.	0.	0.	.34
A23410	2.3	11.4	13.2	15.6	.09	90.9	38.3	0.0	6.0	101.	0.	101.	0.	113.	1.77
A23411	4.8	6.0	12.9	16.7	.34	90.9	30.6	0.0	11.9	57.	0.	99.	0.	124.	6.78
A23412	6.0	5.3	14.4	18.5	.49	90.9	23.0	0.0	14.8	44.	0.	110.	0.	137.	9.48
A23413	5.7	4.2	13.3	18.6	.56	90.9	15.3	0.0	14.1	39.	0.	102.	0.	134.	10.85
A23414	5.4	3.8	12.9	19.2	.54	90.9	7.6	0.0	13.5	37.	0.	99.	0.	127.	10.58
A23415	5.6	3.4	13.8	17.6	.55	90.9	0.0	0.0	13.8	30.	0.	106.	0.	127.	10.80
B23408	.2	0.0	7.3	0.0	.03	90.9	53.6	0.0	.4	0.	0.	56.	0.	0.	.66
B23409	.2	0.0	10.1	0.0	.03	90.9	45.9	0.0	.6	0.	0.	77.	0.	0.	.66
B23410	4.4	9.3	13.0	15.4	.16	90.9	38.3	0.0	11.1	74.	0.	100.	0.	112.	3.24
B23411	4.6	4.8	9.9	18.2	.43	90.9	30.6	0.0	11.6	44.	0.	76.	0.	125.	8.45
B23412	4.9	4.2	14.3	17.2	.42	90.9	23.0	0.0	12.3	41.	0.	109.	0.	126.	8.28
B23413	5.3	3.6	13.9	18.1	.49	90.9	15.3	0.0	13.1	36.	0.	107.	0.	128.	9.67
B23414	5.8	3.8	10.3	18.4	.58	90.9	7.6	0.0	14.2	34.	0.	79.	0.	131.	11.27
B23415	5.9	3.4	14.0	17.1	.59	90.9	0.0	0.0	14.4	34.	0.	107.	0.	124.	11.48
A23306	6.4	3.0	8.8	17.6	.61	90.9	0.0	0.0	15.6	31.	66.	67.	70.	124.	11.86
A23309	5.9	2.9	14.3	17.7	.62	90.9	-7.6	0.0	14.4	29.	0.	110.	0.	128.	12.05
A23310	6.5	3.6	11.6	19.7	.71	90.9	-15.3	0.0	15.7	30.	89.	89.	116.	141.	13.63
A23311	5.6	3.5	9.7	16.6	.56	90.9	-23.0	0.0	13.9	33.	0.	74.	0.	126.	10.77
A23312	5.3	4.4	9.4	15.9	.41	90.9	-30.6	0.0	13.1	37.	0.	72.	0.	113.	8.04
A23313	4.6	5.9	10.6	16.2	.34	90.9	-38.3	0.0	11.6	50.	0.	81.	0.	114.	6.69
A23314	2.6	8.4	13.3	15.0	.14	90.9	-45.9	0.0	6.8	101.	0.	102.	0.	107.	2.79
A23315	.1	0.0	10.1	0.0	.02	90.9	-53.6	0.0	.4	0.	0.	78.	0.	0.	.91
B23308	6.6	3.4	13.5	17.4	.60	90.9	0.0	0.0	16.1	30.	101.	103.	107.	126.	11.68
B23309	6.6	3.8	13.3	17.4	.58	90.9	-7.6	0.0	16.0	35.	101.	102.	106.	129.	11.30
B23310	7.2	3.8	14.2	20.1	.75	90.9	-15.3	0.0	17.3	33.	102.	109.	123.	138.	14.40
B23311	6.2	4.3	13.2	18.5	.54	90.9	-23.0	0.0	15.2	34.	101.	101.	101.	127.	10.49
B23312	6.1	4.6	12.6	17.6	.44	90.9	-30.6	0.0	15.0	40.	96.	96.	97.	124.	8.56
B23313	5.1	5.5	12.1	15.8	.35	90.9	-38.3	0.0	12.7	51.	0.	93.	0.	118.	6.80
B23314	2.2	11.8	13.6	15.3	.07	90.9	-45.9	0.0	5.7	95.	0.	104.	0.	104.	1.43
B23315	.1	0.0	19.4	0.0	.01	90.9	-53.6	0.0	.3	0.	0.	148.	0.	0.	.14
A24308	4.3	4.5	12.7	18.2	.45	140.3	0.0	0.0	10.7	46.	0.	97.	0.	132.	8.86
A24309	4.1	5.4	13.6	19.4	.47	140.3	-7.6	0.0	10.4	42.	0.	104.	0.	138.	9.20
A24310	4.5	4.7	13.8	19.6	.49	140.3	-15.3	0.0	11.3	47.	0.	106.	0.	144.	9.67
A24311	3.7	6.1	12.7	17.8	.35	140.3	-23.0	0.0	9.4	51.	0.	97.	0.	128.	7.01
A24312	3.5	5.3	10.3	16.9	.31	140.3	-30.6	0.0	9.0	56.	0.	79.	0.	128.	6.15

RUN NUMBER 2

FILE NAME	MODEL CONDITIONS: PEAK CONC. (%)	1% ARR. TIME (SEC)	PEAK TIME (SEC)	1% END TIME (SEC)	SUM (X-S)	PROTOTYPE CONDITIONS: POSITION X (M)	Y (M)	Z (M)	PEAK CONC. (%)	5% ARR. TIME (SEC)	15% ARR. TIME (SEC)	PEAK TIME (SEC)	15% END TIME (SEC)	5% END TIME (SEC)	SUM (X-S)
A24313	3.3	6.0	13.6	17.3	.27	140.3	-38.3	0.0	8.4	59.	0.	104.	0.	122.	5.42
A24314	3.6	6.8	13.6	17.7	.23	140.3	-45.9	0.0	9.2	79.	0.	104.	0.	128.	4.68
A24315	1.5	13.4	14.4	16.3	.06	140.3	-53.6	0.0	3.8	0.	0.	110.	0.	0.	1.15
B24308	5.0	4.6	14.5	20.5	.54	140.3	0.0	0.0	12.4	48.	0.	111.	0.	137.	10.59
B24309	4.5	5.0	14.8	20.2	.50	140.3	-7.6	0.0	11.2	39.	0.	113.	0.	146.	9.81
B24310	4.1	4.9	14.7	19.4	.44	140.3	-15.3	0.0	10.3	48.	0.	112.	0.	135.	8.72
B24311	3.4	5.4	13.0	18.9	.35	140.3	-23.0	0.0	8.6	54.	0.	100.	0.	123.	6.96
B24312	3.1	5.5	11.1	17.0	.27	140.3	-30.6	0.0	7.9	58.	0.	85.	0.	126.	5.49
B24313	2.9	6.4	13.3	17.1	.25	140.3	-38.3	0.0	7.3	69.	0.	102.	0.	119.	5.10
B24314	3.0	8.2	13.8	16.1	.19	140.3	-45.9	0.0	7.8	67.	0.	105.	0.	116.	3.87
B24315	1.6	14.8	14.8	15.1	.04	140.3	-53.6	0.0	2.7	0.	0.	113.	0.	0.	.75
A24408	.1	0.0	16.4	0.0	.02	140.3	53.6	0.0	.4	0.	0.	126.	0.	0.	.34
A24409	.2	0.0	14.4	0.0	.02	140.3	45.9	0.0	2.3	0.	0.	110.	0.	0.	.47
A24410	2.2	10.5	14.3	16.4	.12	140.3	38.3	0.0	5.7	106.	0.	110.	0.	117.	2.34
A24411	2.9	7.7	15.8	18.7	.25	140.3	30.6	0.0	7.6	72.	0.	121.	0.	137.	5.04
A24412	3.1	6.4	12.6	18.6	.29	140.3	23.0	0.0	7.9	59.	0.	97.	0.	128.	5.81
A24413	3.4	6.0	13.3	17.7	.33	140.3	15.3	0.0	8.6	58.	0.	102.	0.	123.	6.49
A24414	3.3	5.8	15.2	18.9	.34	140.3	7.6	0.0	8.5	53.	0.	116.	0.	133.	6.88
A24415	3.6	5.4	14.7	18.6	.38	140.3	0.0	0.0	9.2	51.	0.	112.	0.	128.	7.52
B24408	.1	0.0	10.5	0.0	.01	140.3	53.6	0.0	.3	0.	0.	80.	0.	0.	.12
B24409	.2	0.0	11.6	0.0	.02	140.3	45.9	0.0	.5	0.	0.	89.	0.	0.	.39
B24410	2.2	8.2	13.5	15.5	.11	140.3	38.3	0.0	5.7	102.	0.	103.	0.	112.	2.13
B24411	2.5	6.7	12.9	17.0	.22	140.3	30.6	0.0	6.4	74.	0.	99.	0.	127.	4.36
B24412	3.0	5.8	8.7	17.5	.27	140.3	23.0	0.0	7.7	56.	0.	66.	0.	122.	5.39
B24413	3.2	5.4	15.0	18.3	.33	140.3	15.3	0.0	8.1	52.	0.	115.	0.	128.	6.60
B24414	4.0	5.6	13.0	18.2	.35	140.3	7.6	0.0	10.1	51.	0.	100.	0.	133.	7.00
B24415	3.6	4.3	13.3	19.0	.37	140.3	0.0	0.0	9.3	51.	0.	102.	0.	134.	7.36
A25408	.9	0.0	10.4	0.0	.03	242.3	53.6	0.0	2.3	0.	0.	79.	0.	0.	.61
A25409	1.1	10.4	10.4	10.4	.07	242.3	45.9	0.0	2.9	0.	0.	79.	0.	0.	1.35
A25410	1.4	10.4	14.1	18.7	.13	242.3	38.3	0.0	3.8	0.	0.	108.	0.	0.	2.58
A25411	1.5	10.4	15.8	19.0	.13	242.3	30.6	0.0	3.8	0.	0.	121.	0.	0.	2.70
A25412	1.4	10.9	14.8	19.3	.15	242.3	23.0	0.0	3.8	0.	0.	113.	0.	0.	3.01
A25413	1.7	8.9	16.2	19.4	.18	242.3	15.3	0.0	4.4	0.	0.	124.	0.	0.	3.64
A25414	2.0	9.6	16.5	19.9	.19	242.3	7.6	0.0	5.3	126.	0.	126.	0.	130.	3.89
A25415	2.0	8.8	16.4	19.8	.22	242.3	0.0	0.0	5.3	104.	0.	126.	0.	128.	4.50
B25408	.7	0.0	17.0	0.0	.03	242.3	53.6	0.0	1.8	0.	0.	131.	0.	0.	.52
B25409	1.4	14.5	16.8	18.2	.08	242.3	45.9	0.0	3.7	0.	0.	128.	0.	0.	1.60
B25410	1.5	11.8	16.2	17.8	.11	242.3	38.3	0.0	3.9	0.	0.	124.	0.	0.	2.16
B25411	1.5	11.4	14.5	20.0	.15	242.3	30.6	0.0	4.0	0.	0.	111.	0.	0.	3.13
B25412	1.7	11.4	14.5	19.9	.17	242.3	23.0	0.0	4.6	0.	0.	111.	0.	0.	3.44
B25413	1.9	10.0	15.0	20.9	.21	242.3	15.3	0.0	5.0	0.	0.	115.	0.	0.	4.29
B25414	2.0	8.8	14.6	20.4	.22	242.3	7.6	0.0	5.3	112.	0.	112.	0.	115.	4.40
B25415	2.1	8.5	15.5	20.2	.23	242.3	0.0	0.0	5.4	119.	0.	119.	0.	123.	4.62
A25308	2.1	8.1	12.9	19.5	.22	242.3	0.0	0.0	5.4	98.	0.	99.	0.	132.	4.38
A25309	2.0	8.6	14.3	20.5	.23	242.3	-7.6	0.0	5.2	99.	0.	110.	0.	135.	4.72
A25310	2.4	8.2	16.1	21.6	.30	242.3	-15.3	0.0	6.3	78.	0.	123.	0.	144.	5.95
A25311	2.4	8.7	17.2	21.2	.26	242.3	-23.0	0.0	6.2	91.	0.	132.	0.	151.	5.22
A25312	2.1	9.5	16.0	20.2	.19	242.3	-30.6	0.0	5.6	121.	0.	122.	0.	145.	3.82
A25313	1.9	9.8	16.0	19.4	.18	242.3	-38.3	0.0	5.0	122.	0.	122.	0.	123.	3.60
A25314	1.8	10.9	16.2	19.2	.15	242.3	-45.9	0.0	4.6	0.	0.	124.	0.	0.	2.98

RUN NUMBER 2

MODEL CONDITIONS						PROTOTYPE CONDITIONS									
FILE NAME	PEAK CONC. (%)	1% ARR. TIME (SEC)	PEAK TIME (SEC)	1% END TIME (SEC)	SUM (X-S)	POSITION X (M)	POSITION Y (M)	POSITION Z (M)	PEAK CONC. (%)	5% ARR. TIME (SEC)	15% ARR. TIME (SEC)	PEAK TIME (SEC)	15% END TIME (SEC)	5% END TIME (SEC)	SUM (X-S)
A25315	1.8	11.4	15.8	19.6	.13	242.3	-53.6	0.0	4.8	0.	0.	121.	0.	0.	2.64
B25308	2.5	8.0	16.8	19.9	.25	242.3	0.0	0.0	6.4	100.	0.	129.	0.	140.	4.95
B25309	2.2	8.1	15.6	19.9	.22	242.3	-7.6	0.0	5.8	87.	0.	119.	0.	138.	4.45
B25310	2.5	7.2	14.4	21.2	.30	242.3	-15.3	0.0	6.5	86.	0.	110.	0.	151.	6.11
B25311	2.3	8.2	16.7	20.2	.25	242.3	-23.0	0.0	6.0	92.	0.	128.	0.	144.	5.01
B25312	1.9	8.6	17.1	18.9	.17	242.3	-30.6	0.0	5.0	131.	0.	131.	0.	133.	3.39
B25313	1.8	8.9	13.3	19.1	.18	242.3	-38.3	0.0	4.8	0.	0.	102.	0.	0.	3.70
B25314	1.9	9.8	14.0	19.1	.16	242.3	-45.9	0.0	4.9	0.	0.	108.	0.	0.	3.24
B25315	1.7	12.5	16.8	19.6	.13	242.3	-53.6	0.0	4.5	0.	0.	129.	0.	0.	2.74
A26308	1.1	15.4	18.8	21.0	.13	399.8	0.0	0.0	3.0	0.	0.	144.	0.	0.	2.72
A26309	1.2	16.5	20.0	21.0	.13	399.8	-7.6	0.0	3.2	0.	0.	154.	0.	0.	2.57
A26310	1.3	14.0	17.7	22.2	.15	399.8	-15.3	0.0	3.6	0.	0.	135.	0.	0.	3.12
A26311	1.3	13.6	20.6	21.2	.16	399.8	-23.0	0.0	3.6	0.	0.	158.	0.	0.	3.29
A26312	1.3	14.0	17.2	20.6	.15	399.8	-30.6	0.0	3.4	0.	0.	131.	0.	0.	3.05
A26313	.9	0.0	20.4	0.0	.07	399.8	-38.3	0.0	2.5	0.	0.	157.	0.	0.	1.38
A26314	1.1	16.4	16.4	18.1	.13	399.8	-45.9	0.0	2.9	0.	0.	126.	0.	0.	2.60
A26315	1.1	17.2	17.8	18.9	.12	399.8	-53.6	0.0	2.9	0.	0.	137.	0.	0.	2.40
B26308	1.2	13.6	18.4	21.8	.13	399.5	0.0	0.0	3.1	0.	0.	141.	0.	0.	2.70
B26309	1.1	15.2	16.8	21.0	.13	399.5	-7.6	0.0	3.0	0.	0.	129.	0.	0.	2.71
B26310	1.5	14.0	19.4	22.0	.16	399.5	-15.3	0.0	3.9	0.	0.	149.	0.	0.	3.34
B26311	1.5	14.4	20.2	22.8	.16	399.5	-23.0	0.0	3.9	0.	0.	155.	0.	0.	3.31
B26312	1.3	14.8	22.0	23.2	.15	399.5	-30.6	0.0	3.6	0.	0.	169.	0.	0.	3.13
B26313	1.3	14.3	17.3	22.5	.14	399.5	-38.3	0.0	3.3	0.	0.	133.	0.	0.	2.91
B26314	1.0	17.4	17.4	20.2	.11	399.5	-45.9	0.0	2.8	0.	0.	134.	0.	0.	2.24
B26315	1.1	17.4	17.7	20.2	.10	399.5	-53.6	0.0	3.0	0.	0.	136.	0.	0.	1.99
A26408	.7	0.0	10.4	0.0	.03	399.5	53.6	0.0	1.9	0.	0.	80.	0.	0.	.61
A26409	.7	0.0	10.5	0.0	.04	399.5	45.9	0.0	1.9	0.	0.	80.	0.	0.	.76
A26410	1.0	0.0	18.5	0.0	.08	399.5	38.3	0.0	2.6	0.	0.	142.	0.	0.	1.60
A26411	1.0	19.9	19.9	21.2	.11	399.5	30.6	0.0	2.8	0.	0.	153.	0.	0.	2.30
A26412	.9	0.0	18.3	0.0	.11	399.5	23.0	0.0	2.5	0.	0.	140.	0.	0.	2.22
A26413	1.1	18.4	18.4	22.4	.12	399.5	15.3	0.0	2.8	0.	0.	141.	0.	0.	2.54
A26414	1.1	20.0	20.0	21.0	.11	399.5	7.6	0.0	2.9	0.	0.	154.	0.	0.	2.17
A26415	1.1	18.2	18.2	20.6	.12	399.5	0.0	0.0	2.9	0.	0.	140.	0.	0.	2.39
B26408	.6	0.0	20.2	0.0	.03	399.5	53.6	0.0	1.5	0.	0.	155.	0.	0.	.57
B26409	.5	0.0	17.6	0.0	.04	399.5	45.9	0.0	1.3	0.	0.	135.	0.	0.	.84
B26410	.9	0.0	17.8	0.0	.08	399.5	38.3	0.0	2.5	0.	0.	136.	0.	0.	1.54
B26411	1.0	0.0	20.4	0.0	.09	399.5	30.6	0.0	2.6	0.	0.	157.	0.	0.	1.93
B26412	1.0	18.4	18.4	18.6	.11	399.5	23.0	0.0	2.7	0.	0.	141.	0.	0.	2.21
B26413	1.1	16.6	18.4	21.3	.12	399.5	15.3	0.0	3.0	0.	0.	141.	0.	0.	2.52
B26414	1.0	17.8	17.8	22.5	.11	399.5	7.6	0.0	2.8	0.	0.	136.	0.	0.	2.24
B26415	1.2	16.8	17.0	22.0	.13	399.5	0.0	0.0	3.1	0.	0.	130.	0.	0.	2.73

RUN NUMBER 3

FILE NAME	MODEL CONDITIONS: PEAK CONC. (%)	1% ARR. TIME (SEC)	PEAK TIME (SEC)	1% END TIME (SEC)	SUM (X-S)	POSITION X (M)	Y (M)	Z (M)	PROTOTYPE CONDITIONS: PEAK CONC. (%)	5% ARR. TIME (SEC)	15% ARR. TIME (SEC)	PEAK TIME (SEC)	15% END TIME (SEC)	5% END TIME (SEC)	SUM (X-S)
A31308	6.1	13.4	18.4	38.1	1.08	36.6	53.6	0.0	19.3	103.	117.	141.	161.	264.	20.63
A31309	9.0	9.5	17.6	44.9	1.62	36.6	45.9	0.0	21.0	80.	112.	135.	184.	320.	30.78
A31310	13.0	7.8	17.3	49.9	2.64	36.6	38.3	0.0	28.7	63.	85.	133.	227.	357.	48.15
A31311	13.7	6.0	16.2	48.9	3.11	36.6	30.6	0.0	30.0	48.	70.	124.	244.	365.	55.86
A31312	15.0	5.4	16.2	53.5	3.69	36.6	23.0	0.0	32.3	42.	51.	124.	238.	380.	65.41
A31313	16.5	4.1	14.6	57.4	4.10	36.6	15.3	0.0	34.7	33.	40.	112.	260.	402.	72.50
A31314	19.0	3.4	14.3	56.7	4.76	36.6	7.6	0.0	38.8	27.	34.	109.	302.	412.	82.78
A31315	18.0	3.0	15.5	61.2	4.77	36.6	0.0	0.0	37.2	24.	33.	119.	298.	415.	83.38
B31308	8.8	11.1	18.5	37.6	1.49	36.6	53.6	0.0	20.7	85.	107.	142.	203.	279.	27.93
B31309	9.1	9.8	18.4	42.0	1.71	36.6	45.9	0.0	21.4	76.	102.	141.	195.	311.	32.08
B31310	12.9	7.3	16.7	49.4	2.68	36.6	38.3	0.0	28.6	57.	75.	128.	228.	345.	48.60
B31311	13.7	6.1	16.2	51.0	3.05	36.6	30.6	0.0	30.0	52.	65.	124.	237.	366.	54.75
B31312	15.7	5.2	14.8	52.0	3.56	36.6	23.0	0.0	33.6	41.	51.	114.	236.	382.	63.13
B31313	17.1	4.0	13.5	53.8	3.89	36.6	15.3	0.0	35.9	32.	38.	103.	243.	371.	68.37
B31314	18.5	2.9	14.7	54.8	4.55	36.6	7.6	0.0	38.1	24.	30.	113.	282.	380.	79.07
B31315	15.7	2.7	14.8	54.8	4.44	36.6	0.0	0.0	33.5	25.	34.	114.	293.	379.	78.31
A31208	.1	0.0	68.8	0.0	0.00	36.6	107.1	0.0	.3	0.	0.	527.	0.	0.	.03
A31209	.1	0.0	66.6	0.0	.03	36.6	99.4	0.0	.4	0.	0.	519.	0.	0.	.33
A31210	.1	0.0	42.5	0.0	.02	36.6	91.8	0.0	.3	0.	0.	326.	0.	0.	.34
A31211	.2	0.0	33.3	0.0	.02	36.6	84.1	0.0	.5	0.	0.	255.	0.	0.	.50
A31212	.2	0.0	26.0	0.0	.01	36.6	76.5	0.0	.4	0.	0.	199.	0.	0.	.21
A31213	.5	0.0	23.5	0.0	.02	36.6	68.9	0.0	1.2	0.	0.	180.	0.	0.	.36
A31214	3.4	17.8	20.4	28.3	.21	36.6	61.2	0.0	8.7	140.	0.	156.	0.	186.	4.30
A31215	6.2	14.7	17.4	35.4	.79	36.6	53.6	0.0	15.2	114.	133.	133.	135.	259.	15.29
A31408	18.9	2.8	14.7	58.3	5.11	36.6	0.0	0.0	38.7	23.	36.	113.	338.	432.	88.43
A31409	18.3	3.0	14.8	58.1	4.61	36.6	-7.6	0.0	37.7	24.	34.	114.	293.	405.	80.68
A31410	21.7	2.9	14.4	58.1	5.12	36.6	-15.3	0.0	42.8	24.	29.	110.	293.	420.	87.62
A31411	20.3	3.2	14.4	58.2	4.56	36.6	-23.0	0.0	40.7	27.	36.	110.	261.	415.	78.84
A31412	16.5	3.8	15.3	50.0	3.33	36.6	-30.6	0.0	34.8	30.	40.	117.	217.	374.	59.43
A31413	12.8	4.9	15.8	50.3	2.47	36.6	-38.3	0.0	28.3	38.	53.	121.	175.	339.	45.34
A31414	12.2	6.7	16.2	38.0	1.90	36.6	-45.9	0.0	27.3	52.	66.	124.	186.	274.	35.01
A31415	9.7	8.6	16.8	35.4	1.25	36.6	-53.6	0.0	22.6	67.	100.	129.	162.	259.	23.46
B31408	15.9	2.5	19.3	60.0	4.65	36.6	0.0	0.0	33.8	20.	33.	148.	325.	400.	81.54
B31409	14.8	3.1	15.9	56.1	3.89	36.6	-7.6	0.0	31.9	24.	31.	122.	305.	377.	69.64
B31410	19.6	2.7	12.1	57.4	5.11	36.6	-15.3	0.0	39.8	26.	36.	93.	307.	418.	88.07
B31411	18.5	3.3	13.5	57.7	4.50	36.6	-23.0	0.0	38.1	26.	33.	119.	276.	414.	78.88
B31412	16.9	3.8	16.0	54.0	3.48	36.6	-30.6	0.0	35.4	32.	41.	123.	217.	402.	62.26
B31413	14.1	5.1	16.1	47.2	2.77	36.6	-38.3	0.0	30.7	42.	55.	123.	198.	348.	50.20
B31414	12.9	5.6	16.7	42.6	2.35	36.6	-45.9	0.0	28.5	44.	68.	128.	196.	319.	42.98
B31415	10.7	7.2	17.5	38.0	1.71	36.6	-53.6	0.0	24.5	58.	86.	134.	197.	281.	31.86
A31508	11.4	7.4	17.3	39.0	1.81	36.6	-53.6	0.0	25.9	58.	78.	133.	185.	257.	33.34
A31509	7.1	9.6	18.3	31.9	.91	36.6	-61.2	0.0	17.1	77.	121.	140.	143.	224.	17.55
A31510	4.7	11.7	18.2	29.8	.52	36.6	-68.9	0.0	11.7	109.	0.	140.	0.	207.	10.35
A31511	3.2	17.8	19.0	30.1	.30	36.6	-76.5	0.0	8.3	141.	0.	145.	0.	193.	6.07
A31512	2.3	21.5	21.7	28.6	.16	36.6	-84.1	0.0	6.1	165.	0.	166.	0.	186.	3.20
A31513	.9	0.0	28.8	0.0	.07	36.6	-91.8	0.0	2.5	0.	0.	220.	0.	0.	1.45
A31514	.2	0.0	49.6	0.0	.02	36.6	-99.4	0.0	.5	0.	0.	380.	0.	0.	.45
A31515	.1	0.0	.0	0.0	.02	36.6	-107.1	0.0	.2	0.	0.	0.	0.	0.	.35
A32508	8.1	8.6	17.2	47.7	1.72	56.9	-53.6	0.0	19.3	73.	99.	131.	182.	332.	32.65
A32509	7.5	9.3	18.2	43.2	1.52	56.9	-61.2	0.0	18.1	79.	118.	140.	185.	305.	28.82

RUN NUMBER 3

FILE NAME	MODEL CONDITIONS: PEAK CONC. (%)	1% ARR. TIME (SEC)	PEAK TIME (SEC)	1% END TIME (SEC)	SUM (X-S)	PROTOTYPE CONDITIONS: POSITION X (M)	Y (M)	Z (M)	PEAK CONC. (%)	5% ARR. TIME (SEC)	15% ARR. TIME (SEC)	PEAK TIME (SEC)	15% END TIME (SEC)	5% END TIME (SEC)	SUM (X-S)
A32310	7.2	12.1	18.7	39.0	1.29	56.9	-68.9	0.0	17.4	105.	129.	143.	204.	271.	24.51
A32311	5.3	14.6	19.6	37.2	.82	56.9	-76.5	0.0	13.1	118.	0.	150.	0.	262.	15.92
A32312	4.7	16.2	20.2	32.5	.54	56.9	-84.1	0.0	11.7	139.	0.	155.	0.	237.	10.57
A32313	3.1	19.8	22.5	31.0	.30	56.9	-91.8	0.0	8.0	157.	0.	172.	0.	205.	6.06
A32314	1.7	24.9	26.4	29.5	.13	56.9	-99.4	0.0	4.4	0.	0.	202.	0.	0.	2.70
A32315	.1	0.0	50.0	0.0	.03	56.9	-107.1	0.0	.3	0.	0.	383.	0.	0.	.53
A32408	10.5	4.8	18.3	62.3	3.15	56.9	0.0	0.0	24.1	40.	74.	140.	256.	436.	58.46
A32409	8.7	5.5	17.1	58.4	2.38	56.9	-7.6	0.0	20.5	45.	80.	131.	204.	388.	44.99
A32410	9.7	5.0	16.8	60.5	2.80	56.9	-15.3	0.0	22.5	41.	65.	129.	224.	408.	52.52
A32411	9.1	5.6	17.8	56.4	2.51	56.9	-23.0	0.0	21.4	45.	74.	136.	216.	413.	47.38
A32412	8.4	5.0	18.6	55.6	2.37	56.9	-30.6	0.0	19.8	46.	76.	142.	220.	413.	44.79
A32413	7.7	5.6	15.6	58.7	2.20	56.9	-38.3	0.0	18.4	51.	97.	119.	197.	400.	41.95
A32414	7.5	6.8	17.1	56.3	2.00	56.9	-45.9	0.0	17.9	55.	94.	131.	186.	419.	38.22
A32415	7.1	7.8	17.2	51.4	1.74	56.9	-53.6	0.0	17.2	65.	110.	132.	174.	354.	33.34
B32408	11.3	4.6	16.4	58.0	3.37	56.9	0.0	0.0	25.6	41.	73.	126.	266.	432.	62.11
B32409	9.2	5.4	15.1	59.3	2.62	56.9	-7.6	0.0	21.4	49.	86.	116.	223.	396.	49.37
B32410	9.5	5.0	17.2	61.8	2.86	56.9	-15.3	0.0	22.1	43.	63.	131.	225.	397.	53.61
B32411	9.4	5.4	17.3	57.2	2.63	56.9	-23.0	0.0	22.0	47.	85.	133.	220.	402.	49.64
B32412	9.1	5.7	17.8	58.0	2.48	56.9	-30.6	0.0	21.2	47.	87.	136.	199.	417.	46.82
B32413	8.5	6.5	16.7	57.8	2.16	56.9	-38.3	0.0	20.1	56.	98.	128.	199.	412.	41.21
B32414	8.1	7.8	17.3	56.5	1.91	56.9	-45.9	0.0	19.3	63.	113.	132.	201.	359.	36.40
B32415	7.7	8.3	18.2	52.2	1.78	56.9	-53.6	0.0	18.3	71.	120.	140.	185.	361.	34.04
A32308	7.7	12.2	23.0	44.4	1.35	56.9	53.6	0.0	18.4	109.	145.	176.	207.	317.	25.75
A32309	7.6	11.1	22.6	46.2	1.39	56.9	45.9	0.0	16.8	102.	143.	168.	178.	330.	26.73
A32310	9.1	9.6	20.8	48.9	2.01	56.9	38.3	0.0	21.3	75.	116.	159.	231.	367.	37.74
A32311	9.8	7.9	18.5	52.0	2.42	56.9	30.6	0.0	22.7	68.	102.	142.	237.	377.	44.98
A32312	10.3	7.6	19.7	53.9	2.77	56.9	23.0	0.0	23.7	59.	87.	151.	260.	379.	51.17
A32313	10.4	6.4	19.9	55.2	3.15	56.9	15.3	0.0	23.8	51.	71.	152.	263.	416.	57.99
A32314	11.1	5.7	19.4	59.3	3.43	56.9	7.6	0.0	25.2	48.	71.	149.	277.	427.	62.95
A32315	9.4	5.2	21.0	63.4	3.33	56.9	0.0	0.0	22.0	44.	79.	161.	269.	467.	61.98
A32208	.1	0.0	88.0	0.0	.01	56.9	107.1	0.0	.3	0.	0.	674.	0.	0.	.12
A32209	.1	0.0	3.6	0.0	.01	56.9	99.4	0.0	.3	0.	0.	27.	0.	0.	.11
A32210	.5	0.0	27.6	0.0	.02	56.9	91.8	0.0	1.3	0.	0.	211.	0.	0.	.47
A32211	.6	0.0	26.9	0.0	.04	56.9	84.1	0.0	1.6	0.	0.	206.	0.	0.	.89
A32212	2.5	21.5	23.9	28.8	.18	56.9	76.5	0.0	6.4	169.	0.	183.	0.	214.	3.64
A32213	3.4	18.6	22.8	31.6	.37	56.9	68.9	0.0	8.6	150.	0.	174.	0.	235.	7.34
A32214	4.9	15.2	20.6	38.8	.85	56.9	61.2	0.0	12.3	123.	0.	158.	0.	286.	16.59
A32215	5.5	13.5	21.2	38.0	.95	56.9	53.6	0.0	13.6	106.	0.	163.	0.	275.	18.45
A33308	4.2	15.0	24.7	44.5	.81	90.9	53.6	0.0	10.6	138.	0.	189.	0.	299.	15.99
A33309	4.1	14.2	24.1	46.9	.90	90.9	45.9	0.0	10.5	121.	0.	185.	0.	305.	17.86
A33310	4.6	13.9	23.8	51.9	1.15	90.9	38.3	0.0	11.5	116.	0.	183.	0.	335.	22.67
A33311	5.1	11.9	24.2	56.4	1.51	90.9	30.6	0.0	12.8	104.	0.	185.	0.	388.	29.51
A33312	5.6	11.5	23.7	58.0	1.74	90.9	23.0	0.0	13.7	93.	0.	181.	0.	417.	33.77
A33313	5.5	9.9	22.5	63.2	1.87	90.9	15.3	0.0	13.5	83.	0.	173.	0.	440.	36.45
A33314	5.4	9.6	21.5	65.4	1.92	90.9	7.6	0.0	13.4	78.	0.	165.	0.	415.	37.32
A33315	4.9	8.8	23.1	66.5	1.88	90.9	0.0	0.0	12.2	78.	0.	177.	0.	449.	36.67
A33208	.1	0.0	21.6	0.0	.01	90.9	107.1	0.0	.3	0.	0.	166.	0.	0.	.27
A33209	.2	0.0	6.2	0.0	.02	90.9	99.4	0.0	.4	0.	0.	47.	0.	0.	.35
A33210	.2	0.0	8.1	0.0	.02	90.9	91.8	0.0	.4	0.	0.	62.	0.	0.	.36
A33211	.4	0.0	23.6	0.0	.01	90.9	84.1	0.0	1.0	0.	0.	181.	0.	0.	.26

RUN NUMBER 3

FILE NAME	MODEL CONDITIONS PEAK CONC. (%)	1% ARR. TIME (SEC)	PEAK TIME (SEC)	1% END TIME (SEC)	SUM (X-S)	PROTOTYPE CONDITIONS POSITION X (M)	Y (M)	Z (M)	PEAK CONC. (%)	5% ARR. TIME (SEC)	15% ARR. TIME (SEC)	PEAK TIME (SEC)	15% END TIME (SEC)	5% END TIME (SEC)	SUM (X-S)
A33212	2.3	21.0	24.0	30.3	.18	90.9	76.5	0.0	6.0	170.	0.	184.	0.	230.	3.56
A33213	2.3	19.6	28.6	33.4	.29	90.9	68.9	0.0	6.0	157.	0.	219.	0.	231.	5.81
A33214	3.0	18.3	27.4	40.5	.50	90.9	61.2	0.0	7.6	149.	0.	210.	0.	286.	10.09
A33215	3.3	16.3	26.1	40.5	.67	90.9	53.6	0.0	8.5	140.	0.	200.	0.	276.	13.34
A33408	5.7	7.4	25.0	59.7	1.95	90.9	0.0	0.0	14.0	69.	0.	191.	0.	426.	37.80
A33409	4.9	8.4	24.7	57.6	1.62	90.9	-7.6	0.0	12.2	85.	0.	189.	0.	394.	31.67
A33410	4.9	9.1	24.0	56.7	1.61	90.9	-15.3	0.0	12.1	83.	0.	184.	0.	396.	31.44
A33411	4.6	8.3	21.5	56.8	1.59	90.9	-23.0	0.0	11.5	80.	0.	165.	0.	395.	31.15
A33412	4.7	9.2	19.6	59.2	1.60	90.9	-30.6	0.0	11.7	79.	0.	150.	0.	399.	31.28
A33413	4.4	9.2	22.4	61.0	1.48	90.9	-38.3	0.0	11.1	77.	0.	171.	0.	347.	29.12
A33414	4.6	11.2	20.0	56.6	1.28	90.9	-45.9	0.0	11.5	89.	0.	153.	0.	297.	25.15
A33415	4.0	11.6	20.4	47.7	.91	90.9	-53.6	0.0	10.0	111.	0.	156.	0.	294.	18.02
A33508	3.8	12.6	19.9	44.1	.80	90.9	-53.6	0.0	9.6	111.	0.	152.	0.	273.	15.89
A33509	3.1	12.3	21.0	42.0	.65	90.9	-61.2	0.0	8.1	117.	0.	161.	0.	232.	12.97
A33510	3.7	13.1	21.1	44.1	.76	90.9	-68.9	0.0	9.3	120.	0.	161.	0.	316.	15.01
A33511	3.5	15.6	19.3	43.2	.63	90.9	-76.5	0.0	8.9	127.	0.	148.	0.	305.	12.57
A33512	3.8	16.2	20.4	42.8	.72	90.9	-84.1	0.0	9.7	133.	0.	156.	0.	304.	14.32
A33513	3.5	18.0	22.0	38.2	.58	90.9	-91.8	0.0	9.0	149.	0.	169.	0.	267.	11.45
A33514	3.6	20.2	32.8	37.6	.47	90.9	-99.4	0.0	9.1	161.	0.	251.	0.	269.	9.40
A33515	2.7	23.3	24.2	32.2	.19	90.9	-107.1	0.0	6.9	181.	0.	186.	0.	221.	3.91
A34408	3.4	12.1	24.5	61.5	1.29	140.3	0.0	0.0	8.7	123.	0.	188.	0.	415.	25.63
A34409	3.1	12.9	27.2	62.6	1.17	140.3	-7.6	0.0	7.9	130.	0.	209.	0.	371.	23.43
A34410	3.2	12.9	28.9	62.8	1.22	140.3	-15.3	0.0	8.3	124.	0.	222.	0.	392.	24.28
A34411	2.9	15.1	29.0	57.9	1.02	140.3	-23.0	0.0	7.4	142.	0.	222.	0.	377.	20.34
A34412	2.5	14.6	25.2	58.8	.89	140.3	-30.6	0.0	6.6	142.	0.	193.	0.	311.	17.97
A34413	2.6	15.1	25.1	60.6	.93	140.3	-38.3	0.0	6.8	136.	0.	192.	0.	332.	18.62
A34414	2.9	15.2	26.0	53.3	.87	140.3	-45.9	0.0	7.4	142.	0.	199.	0.	325.	17.39
A34415	2.6	16.5	28.4	52.1	.78	140.3	-53.6	0.0	6.8	149.	0.	218.	0.	298.	15.61
A34508	2.8	14.6	26.4	58.3	.89	140.3	-53.6	0.0	7.4	135.	0.	203.	0.	310.	17.82
A34509	2.3	15.8	31.1	50.2	.65	140.3	-61.2	0.0	6.1	156.	0.	238.	0.	247.	13.12
A34510	2.8	16.0	29.2	46.3	.64	140.3	-68.9	0.0	7.2	160.	0.	223.	0.	304.	12.81
A34511	2.3	19.6	33.2	47.8	.56	140.3	-76.5	0.0	5.9	195.	0.	255.	0.	282.	11.21
A34512	2.0	22.3	33.4	44.1	.47	140.3	-84.1	0.0	5.3	252.	0.	256.	0.	274.	9.41
A34513	1.8	23.5	32.0	43.0	.38	140.3	-91.8	0.0	4.6	0.	0.	245.	0.	0.	7.74
A34514	1.6	23.6	29.1	44.1	.35	140.3	-99.4	0.0	4.3	0.	0.	223.	0.	0.	7.03
A34515	1.8	22.6	30.6	45.2	.36	140.3	-107.1	0.0	4.6	0.	0.	234.	0.	0.	7.20
A34308	2.6	20.3	30.8	48.8	.58	140.3	53.6	0.0	6.7	181.	0.	236.	0.	287.	11.76
A34309	2.3	21.0	29.2	50.4	.59	140.3	45.9	0.0	6.0	186.	0.	224.	0.	281.	11.81
A34310	2.8	16.8	31.7	55.3	.86	140.3	38.3	0.0	7.3	153.	0.	243.	0.	349.	17.24
A34311	2.9	16.5	27.4	55.3	.90	140.3	30.6	0.0	7.5	146.	0.	210.	0.	360.	17.94
A34312	3.3	17.4	26.9	57.0	.97	140.3	23.0	0.0	8.4	150.	0.	206.	0.	354.	19.31
A34313	3.4	15.0	29.5	61.9	1.14	140.3	15.3	0.0	8.7	137.	0.	226.	0.	394.	22.66
A34314	3.4	13.5	30.2	63.4	1.18	140.3	7.6	0.0	8.7	138.	0.	232.	0.	385.	23.45
A34315	3.1	13.8	31.3	61.2	1.09	140.3	0.0	0.0	8.0	140.	0.	240.	0.	362.	21.74
A34208	.1	0.0	79.4	0.0	.01	140.3	107.1	0.0	.3	0.	0.	608.	0.	0.	.10
A34209	.2	0.0	14.1	0.0	.01	140.3	99.4	0.0	.5	0.	0.	108.	0.	0.	.26
A34210	.7	0.0	32.8	0.0	.05	140.3	91.8	0.0	1.8	0.	0.	251.	0.	0.	.94
A34211	1.2	27.9	30.3	34.4	.16	140.3	84.1	0.0	3.2	0.	0.	232.	0.	0.	3.26
A34212	1.2	26.4	27.6	33.3	.17	140.3	76.5	0.0	3.3	0.	0.	211.	0.	0.	3.44
A34213	1.5	24.0	27.8	37.2	.26	140.3	68.9	0.0	3.9	0.	0.	213.	0.	0.	5.27

RUN NUMBER 3

FILE NAME	MODEL CONDITIONS PEAK CONC. (%)	1% ARR. TIME (SEC)	PEAK TIME (SEC)	1% END TIME (SEC)	SUM (X-S)	POSITION X (M)	Y (M)	Z (M)	PROTOTYPE CONDITIONS PEAK CONC. (%)	5% ARR. TIME (SEC)	15% ARR. TIME (SEC)	PEAK TIME (SEC)	15% END TIME (SEC)	5% END TIME (SEC)	SUM (X-S)
A34214	1.9	22.5	29.2	41.7	.35	140.3	61.2	0.0	4.9	0.	0.	223.	0.	0.	7.16
A34215	2.1	21.0	31.3	43.4	.44	140.3	53.6	0.0	5.5	218.	0.	240.	0.	279.	8.82
A35308	1.2	34.9	41.6	45.4	.23	242.3	53.6	0.0	3.1	0.	0.	318.	0.	0.	4.60
A35309	1.1	38.0	38.9	43.1	.25	242.3	45.9	0.0	2.9	0.	0.	291.	0.	0.	5.03
A35310	1.4	30.2	39.6	53.4	.35	242.3	38.3	0.0	3.8	0.	0.	303.	0.	0.	7.13
A35311	1.4	29.3	39.0	50.7	.36	242.3	30.6	0.0	3.6	0.	0.	299.	0.	0.	7.28
A35312	1.4	32.4	41.8	49.5	.34	242.3	23.0	0.0	3.7	0.	0.	320.	0.	0.	7.01
A35313	1.4	27.5	34.3	51.7	.40	242.3	15.3	0.0	3.8	0.	0.	263.	0.	0.	8.07
A35314	1.6	26.3	33.4	53.3	.47	242.3	7.6	0.0	4.3	0.	0.	256.	0.	0.	9.47
A35315	1.6	23.0	41.8	57.5	.56	242.3	0.0	0.0	4.2	0.	0.	320.	0.	0.	11.27
B35308	1.3	33.8	35.6	48.2	.28	242.3	53.6	0.0	3.4	0.	0.	273.	0.	0.	5.63
B35309	1.3	32.3	35.4	48.8	.31	242.3	45.9	0.0	3.3	0.	0.	271.	0.	0.	6.26
B35310	1.5	30.6	43.1	52.6	.41	242.3	38.3	0.0	4.1	0.	0.	330.	0.	0.	8.41
B35311	1.4	30.2	31.7	50.5	.41	242.3	30.6	0.0	3.8	0.	0.	243.	0.	0.	8.36
B35312	1.6	30.5	36.3	55.6	.48	242.3	23.0	0.0	4.1	0.	0.	278.	0.	0.	9.86
B35313	1.6	25.0	30.5	41.6	.41	242.3	15.3	0.0	4.3	0.	0.	234.	0.	0.	8.41
B35314	1.6	24.0	33.0	63.1	.61	242.3	7.6	0.0	4.3	0.	0.	253.	0.	0.	12.47
B35315	1.7	25.4	35.9	61.6	.61	242.3	0.0	0.0	4.4	0.	0.	275.	0.	0.	12.36
A35408	1.9	25.3	37.2	66.1	.68	242.3	0.0	0.0	4.9	0.	0.	285.	0.	0.	13.82
A35409	1.7	25.3	39.5	65.1	.64	242.3	-7.6	0.0	4.4	0.	0.	302.	0.	0.	12.90
A35410	1.8	27.7	39.5	68.4	.69	242.3	-15.3	0.0	4.8	0.	0.	302.	0.	0.	13.91
A35411	1.9	27.1	40.4	61.8	.67	242.3	-23.0	0.0	5.1	309.	0.	309.	0.	334.	13.57
A35412	1.6	29.4	37.3	54.6	.51	242.3	-30.6	0.0	4.3	0.	0.	286.	0.	0.	10.33
A35413	1.9	24.4	40.1	60.6	.68	242.3	-38.3	0.0	4.9	0.	0.	307.	0.	0.	13.86
A35414	1.8	27.2	39.7	61.7	.65	242.3	-45.9	0.0	4.7	0.	0.	304.	0.	0.	13.13
A35415	1.6	28.4	45.4	62.1	.58	242.3	-53.6	0.0	4.3	0.	0.	348.	0.	0.	11.81
B35408	1.8	28.2	41.9	55.6	.59	242.3	0.0	0.0	4.6	0.	0.	321.	0.	0.	12.07
B35409	1.4	31.8	47.8	58.2	.52	242.3	-7.6	0.0	3.8	0.	0.	366.	0.	0.	10.66
B35410	1.6	29.8	37.9	62.5	.61	242.3	-15.3	0.0	4.2	0.	0.	290.	0.	0.	12.43
B35411	1.7	29.3	38.2	59.9	.60	242.3	-23.0	0.0	4.4	0.	0.	293.	0.	0.	12.24
B35412	1.5	26.1	39.0	61.7	.56	242.3	-30.6	0.0	4.0	0.	0.	299.	0.	0.	11.44
B35413	1.6	26.4	39.3	60.8	.57	242.3	-38.3	0.0	4.2	0.	0.	301.	0.	0.	11.61
B35414	1.4	27.7	34.0	53.1	.51	242.3	-45.9	0.0	3.8	0.	0.	261.	0.	0.	10.31
B35415	1.5	26.2	34.6	55.1	.58	242.3	-53.6	0.0	3.9	0.	0.	265.	0.	0.	11.81
A36908	.7	0.0	56.0	0.0	.15	399.5	23.0	0.0	1.9	0.	0.	429.	0.	0.	3.02
A36909	.6	0.0	47.5	0.0	.14	399.5	15.3	0.0	1.5	0.	0.	364.	0.	0.	2.90
A36910	.9	0.0	49.1	0.0	.23	399.5	7.6	0.0	2.3	0.	0.	376.	0.	0.	4.78
A36911	.8	0.0	42.4	0.0	.29	399.5	0.0	0.0	2.2	0.	0.	324.	0.	0.	5.85
A36912	.7	0.0	57.0	0.0	.24	399.5	-7.6	0.0	2.0	0.	0.	437.	0.	0.	4.99
A36913	.8	0.0	49.8	0.0	.32	399.5	-15.3	0.0	2.2	0.	0.	381.	0.	0.	6.49
A36914	.9	0.0	55.0	0.0	.34	399.5	-23.0	0.0	2.4	0.	0.	421.	0.	0.	6.97
A36915	.8	0.0	55.5	0.0	.34	399.5	-30.6	0.0	2.1	0.	0.	425.	0.	0.	6.94

RUN NUMBER 4

FILE NAME	MODEL CONDITIONS PEAK CONC. (%)	1% ARR. TIME (SEC)	PEAK TIME (SEC)	1% END TIME (SEC)	SUM (X-S)	POSITION X (M)	Y (M)	Z (M)	PROTOTYPE CONDITIONS PEAK CONC. (%)	5% ARR. TIME (SEC)	15% ARR. TIME (SEC)	PEAK TIME (SEC)	15% END TIME (SEC)	5% END TIME (SEC)	SUM (X-S)
A41308	.2	0.0	29.8	0.0	.02	36.5	84.0	0.0	.6	0.	0.	387.	0.	0.	.60
A41309	.1	0.0	11.8	0.0	0.00	36.5	72.0	0.0	.4	0.	0.	154.	0.	0.	.08
A41310	.1	0.0	25.9	0.0	.01	36.5	60.0	0.0	.4	0.	0.	337.	0.	0.	.23
A41311	.1	0.0	7.0	0.0	0.00	36.5	48.0	0.0	.4	0.	0.	91.	0.	0.	.12
A41312	.1	0.0	5.3	0.0	.01	36.5	36.0	0.0	.4	0.	0.	69.	0.	0.	.51
A41313	.1	0.0	33.7	0.0	.01	36.5	24.0	0.0	.3	0.	0.	438.	0.	0.	.39
A41314	9.0	1.5	11.7	23.5	.36	36.5	12.0	0.0	21.1	72.	152.	152.	174.	189.	11.91
A41315	14.6	.8	11.6	30.8	1.47	36.5	0.0	0.0	31.6	23.	64.	150.	198.	304.	45.85
B41308	.1	0.0	33.4	0.0	.01	36.5	84.0	0.0	.4	0.	0.	434.	0.	0.	.48
B41309	.2	0.0	14.6	0.0	.01	36.5	72.0	0.0	.4	0.	0.	190.	0.	0.	.40
B41310	.2	0.0	4.8	0.0	0.00	36.5	60.0	0.0	.6	0.	0.	62.	0.	0.	.02
B41311	.1	0.0	37.1	0.0	0.00	36.5	48.0	0.0	.4	0.	0.	483.	0.	0.	.16
B41312	.0	0.0	.1	0.0	0.00	36.5	36.0	0.0	.1	0.	0.	2.	0.	0.	.17
B41313	.3	0.0	19.4	0.0	.01	36.5	24.0	0.0	.8	0.	0.	252.	0.	0.	.24
B41314	6.2	10.6	17.5	26.8	.29	36.5	12.0	0.0	15.1	139.	228.	228.	241.	344.	9.62
B41315	14.0	5.7	13.1	30.3	1.41	36.5	0.0	0.0	30.5	87.	121.	171.	263.	353.	43.59
A41408	14.4	1.0	8.9	27.8	1.44	36.5	0.0	0.0	31.3	18.	49.	116.	190.	282.	44.46
A41409	9.6	1.3	11.2	27.0	1.09	36.5	-12.0	0.0	22.4	25.	62.	146.	196.	282.	35.10
A41410	5.8	4.8	11.1	16.0	.21	36.5	-24.0	0.0	14.3	63.	0.	144.	0.	193.	6.92
A41411	.2	0.0	35.4	0.0	.01	36.5	-36.0	0.0	.4	0.	0.	461.	0.	0.	.41
A41412	.1	0.0	45.8	0.0	.01	36.5	-48.0	0.0	.3	0.	0.	596.	0.	0.	.41
A41413	.2	0.0	22.3	0.0	.02	36.5	-60.0	0.0	.4	0.	0.	290.	0.	0.	.70
A41414	.1	0.0	26.7	0.0	.01	36.5	-72.0	0.0	.4	0.	0.	347.	0.	0.	.48
A41415	.1	0.0	38.9	0.0	.01	36.5	-84.0	0.0	.3	0.	0.	505.	0.	0.	.19
B41408	13.1	1.2	10.4	27.0	1.23	36.5	0.0	0.0	29.0	26.	69.	135.	186.	307.	38.99
B41409	10.8	1.4	10.4	25.5	1.14	36.5	-12.0	0.0	24.7	29.	56.	135.	186.	254.	36.10
B41410	7.9	2.3	7.0	18.6	.31	36.5	-24.0	0.0	16.8	62.	90.	91.	138.	204.	10.41
B41411	.2	0.0	39.5	0.0	.03	36.5	-36.0	0.0	.4	0.	0.	514.	0.	0.	.91
B41412	.2	0.0	48.6	0.0	0.00	36.5	-48.0	0.0	.5	0.	0.	632.	0.	0.	.06
B41413	.1	0.0	3.6	0.0	0.00	36.5	-60.0	0.0	.3	0.	0.	47.	0.	0.	.14
B41414	.1	0.0	35.4	0.0	0.00	36.5	-72.0	0.0	.4	0.	0.	461.	0.	0.	.12
B41415	.1	0.0	48.4	0.0	0.00	36.5	-84.0	0.0	.2	0.	0.	629.	0.	0.	.16
A42408	6.5	2.4	9.8	22.4	.59	56.9	0.0	0.0	15.8	33.	124.	127.	152.	210.	19.72
A42409	7.9	2.7	11.6	18.7	.49	56.9	-12.0	0.0	18.8	51.	137.	151.	152.	211.	16.46
A42410	4.2	6.7	11.6	17.2	.11	56.9	-24.0	0.0	10.6	88.	0.	151.	0.	155.	3.79
A42411	1.1	12.0	12.0	12.1	.01	56.9	-36.0	0.0	2.9	0.	0.	155.	0.	0.	.23
A42412	.0	0.0	43.9	0.0	0.00	56.9	-48.0	0.0	.0	0.	0.	570.	0.	0.	.05
A42413	.1	0.0	13.2	0.0	0.00	56.9	-60.0	0.0	.3	0.	0.	172.	0.	0.	.11
A42414	.1	0.0	35.4	0.0	.01	56.9	-72.0	0.0	.3	0.	0.	461.	0.	0.	.23
A42415	.3	0.0	13.2	0.0	0.00	56.9	-84.0	0.0	.8	0.	0.	172.	0.	0.	.13
B42408	7.7	1.8	11.2	22.5	.73	56.9	0.0	0.0	18.5	48.	103.	146.	185.	255.	23.90
B42409	7.4	2.7	9.6	23.5	.58	56.9	-12.0	0.0	17.7	61.	116.	125.	192.	212.	19.37
B42410	4.3	3.4	8.7	14.8	.17	56.9	-24.0	0.0	10.8	86.	0.	113.	0.	187.	5.70
B42411	.9	0.0	9.9	0.0	.03	56.9	-36.0	0.0	2.5	0.	0.	129.	0.	0.	1.07
B42412	.3	0.0	21.8	0.0	.07	56.9	-48.0	0.0	.9	0.	0.	283.	0.	0.	2.51
B42413	.1	0.0	1.1	0.0	0.00	56.9	-60.0	0.0	.3	0.	0.	15.	0.	0.	.04
B42414	.1	0.0	45.9	0.0	.01	56.9	-72.0	0.0	.4	0.	0.	597.	0.	0.	.26
B42415	.1	0.0	35.9	0.0	0.00	56.9	-84.0	0.0	.3	0.	0.	467.	0.	0.	.15
B42308	.1	0.0	.3	0.0	.01	56.9	84.0	0.0	.3	0.	0.	4.	0.	0.	.18
A42309	.1	0.0	35.0	0.0	0.00	56.9	72.0	0.0	.4	0.	0.	456.	0.	0.	.02

RUN NUMBER 4

FILE NAME	MODEL CONDITIONS PEAK CONC. (%)	1% ARR. TIME (SEC)	PEAK TIME (SEC)	1% END TIME (SEC)	SUM (X-S)	PROTOTYPE CONDITIONS POSITION X (M)	Y (M)	Z (M)	PEAK CONC. (%)	5% ARR. TIME (SEC)	15% ARR. TIME (SEC)	PEAK TIME (SEC)	15% END TIME (SEC)	5% END TIME (SEC)	SUM (X-S)
A42310	.1	0.0	44.3	0.0	.01	56.9	60.0	0.0	.2	0.	0.	576.	0.	0.	.25
A42311	.1	0.0	2.1	0.0	0.00	56.9	48.0	0.0	.2	0.	0.	28.	0.	0.	.12
A42312	.1	0.0	9.0	0.0	.01	56.9	36.0	0.0	.3	0.	0.	117.	0.	0.	.19
A42313	.2	0.0	13.2	0.0	.01	56.9	24.0	0.0	.6	0.	0.	172.	0.	0.	.31
A42314	4.5	4.3	11.7	14.1	.17	56.9	12.0	0.0	11.2	101.	0.	152.	0.	172.	5.87
A42315	7.3	1.4	11.4	19.9	.60	56.9	0.0	0.0	17.6	42.	147.	148.	164.	229.	19.82
B42308	.2	0.0	5.5	0.0	.01	56.9	84.0	0.0	.5	0.	0.	71.	0.	0.	.48
B42309	.2	0.0	34.4	0.0	.01	56.9	72.0	0.0	.5	0.	0.	447.	0.	0.	.49
B42310	.1	0.0	25.4	0.0	0.00	56.9	60.0	0.0	.3	0.	0.	331.	0.	0.	.11
B42311	.1	0.0	44.1	0.0	0.00	56.9	48.0	0.0	.2	0.	0.	573.	0.	0.	.15
B42312	.1	0.0	42.2	0.0	0.00	56.9	36.0	0.0	.3	0.	0.	549.	0.	0.	0.00
B42313	.5	0.0	12.4	0.0	0.00	56.9	24.0	0.0	1.3	0.	0.	162.	0.	0.	.09
B42314	3.2	4.2	10.4	19.2	.19	56.9	12.0	0.0	8.3	96.	0.	135.	0.	178.	6.37
B42315	8.0	3.8	13.4	21.9	.61	56.9	0.0	0.0	19.1	50.	121.	175.	183.	239.	20.32
A43308	.1	0.0	1.6	0.0	0.00	91.2	84.0	0.0	.2	0.	0.	21.	0.	0.	.06
A43309	.1	0.0	28.6	0.0	0.00	91.2	72.0	0.0	.2	0.	0.	371.	0.	0.	.07
A43310	.1	0.0	.2	0.0	0.00	91.2	60.0	0.0	.2	0.	0.	3.	0.	0.	.03
A43311	.1	0.0	15.6	0.0	.01	91.2	48.0	0.0	.3	0.	0.	203.	0.	0.	.26
A43312	.1	0.0	12.4	0.0	.01	91.2	36.0	0.0	.2	0.	0.	161.	0.	0.	.47
A43313	.2	0.0	14.7	0.0	.01	91.2	24.0	0.0	.4	0.	0.	191.	0.	0.	.49
A43314	2.1	9.8	10.0	10.2	.04	91.2	12.0	0.0	5.4	131.	0.	131.	0.	131.	1.35
A43315	3.7	6.3	12.5	17.1	.22	91.2	0.0	0.0	9.4	116.	0.	162.	0.	191.	7.36
B43308	.3	0.0	15.5	0.0	.03	91.2	84.0	0.0	.7	0.	0.	201.	0.	0.	.95
B43309	.2	0.0	19.1	0.0	.02	91.2	72.0	0.0	.5	0.	0.	248.	0.	0.	.68
B43310	.1	0.0	25.4	0.0	.02	91.2	60.0	0.0	.4	0.	0.	331.	0.	0.	.69
B43311	.3	0.0	18.5	0.0	.03	91.2	48.0	0.0	.7	0.	0.	240.	0.	0.	1.19
B43312	.3	0.0	18.0	0.0	.03	91.2	36.0	0.0	.9	0.	0.	235.	0.	0.	1.07
B43313	.4	0.0	18.0	0.0	.04	91.2	24.0	0.0	1.2	0.	0.	235.	0.	0.	1.42
B43314	2.3	14.2	16.2	16.8	.09	91.2	12.0	0.0	5.9	187.	0.	211.	0.	216.	3.08
B43315	3.3	9.0	15.4	22.5	.26	91.2	0.0	0.0	8.4	179.	0.	200.	0.	268.	8.73
B43408	4.4	3.8	12.0	17.0	.27	91.2	0.0	0.0	11.1	88.	0.	156.	0.	196.	9.25
B43409	4.0	4.0	12.9	18.7	.30	91.2	-12.0	0.0	10.1	63.	0.	168.	0.	200.	10.22
B43410	2.7	3.8	10.0	15.4	.15	91.2	-24.0	0.0	7.0	121.	0.	129.	0.	135.	5.17
B43411	1.2	5.2	5.3	5.6	.02	91.2	-36.0	0.0	3.1	0.	0.	69.	0.	0.	.54
B43412	.1	0.0	45.4	0.0	0.00	91.2	-48.0	0.0	.3	0.	0.	590.	0.	0.	.17
B43413	.1	0.0	14.4	0.0	.01	91.2	-60.0	0.0	.4	0.	0.	188.	0.	0.	.35
B43414	.2	0.0	16.6	0.0	.02	91.2	-72.0	0.0	.4	0.	0.	215.	0.	0.	.58
B43415	.1	0.0	45.4	0.0	0.00	91.2	-84.0	0.0	.3	0.	0.	590.	0.	0.	.17
A43408	4.4	3.7	11.1	16.9	.30	91.2	0.0	0.0	11.0	66.	0.	145.	0.	202.	10.32
A43409	4.2	3.6	14.0	20.7	.34	91.2	-12.0	0.0	10.5	86.	0.	181.	0.	192.	11.52
A43410	2.9	5.5	14.6	15.6	.24	91.2	-24.0	0.0	7.5	99.	0.	189.	0.	197.	8.28
A43411	1.4	7.9	13.1	15.0	.06	91.2	-36.0	0.0	3.7	0.	0.	170.	0.	0.	2.23
A43412	.1	0.0	20.2	0.0	.02	91.2	-48.0	0.0	.4	0.	0.	263.	0.	0.	.62
A43413	.1	0.0	7.1	0.0	0.00	91.2	-60.0	0.0	.3	0.	0.	93.	0.	0.	.10
A43414	.1	0.0	40.8	0.0	.01	91.2	-72.0	0.0	.2	0.	0.	530.	0.	0.	.49
A43415	.0	0.0	42.5	0.0	.01	91.2	-84.0	0.0	.1	0.	0.	552.	0.	0.	.19
A44408	1.7	6.3	7.5	16.6	.17	139.9	0.0	0.0	4.3	0.	0.	97.	0.	0.	5.96
A44409	2.2	5.6	8.9	17.1	.25	139.9	-12.0	0.0	5.8	103.	0.	115.	0.	183.	8.59
A44410	3.0	4.2	11.9	20.6	.33	139.9	-24.0	0.0	7.6	126.	0.	154.	0.	187.	11.45
A44411	1.4	4.9	14.6	15.4	.08	139.9	-36.0	0.0	3.6	0.	0.	190.	0.	0.	2.80

RUN NUMBER 4

FILE NAME	MODEL CONDITIONS: PEAK CONC. (%)	1% ARR. TIME (SEC)	PEAK TIME (SEC)	1% END TIME (SEC)	SUM (X-S)	POSITION X (M)	POSITION Y (M)	POSITION Z (M)	PROTOTYPE CONDITIONS: PEAK CONC. (%)	5% ARR. TIME (SEC)	15% ARR. TIME (SEC)	PEAK TIME (SEC)	15% END TIME (SEC)	5% END TIME (SEC)	SUM (X-S)
A44412	.5	0.0	15.3	0.0	.02	139.9	-48.0	0.0	1.4	0.	0.	199.	0.	0.	.71
A44413	.1	0.0	2.6	0.0	.01	139.9	-60.0	0.0	.4	0.	0.	34.	0.	0.	.27
A44414	.1	0.0	9.7	0.0	.01	139.9	-72.0	0.0	.3	0.	0.	126.	0.	0.	.21
A44415	.1	0.0	45.6	0.0	0.00	139.9	-84.0	0.0	.3	0.	0.	593.	0.	0.	.02
B44408	4.1	5.5	14.0	17.8	.37	139.9	0.0	0.0	10.4	103.	0.	183.	0.	210.	12.46
B44409	3.5	5.2	13.0	17.9	.27	139.9	-12.0	0.0	8.8	103.	0.	170.	0.	177.	9.38
B44410	1.6	8.2	13.2	14.4	.11	139.9	-24.0	0.0	4.2	0.	0.	171.	0.	0.	3.66
B44411	.1	0.0	24.9	0.0	.01	139.9	-36.0	0.0	.3	0.	0.	324.	0.	0.	.29
B44412	.0	0.0	26.0	0.0	.01	139.9	-48.0	0.0	.1	0.	0.	338.	0.	0.	.37
B44413	.1	0.0	3.4	0.0	0.00	139.9	-60.0	0.0	.3	0.	0.	45.	0.	0.	.02
B44414	.2	0.0	18.5	0.0	.01	139.9	-72.0	0.0	.5	0.	0.	241.	0.	0.	.45
B44415	.1	0.0	9.6	0.0	.02	139.9	-84.0	0.0	.3	0.	0.	125.	0.	0.	.58
C44408	2.1	8.4	14.9	15.5	.17	139.9	0.0	0.0	5.6	124.	0.	194.	0.	194.	5.89
C44409	2.4	5.8	14.1	16.2	.18	139.9	-12.0	0.0	6.3	151.	0.	183.	0.	193.	6.10
C44410	1.9	7.4	12.6	14.3	.11	139.9	-24.0	0.0	5.0	164.	0.	164.	0.	164.	3.84
C44411	.7	0.0	7.9	0.0	.03	139.9	-36.0	0.0	1.8	0.	0.	102.	0.	0.	.91
C44412	.2	0.0	11.1	0.0	.01	139.9	-48.0	0.0	.5	0.	0.	145.	0.	0.	.22
C44413	.0	0.0	.2	0.0	.01	139.9	-60.0	0.0	.2	0.	0.	2.	0.	0.	.53
C44414	.2	0.0	.6	0.0	.01	139.9	-72.0	0.0	.4	0.	0.	8.	0.	0.	.29
C44415	.1	0.0	37.1	0.0	0.00	139.9	-84.0	0.0	.2	0.	0.	483.	0.	0.	.14
D44408	2.3	5.2	11.7	13.7	.17	139.9	0.0	0.0	5.9	144.	0.	152.	0.	166.	5.95
D44409	2.4	6.3	11.2	14.8	.21	139.9	-12.0	0.0	6.1	139.	0.	145.	0.	175.	7.25
D44410	2.1	6.9	13.8	16.2	.17	139.9	-24.0	0.0	5.5	180.	0.	180.	0.	192.	5.85
D44411	1.1	15.5	15.5	15.6	.06	139.9	-36.0	0.0	3.0	0.	0.	201.	0.	0.	1.94
D44412	.2	0.0	16.7	0.0	.01	139.9	-48.0	0.0	.5	0.	0.	217.	0.	0.	.44
D44413	.1	0.0	35.8	0.0	.01	139.9	-60.0	0.0	.3	0.	0.	465.	0.	0.	.23
D44414	.2	0.0	7.8	0.0	.01	139.9	-72.0	0.0	.4	0.	0.	101.	0.	0.	.34
D44415	.1	0.0	1.8	0.0	0.00	139.9	-84.0	0.0	.3	0.	0.	24.	0.	0.	.13
A44308	.1	0.0	45.2	0.0	.02	139.9	84.0	0.0	.3	0.	0.	587.	0.	0.	.64
A44309	.1	0.0	29.1	0.0	0.00	139.9	72.0	0.0	.4	0.	0.	378.	0.	0.	.12
A44310	.6	0.0	27.3	0.0	.09	139.9	60.0	0.0	1.5	0.	0.	355.	0.	0.	3.04
A44311	.2	0.0	9.6	0.0	.01	139.9	48.0	0.0	.4	0.	0.	125.	0.	0.	.52
A44312	.1	0.0	.3	0.0	.01	139.9	36.0	0.0	.2	0.	0.	4.	0.	0.	.43
A44313	.3	0.0	10.8	0.0	.02	139.9	24.0	0.0	.8	0.	0.	141.	0.	0.	.77
A44314	1.5	8.2	8.4	15.1	.08	139.9	12.0	0.0	4.0	0.	0.	109.	0.	0.	2.75
A44315	1.9	7.8	10.9	16.2	.18	139.9	0.0	0.0	5.1	142.	0.	142.	0.	142.	6.32
B44308	.1	0.0	.2	0.0	.01	139.9	84.0	0.0	.3	0.	0.	3.	0.	0.	.21
B44309	.2	0.0	39.1	0.0	.01	139.9	72.0	0.0	.4	0.	0.	508.	0.	0.	.28
B44310	.1	0.0	41.9	0.0	.01	139.9	60.0	0.0	.4	0.	0.	544.	0.	0.	.19
B44311	.1	0.0	41.7	0.0	.01	139.9	48.0	0.0	.3	0.	0.	542.	0.	0.	.30
B44312	.1	0.0	29.1	0.0	.01	139.9	36.0	0.0	.3	0.	0.	378.	0.	0.	.19
B44313	.2	0.0	6.6	0.0	.01	139.9	24.0	0.0	.5	0.	0.	86.	0.	0.	.34
B44314	1.0	14.8	14.8	14.8	.05	139.9	12.0	0.0	2.7	0.	0.	192.	0.	0.	1.76
B44315	1.8	6.2	11.4	15.2	.15	139.9	0.0	0.0	4.8	0.	0.	148.	0.	0.	5.37
A45308	.3	0.0	19.2	0.0	.03	242.4	84.0	0.0	.7	0.	0.	250.	0.	0.	1.03
A45309	.2	0.0	23.2	0.0	.02	242.4	72.0	0.0	.5	0.	0.	391.	0.	0.	.69
A45310	.2	0.0	6.0	0.0	.02	242.4	60.0	0.0	.4	0.	0.	77.	0.	0.	.55
A45311	.2	0.0	27.5	0.0	.01	242.4	48.0	0.0	.5	0.	0.	358.	0.	0.	.48
A45312	.1	0.0	23.5	0.0	.01	242.4	36.0	0.0	.3	0.	0.	306.	0.	0.	.32
A45313	.1	0.0	28.9	0.0	.01	242.4	24.0	0.0	.4	0.	0.	375.	0.	0.	.21

RUN NUMBER

FILE NAME	MODEL CONDITIONS: PEAK CONC. (%)	1% ARR. TIME (SEC)	PEAK TIME (SEC)	1% END TIME (SEC)	SUM (X-S)	POSITION X (M)	POSITION Y (M)	POSITION Z (M)	PROTOTYPE CONDITIONS: PEAK CONC. (%)	5% ARR. TIME (SEC)	15% ARR. TIME (SEC)	PEAK TIME (SEC)	15% END TIME (SEC)	5% END TIME (SEC)	SUM (X-S)
A45314	.4	0.0	11.8	0.0	.03	242.4	12.0	0.0	1.0	0.	0.	153.	0.	0.	.99
A45315	.8	0.0	12.0	0.0	.07	242.4	0.0	0.0	2.2	0.	0.	157.	0.	0.	2.60
B45308	.2	0.0	38.0	0.0	.03	242.4	84.0	0.0	.5	0.	0.	494.	0.	0.	1.22
B45309	.2	0.0	6.2	0.0	.03	242.4	72.0	0.0	.5	0.	0.	81.	0.	0.	1.03
B45310	.3	0.0	16.4	0.0	.05	242.4	60.0	0.0	.7	0.	0.	213.	0.	0.	1.60
B45311	.2	0.0	18.1	0.0	.02	242.4	48.0	0.0	.6	0.	0.	236.	0.	0.	.84
B45312	.1	0.0	39.1	0.0	.01	242.4	36.0	0.0	.3	0.	0.	509.	0.	0.	.45
B45313	.2	0.0	19.0	0.0	.02	242.4	24.0	0.0	.5	0.	0.	246.	0.	0.	.75
B45314	.4	0.0	10.7	0.0	.03	242.4	12.0	0.0	.9	0.	0.	139.	0.	0.	1.20
B45315	.8	0.0	14.7	0.0	.07	242.4	0.0	0.0	2.1	0.	0.	191.	0.	0.	2.44
B45408	1.8	13.0	13.0	13.0	.08	242.4	0.0	0.0	4.6	0.	0.	169.	0.	0.	2.78
B45409	1.4	13.0	13.0	13.1	.10	242.4	-12.0	0.0	3.7	0.	0.	170.	0.	0.	3.46
B45410	1.1	13.0	13.0	13.1	.09	242.4	-24.0	0.0	3.0	0.	0.	170.	0.	0.	3.07
B45411	1.2	13.0	13.0	13.1	.04	242.4	-36.0	0.0	3.2	0.	0.	170.	0.	0.	1.29
B45412	.3	0.0	13.0	0.0	.01	242.4	-48.0	0.0	.8	0.	0.	169.	0.	0.	.41
B45413	.3	0.0	13.0	0.0	0.00	242.4	-60.0	0.0	.7	0.	0.	169.	0.	0.	.07
B45414	.8	0.0	13.0	0.0	0.00	242.4	-72.0	0.0	2.1	0.	0.	169.	0.	0.	.04
B45415	.1	0.0	13.4	0.0	0.00	242.4	-84.0	0.0	.2	0.	0.	174.	0.	0.	.04
C45408	1.1	10.8	10.8	10.8	.10	242.4	0.0	0.0	2.9	0.	0.	140.	0.	0.	3.65
C45409	1.2	14.7	14.9	15.0	.11	242.4	-12.0	0.0	3.2	0.	0.	194.	0.	0.	3.79
C45410	1.2	12.1	13.2	13.4	.09	242.4	-24.0	0.0	3.2	0.	0.	171.	0.	0.	3.21
C45411	.8	0.0	15.7	0.0	.05	242.4	-36.0	0.0	2.1	0.	0.	204.	0.	0.	1.63
C45412	.3	0.0	18.2	0.0	.02	242.4	-48.0	0.0	.9	0.	0.	237.	0.	0.	.61
C45413	.1	0.0	32.1	0.0	.01	242.4	-60.0	0.0	.2	0.	0.	418.	0.	0.	.50
C45414	.2	0.0	25.1	0.0	.02	242.4	-72.0	0.0	.6	0.	0.	326.	0.	0.	.86
C45415	.1	0.0	3.8	0.0	.02	242.4	-84.0	0.0	.4	0.	0.	49.	0.	0.	.58

RUN NUMBER 5

FILE NAME	MODEL CONDITIONS PEAK CONC. (%)	1% ARR. TIME (SEC)	PEAK TIME (SEC)	1% END TIME (SEC)	SUM (X-S)	POSITION X (M)	Y (M)	Z (M)	PROTOTYPE CONDITIONS PEAK CONC. (%)	5% ARR. TIME (SEC)	15% ARR. TIME (SEC)	PEAK TIME (SEC)	15% END TIME (SEC)	5% END TIME (SEC)	SUM (X-S)
A51308	.2	0.0	18.3	0.0	.02	36.5	84.0	0.0	.5	0.	0.	238.	0.	0.	.73
A51309	.2	0.0	26.9	0.0	.02	36.5	72.0	0.0	.5	0.	0.	349.	0.	0.	.55
A51310	.1	0.0	14.3	0.0	.02	36.5	60.0	0.0	.4	0.	0.	188.	0.	0.	.59
A51311	.1	0.0	46.9	0.0	.01	36.5	48.0	0.0	.2	0.	0.	609.	0.	0.	.49
A51312	.1	0.0	2.2	0.0	.01	36.5	36.0	0.0	.3	0.	0.	29.	0.	0.	.29
A51313	.3	0.0	13.3	0.0	.01	36.5	24.0	0.0	.8	0.	0.	173.	0.	0.	.43
A51314	11.3	1.6	12.3	20.6	.44	36.5	12.0	0.0	25.6	60.	156.	160.	197.	208.	14.33
A51315	13.2	1.2	13.1	27.3	1.47	36.5	0.0	0.0	29.2	28.	64.	170.	206.	291.	45.67
B51308	.1	0.0	.3	0.0	.02	36.5	84.0	0.0	.3	0.	0.	4.	0.	0.	.74
B51309	.2	0.0	15.0	0.0	.02	36.5	72.0	0.0	.5	0.	0.	195.	0.	0.	.74
B51310	.1	0.0	.0	0.0	.02	36.5	60.0	0.0	.2	0.	0.	1.	0.	0.	.64
B51311	.2	0.0	27.8	0.0	.01	36.5	48.0	0.0	.4	0.	0.	361.	0.	0.	.27
B51312	.1	0.0	9.4	0.0	.01	36.5	36.0	0.0	.3	0.	0.	122.	0.	0.	.31
B51313	.4	0.0	6.5	0.0	.01	36.5	24.0	0.0	1.0	0.	0.	84.	0.	0.	.38
B51314	10.1	1.7	14.1	22.2	.48	36.5	12.0	0.0	23.3	48.	81.	184.	192.	220.	15.75
B51315	13.3	1.4	11.9	28.2	1.39	36.5	0.0	0.0	29.3	27.	62.	155.	209.	269.	43.53
A51408	15.1	1.1	12.6	29.0	1.74	36.5	0.0	0.0	32.4	25.	47.	163.	210.	303.	52.99
A51409	12.5	1.7	11.0	29.2	1.40	36.5	-12.0	0.0	28.0	32.	69.	144.	205.	346.	44.94
A51410	8.8	1.1	12.6	18.0	.35	36.5	-24.0	0.0	20.7	49.	162.	164.	191.	206.	11.70
A51411	.9	0.0	12.9	0.0	.01	36.5	-36.0	0.0	2.4	0.	0.	168.	0.	0.	.26
A51412	.1	0.0	15.9	0.0	.01	36.5	-48.0	0.0	.3	0.	0.	207.	0.	0.	.25
A51413	.1	0.0	12.0	0.0	.01	36.5	-60.0	0.0	.4	0.	0.	155.	0.	0.	.25
A51414	.2	0.0	2.4	0.0	.02	36.5	-72.0	0.0	.5	0.	0.	32.	0.	0.	.57
A51415	.1	0.0	.2	0.0	.02	36.5	-84.0	0.0	.3	0.	0.	2.	0.	0.	.68
B51408	14.8	1.4	12.8	30.6	1.64	36.5	0.0	0.0	31.9	27.	51.	166.	205.	295.	50.52
B51409	12.3	2.0	11.9	31.8	1.38	36.5	-12.0	0.0	27.6	39.	70.	154.	212.	363.	43.67
B51410	7.8	4.8	14.0	24.8	.29	36.5	-24.0	0.0	18.6	63.	154.	183.	187.	205.	9.55
B51411	.6	0.0	12.2	0.0	.01	36.5	-36.0	0.0	1.7	0.	0.	159.	0.	0.	.22
B51412	.1	0.0	13.8	0.0	.01	36.5	-48.0	0.0	.3	0.	0.	179.	0.	0.	.23
B51413	.3	0.0	13.8	0.0	.01	36.5	-60.0	0.0	.8	0.	0.	179.	0.	0.	.23
B51414	.5	0.0	13.8	0.0	.02	36.5	-72.0	0.0	1.3	0.	0.	179.	0.	0.	.57
B51415	.1	0.0	13.8	0.0	.01	36.5	-84.0	0.0	.4	0.	0.	179.	0.	0.	.47
A52408	9.5	2.6	11.4	24.2	1.04	56.9	0.0	0.0	22.1	41.	80.	148.	207.	310.	33.64
A52409	7.3	2.8	10.2	25.8	.65	56.9	-12.0	0.0	17.5	54.	113.	133.	175.	228.	21.38
A52410	5.4	3.2	13.7	17.0	.26	56.9	-24.0	0.0	13.3	72.	0.	178.	0.	201.	8.89
A52411	2.0	10.6	14.6	15.3	.03	56.9	-36.0	0.0	5.2	189.	0.	189.	0.	190.	1.09
A52412	.1	0.0	34.2	0.0	.01	56.9	-48.0	0.0	.3	0.	0.	444.	0.	0.	.23
A52413	.1	0.0	5.1	0.0	0.00	56.9	-60.0	0.0	.2	0.	0.	66.	0.	0.	.12
A52414	.1	0.0	11.4	0.0	.01	56.9	-72.0	0.0	.3	0.	0.	148.	0.	0.	.18
A52415	.1	0.0	48.2	0.0	0.00	56.9	-84.0	0.0	.2	0.	0.	627.	0.	0.	.05
B52408	6.3	2.0	10.4	25.1	.86	56.9	0.0	0.0	19.7	43.	127.	135.	203.	279.	28.22
B52409	8.4	3.0	11.3	28.7	.91	56.9	-12.0	0.0	19.8	53.	106.	147.	210.	260.	29.69
B52410	6.1	3.1	10.0	21.3	.56	56.9	-24.0	0.0	14.9	67.	0.	130.	0.	259.	18.46
B52411	.9	0.0	11.5	0.0	.04	56.9	-36.0	0.0	2.4	0.	0.	150.	0.	0.	1.45
B52412	.1	0.0	.4	0.0	.01	56.9	-48.0	0.0	.2	0.	0.	5.	0.	0.	.39
B52413	.0	0.0	.0	0.0	.01	56.9	-60.0	0.0	.0	0.	0.	1.	0.	0.	.22
B52414	.1	0.0	32.5	0.0	.01	56.9	-72.0	0.0	.3	0.	0.	422.	0.	0.	.29
B52415	.1	0.0	.3	0.0	0.00	56.9	-84.0	0.0	.2	0.	0.	4.	0.	0.	.10
A52308	.1	0.0	43.9	0.0	0.00	56.9	84.0	0.0	.4	0.	0.	571.	0.	0.	.01
A52309	.1	0.0	48.7	0.0	.01	56.9	72.0	0.0	.4	0.	0.	633.	0.	0.	.29

RUN NUMBER 5

FILE NAME	MODEL CONDITIONS PEAK CONC. (%)	1% ARR. TIME (SEC)	PEAK TIME (SEC)	1% END TIME (SEC)	SUM (X-S)	POSITION X (M)	Y (M)	Z (M)	PROTOTYPE CONDITIONS PEAK CONC. (%)	5% ARR. TIME (SEC)	15% ARR. TIME (SEC)	PEAK TIME (SEC)	15% END TIME (SEC)	5% END TIME (SEC)	SUM (X-S)
A52310	.1	0.0	15.6	0.0	.01	56.9	60.0	0.0	.3	0.	0.	203.	0.	0.	.30
A52311	.1	0.0	33.2	0.0	.01	56.9	48.0	0.0	.3	0.	0.	431.	0.	0.	.35
A52312	.1	0.0	33.9	0.0	.01	56.9	36.0	0.0	.3	0.	0.	441.	0.	0.	.31
A52313	.5	0.0	15.5	0.0	.01	56.9	24.0	0.0	1.4	0.	0.	202.	0.	0.	.46
A52314	5.1	3.5	15.1	20.9	.31	56.9	12.0	0.0	12.6	102.	0.	196.	0.	213.	10.42
A52315	7.1	2.3	15.2	26.4	.72	56.9	0.0	0.0	17.2	48.	159.	198.	199.	232.	23.90
B52308	.2	0.0	15.3	0.0	0.00	56.9	84.0	0.0	.4	0.	0.	199.	0.	0.	.12
B52309	.3	0.0	22.8	0.0	.05	56.9	72.0	0.0	.7	0.	0.	297.	0.	0.	1.76
B52310	.1	0.0	.0	0.0	.02	56.9	60.0	0.0	.3	0.	0.	1.	0.	0.	.63
B52311	.1	0.0	41.2	0.0	0.00	56.9	48.0	0.0	.3	0.	0.	535.	0.	0.	.03
B52312	.0	0.0	28.2	0.0	.01	56.9	36.0	0.0	.1	0.	0.	367.	0.	0.	.29
B52313	.9	0.0	12.8	0.0	.02	56.9	24.0	0.0	2.4	0.	0.	166.	0.	0.	.55
B52314	4.6	4.0	12.7	16.4	.23	56.9	12.0	0.0	11.6	67.	0.	165.	0.	209.	7.69
B52315	6.3	3.2	15.4	23.2	.59	56.9	0.0	0.0	15.5	51.	158.	200.	203.	244.	19.61
A53308	.2	0.0	37.0	0.0	.02	91.2	84.0	0.0	.5	0.	0.	482.	0.	0.	.69
A53309	.2	0.0	7.4	0.0	.01	91.2	72.0	0.0	.4	0.	0.	97.	0.	0.	.45
A53310	.1	0.0	29.9	0.0	.02	91.2	60.0	0.0	.2	0.	0.	389.	0.	0.	.81
A53311	.2	0.0	37.6	0.0	.01	91.2	48.0	0.0	.4	0.	0.	489.	0.	0.	.38
A53312	.1	0.0	23.1	0.0	.01	91.2	36.0	0.0	.4	0.	0.	301.	0.	0.	.51
A53313	.9	0.0	11.6	0.0	.03	91.2	24.0	0.0	2.4	0.	0.	151.	0.	0.	.98
A53314	2.8	6.5	14.8	15.4	.12	91.2	12.0	0.0	7.1	190.	0.	192.	0.	199.	4.21
A53315	4.0	4.8	14.7	16.8	.29	91.2	0.0	0.0	10.2	95.	0.	191.	0.	206.	9.91
B53308	.1	0.0	43.8	0.0	.01	91.2	84.0	0.0	.2	0.	0.	569.	0.	0.	.41
B53309	.1	0.0	1.9	0.0	.01	91.2	72.0	0.0	.3	0.	0.	24.	0.	0.	.38
B53310	.1	0.0	8.9	0.0	0.00	91.2	60.0	0.0	.2	0.	0.	115.	0.	0.	.01
B53311	.0	0.0	12.1	0.0	.01	91.2	48.0	0.0	.1	0.	0.	157.	0.	0.	.33
B53312	.1	0.0	.1	0.0	.01	91.2	36.0	0.0	.2	0.	0.	1.	0.	0.	.28
B53313	.3	0.0	21.5	0.0	.01	91.2	24.0	0.0	.8	0.	0.	279.	0.	0.	.50
B53314	1.1	9.0	9.0	9.0	.04	91.2	12.0	0.0	3.0	0.	0.	117.	0.	0.	1.29
B53315	3.1	3.7	9.8	18.0	.20	91.2	0.0	0.0	8.9	112.	0.	127.	0.	153.	6.95
A53408	4.7	4.0	15.2	20.2	.43	91.2	0.0	0.0	11.7	67.	0.	198.	0.	223.	14.44
A53409	4.1	4.9	8.3	22.2	.46	91.2	-12.0	0.0	10.4	85.	0.	108.	0.	245.	15.48
A53410	3.3	6.8	8.4	19.4	.21	91.2	-24.0	0.0	8.5	97.	0.	110.	0.	163.	7.05
A53411	1.9	8.6	10.0	15.9	.08	91.2	-36.0	0.0	4.9	0.	0.	129.	0.	0.	2.86
A53412	.3	0.0	19.1	0.0	.01	91.2	-48.0	0.0	.7	0.	0.	131.	0.	0.	.33
A53413	.1	0.0	46.6	0.0	0.00	91.2	-60.0	0.0	.3	0.	0.	606.	0.	0.	.09
A53414	.1	0.0	.2	0.0	.01	91.2	-72.0	0.0	.3	0.	0.	3.	0.	0.	.18
A53415	.1	0.0	45.2	0.0	.01	91.2	-84.0	0.0	.2	0.	0.	588.	0.	0.	.23
B53408	4.2	6.7	13.0	22.7	.40	91.2	0.0	0.0	10.5	94.	0.	169.	0.	228.	13.51
B53409	5.8	3.3	12.8	22.8	.63	91.2	-12.0	0.0	14.2	78.	0.	166.	0.	258.	20.93
B53410	4.9	5.1	13.4	23.3	.40	91.2	-24.0	0.0	12.2	79.	0.	174.	0.	234.	13.41
B53411	1.6	9.6	10.0	10.1	.05	91.2	-36.0	0.0	4.3	0.	0.	129.	0.	0.	1.68
B53412	.1	0.0	44.6	0.0	.01	91.2	-48.0	0.0	.2	0.	0.	580.	0.	0.	.36
B53413	.0	0.0	37.0	0.0	.01	91.2	-60.0	0.0	.1	0.	0.	481.	0.	0.	.21
B53414	.1	0.0	.3	0.0	.01	91.2	-72.0	0.0	.2	0.	0.	4.	0.	0.	.34
B53415	.1	0.0	22.5	0.0	.01	91.2	-84.0	0.0	.2	0.	0.	292.	0.	0.	.20
A54308	.2	0.0	10.5	0.0	.02	139.9	84.0	0.0	.5	0.	0.	136.	0.	0.	.66
A54309	.3	0.0	10.3	0.0	.02	139.9	72.0	0.0	.7	0.	0.	134.	0.	0.	.84
A54310	.1	0.0	48.1	0.0	.01	139.9	60.0	0.0	.3	0.	0.	626.	0.	0.	.33
A54311	.1	0.0	43.9	0.0	.01	139.9	48.0	0.0	.3	0.	0.	571.	0.	0.	.24

RUN NUMBER 5

FILE NAME	MODEL CONDITIONS PEAK CONC. (%)	1% ARR. TIME (SEC)	PEAK TIME (SEC)	1% END TIME (SEC)	SUM (X-S)	POSITION X (M)	Y (M)	Z (M)	PROTOTYPE CONDITIONS PEAK CONC. (%)	5% ARR. TIME (SEC)	15% ARR. TIME (SEC)	PEAK TIME (SEC)	15% END TIME (SEC)	5% END TIME (SEC)	SUM (X-S)
A54312	.1	0.0	1.0	0.0	.01	139.9	36.0	0.0	.3	0.	0.	14.	0.	0.	.33
A54313	.2	0.0	12.4	0.0	.02	139.9	24.0	0.0	.5	0.	0.	161.	0.	0.	.57
A54314	.5	0.0	8.4	0.0	.04	139.9	12.0	0.0	1.5	0.	0.	109.	0.	0.	1.38
A54315	1.7	8.1	12.9	14.0	.10	139.9	0.0	0.0	4.4	0.	0.	168.	0.	0.	3.30
B54308	.2	0.0	41.9	0.0	.02	139.9	84.0	0.0	.4	0.	0.	544.	0.	0.	.61
B54309	.1	0.0	45.7	0.0	.02	139.9	72.0	0.0	.3	0.	0.	594.	0.	0.	.61
B54310	.2	0.0	18.0	0.0	.02	139.9	60.0	0.0	.4	0.	0.	234.	0.	0.	.56
B54311	.1	0.0	4.3	0.0	.01	139.9	48.0	0.0	.3	0.	0.	56.	0.	0.	.44
B54312	.1	0.0	26.2	0.0	.01	139.9	36.0	0.0	.4	0.	0.	341.	0.	0.	.49
B54313	.2	0.0	13.8	0.0	.02	139.9	24.0	0.0	.6	0.	0.	179.	0.	0.	.83
B54314	1.3	12.4	13.4	14.6	.08	139.9	12.0	0.0	3.6	0.	0.	175.	0.	0.	2.65
B54315	2.6	7.9	14.4	16.9	.18	139.9	0.0	0.0	6.7	173.	0.	187.	0.	199.	6.05
B54408	2.5	6.2	10.4	15.0	.20	139.9	0.0	0.0	6.4	123.	0.	135.	0.	140.	6.87
A54409	2.4	5.7	15.2	20.4	.31	139.9	-12.0	0.0	6.3	172.	0.	198.	0.	223.	10.54
A54410	2.8	5.1	15.8	19.8	.33	139.9	-24.0	0.0	7.3	112.	0.	206.	0.	232.	11.38
A54411	1.7	12.4	15.4	16.4	.11	139.9	-36.0	0.0	4.6	0.	0.	200.	0.	0.	3.74
A54412	1.6	13.0	15.6	16.5	.08	139.9	-48.0	0.0	4.1	0.	0.	202.	0.	0.	2.70
A54413	.3	0.0	16.0	0.0	.02	139.9	-60.0	0.0	.8	0.	0.	209.	0.	0.	.59
A54414	.1	0.0	.1	0.0	.01	139.9	-72.0	0.0	.2	0.	0.	2.	0.	0.	.26
A54415	.0	0.0	.1	0.0	0.00	139.9	-84.0	0.0	.1	0.	0.	1.	0.	0.	.11
B34408	2.4	6.8	12.6	17.0	.21	139.9	0.0	0.0	6.3	123.	0.	164.	0.	167.	7.39
B34409	3.2	5.3	16.3	19.2	.32	139.9	-12.0	0.0	8.2	109.	0.	212.	0.	230.	11.09
B34410	3.1	6.2	16.1	19.2	.29	139.9	-24.0	0.0	8.1	147.	0.	210.	0.	220.	10.06
B34411	1.1	13.9	13.9	14.0	.06	139.9	-36.0	0.0	3.0	0.	0.	181.	0.	0.	1.95
B34412	.6	0.0	13.8	0.0	.03	139.9	-48.0	0.0	1.7	0.	0.	179.	0.	0.	1.01
B34413	.1	0.0	.1	0.0	.01	139.9	-60.0	0.0	.2	0.	0.	2.	0.	0.	.44
B34414	.1	0.0	.1	0.0	.02	139.9	-72.0	0.0	.3	0.	0.	1.	0.	0.	.56
B34415	.1	0.0	1.9	0.0	.01	139.9	-84.0	0.0	.4	0.	0.	25.	0.	0.	.46
A55408	1.1	14.8	14.8	16.4	.09	242.4	0.0	0.0	3.0	0.	0.	192.	0.	0.	3.19
A55409	1.4	11.0	15.3	15.9	.14	242.4	-12.0	0.0	3.7	0.	0.	199.	0.	0.	4.74
A55410	1.2	13.8	17.4	17.6	.13	242.4	-24.0	0.0	3.2	0.	0.	226.	0.	0.	4.53
A55411	1.0	17.2	17.2	17.4	.10	242.4	-36.0	0.0	2.7	0.	0.	224.	0.	0.	3.32
A55412	.6	0.0	16.0	0.0	.05	242.4	-48.0	0.0	1.6	0.	0.	209.	0.	0.	1.68
A55413	.3	0.0	17.6	0.0	.02	242.4	-60.0	0.0	.7	0.	0.	229.	0.	0.	.69
A55414	.3	0.0	24.9	0.0	.03	242.4	-72.0	0.0	.7	0.	0.	324.	0.	0.	1.18
A55415	.2	0.0	14.2	0.0	.03	242.4	-84.0	0.0	.5	0.	0.	185.	0.	0.	1.01
B55408	1.0	11.2	11.2	11.8	.07	242.4	0.0	0.0	2.7	0.	0.	145.	0.	0.	2.59
B55409	1.3	13.6	14.8	18.7	.14	242.4	-12.0	0.0	3.4	0.	0.	192.	0.	0.	4.75
B55410	1.4	10.0	16.8	18.7	.13	242.4	-24.0	0.0	3.6	0.	0.	219.	0.	0.	4.66
B55411	1.1	17.3	17.3	18.0	.11	242.4	-36.0	0.0	2.8	0.	0.	225.	0.	0.	3.66
B55412	.7	0.0	14.6	0.0	.05	242.4	-48.0	0.0	1.8	0.	0.	190.	0.	0.	1.84
B55413	.4	0.0	14.6	0.0	.03	242.4	-60.0	0.0	.9	0.	0.	189.	0.	0.	1.16
B55414	.2	0.0	15.8	0.0	.03	242.4	-72.0	0.0	.5	0.	0.	205.	0.	0.	.96
B55415	.2	0.0	36.8	0.0	.01	242.4	-84.0	0.0	.5	0.	0.	478.	0.	0.	.48
A55308	.2	0.0	4.4	0.0	0.00	242.4	84.0	0.0	.4	0.	0.	57.	0.	0.	.13
A55309	.1	0.0	41.2	0.0	0.00	242.4	72.0	0.0	.4	0.	0.	536.	0.	0.	.06
A55310	.1	0.0	20.0	0.0	.01	242.4	60.0	0.0	.3	0.	0.	260.	0.	0.	.25
A55311	.2	0.0	13.3	0.0	.02	242.4	48.0	0.0	.5	0.	0.	173.	0.	0.	.53
A55312	.2	0.0	4.7	0.0	.01	242.4	36.0	0.0	.4	0.	0.	61.	0.	0.	.45
A55313	.1	0.0	46.4	0.0	.01	242.4	24.0	0.0	.2	0.	0.	603.	0.	0.	.37

RUN NUMBER 5

FILE NAME	MODEL CONDITIONS PEAK CONC. (%)	1% ARR. TIME (SEC)	PEAK TIME (SEC)	1% END TIME (SEC)	SUM (X-S)	POSITION X (M)	Y (M)	Z (M)	PROTOTYPE CONDITIONS PEAK CONC. (%)	5% ARR. TIME (SEC)	15% ARR. TIME (SEC)	PEAK TIME (SEC)	15% END TIME (SEC)	5% END TIME (SEC)	SUM (X-S)
A55314	.2	0.0	14.6	0.0	.01	242.4	12.0	0.0	.6	0.	0.	190.	0.	0.	.30
A55315	.4	0.0	14.1	0.0	.02	242.4	0.0	0.0	1.2	0.	0.	183.	0.	0.	.73

RUN NUMBER 7

FILE NAME	MODEL CONDITIONS PEAK CONC. (%)	1% ARR. TIME (SEC)	PEAK TIME (SEC)	1% END TIME (SEC)	SUM (X-S)	POSITION X (M)	Y (M)	Z (M)	PROTOTYPE CONDITIONS PEAK CONC. (%)	5% ARR. TIME (SEC)	15% ARR. TIME (SEC)	PEAK TIME (SEC)	15% END TIME (SEC)	5% END TIME (SEC)	SUM (X-S)
A71408	15.8	1.0	8.4	27.8	1.55	36.5	0.0	0.0	33.7	20.	49.	109.	187.	310.	47.62
A71409	12.4	1.1	9.3	25.9	1.18	36.5	-12.0	0.0	27.6	24.	68.	121.	184.	270.	37.08
A71410	5.5	3.6	8.2	15.0	.17	36.5	-24.0	0.0	13.5	79.	0.	107.	0.	164.	5.69
A71411	.2	0.0	49.4	0.0	.01	36.5	-36.0	0.0	.4	0.	0.	643.	0.	0.	.28
A71412	.1	0.0	.4	0.0	.01	36.5	-48.0	0.0	.2	0.	0.	5.	0.	0.	.27
A71413	.1	0.0	6.8	0.0	.01	36.5	-60.0	0.0	.3	0.	0.	88.	0.	0.	.24
A71414	.2	0.0	24.0	0.0	.02	36.5	-72.0	0.0	.5	0.	0.	311.	0.	0.	.62
A71415	.1	0.0	21.6	0.0	.01	36.5	-84.0	0.0	.3	0.	0.	281.	0.	0.	.46
B71408	17.6	.8	12.8	24.5	1.50	36.5	0.0	0.0	36.6	19.	42.	166.	183.	275.	45.52
B71409	15.3	1.7	12.9	26.8	1.27	36.5	-12.0	0.0	32.8	28.	48.	168.	186.	274.	39.69
B71410	7.1	3.3	6.3	16.9	.20	36.5	-24.0	0.0	17.1	59.	82.	82.	144.	183.	6.86
B71411	.2	0.0	41.6	0.0	0.00	36.5	-36.0	0.0	.4	0.	0.	540.	0.	0.	.16
B71412	.1	0.0	.4	0.0	0.00	36.5	-48.0	0.0	.2	0.	0.	5.	0.	0.	.16
B71413	.1	0.0	.5	0.0	.01	36.5	-60.0	0.0	.2	0.	0.	7.	0.	0.	.35
B71414	.1	0.0	.2	0.0	.01	36.5	-72.0	0.0	.3	0.	0.	2.	0.	0.	.28
B71415	.1	0.0	20.2	0.0	0.00	36.5	-84.0	0.0	.2	0.	0.	263.	0.	0.	.17
C71308	.1	0.0	33.6	0.0	.01	36.5	84.0	0.0	.2	0.	0.	436.	0.	0.	.42
C71309	.1	0.0	.0	0.0	.01	36.5	72.0	0.0	.2	0.	0.	1.	0.	0.	.37
C71310	.1	0.0	34.0	0.0	.01	36.5	60.0	0.0	.2	0.	0.	443.	0.	0.	.41
C71311	.2	0.0	38.0	0.0	.01	36.5	48.0	0.0	.4	0.	0.	494.	0.	0.	.32
C71312	.1	0.0	17.7	0.0	0.00	36.5	36.0	0.0	.3	0.	0.	230.	0.	0.	.05
C71313	.6	0.0	12.6	0.0	0.00	36.5	24.0	0.0	1.7	0.	0.	164.	0.	0.	.16
C71314	12.1	1.8	11.3	19.1	.70	36.5	12.0	0.0	27.1	44.	64.	147.	175.	228.	22.18
C71315	14.5	.8	10.3	25.7	1.44	36.5	0.0	0.0	31.4	21.	46.	134.	186.	301.	44.19
D71308	.2	0.0	.4	0.0	.01	36.5	84.0	0.0	.4	0.	0.	5.	0.	0.	.27
D71309	.1	0.0	25.6	0.0	.01	36.5	72.0	0.0	.3	0.	0.	333.	0.	0.	.26
D71310	.1	0.0	26.0	0.0	.01	36.5	60.0	0.0	.3	0.	0.	337.	0.	0.	.22
D71311	.1	0.0	.3	0.0	.01	36.5	48.0	0.0	.3	0.	0.	4.	0.	0.	.32
D71312	.1	0.0	.2	0.0	.01	36.5	36.0	0.0	.2	0.	0.	2.	0.	0.	.29
D71313	.8	0.0	13.7	0.0	.01	36.5	24.0	0.0	2.0	0.	0.	178.	0.	0.	.32
D71314	14.3	1.7	12.5	22.3	.75	36.5	12.0	0.0	31.1	23.	63.	162.	179.	276.	23.76
D71315	16.0	.9	12.1	28.9	1.64	36.5	0.0	0.0	34.0	17.	52.	158.	187.	269.	49.79
A72308	.2	0.0	17.0	0.0	.02	56.9	84.0	0.0	.6	0.	0.	222.	0.	0.	.67
A72309	.1	0.0	28.4	0.0	.01	56.9	72.0	0.0	.3	0.	0.	370.	0.	0.	.28
A72310	.1	0.0	27.7	0.0	.01	56.9	60.0	0.0	.4	0.	0.	360.	0.	0.	.38
A72311	.2	0.0	27.2	0.0	.01	56.9	48.0	0.0	.5	0.	0.	353.	0.	0.	.43
A72312	.1	0.0	48.1	0.0	.01	56.9	36.0	0.0	.3	0.	0.	625.	0.	0.	.23
A72313	.3	0.0	13.9	0.0	.02	56.9	24.0	0.0	.8	0.	0.	181.	0.	0.	.65
A72314	9.6	3.8	9.8	15.4	.30	56.9	12.0	0.0	22.2	99.	118.	128.	132.	195.	9.80
A72315	10.5	1.6	12.6	22.3	.89	56.9	0.0	0.0	24.2	38.	94.	163.	187.	256.	28.50
B72308	.2	0.0	41.6	0.0	.01	56.9	84.0	0.0	.4	0.	0.	540.	0.	0.	.34
B72309	.1	0.0	45.8	0.0	0.00	56.9	72.0	0.0	.3	0.	0.	595.	0.	0.	.96
B72310	.1	0.0	.1	0.0	0.00	56.9	60.0	0.0	.4	0.	0.	1.	0.	0.	.17
B72311	.1	0.0	48.0	0.0	0.00	56.9	48.0	0.0	.3	0.	0.	624.	0.	0.	.96
B72312	.1	0.0	1.6	0.0	0.00	56.9	36.0	0.0	.2	0.	0.	21.	0.	0.	.02
B72313	1.1	12.4	12.4	12.5	.01	56.9	24.0	0.0	3.0	0.	0.	161.	0.	0.	.41
B72314	7.5	3.4	11.5	14.7	.35	56.9	12.0	0.0	18.1	58.	149.	150.	158.	176.	11.34
B72315	9.3	2.1	13.0	20.5	.75	56.9	0.0	0.0	21.6	41.	74.	170.	174.	219.	24.56
A72408	10.1	1.4	12.0	22.2	.91	56.9	0.0	0.0	23.3	30.	66.	157.	168.	250.	29.51
A72409	9.0	3.6	12.6	17.0	.47	56.9	-12.0	0.0	21.1	49.	151.	164.	173.	206.	15.70

RUN NUMBER 7

FILE NAME	MODEL CONDITIONS PEAK CONC. (%)	1% ARR. TIME (SEC)	PEAK TIME (SEC)	1% END TIME (SEC)	SUM (X-S)	PROTOTYPE CONDITIONS POSITION X (M)	Y (M)	Z (M)	PEAK CONC. (%)	5% ARR. TIME (SEC)	15% ARR. TIME (SEC)	PEAK TIME (SEC)	15% END TIME (SEC)	5% END TIME (SEC)	SUM (X-S)
A72410	3.2	5.4	13.2	13.9	.10	56.9	-24.0	0.0	8.3	127.	0.	172.	0.	178.	3.40
A72411	.2	0.0	20.0	0.0	.02	56.9	-36.0	0.0	.5	0.	0.	260.	0.	0.	.73
A72412	.1	0.0	14.4	0.0	.01	56.9	-48.0	0.0	.3	0.	0.	187.	0.	0.	.49
A72413	.2	0.0	26.6	0.0	.02	56.9	-60.0	0.0	.5	0.	0.	345.	0.	0.	.66
A72414	.2	0.0	32.2	0.0	.03	56.9	-72.0	0.0	.6	0.	0.	419.	0.	0.	.96
A72415	.2	0.0	26.8	0.0	.03	56.9	-84.0	0.0	.5	0.	0.	349.	0.	0.	.88
B72408	10.7	1.8	13.1	27.8	.96	56.9	0.0	0.0	24.5	34.	78.	170.	185.	266.	31.12
B72409	7.7	2.6	10.7	22.5	.57	56.9	-12.0	0.0	18.4	41.	127.	139.	179.	274.	18.63
B72410	2.5	6.2	10.7	15.1	.07	56.9	-24.0	0.0	6.6	83.	0.	139.	0.	148.	2.31
B72411	.2	0.0	6.2	0.0	.01	56.9	-36.0	0.0	.4	0.	0.	81.	0.	0.	.33
B72412	.1	0.0	35.9	0.0	.01	56.9	-48.0	0.0	.3	0.	0.	467.	0.	0.	.30
B72413	.1	0.0	16.2	0.0	.01	56.9	-60.0	0.0	.3	0.	0.	210.	0.	0.	.30
B72414	.2	0.0	27.0	0.0	.01	56.9	-72.0	0.0	.4	0.	0.	351.	0.	0.	.30
B72415	.1	0.0	20.4	0.0	.01	56.9	-84.0	0.0	.2	0.	0.	265.	0.	0.	.22
A73408	6.0	3.1	10.2	20.1	.48	91.2	0.0	0.0	14.7	57.	0.	133.	0.	242.	16.27
A73409	3.9	4.5	11.6	21.7	.25	91.2	-12.0	0.0	10.0	65.	0.	151.	0.	171.	8.64
A73410	1.4	5.1	5.2	8.4	.07	91.2	-24.0	0.0	3.8	0.	0.	67.	0.	0.	2.34
A73411	1.2	7.4	7.4	7.4	.01	91.2	-36.0	0.0	3.3	0.	0.	96.	0.	0.	.26
A73412	.0	0.0	20.4	0.0	.01	91.2	-48.0	0.0	.1	0.	0.	266.	0.	0.	.35
A73413	.1	0.0	40.8	0.0	.01	91.2	-60.0	0.0	.2	0.	0.	530.	0.	0.	.41
A73414	.1	0.0	42.9	0.0	.01	91.2	-72.0	0.0	.4	0.	0.	545.	0.	0.	.27
A73415	.0	0.0	39.7	0.0	.01	91.2	-84.0	0.0	.1	0.	0.	516.	0.	0.	.31
B73408	6.6	2.7	9.3	18.1	.53	91.2	0.0	0.0	16.0	59.	120.	121.	122.	209.	17.63
B73409	6.7	3.9	14.1	21.1	.52	91.2	-12.0	0.0	16.3	56.	183.	184.	185.	210.	17.43
B73410	3.5	5.7	13.9	14.8	.21	91.2	-24.0	0.0	9.0	141.	0.	180.	0.	186.	7.31
B73411	.6	0.0	14.6	0.0	.02	91.2	-36.0	0.0	1.5	0.	0.	190.	0.	0.	.86
B73412	.1	0.0	13.4	0.0	.01	91.2	-48.0	0.0	.3	0.	0.	175.	0.	0.	.30
B73413	.1	0.0	39.2	0.0	.01	91.2	-60.0	0.0	.4	0.	0.	510.	0.	0.	.36
B73414	.3	0.0	12.0	0.0	.01	91.2	-72.0	0.0	.9	0.	0.	155.	0.	0.	.42
B73415	.2	0.0	12.0	0.0	.02	91.2	-84.0	0.0	.4	0.	0.	155.	0.	0.	.74
A73308	.1	0.0	45.5	0.0	0.00	91.2	84.0	0.0	.3	0.	0.	591.	0.	0.	.15
A73309	.1	0.0	44.3	0.0	.02	91.2	72.0	0.0	.3	0.	0.	576.	0.	0.	.56
A73310	.1	0.0	44.6	0.0	0.00	91.2	60.0	0.0	.3	0.	0.	580.	0.	0.	.06
A73311	.1	0.0	44.7	0.0	.01	91.2	48.0	0.0	.2	0.	0.	581.	0.	0.	.31
A73312	.1	0.0	.0	0.0	.01	91.2	36.0	0.0	.2	0.	0.	1.	0.	0.	.22
A73313	.4	0.0	7.6	0.0	.01	91.2	24.0	0.0	1.1	0.	0.	99.	0.	0.	.37
A73314	2.5	5.8	6.2	14.0	.07	91.2	12.0	0.0	6.4	80.	0.	81.	0.	87.	2.57
A73315	4.3	3.7	11.9	18.6	.37	91.2	0.0	0.0	10.8	70.	0.	154.	0.	179.	12.54
B73308	.2	0.0	10.9	0.0	.01	91.2	84.0	0.0	.5	0.	0.	129.	0.	0.	.37
B73309	.1	0.0	12.6	0.0	0.00	91.2	72.0	0.0	.2	0.	0.	164.	0.	0.	.09
B73310	.0	0.0	39.4	0.0	0.00	91.2	60.0	0.0	.1	0.	0.	512.	0.	0.	.17
B73311	.1	0.0	35.4	0.0	0.00	91.2	48.0	0.0	.3	0.	0.	461.	0.	0.	.01
B73312	.1	0.0	37.2	0.0	.01	91.2	36.0	0.0	.3	0.	0.	484.	0.	0.	.29
B73313	.6	0.0	13.4	0.0	.02	91.2	24.0	0.0	1.7	0.	0.	174.	0.	0.	.59
B73314	3.4	5.9	7.2	15.1	.16	91.2	12.0	0.0	8.7	86.	0.	94.	0.	192.	5.42
B73315	5.3	2.6	11.2	18.4	.38	91.2	0.0	0.0	13.2	55.	0.	145.	0.	186.	12.75
A74308	.1	0.0	14.2	0.0	.01	139.9	84.0	0.0	.4	0.	0.	185.	0.	0.	.23
A74309	.1	0.0	39.6	0.0	0.00	139.9	72.0	0.0	.4	0.	0.	515.	0.	0.	.03
A74310	.0	0.0	.3	0.0	.01	139.9	60.0	0.0	.1	0.	0.	4.	0.	0.	.33
A74311	.1	0.0	33.6	0.0	0.00	139.9	48.0	0.0	.3	0.	0.	437.	0.	0.	.12

RUN NUMBER 7

FILE NAME	MODEL CONDITIONS: PEAK CONC. (%)	1% ARR. TIME (SEC)	PEAK TIME (SEC)	1% END TIME (SEC)	SUM (X-S)	PROTOTYPE CONDITIONS: POSITION X (M)	Y (M)	Z (M)	PEAK CONC. (%)	5% ARR. TIME (SEC)	15% ARR. TIME (SEC)	PEAK TIME (SEC)	15% END TIME (SEC)	5% END TIME (SEC)	SUM (X-S)
A74312	.1	0.0	10.5	0.0	.01	139.9	36.0	0.0	.3	0.	0.	137.	0.	0.	.20
A74313	.2	0.0	13.7	0.0	0.00	139.9	24.0	0.0	.4	0.	0.	178.	0.	0.	.15
A74314	1.5	9.7	14.0	14.7	.06	139.9	12.0	0.0	3.9	0.	0.	183.	0.	0.	2.10
A74315	2.3	5.0	10.7	15.0	.17	139.9	0.0	0.0	6.1	135.	0.	139.	0.	178.	5.84
B74308	.2	0.0	24.8	0.0	.01	139.9	84.0	0.0	.4	0.	0.	322.	0.	0.	.41
B74309	.2	0.0	24.4	0.0	.02	139.9	72.0	0.0	.5	0.	0.	317.	0.	0.	.81
B74310	.3	0.0	29.7	0.0	.01	139.9	60.0	0.0	.7	0.	0.	386.	0.	0.	.59
B74311	.1	0.0	38.0	0.0	.02	139.9	48.0	0.0	.3	0.	0.	495.	0.	0.	.67
B74312	.1	0.0	8.5	0.0	.01	139.9	36.0	0.0	.3	0.	0.	110.	0.	0.	.34
B74313	.1	0.0	11.2	0.0	0.00	139.9	24.0	0.0	.3	0.	0.	145.	0.	0.	.07
B74314	1.3	11.5	11.8	14.2	.06	139.9	12.0	0.0	3.6	0.	0.	153.	0.	0.	1.98
B74315	4.4	6.5	11.6	15.8	.30	139.9	0.0	0.0	11.1	108.	0.	151.	0.	201.	10.02
A74408	3.5	4.2	10.3	16.3	.28	139.9	0.0	0.0	8.9	99.	0.	134.	0.	194.	9.46
A74409	3.1	4.5	8.6	16.4	.25	139.9	-12.0	0.0	7.9	97.	0.	112.	0.	190.	8.65
A74410	2.2	6.0	11.3	13.2	.16	139.9	-24.0	0.0	5.7	146.	0.	147.	0.	164.	5.46
A74411	.6	0.0	11.9	0.0	.03	139.9	-36.0	0.0	1.7	0.	0.	155.	0.	0.	.97
A74412	.2	0.0	13.0	0.0	.01	139.9	-48.0	0.0	.6	0.	0.	169.	0.	0.	.29
A74413	.0	0.0	47.2	0.0	0.00	139.9	-60.0	0.0	.1	0.	0.	613.	0.	0.	.16
A74414	.1	0.0	44.4	0.0	0.00	139.9	-72.0	0.0	.3	0.	0.	577.	0.	0.	.09
A74415	.0	0.0	47.4	0.0	0.00	139.9	-84.0	0.0	.1	0.	0.	617.	0.	0.	.06
B74408	3.8	4.7	9.3	17.2	.31	139.9	0.0	0.0	9.6	87.	0.	121.	0.	188.	10.70
B74409	4.1	5.0	13.3	18.3	.37	139.9	-12.0	0.0	10.4	86.	0.	173.	0.	213.	12.46
B74410	4.2	7.8	13.2	17.9	.25	139.9	-24.0	0.0	10.7	137.	0.	172.	0.	190.	8.43
B74411	1.3	13.8	13.8	14.7	.04	139.9	-36.0	0.0	3.5	0.	0.	180.	0.	0.	1.29
B74412	.1	0.0	6.0	0.0	.01	139.9	-48.0	0.0	.4	0.	0.	79.	0.	0.	.39
B74413	.1	0.0	47.9	0.0	.01	139.9	-60.0	0.0	.4	0.	0.	623.	0.	0.	.48
B74414	.2	0.0	2.6	0.0	.02	139.9	-72.0	0.0	.4	0.	0.	33.	0.	0.	.59
B74415	.1	0.0	30.3	0.0	.02	139.9	-84.0	0.0	.4	0.	0.	394.	0.	0.	.68
A75408	2.2	11.9	13.9	15.3	.11	242.4	0.0	0.0	5.7	178.	0.	180.	0.	189.	3.94
A75409	2.0	11.3	14.9	16.7	.15	242.4	-12.0	0.0	5.3	193.	0.	193.	0.	197.	5.08
A75410	1.3	9.0	10.6	16.7	.12	242.4	-24.0	0.0	3.4	0.	0.	138.	0.	0.	4.23
A75411	1.2	8.8	9.2	18.2	.11	242.4	-36.0	0.0	3.3	0.	0.	120.	0.	0.	3.95
A75412	1.0	0.0	9.4	0.0	.06	242.4	-48.0	0.0	2.5	0.	0.	122.	0.	0.	2.11
A75413	.5	0.0	10.7	0.0	.04	242.4	-60.0	0.0	1.5	0.	0.	139.	0.	0.	1.32
A75414	.2	0.0	17.8	0.0	.03	242.4	-72.0	0.0	.7	0.	0.	231.	0.	0.	.94
A75415	.1	0.0	30.3	0.0	.02	242.4	-84.0	0.0	.4	0.	0.	394.	0.	0.	.65
B75408	1.9	10.9	15.9	17.5	.15	242.4	0.0	0.0	5.0	0.	0.	207.	0.	0.	5.08
B75409	2.1	9.1	15.6	17.9	.20	242.4	-12.0	0.0	5.6	203.	0.	203.	0.	213.	6.83
B75410	1.7	7.4	15.6	16.7	.17	242.4	-24.0	0.0	4.5	0.	0.	203.	0.	0.	5.75
B75411	1.1	10.0	10.0	11.4	.06	242.4	-36.0	0.0	2.9	0.	0.	131.	0.	0.	2.18
B75412	.3	0.0	14.6	0.0	.01	242.4	-48.0	0.0	.8	0.	0.	189.	0.	0.	.38
B75413	.1	0.0	7.9	0.0	0.00	242.4	-60.0	0.0	.3	0.	0.	102.	0.	0.	.17
B75414	.2	0.0	.1	0.0	.01	242.4	-72.0	0.0	.4	0.	0.	1.	0.	0.	.29
B75415	.1	0.0	8.8	0.0	0.00	242.4	-84.0	0.0	.2	0.	0.	114.	0.	0.	.03
A75308	.1	0.0	20.1	0.0	.01	242.4	84.0	0.0	.4	0.	0.	261.	0.	0.	.40
A75309	.1	0.0	47.8	0.0	.01	242.4	72.0	0.0	.4	0.	0.	621.	0.	0.	.32
A75310	.1	0.0	.6	0.0	.01	242.4	60.0	0.0	.4	0.	0.	8.	0.	0.	.25
A75311	.1	0.0	47.5	0.0	0.00	242.4	48.0	0.0	.3	0.	0.	617.	0.	0.	.08
A75312	.3	0.0	23.2	0.0	.04	242.4	36.0	0.0	.9	0.	0.	302.	0.	0.	1.54
A75313	.2	0.0	14.7	0.0	.01	242.4	24.0	0.0	.4	0.	0.	191.	0.	0.	.19

RUN NUMBER 7

FILE NAME	MODEL CONDITIONS PEAK CONC. (%)	1% ARR. TIME (SEC)	PEAK TIME (SEC)	1% END TIME (SEC)	SUM (X-S)	POSITION X (M)	Y (M)	Z (M)	PROTOTYPE CONDITIONS PEAK CONC. (%)	5% ARR. TIME (SEC)	15% ARR. TIME (SEC)	PEAK TIME (SEC)	15% END TIME (SEC)	5% END TIME (SEC)	SUM (X-S)
A75314	.5	0.0	14.6	0.0	.03	242.4	12.0	0.0	1.4	0.	0.	190.	0.	0.	.96
A75315	1.4	12.2	14.4	14.8	.09	242.4	0.0	0.0	3.7	0.	0.	187.	0.	0.	3.13
B75308	.1	0.0	32.2	0.0	.01	242.4	84.0	0.0	.4	0.	0.	418.	0.	0.	.18
B75309	.2	0.0	2.3	0.0	.01	242.4	72.0	0.0	.5	0.	0.	30.	0.	0.	.27
B75310	.0	0.0	44.8	0.0	.01	242.4	60.0	0.0	.2	0.	0.	583.	0.	0.	.33
B75311	.1	0.0	.0	0.0	.01	242.4	48.0	0.0	.2	0.	0.	1.	0.	0.	.43
B75312	.1	0.0	.1	0.0	.01	242.4	36.0	0.0	.3	0.	0.	2.	0.	0.	.25
B75313	.1	0.0	.4	0.0	.01	242.4	24.0	0.0	.4	0.	0.	5.	0.	0.	.40
B75314	1.2	12.7	12.9	14.3	.07	242.4	12.0	0.0	3.2	0.	0.	167.	0.	0.	2.51
B75315	1.4	9.8	10.6	12.7	.11	242.4	0.0	0.0	3.6	0.	0.	138.	0.	0.	3.83
A76308	.2	0.0	45.1	0.0	.01	399.8	84.0	0.0	.4	0.	0.	587.	0.	0.	.19
A76309	.2	0.0	35.1	0.0	.01	399.8	72.0	0.0	.4	0.	0.	457.	0.	0.	.31
A76310	.1	0.0	28.6	0.0	.01	399.8	60.0	0.0	.3	0.	0.	371.	0.	0.	.35
A76311	.1	0.0	47.8	0.0	.02	399.8	48.0	0.0	.3	0.	0.	622.	0.	0.	.55
A76312	.1	0.0	44.2	0.0	.01	399.8	36.0	0.0	.2	0.	0.	574.	0.	0.	.37
A76313	.1	0.0	20.7	0.0	0.00	399.8	24.0	0.0	.3	0.	0.	269.	0.	0.	.16
A76314	.2	0.0	34.3	0.0	.01	399.8	12.0	0.0	.4	0.	0.	446.	0.	0.	.40
A76315	.4	0.0	12.2	0.0	.03	399.8	0.0	0.0	1.2	0.	0.	158.	0.	0.	1.07
B76308	.2	0.0	48.1	0.0	.01	399.8	84.0	0.0	.5	0.	0.	625.	0.	0.	.23
B76309	.1	0.0	46.0	0.0	0.00	399.8	72.0	0.0	.4	0.	0.	598.	0.	0.	.14
B76310	.1	0.0	4.2	0.0	0.00	399.8	60.0	0.0	.3	0.	0.	55.	0.	0.	.14
B76311	.1	0.0	.2	0.0	.01	399.8	48.0	0.0	.2	0.	0.	3.	0.	0.	.18
B76312	.1	0.0	.2	0.0	0.00	399.8	36.0	0.0	.2	0.	0.	3.	0.	0.	.13
B76313	.1	0.0	41.8	0.0	0.00	399.8	24.0	0.0	.3	0.	0.	544.	0.	0.	.02
B76314	.1	0.0	.2	0.0	0.00	399.8	12.0	0.0	.3	0.	0.	3.	0.	0.	.16
B76315	.4	0.0	11.5	0.0	.02	399.8	0.0	0.0	1.2	0.	0.	150.	0.	0.	.74

RUN NUMBER 8

FILE NAME	MODEL CONDITIONS PEAK CONC. (%)	1% ARR. TIME (SEC)	PEAK TIME (SEC)	1% END TIME (SEC)	SUM (X-S)	POSITION X (M)	Y (M)	Z (M)	PROTOTYPE CONDITIONS PEAK CONC. (%)	5% ARR. TIME (SEC)	15% ARR. TIME (SEC)	PEAK TIME (SEC)	15% END TIME (SEC)	5% END TIME (SEC)	SUM (X-S)
A81308	.7	0.0	16.0	0.0	.03	36.5	84.0	0.0	1.8	0.	0.	209.	0.	0.	.96
A81309	2.6	10.8	12.0	15.6	.11	36.5	72.0	0.0	6.8	144.	0.	135.	0.	189.	3.85
A81310	4.3	8.9	10.2	16.0	.22	36.5	60.0	0.0	10.9	116.	0.	132.	0.	193.	7.37
A81311	7.6	6.6	9.6	28.4	.51	36.5	48.0	0.0	18.2	89.	110.	124.	142.	210.	16.68
A81312	8.9	5.4	9.5	30.2	.78	36.5	36.0	0.0	20.8	72.	98.	124.	151.	363.	25.37
A81313	11.5	2.9	8.6	32.1	1.34	36.5	24.0	0.0	26.1	45.	76.	112.	163.	365.	42.70
A81314	13.5	1.7	9.2	40.8	1.94	36.5	12.0	0.0	29.6	34.	58.	119.	192.	484.	60.92
A81315	9.6	2.6	8.5	48.4	1.74	36.5	0.0	0.0	22.3	42.	71.	111.	187.	415.	56.06
B81308	.2	0.0	13.0	0.0	.01	36.5	84.0	0.0	.4	0.	0.	168.	0.	0.	.47
B81309	.4	0.0	18.4	0.0	.01	36.5	72.0	0.0	1.2	0.	0.	239.	0.	0.	.34
B81310	3.3	16.2	17.2	19.3	.08	36.5	60.0	0.0	8.5	214.	0.	224.	0.	236.	2.81
B81311	5.4	8.6	15.3	25.2	.51	36.5	48.0	0.0	13.4	117.	0.	199.	0.	265.	16.99
B81312	6.1	6.0	14.9	26.7	.75	36.5	36.0	0.0	14.8	82.	0.	193.	0.	333.	24.72
B81313	9.0	4.4	9.2	28.6	1.18	36.5	24.0	0.0	21.1	58.	81.	120.	194.	360.	37.99
B81314	13.0	2.9	8.9	43.2	2.09	36.5	12.0	0.0	28.8	43.	59.	116.	234.	527.	65.53
B81315	10.6	2.0	9.2	47.7	2.02	36.5	0.0	0.0	24.2	39.	72.	120.	235.	544.	65.01
A81408	9.9	2.8	8.8	40.0	1.70	36.5	0.0	0.0	22.8	38.	72.	115.	194.	421.	54.54
A81409	10.9	3.6	8.1	41.1	1.57	36.5	-12.0	0.0	24.8	48.	72.	106.	180.	459.	50.47
A81410	7.5	4.5	11.0	35.6	.97	36.5	-24.0	0.0	18.0	68.	102.	143.	150.	445.	32.09
A81411	6.3	5.8	11.4	34.1	.49	36.5	-36.0	0.0	15.3	80.	148.	148.	149.	211.	16.48
A81412	3.1	12.0	12.6	16.4	.12	36.5	-48.0	0.0	8.0	158.	0.	164.	0.	184.	4.07
A81413	1.7	13.3	13.5	14.6	.03	36.5	-60.0	0.0	4.4	0.	0.	176.	0.	0.	1.16
A81414	.2	0.0	.3	0.0	.01	36.5	-72.0	0.0	.5	0.	0.	4.	0.	0.	.47
A81415	.1	0.0	33.8	0.0	.01	36.5	-84.0	0.0	.2	0.	0.	440.	0.	0.	.24
B81408	13.6	2.2	9.0	40.5	1.98	36.5	0.0	0.0	28.8	37.	65.	118.	212.	441.	62.80
B81409	9.7	2.6	9.2	35.4	1.46	36.5	-12.0	0.0	22.6	41.	81.	120.	160.	452.	47.17
B81410	4.8	3.6	9.0	30.6	.68	36.5	-24.0	0.0	12.0	50.	0.	117.	0.	393.	22.79
B81411	2.3	8.5	11.6	14.8	.12	36.5	-36.0	0.0	5.9	147.	0.	151.	0.	163.	4.03
B81412	.1	0.0	7.3	0.0	.01	36.5	-48.0	0.0	.3	0.	0.	95.	0.	0.	.22
B81413	.1	0.0	80.0	0.0	.02	36.5	-60.0	0.0	.3	0.	0.	1041.	0.	0.	.80
B81414	.2	0.0	87.0	0.0	.03	36.5	-72.0	0.0	.4	0.	0.	1131.	0.	0.	1.08
B81415	.1	0.0	86.0	0.0	.01	36.5	-84.0	0.0	.2	0.	0.	1117.	0.	0.	.33
A82408	5.8	4.4	10.2	35.9	.94	56.9	0.0	0.0	14.3	64.	0.	132.	0.	370.	31.33
A82409	5.4	4.9	10.5	42.3	.85	56.9	-12.0	0.0	13.3	73.	0.	136.	0.	320.	28.59
A82410	4.2	5.7	9.4	28.1	.52	56.9	-24.0	0.0	10.6	85.	0.	122.	0.	310.	17.49
A82411	3.8	6.3	8.5	28.2	.48	56.9	-36.0	0.0	9.5	92.	0.	111.	0.	325.	16.18
A82412	2.8	7.9	10.0	27.8	.36	56.9	-48.0	0.0	7.1	106.	0.	131.	0.	291.	12.22
A82413	2.4	9.0	10.8	26.2	.25	56.9	-60.0	0.0	6.1	133.	0.	140.	0.	301.	8.64
A82414	1.6	11.8	21.5	22.6	.10	56.9	-72.0	0.0	4.2	0.	0.	280.	0.	0.	3.53
A82415	.4	0.0	21.2	0.0	.03	56.9	-84.0	0.0	1.1	0.	0.	276.	0.	0.	1.08
B82408	5.9	4.1	14.1	43.3	1.00	56.9	0.0	0.0	14.5	68.	0.	184.	0.	366.	33.30
B82409	4.6	4.7	15.5	32.8	.80	56.9	-12.0	0.0	11.6	74.	0.	201.	0.	372.	26.78
B82410	3.6	5.3	10.2	33.5	.60	56.9	-24.0	0.0	9.2	100.	0.	132.	0.	267.	20.32
B82411	2.7	6.5	9.7	35.9	.46	56.9	-36.0	0.0	7.1	110.	0.	126.	0.	394.	15.77
B82412	2.1	17.7	20.5	21.8	.17	56.9	-48.0	0.0	5.4	265.	0.	266.	0.	272.	5.75
B82413	.7	0.0	21.4	0.0	.06	56.9	-60.0	0.0	1.9	0.	0.	278.	0.	0.	1.95
B82414	.4	0.0	56.5	0.0	.07	56.9	-72.0	0.0	1.0	0.	0.	734.	0.	0.	2.32
B82415	.2	0.0	81.1	0.0	.02	56.9	-84.0	0.0	.5	0.	0.	1055.	0.	0.	.66
A82308	.2	0.0	21.5	0.0	.02	56.9	84.0	0.0	.5	0.	0.	280.	0.	0.	.56
A82309	.2	0.0	68.6	0.0	.03	56.9	72.0	0.0	.4	0.	0.	891.	0.	0.	.97

RUN NUMBER 8

FILE NAME	MODEL CONDITIONS: PEAK CONC. (%)	1% ARR. TIME (SEC)	PEAK TIME (SEC)	1% END TIME (SEC)	SUM (X-S)	POSITION X (M)	POSITION Y (M)	POSITION Z (M)	PROTOTYPE CONDITIONS: PEAK CONC. (%)	5% ARR. TIME (SEC)	15% ARR. TIME (SEC)	PEAK TIME (SEC)	15% END TIME (SEC)	5% END TIME (SEC)	SUM (X-S)
A82310	2.8	12.8	14.7	18.4	.17	56.9	60.0	0.0	7.2	176.	0.	191.	0.	232.	5.96
A82311	4.5	11.1	16.4	31.6	.61	56.9	48.0	0.0	11.3	147.	0.	213.	0.	317.	20.62
A82312	4.9	5.2	13.9	31.1	.71	56.9	36.0	0.0	12.3	100.	0.	181.	0.	302.	23.69
A82313	6.8	3.3	11.4	42.4	1.08	56.9	24.0	0.0	16.4	66.	143.	148.	191.	380.	35.55
A82314	8.2	3.0	10.9	45.8	1.31	56.9	12.0	0.0	19.5	52.	121.	142.	196.	383.	42.81
A82315	7.5	4.0	10.5	41.0	1.07	56.9	0.0	0.0	17.9	82.	118.	137.	162.	376.	35.46
A82308	.2	0.0	46.3	0.0	.04	56.9	84.0	0.0	.6	0.	0.	602.	0.	0.	1.42
A82309	2.1	12.2	12.9	18.0	.14	56.9	72.0	0.0	5.5	164.	0.	168.	0.	173.	4.80
A82310	3.6	8.0	14.6	22.5	.43	56.9	60.0	0.0	9.1	114.	0.	190.	0.	252.	14.57
A82311	5.3	6.2	10.9	22.8	.58	56.9	48.0	0.0	13.0	90.	0.	142.	0.	284.	19.20
A82312	6.1	5.7	10.5	26.0	.67	56.9	36.0	0.0	14.8	83.	0.	136.	0.	302.	22.36
A82313	8.2	4.3	9.8	38.6	.96	56.9	24.0	0.0	19.4	63.	114.	127.	163.	316.	31.33
A82314	7.4	4.1	11.0	37.0	1.11	56.9	12.0	0.0	17.7	63.	127.	144.	164.	336.	36.73
A82315	6.6	3.8	13.0	37.2	1.09	56.9	0.0	0.0	15.9	65.	139.	170.	173.	333.	36.43
A83308	.2	0.0	38.1	0.0	.02	91.2	84.0	0.0	.5	0.	0.	495.	0.	0.	.55
A83309	.1	0.0	49.9	0.0	.01	91.2	72.0	0.0	.4	0.	0.	648.	0.	0.	.41
A83310	1.4	24.6	25.1	27.5	.07	91.2	60.0	0.0	3.8	0.	0.	327.	0.	0.	2.36
A83311	1.9	13.9	20.3	33.4	.22	91.2	48.0	0.0	5.1	263.	0.	264.	0.	265.	7.61
A83312	2.5	13.1	16.2	24.9	.29	91.2	36.0	0.0	6.6	197.	0.	211.	0.	263.	9.89
A83313	3.3	10.8	15.6	30.5	.42	91.2	24.0	0.0	8.4	157.	0.	203.	0.	309.	14.12
A83314	3.5	8.1	14.0	31.7	.58	91.2	12.0	0.0	8.9	115.	0.	183.	0.	365.	19.67
A83315	3.3	7.6	13.8	37.0	.60	91.2	0.0	0.0	8.6	124.	0.	180.	0.	357.	20.60
A83306	.3	0.0	59.5	0.0	.05	91.2	84.0	0.0	.8	0.	0.	774.	0.	0.	1.70
A83309	.7	0.0	28.0	0.0	.05	91.2	72.0	0.0	1.9	0.	0.	364.	0.	0.	1.87
A83310	1.4	25.6	26.8	27.8	.09	91.2	60.0	0.0	3.6	0.	0.	348.	0.	0.	3.09
A83311	2.3	13.6	15.0	27.4	.23	91.2	48.0	0.0	5.9	191.	0.	195.	0.	343.	7.89
A83312	2.4	12.6	14.0	26.8	.23	91.2	36.0	0.0	6.2	175.	0.	183.	0.	253.	7.94
A83313	3.5	9.2	13.9	30.2	.44	91.2	24.0	0.0	8.9	164.	0.	180.	0.	322.	14.96
A83314	3.4	7.2	17.9	30.7	.59	91.2	12.0	0.0	8.7	122.	0.	233.	0.	326.	20.07
A83315	3.6	5.7	12.0	30.2	.62	91.2	0.0	0.0	9.1	105.	0.	157.	0.	310.	20.91
A83408	3.6	7.5	13.4	23.8	.44	91.2	0.0	0.0	9.0	138.	0.	174.	0.	292.	14.86
A83409	3.7	7.6	14.3	30.4	.52	91.2	-12.0	0.0	9.3	150.	0.	186.	0.	302.	17.61
A83410	2.8	8.0	16.8	31.7	.47	91.2	-24.0	0.0	7.3	177.	0.	218.	0.	268.	16.10
A83411	2.8	8.1	15.4	31.5	.44	91.2	-36.0	0.0	7.1	170.	0.	200.	0.	251.	14.94
A83412	2.0	13.6	15.7	27.8	.24	91.2	-48.0	0.0	5.1	204.	0.	204.	0.	209.	8.34
A83413	1.9	14.4	20.3	27.0	.22	91.2	-60.0	0.0	5.1	196.	0.	264.	0.	269.	7.57
A83414	2.0	15.4	15.8	21.6	.20	91.2	-72.0	0.0	5.2	205.	0.	205.	0.	259.	6.98
A83415	1.6	16.2	17.4	19.2	.08	91.2	-84.0	0.0	4.3	0.	0.	226.	0.	0.	2.87
A83408	3.2	7.0	12.3	33.5	.53	91.2	0.0	0.0	8.3	124.	0.	160.	0.	269.	17.92
A83409	3.8	6.6	12.8	32.8	.65	91.2	-12.0	0.0	9.6	122.	0.	166.	0.	304.	21.87
A83410	3.5	7.0	12.9	28.4	.58	91.2	-24.0	0.0	8.9	134.	0.	167.	0.	301.	19.58
A83411	3.1	8.8	14.1	25.8	.47	91.2	-36.0	0.0	7.9	145.	0.	183.	0.	293.	16.11
A83412	2.6	10.4	14.7	25.3	.32	91.2	-48.0	0.0	6.8	183.	0.	191.	0.	210.	10.88
A83413	2.8	10.2	14.3	29.2	.34	91.2	-60.0	0.0	7.2	178.	0.	186.	0.	331.	11.68
A83414	2.6	13.0	15.4	26.3	.29	91.2	-72.0	0.0	6.6	187.	0.	200.	0.	332.	10.05
A83415	2.2	15.0	16.6	25.7	.14	91.2	-84.0	0.0	5.6	210.	0.	216.	0.	220.	4.91
A83508	1.1	22.5	22.5	22.5	.05	91.2	-84.0	0.0	2.8	0.	0.	292.	0.	0.	1.57
A83509	.2	0.0	24.4	0.0	.02	91.2	-96.0	0.0	.6	0.	0.	317.	0.	0.	.71
A83510	.1	0.0	74.9	0.0	.01	91.2	-108.0	0.0	.3	0.	0.	973.	0.	0.	.41
A83511	.2	0.0	33.9	0.0	.01	91.2	-120.0	0.0	.4	0.	0.	440.	0.	0.	.46

RUN NUMBER 8

FILE NAME	MODEL CONDITIONS PEAK CONC. (%)	1% ARR. TIME (SEC)	PEAK TIME (SEC)	1% END TIME (SEC)	SUM (X-S)	POSITION X (M)	Y (M)	Z (M)	PROTOTYPE CONDITIONS PEAK CONC. (%)	5% ARR. TIME (SEC)	15% ARR. TIME (SEC)	PEAK TIME (SEC)	15% END TIME (SEC)	5% END TIME (SEC)	SUM (X-S)
A03512	.1	0.0	83.2	0.0	.01	91.2	-132.0	0.0	.2	0.	0.	1107.	0.	0.	.20
A03513	.1	0.0	16.6	0.0	.01	91.2	-144.0	0.0	.2	0.	0.	215.	0.	0.	.24
A03514	.2	0.0	50.8	0.0	.02	91.2	-156.0	0.0	.3	0.	0.	660.	0.	0.	.69
A03515	.1	0.0	70.7	0.0	.01	91.2	-168.0	0.0	.3	0.	0.	919.	0.	0.	.30
A03508	.3	0.0	58.6	0.0	.03	91.2	-84.0	0.0	.7	0.	0.	762.	0.	0.	.99
A03509	.1	0.0	12.0	0.0	.02	91.2	-96.0	0.0	.3	0.	0.	155.	0.	0.	.62
A03510	.0	0.0	.0	0.0	.01	91.2	-108.0	0.0	.1	0.	0.	1.	0.	0.	.39
A03511	.1	0.0	81.6	0.0	.01	91.2	-120.0	0.0	.3	0.	0.	1061.	0.	0.	.31
A03512	.1	0.0	76.8	0.0	.01	91.2	-132.0	0.0	.3	0.	0.	998.	0.	0.	.38
A03513	.0	0.0	.0	0.0	.02	91.2	-144.0	0.0	.1	0.	0.	1.	0.	0.	.74
A03514	.2	0.0	86.4	0.0	0.00	91.2	-156.0	0.0	.5	0.	0.	1124.	0.	0.	.15
A03515	.1	0.0	87.1	0.0	0.00	91.2	-168.0	0.0	.2	0.	0.	1133.	0.	0.	.08
A04406	2.4	11.9	17.4	25.0	.31	139.9	0.0	0.0	6.3	184.	0.	227.	0.	265.	10.39
A04409	2.3	8.0	19.1	26.1	.40	139.9	-12.0	0.0	5.9	190.	0.	249.	0.	277.	13.77
A04410	2.2	10.0	18.2	27.3	.37	139.9	-24.0	0.0	5.7	197.	0.	237.	0.	258.	12.89
A04411	2.2	11.2	17.9	31.2	.33	139.9	-36.0	0.0	5.6	202.	0.	233.	0.	262.	11.39
A04412	1.8	17.2	18.3	21.2	.19	139.9	-48.0	0.0	4.7	0.	0.	238.	0.	0.	6.73
A04413	1.5	21.1	21.9	32.9	.19	139.9	-60.0	0.0	4.1	0.	0.	284.	0.	0.	6.50
A04414	1.3	8.0	8.0	29.9	.10	139.9	-72.0	0.0	3.4	0.	0.	103.	0.	0.	3.38
A04415	.1	0.0	71.2	0.0	.01	139.9	-84.0	0.0	.3	0.	0.	926.	0.	0.	.38
A04406	2.0	11.7	19.0	30.6	.37	139.9	0.0	0.0	5.3	248.	0.	248.	0.	270.	12.82
A04409	2.2	10.6	15.7	30.1	.40	139.9	-12.0	0.0	5.6	160.	0.	204.	0.	244.	13.81
A04410	1.9	10.4	15.0	29.2	.36	139.9	-24.0	0.0	5.1	195.	0.	195.	0.	232.	12.43
A04411	1.9	11.6	15.5	30.6	.36	139.9	-36.0	0.0	5.1	201.	0.	201.	0.	207.	12.26
A04412	1.3	14.9	16.1	28.0	.23	139.9	-48.0	0.0	3.5	0.	0.	209.	0.	0.	8.06
A04413	1.3	17.0	18.0	28.9	.17	139.9	-60.0	0.0	3.5	0.	0.	234.	0.	0.	5.99
A04414	.3	0.0	6.2	0.0	.04	139.9	-72.0	0.0	.9	0.	0.	81.	0.	0.	1.33
A04415	.1	0.0	56.8	0.0	.02	139.9	-84.0	0.0	.3	0.	0.	738.	0.	0.	.78
A04308	.2	0.0	2.1	0.0	.02	139.9	84.0	0.0	.4	0.	0.	27.	0.	0.	.78
A04309	.7	0.0	23.7	0.0	.04	139.9	72.0	0.0	1.8	0.	0.	308.	0.	0.	1.31
A04310	1.2	22.1	23.9	25.4	.11	139.9	60.0	0.0	3.0	0.	0.	310.	0.	0.	3.75
A04311	1.7	19.4	24.6	30.0	.22	139.9	48.0	0.0	4.3	0.	0.	320.	0.	0.	7.50
A04312	1.5	14.3	19.3	24.4	.19	139.9	36.0	0.0	4.1	0.	0.	251.	0.	0.	6.47
A04313	2.6	12.8	17.8	28.9	.30	139.9	24.0	0.0	6.6	178.	0.	231.	0.	264.	10.44
A04314	2.7	12.1	16.2	27.6	.36	139.9	12.0	0.0	7.0	183.	0.	211.	0.	269.	12.34
A04315	2.2	11.9	16.8	24.0	.29	139.9	0.0	0.0	5.8	186.	0.	219.	0.	253.	10.08
A04308	.9	0.0	22.3	0.0	.05	139.9	84.0	0.0	2.3	0.	0.	290.	0.	0.	1.69
A04309	1.3	20.3	21.2	24.6	.09	139.9	72.0	0.0	3.6	0.	0.	276.	0.	0.	3.14
A04310	2.0	14.8	16.3	25.5	.19	139.9	60.0	0.0	5.2	212.	0.	212.	0.	222.	6.57
A04311	2.2	13.3	18.9	26.4	.25	139.9	48.0	0.0	5.8	191.	0.	245.	0.	254.	8.46
A04312	2.0	12.6	18.8	22.1	.22	139.9	36.0	0.0	5.2	245.	0.	245.	0.	250.	7.41
A04313	2.3	11.1	16.2	22.9	.31	139.9	24.0	0.0	6.0	173.	0.	211.	0.	264.	10.62
A04314	2.4	10.4	19.8	28.8	.39	139.9	12.0	0.0	6.1	156.	0.	257.	0.	274.	13.23
A04315	1.8	10.0	12.8	27.8	.29	139.9	0.0	0.0	4.8	0.	0.	166.	0.	0.	9.93
A05308	.6	0.0	23.2	0.0	.09	242.4	84.0	0.0	1.6	0.	0.	302.	0.	0.	3.09
A05309	.9	0.0	20.1	0.0	.10	242.4	72.0	0.0	2.3	0.	0.	262.	0.	0.	3.45
A05310	.6	0.0	18.4	0.0	.07	242.4	60.0	0.0	1.5	0.	0.	239.	0.	0.	2.41
A05311	.5	0.0	18.5	0.0	.07	242.4	48.0	0.0	1.4	0.	0.	241.	0.	0.	2.37
A05312	.4	0.0	25.4	0.0	.07	242.4	36.0	0.0	1.2	0.	0.	330.	0.	0.	2.29
A05313	.5	0.0	27.8	0.0	.08	242.4	24.0	0.0	1.4	0.	0.	362.	0.	0.	2.64

RUN NUMBER 8

FILE NAME	MODEL CONDITIONS PEAK CONC. (%)	1% ARR. TIME (SEC)	PEAK TIME (SEC)	1% END TIME (SEC)	SUM (X-S)	POSITION X (M)	Y (M)	Z (M)	PROTOTYPE CONDITIONS PEAK CONC. (%)	5% ARR. TIME (SEC)	15% ARR. TIME (SEC)	PEAK TIME (SEC)	15% END TIME (SEC)	5% END TIME (SEC)	SUM (X-S)
B85314	.7	0.0	25.7	0.0	.10	242.4	12.0	0.0	1.8	0.	0.	334.	0.	0.	3.36
B85315	.9	0.0	24.0	0.0	.15	242.4	0.0	0.0	2.3	0.	0.	311.	0.	0.	5.32
B85308	.4	0.0	22.6	0.0	.02	242.4	84.0	0.0	1.0	0.	0.	293.	0.	0.	.60
B85309	1.0	21.6	21.6	22.5	.14	242.4	72.0	0.0	2.7	0.	0.	281.	0.	0.	4.79
B85310	.9	0.0	20.4	0.0	.14	242.4	60.0	0.0	2.5	0.	0.	265.	0.	0.	4.96
B85311	1.1	21.2	21.2	21.4	.13	242.4	48.0	0.0	2.9	0.	0.	275.	0.	0.	4.50
B85312	.7	0.0	18.2	0.0	.10	242.4	36.0	0.0	1.8	0.	0.	236.	0.	0.	3.58
B85313	1.2	17.9	18.5	23.7	.17	242.4	24.0	0.0	3.1	0.	0.	240.	0.	0.	5.78
B85314	1.0	20.5	24.0	24.3	.18	242.4	12.0	0.0	2.7	0.	0.	311.	0.	0.	6.23
B85315	.7	0.0	21.5	0.0	.13	242.4	0.0	0.0	1.9	0.	0.	280.	0.	0.	4.49
B85408	.8	0.0	28.7	0.0	.14	242.4	0.0	0.0	2.2	0.	0.	373.	0.	0.	4.76
B85409	1.1	26.2	26.2	26.5	.18	242.4	-12.0	0.0	2.8	0.	0.	341.	0.	0.	6.15
B85410	.9	0.0	25.7	0.0	.16	242.4	-24.0	0.0	2.3	0.	0.	334.	0.	0.	5.41
B85411	1.2	24.8	27.3	27.9	.19	242.4	-36.0	0.0	3.0	0.	0.	355.	0.	0.	6.71
B85412	.8	0.0	28.2	0.0	.14	242.4	-48.0	0.0	2.0	0.	0.	367.	0.	0.	4.89
B85413	.6	0.0	20.9	0.0	.10	242.4	-60.0	0.0	2.2	0.	0.	271.	0.	0.	3.43
B85414	1.1	21.6	21.6	21.7	.06	242.4	-72.0	0.0	2.8	0.	0.	281.	0.	0.	2.05
B85415	.7	0.0	18.4	0.0	.02	242.4	-84.0	0.0	1.9	0.	0.	239.	0.	0.	.56
B85408	1.0	0.0	29.9	0.0	.14	242.4	0.0	0.0	2.5	0.	0.	388.	0.	0.	4.88
B85409	1.1	20.5	29.1	29.9	.19	242.4	-12.0	0.0	3.0	0.	0.	379.	0.	0.	6.66
B85410	1.2	17.6	28.1	30.7	.22	242.4	-24.0	0.0	3.2	0.	0.	366.	0.	0.	7.56
B85411	1.2	16.8	30.1	33.2	.22	242.4	-36.0	0.0	3.2	0.	0.	391.	0.	0.	7.66
B85412	.9	0.0	19.6	0.0	.17	242.4	-48.0	0.0	2.3	0.	0.	255.	0.	0.	5.99
B85413	1.0	0.0	23.8	0.0	.10	242.4	-60.0	0.0	2.6	0.	0.	310.	0.	0.	3.47
B85414	1.0	24.0	24.0	25.3	.08	242.4	-72.0	0.0	2.7	0.	0.	311.	0.	0.	2.96
B85415	.2	0.0	26.5	0.0	.02	242.4	-84.0	0.0	.6	0.	0.	345.	0.	0.	.69

RUN NUMBER 9

FILE NAME	MODEL CONDITIONS: PEAK CONC. (%)	1% ARR. TIME (SEC)	PEAK TIME (SEC)	1% END TIME (SEC)	SUM (X-S)	POSITION X (M)	Y (M)	Z (M)	PROTOTYPE CONDITIONS: PEAK CONC. (%)	5% ARR. TIME (SEC)	15% ARR. TIME (SEC)	PEAK TIME (SEC)	15% END TIME (SEC)	5% END TIME (SEC)	SUM (X-S)
A91408	14.7	1.6	6.7	27.6	1.44	36.5	0.0	0.0	31.8	25.	39.	87.	165.	309.	44.70
A91409	14.3	2.3	7.2	21.4	.90	36.5	-12.0	0.0	31.1	31.	49.	93.	129.	186.	28.15
A91410	9.1	3.0	5.9	8.9	.20	36.5	-24.0	0.0	21.3	39.	64.	76.	96.	101.	6.57
A91411	.2	0.0	5.0	0.0	.01	36.5	-36.0	0.0	.5	0.	0.	65.	0.	0.	.38
A91412	.1	0.0	27.1	0.0	.01	36.5	-48.0	0.0	.3	0.	0.	352.	0.	0.	.39
A91413	.1	0.0	20.0	0.0	.01	36.5	-60.0	0.0	.3	0.	0.	261.	0.	0.	.31
A91414	.3	0.0	27.8	0.0	.03	36.5	-72.0	0.0	.7	0.	0.	361.	0.	0.	.91
A91415	.1	0.0	26.7	0.0	.02	36.5	-84.0	0.0	.4	0.	0.	347.	0.	0.	.61
B91408	16.5	1.4	6.9	24.2	1.40	36.5	0.0	0.0	34.8	26.	41.	89.	141.	274.	42.88
B91409	12.9	.7	5.6	21.2	.68	36.5	-12.0	0.0	28.6	34.	59.	73.	105.	220.	21.84
B91410	4.4	5.8	6.4	6.8	.03	36.5	-24.0	0.0	11.1	76.	0.	83.	0.	88.	1.15
B91411	.4	0.0	6.1	0.0	.01	36.5	-36.0	0.0	1.0	0.	0.	80.	0.	0.	.20
B91412	.1	0.0	46.1	0.0	.01	36.5	-48.0	0.0	.2	0.	0.	599.	0.	0.	.24
B91413	.1	0.0	47.2	0.0	.01	36.5	-60.0	0.0	.3	0.	0.	613.	0.	0.	.39
B91414	.3	0.0	37.7	0.0	.03	36.5	-72.0	0.0	.8	0.	0.	490.	0.	0.	1.22
B91415	.2	0.0	9.2	0.0	.03	36.5	-84.0	0.0	.4	0.	0.	120.	0.	0.	1.08
A91308	.1	0.0	32.2	0.0	0.00	36.5	84.0	0.0	.3	0.	0.	418.	0.	0.	.15
A91309	.1	0.0	25.4	0.0	.01	36.5	72.0	0.0	.4	0.	0.	331.	0.	0.	.27
A91310	.1	0.0	19.5	0.0	.01	36.5	60.0	0.0	.3	0.	0.	254.	0.	0.	.28
A91311	.2	0.0	36.9	0.0	.02	36.5	48.0	0.0	.4	0.	0.	480.	0.	0.	.61
A91312	.1	0.0	20.3	0.0	.01	36.5	36.0	0.0	.4	0.	0.	264.	0.	0.	.44
A91313	14.7	3.2	6.3	9.5	.36	36.5	24.0	0.0	31.7	47.	68.	82.	107.	122.	11.30
A91314	18.8	1.2	7.5	27.4	1.18	36.5	12.0	0.0	38.5	28.	37.	97.	137.	201.	35.28
A91315	18.6	.9	7.1	27.8	1.52	36.5	0.0	0.0	37.3	17.	37.	92.	153.	268.	46.15
B91308	.2	0.0	6.3	0.0	.03	36.5	84.0	0.0	.6	0.	0.	82.	0.	0.	.97
B91309	.1	0.0	41.3	0.0	.01	36.5	72.0	0.0	.4	0.	0.	537.	0.	0.	.20
B91310	.0	0.0	.0	0.0	.01	36.5	60.0	0.0	.1	0.	0.	1.	0.	0.	.21
B91311	.1	0.0	.1	0.0	.01	36.5	48.0	0.0	.4	0.	0.	2.	0.	0.	.28
B91312	3.6	7.4	10.8	11.5	.05	36.5	36.0	0.0	9.2	101.	0.	141.	0.	144.	1.79
B91313	10.8	3.2	7.3	12.3	.53	36.5	24.0	0.0	24.6	42.	48.	95.	138.	158.	16.94
B91314	16.6	1.4	7.3	30.4	1.45	36.5	12.0	0.0	35.0	23.	35.	95.	138.	303.	44.50
B91315	16.3	.7	6.9	27.9	1.50	36.5	0.0	0.0	34.4	18.	42.	89.	148.	300.	45.91
A92308	.1	0.0	46.6	0.0	0.00	56.9	84.0	0.0	.4	0.	0.	605.	0.	0.	.14
A92309	.1	0.0	2.9	0.0	0.00	56.9	72.0	0.0	.4	0.	0.	37.	0.	0.	.10
A92310	.1	0.0	42.7	0.0	0.00	56.9	60.0	0.0	.2	0.	0.	555.	0.	0.	.13
A92311	.1	0.0	10.8	0.0	0.00	56.9	48.0	0.0	.3	0.	0.	141.	0.	0.	.11
A92312	.1	0.0	8.0	0.0	0.00	56.9	36.0	0.0	.2	0.	0.	103.	0.	0.	.08
A92313	3.0	7.9	8.0	8.3	.03	56.9	24.0	0.0	7.8	103.	0.	103.	0.	107.	1.01
A92314	12.2	2.5	7.3	12.9	.54	56.9	12.0	0.0	27.3	46.	73.	95.	121.	165.	17.09
A92315	10.9	2.0	6.8	21.7	.78	56.9	0.0	0.0	24.8	33.	55.	88.	139.	170.	25.06
B92308	.2	0.0	27.4	0.0	.01	56.9	84.0	0.0	.5	0.	0.	356.	0.	0.	.42
B92309	.1	0.0	40.7	0.0	.01	56.9	72.0	0.0	.3	0.	0.	529.	0.	0.	.30
B92310	.1	0.0	27.6	0.0	0.00	56.9	60.0	0.0	.2	0.	0.	359.	0.	0.	.13
B92311	.1	0.0	39.0	0.0	0.00	56.9	48.0	0.0	.3	0.	0.	508.	0.	0.	.13
B92312	.1	0.0	34.3	0.0	0.00	56.9	36.0	0.0	.2	0.	0.	446.	0.	0.	.08
B92313	4.9	5.9	7.0	12.1	.14	56.9	24.0	0.0	12.2	77.	0.	91.	0.	118.	4.65
B92314	19.8	4.0	6.9	19.0	.68	56.9	12.0	0.0	24.6	67.	72.	90.	146.	241.	21.75
B92315	9.8	1.7	8.6	23.6	.95	56.9	0.0	0.0	22.7	34.	62.	111.	142.	270.	30.86
A92408	10.3	2.4	8.1	21.4	.72	56.9	0.0	0.0	23.7	36.	60.	105.	126.	182.	23.49
A92409	6.0	3.1	5.9	12.6	.35	56.9	-12.0	0.0	14.8	45.	0.	77.	0.	157.	11.78

RUN NUMBER 9

FILE NAME	MODEL CONDITIONS PEAK CONC. (%)	1% ARR. TIME (SEC)	PEAK TIME (SEC)	1% END TIME (SEC)	SUM (X-S)	PROTOTYPE CONDITIONS POSITION X (M)	Y (M)	Z (M)	PEAK CONC. (%)	5% ARR. TIME (SEC)	15% ARR. TIME (SEC)	PEAK TIME (SEC)	15% END TIME (SEC)	5% END TIME (SEC)	SUM (X-S)
A92410	5.2	2.8	6.0	12.3	.17	56.9	-24.0	0.0	12.8	51.	0.	77.	0.	106.	5.92
A92411	1.2	4.6	4.7	8.7	.05	56.9	-36.0	0.0	3.2	0.	0.	61.	0.	0.	1.65
A92412	.1	0.0	23.4	0.0	.01	56.9	-48.0	0.0	.3	0.	0.	304.	0.	0.	.35
A92413	.2	0.0	24.2	0.0	.02	56.9	-60.0	0.0	.5	0.	0.	315.	0.	0.	.68
A92414	.3	0.0	18.6	0.0	.03	56.9	-72.0	0.0	.9	0.	0.	241.	0.	0.	1.06
A92415	.1	0.0	6.2	0.0	0.00	56.9	-84.0	0.0	.2	0.	0.	81.	0.	0.	.15
B92408	9.5	2.1	7.6	21.6	.82	56.9	0.0	0.0	22.2	34.	50.	99.	119.	245.	26.43
B92409	8.0	2.2	8.1	25.2	.57	56.9	-12.0	0.0	19.0	36.	68.	105.	121.	212.	18.80
B92410	4.4	3.1	6.4	14.2	.23	56.9	-24.0	0.0	11.1	54.	0.	84.	0.	127.	7.72
B92411	2.1	5.6	6.6	7.3	.06	56.9	-36.0	0.0	5.4	84.	0.	85.	0.	87.	2.24
B92412	.2	0.0	6.8	0.0	.02	56.9	-48.0	0.0	.6	0.	0.	88.	0.	0.	.66
B92413	.2	0.0	22.7	0.0	.03	56.9	-60.0	0.0	.5	0.	0.	295.	0.	0.	.95
B92414	.3	0.0	18.7	0.0	.04	56.9	-72.0	0.0	.9	0.	0.	243.	0.	0.	1.56
B92415	.1	0.0	16.7	0.0	.01	56.9	-84.0	0.0	.4	0.	0.	217.	0.	0.	.36
A93408	6.1	3.6	8.2	19.2	.42	91.2	0.0	0.0	14.9	59.	0.	106.	0.	196.	13.94
A93409	5.5	5.3	11.0	14.7	.36	91.2	-12.0	0.0	13.6	76.	0.	143.	0.	167.	12.06
A93410	4.7	6.3	8.8	11.5	.17	91.2	-24.0	0.0	11.8	85.	0.	115.	0.	138.	5.72
A93411	2.2	6.8	9.0	9.8	.07	91.2	-36.0	0.0	5.7	113.	0.	117.	0.	124.	2.39
A93412	.1	0.0	30.9	0.0	.01	91.2	-48.0	0.0	.3	0.	0.	402.	0.	0.	.37
A93413	.1	0.0	44.7	0.0	.01	91.2	-60.0	0.0	.3	0.	0.	581.	0.	0.	.28
A93414	.1	0.0	41.1	0.0	.01	91.2	-72.0	0.0	.2	0.	0.	535.	0.	0.	.46
A93415	.1	0.0	46.7	0.0	0.00	91.2	-84.0	0.0	.2	0.	0.	607.	0.	0.	.07
B93408	4.4	3.9	6.8	15.4	.35	91.2	0.0	0.0	11.0	67.	0.	88.	0.	139.	11.70
B93409	3.9	4.5	6.9	11.6	.20	91.2	-12.0	0.0	10.0	62.	0.	89.	0.	135.	6.90
B93410	3.7	5.5	7.1	9.8	.10	91.2	-24.0	0.0	9.4	75.	0.	92.	0.	110.	3.48
B93411	1.9	5.9	6.8	7.1	.04	91.2	-36.0	0.0	4.9	0.	0.	88.	0.	0.	1.27
B93412	.1	0.0	7.7	0.0	0.00	91.2	-48.0	0.0	.2	0.	0.	100.	0.	0.	.03
B93413	.1	0.0	4.8	0.0	0.00	91.2	-60.0	0.0	.2	0.	0.	63.	0.	0.	.11
B93414	.6	0.0	6.0	0.0	.01	91.2	-72.0	0.0	1.5	0.	0.	79.	0.	0.	.42
B93415	.1	0.0	11.0	0.0	.01	91.2	-84.0	0.0	.3	0.	0.	142.	0.	0.	.24
A93308	.2	0.0	11.0	0.0	.03	91.2	84.0	0.0	.5	0.	0.	142.	0.	0.	.96
A93309	.1	0.0	.1	0.0	.02	91.2	72.0	0.0	.3	0.	0.	2.	0.	0.	.66
A93310	.0	0.0	39.6	0.0	.01	91.2	60.0	0.0	.1	0.	0.	515.	0.	0.	.34
A93311	.2	0.0	18.7	0.0	.02	91.2	48.0	0.0	.4	0.	0.	243.	0.	0.	.58
A93312	.1	0.0	13.1	0.0	.01	91.2	36.0	0.0	.3	0.	0.	170.	0.	0.	.34
A93313	4.2	6.5	8.1	9.2	.08	91.2	24.0	0.0	10.5	98.	0.	105.	0.	112.	2.80
A93314	4.5	2.7	8.4	15.9	.21	91.2	12.0	0.0	11.3	78.	0.	110.	0.	136.	6.99
A93315	5.4	2.6	8.3	17.2	.38	91.2	0.0	0.0	13.3	58.	0.	108.	0.	203.	12.72
B93308	.2	0.0	49.4	0.0	.01	91.2	84.0	0.0	.4	0.	0.	642.	0.	0.	.29
B93309	.2	0.0	45.0	0.0	0.00	91.2	72.0	0.0	.4	0.	0.	585.	0.	0.	.08
B93310	.1	0.0	.2	0.0	0.00	91.2	60.0	0.0	.3	0.	0.	2.	0.	0.	.11
B93311	.2	0.0	6.6	0.0	.01	91.2	48.0	0.0	.4	0.	0.	86.	0.	0.	.31
B93312	.1	0.0	24.4	0.0	.01	91.2	36.0	0.0	.3	0.	0.	318.	0.	0.	.32
B93313	3.2	7.3	8.6	10.2	.07	91.2	24.0	0.0	8.3	100.	0.	112.	0.	115.	2.36
B93314	4.0	4.4	8.1	11.2	.21	91.2	12.0	0.0	10.1	92.	0.	105.	0.	140.	7.02
B93315	5.1	3.8	6.8	18.2	.34	91.2	0.0	0.0	12.6	58.	0.	88.	0.	136.	11.56
A94308	.2	0.0	29.8	0.0	.02	139.9	84.0	0.0	.6	0.	0.	387.	0.	0.	.67
A94309	.2	0.0	29.2	0.0	.01	139.9	72.0	0.0	.4	0.	0.	379.	0.	0.	.35
A94310	.1	0.0	39.2	0.0	0.00	139.9	60.0	0.0	.3	0.	0.	510.	0.	0.	.03
A94311	.1	0.0	35.2	0.0	0.00	139.9	48.0	0.0	.4	0.	0.	458.	0.	0.	.01

RUN NUMBER 9

FILE NAME	MODEL CONDITIONS PEAK CONC (%)	1% ARR. TIME (SEC)	PEAK TIME (SEC)	1% END TIME (SEC)	SUM (X-S)	POSITION X (M)	Y (M)	Z (M)	PROTOTYPE CONDITIONS PEAK CONC (%)	5% ARR. TIME (SEC)	15% ARR. TIME (SEC)	PEAK TIME (SEC)	15% END TIME (SEC)	5% END TIME (SEC)	SUM (X-S)
A94312	.1	0.0	39.4	0.0	.01	139.9	36.0	0.0	.3	0.	0.	512.	0.	0.	.25
A94313	.4	0.0	8.3	0.0	.01	139.9	24.0	0.0	1.2	0.	0.	108.	0.	0.	.49
A94314	2.9	6.8	11.4	14.3	.16	139.9	12.0	0.0	7.6	107.	0.	148.	0.	158.	3.44
A94315	4.0	4.9	10.3	17.8	.32	139.9	0.0	0.0	10.1	90.	0.	134.	0.	173.	10.72
B94313	.7	0.0	8.8	0.0	.02	139.9	24.0	0.0	1.9	0.	0.	114.	0.	0.	.68
B94314	3.1	7.4	10.2	12.6	.14	139.9	12.0	0.0	7.9	110.	0.	133.	0.	155.	4.66
B94315	4.1	5.9	9.6	13.8	.23	139.9	0.0	0.0	10.3	94.	0.	125.	0.	137.	7.88
A94408	4.4	5.0	9.8	15.7	.36	139.9	0.0	0.0	11.1	77.	0.	128.	0.	178.	12.23
A94409	2.6	5.2	10.0	14.5	.20	139.9	-12.0	0.0	6.7	101.	0.	129.	0.	144.	6.80
A94410	2.1	6.2	8.7	11.3	.14	139.9	-24.0	0.0	5.6	111.	0.	113.	0.	121.	4.77
A94411	1.4	9.5	9.6	12.0	.08	139.9	-36.0	0.0	3.6	0.	0.	125.	0.	0.	2.77
A94412	.7	0.0	10.2	0.0	.05	139.9	-48.0	0.0	1.9	0.	0.	133.	0.	0.	1.81
A94413	.2	0.0	28.2	0.0	.02	139.9	-60.0	0.0	.4	0.	0.	367.	0.	0.	.63
A94414	.2	0.0	43.2	0.0	.02	139.9	-72.0	0.0	.5	0.	0.	562.	0.	0.	.63
A94415	.1	0.0	.7	0.0	0.00	139.9	-84.0	0.0	.3	0.	0.	9.	0.	0.	.16
B94408	4.1	6.6	10.0	15.7	.24	139.9	0.0	0.0	10.3	90.	0.	129.	0.	147.	8.26
B94409	4.2	4.7	9.5	19.7	.33	139.9	-12.0	0.0	10.5	83.	0.	123.	0.	167.	11.28
B94410	3.8	5.0	7.4	18.9	.29	139.9	-24.0	0.0	9.5	74.	0.	96.	0.	154.	9.74
B94411	2.3	5.9	9.2	13.0	.18	139.9	-36.0	0.0	5.9	93.	0.	119.	0.	138.	6.30
B94412	1.1	8.1	8.9	10.4	.04	139.9	-48.0	0.0	3.0	0.	0.	115.	0.	0.	1.46
B94413	.4	0.0	8.2	0.0	.03	139.9	-60.0	0.0	1.1	0.	0.	107.	0.	0.	.89
B94414	.3	0.0	7.9	0.0	.01	139.9	-72.0	0.0	.7	0.	0.	103.	0.	0.	.50
B94415	.1	0.0	43.8	0.0	0.00	139.9	-84.0	0.0	.2	0.	0.	569.	0.	0.	.04
A95408	.7	0.0	9.8	0.0	.05	242.4	0.0	0.0	1.8	0.	0.	128.	0.	0.	1.78
A95409	1.3	9.8	10.4	14.8	.12	242.4	-12.0	0.0	3.6	0.	0.	136.	0.	0.	4.30
A95410	1.6	8.3	12.8	16.1	.14	242.4	-24.0	0.0	4.3	0.	0.	166.	0.	0.	4.90
A95411	1.9	8.1	11.8	16.2	.15	242.4	-36.0	0.0	4.9	0.	0.	153.	0.	0.	5.16
A95412	1.5	10.1	12.0	13.2	.06	242.4	-48.0	0.0	4.1	0.	0.	155.	0.	0.	2.09
A95413	1.8	10.4	11.7	12.8	.06	242.4	-60.0	0.0	4.7	0.	0.	152.	0.	0.	1.93
A95414	.8	0.0	12.0	0.0	.04	242.4	-72.0	0.0	2.2	0.	0.	157.	0.	0.	1.30
A95415	.2	0.0	15.0	0.0	.02	242.4	-84.0	0.0	.4	0.	0.	196.	0.	0.	.81
B95408	1.2	8.9	12.7	13.2	.07	242.4	0.0	0.0	3.2	0.	0.	165.	0.	0.	2.52
B95409	1.7	8.8	12.0	14.7	.12	242.4	-12.0	0.0	4.6	0.	0.	155.	0.	0.	4.20
B95410	1.9	8.9	11.4	15.1	.16	242.4	-24.0	0.0	4.9	0.	0.	148.	0.	0.	5.65
B95411	2.0	8.8	11.7	18.2	.19	242.4	-36.0	0.0	5.3	152.	0.	132.	0.	157.	6.46
B95412	1.5	10.9	11.6	12.9	.08	242.4	-48.0	0.0	3.9	0.	0.	151.	0.	0.	2.78
B95413	1.0	0.0	12.0	0.0	.05	242.4	-60.0	0.0	2.6	0.	0.	157.	0.	0.	1.59
B95414	.6	0.0	12.1	0.0	.04	242.4	-72.0	0.0	1.6	0.	0.	158.	0.	0.	1.23
B95415	.1	0.0	16.9	0.0	.01	242.4	-84.0	0.0	.3	0.	0.	207.	0.	0.	.29
A95308	.2	0.0	35.5	0.0	.02	242.4	84.0	0.0	.5	0.	0.	462.	0.	0.	.70
A95309	.2	0.0	25.0	0.0	.03	242.4	72.0	0.0	.5	0.	0.	324.	0.	0.	1.12
A95310	.2	0.0	27.5	0.0	.04	242.4	60.0	0.0	.6	0.	0.	358.	0.	0.	1.53
A95311	.3	0.0	19.2	0.0	.06	242.4	48.0	0.0	.9	0.	0.	249.	0.	0.	2.10
A95312	.2	0.0	11.2	0.0	.02	242.4	36.0	0.0	.4	0.	0.	146.	0.	0.	.60
A95313	.6	0.0	10.8	0.0	.04	242.4	24.0	0.0	1.6	0.	0.	140.	0.	0.	1.26
A95314	1.8	10.4	12.2	12.8	.07	242.4	12.0	0.0	4.6	0.	0.	158.	0.	0.	2.40
A95315	1.6	9.6	11.5	14.2	.08	242.4	0.0	0.0	4.2	0.	0.	150.	0.	0.	2.88
C95308	.1	0.0	20.2	0.0	.01	242.4	84.0	0.0	.3	0.	0.	262.	0.	0.	.29
C95309	.2	0.0	2.4	0.0	.01	242.4	72.0	0.0	.4	0.	0.	32.	0.	0.	.39
C95310	.1	0.0	44.9	0.0	.01	242.4	60.0	0.0	.2	0.	0.	583.	0.	0.	.32

RUN NUMBER 9

FILE NAME	MODEL CONDITIONS PEAK CONC. (%)	1% ARR. TIME (SEC)	PEAK TIME (SEC)	1% END TIME (SEC)	SUM (X-S)	PROTOTYPE CONDITIONS POSITION X (M)	Y (M)	Z (M)	PEAK CONC. (%)	5% ARR. TIME (SEC)	15% ARR. TIME (SEC)	PEAK TIME (SEC)	15% END TIME (SEC)	5% END TIME (SEC)	SUM (X-S)
C95311	.1	0.0	6.2	0.0	.01	242.4	48.0	0.0	.4	0.	0.	80.	0.	0.	.22
C95312	.1	0.0	11.2	0.0	0.00	242.4	36.0	0.0	.2	0.	0.	146.	0.	0.	.10
C95313	.1	0.0	9.4	0.0	0.00	242.4	24.0	0.0	.2	0.	0.	122.	0.	0.	.07
C95314	.2	0.0	7.4	0.0	.01	242.4	12.0	0.0	.6	0.	0.	96.	0.	0.	.34
C95315	1.1	9.3	9.3	9.6	.03	242.4	0.0	0.0	2.9	0.	0.	121.	0.	0.	1.01
A96308	.1	0.0	48.1	0.0	.01	399.8	84.0	0.0	.4	0.	0.	626.	0.	0.	0.00
A96309	.1	0.0	47.1	0.0	.01	399.8	72.0	0.0	.4	0.	0.	612.	0.	0.	0.00
A96310	.1	0.0	36.8	0.0	0.00	399.8	60.0	0.0	.3	0.	0.	478.	0.	0.	0.00
A96311	.2	0.0	27.5	0.0	.02	399.8	48.0	0.0	.5	0.	0.	357.	0.	0.	0.00
A96312	.2	0.0	5.1	0.0	.01	399.8	36.0	0.0	.4	0.	0.	67.	0.	0.	0.00
A96313	.1	0.0	27.3	0.0	.01	399.8	24.0	0.0	.4	0.	0.	355.	0.	0.	0.00
A96314	.2	0.0	26.6	0.0	.02	399.8	12.0	0.0	.6	0.	0.	346.	0.	0.	0.00
A96315	.4	0.0	11.5	0.0	.02	399.8	0.0	0.0	1.0	0.	0.	149.	0.	0.	0.00